THE ROLE OF BPIFA1 IN OTITIS MEDIA

APOORVA MULAY

A thesis submitted for the degree of

Doctor of Philosophy (Ph.D.)

September 2016

University of Sheffield

Faculty of Medicine, Dentistry and Health

Department of Infection, Immunity and Cardiovascular Disease

Supervisors: Professor Colin Bingle
Dr Lynne Bingle
Professor Michael Cheeseman

Dedicated to my grandfather, Mr Vasant Mulay

You are an inspiration and I miss you everyday!

ABSTRACT

Otitis Media (OM) is the most common paediatric disease and a leading cause of conductive hearing impairment. This multifactorial disease shows significant involvement of innate immunity genes and epithelial abnormalities are also commonly implicated. BPIFA1, a member of BPI fold containing family of putative innate defence proteins, is one of the most abundant secretory proteins in the upper airways and SNPs in *BPIFA1* have been associated with OM susceptibility. Recent studies suggest that BPIFA1 plays a pleiotropic host defense role. This thesis describes experiments aimed at investigating the role of BPIFA1 in protection of the middle ear and in the development of OM.

Bpifa1$^{-/-}$ mice do not spontaneously develop OM and do not demonstrate increased nasopharyngeal carriage of the human otopathogen, NT*Hi.* However, deletion of *Bpifa1* in *Junbo (Evi1*$^{Jbo/+}$*)* mice, an established model of chronic OM, leads to significant exacerbation of OM severity and ME mucosal thickness. This thesis also describes the development of a novel *in vitro* model of the murine middle ear epithelium. Using a combination of transcriptional and proteomic approaches, I demonstrate that the model closely mimics the native middle ear epithelium and differentiates into ciliated cells, goblet cells and secretory cells and also supports infection by NT*Hi*. Attempts were made to recapitulate the OM phenotype *in vitro* using this culture system.

Overall, the data from this thesis indicate that BPIFA1 is involved in maintaining homeostasis within the middle ear under steady state conditions through nonspecific defence of the middle ear mucosa. Loss of BPIFA1 in presence of infection or inflammation increases the sensitivity of the epithelium and leads to an exacerbated host defence response and excessive epithelial remodelling. Furthermore, the novel *in vitro* culture

system can be applied as an effective tool to study the interaction between the middle ear epithelium and various otopathogens.

ACKNOWLEDGEMENTS

First and foremost, I would like to thank my supervisor, Professor Colin Bingle. I came to the UK 6 years ago as a Master's student in Colin's lab and he has always been extremely supportive and approachable. This thesis would not have been possible without his invaluable help, guidance and encouragement. Also a heartfelt thank you to Dr Lynne Bingle for her very helpful advice with planning experiments during this study and invaluable suggestions while drafting the paper. A special thank you to Dr Khondoker Akram for being an amazing teacher and guide throughout my PhD. I have learnt a lot about being a researcher from you!

I would like to thank Professor Steve Brown for providing me with the opportunity to spend the first year of my PhD at MRC, Harwell and always making the taking the time to regularly meet and discuss my project. Thank you to Professor Michael Cheeseman for the support and scientific discussions throughout. I am grateful to Dr Derek Hood for always patiently tending to my microbiology doubts. I would like to thank the past and present members of the deafness group and especially Tom Purnell, Hayley Tyrer and Lauren Chessum for helping me settle into the PhD life initially and always making me feel welcome when I went back to Harwell for experiments. Special thanks to Dr Nanda Rodrigues and Dr Sneha Anand for all their advice in helping me figure out the logistics of working between two places.

I would like to thank our collaborating researchers: Professor Ralph Shohet at University of Hawaii for generating the *Bpifa1*$^{-/-}$ mice and Professor James Stewart and Stuart Armstrong at the University of Liverpool for the MS secretome analysis. My thanks also go to the staff of the Mary Lyon Centre: Sara Wells, Lucie Vizor and Lisa Ireson, in particular, for looking after my mouse lines and co-ordinating complicated breeding for multiple simultaneous experiments. I am grateful to the core facilities at MRC Harwell: Deen Quwailid, Adele Traynor and Rumana Zaman from the GEMS core for genotyping my mice, and Adele Austin, Caroline Barker and Naomi Busk from histology and necropsy for processing the large number of histological sections used in my project. A huge thank you to Debbie Williams for coming to my rescue with her RT-qPCR expertise. You are a star! Thank you to Roland Quinney for organising mouse exports to Sheffield and to Dr Helen Marriott and Lynne Williams for their assistance with dissections at Sheffield. I would also like to thank

Hannah and Catherine for helping me with RT-PCRs and Immunohistochemistry experiments.

A big thank you to the lovely members of the Bingle group and my PhD buddies who have made this process an extremely enjoyable experience. I do not know how I would have survived in a quiet office! Thank you Chloe, Emily, Lucy, Renata, Priyanka, Andreea, and Jess for the numerous gossip sessions and cakes! A big thank you to my amazing roomie, Sayali and to Furaha for always comforting me when I was struggling with experiments. A massive thank you to Hrishi for going through my drafts and making sure I hang in there in my most stressful moments.

Most importantly, a huge thank you to my family: Mom, for being a sponge that absorbs all my worries; Dad, for your perpetual enthusiasm and encouragement to follow my dreams and Renu, for your unconditional love. I could never have reached this stage without you three.

Finally, I would like to extend my gratitude to the University of Sheffield and the Medical Research Council for funding my PhD and the Biochemical Society, Genetics society and Action on Hearing Loss for enabling me to attend a number of international meetings during the course of my PhD.

PUBLICATIONS

- **Apoorva Mulay,** Khondoker Akram, Debbie Williams, Hannah Armes, Catherine Russell, Derek Hood, Stuart Armstrong, James P. Stewart, Steve D. M. Brown, Lynne Bingle, Colin D. Bingle *"*An *in vitro* model of murine middle ear epithelium*"* **Disease Models & Mechanisms Sept. 2016** *[Epub ahead of print].*

- **Apoorva Mulay,** Debbie Williams, Michael Cheeseman, Derek Hood, Thomas Purnell, Catherine Russell, Steve D. M. Brown, Lynne Bingle, Colin D. Bingle "Loss of the homeostatic protein, BPIFA1 leads to exacerbation of Otitis media", *Manuscript in preparation.*

CONFERENCE PRESENTATIONS

- Poster presentation: The role of BPIFA1 in Otitis media. **British Association of Lung Research** Summer Meeting, Sheffield, UK July 2016.
- Poster presentation: The role of BPIFA1 in Otitis media. **10th International Molecular Biology of Hearing and Deafness** Meeting, Hinxton, UK, May 2016.
- Podium presentation: The role of BPIFA1 in Otitis media. **2nd International Annual Florey Symposium**, Sheffield, UK September 2015.
- Podium presentation: Isolation and characterisation of middle ear and nasal epithelial cells for development of an in vitro ototpathogenic infection model. **18th International Symposium on Recent Advances in Otitis Media**, Maryland, USA, June 2015.
- Seminar: An *in vitro* otopathogenic model of the middle ear epithelium. **The Children's National Medical Centre, Washington D.C**, USA, June 2015
- Podium presentation: An *in vitro* otopathogenic model of the middle ear epithelium **51st International Inner Ear Biology Workshop**, Sheffield, UK, April 2014.
- Podium presentation: Mucociliary abnormalities lead to altered expression BPIF/PLUNC proteins in murine models of otitis media of **17th Extraordinary International Symposium on Otitis Media**, Stockholm, Sweden, June 2013.

ABBREVIATIONS

ABR	Auditory Brainstem Response
ALI	Air liquid interface
ANOVA	analysis of variance
AOM	Acute Otitis media
AP-1	Activator protein 1
ASL	Airway surface liquid
ASOM	Acute suppurative Otitis media
B.cepacia	*Burkholderia cepacia*
BAL	Broncheoalvealoar lavage
BHI	Brain heart infusion
BPI	Bacterial permeability increasing protein
BPIF protein	Bacterial permeability increasing fold-containing protein
BPIFA1	Bacterial permeability increasing fold-containing protein A1
BPIFB1	Bacterial permeability increasing fold-containing protein B1
CD	Cluster of differentiation
CETP	Cholesterol ester transfer protein
CF	Cystic fibrosis
COME	Chronic Otitis media with effusion
COPD	Chronic obstructive pulmonary disease
CSOM	Chronic supparative Otitis media
CT	Cycle threshold
CtBP	Carboxy terminal binding protein
dB	decibels
DPPC	Dipalmitoylphosphatidylcholine
e	embryonic day
ECM	extracellular matrix
ENaC	Epithelial sodium channel
ENU	N-Ethyl Nitrosourea
ERP	Ethical Review Process
ET	Eustachian tube
EVI1	Ecotropic viral integration site-1
FACs	Fluorescence associated cell sorting
FBS	Foetal bovine serum
FBXO11	F-box 11
Foxj1	Forkhead box protein J1
G	Generation
GWAS	Genome-wide association study
GWLS	Genome-wide linkage study
H&E	haematoxylin and eosin
HBE cells	Human bronchial epithelial cells
HIF	Hypoxia inducible factor
Hm	Hemin
hpi	Hours post infection

HSC	Haematopeitic stem cell
IFC	Fluorescence Immunocytochemistry
IHC	Immunohistochemistry
IL	Interleukin
IN	Intranasal
JNK	c-JUN kinase
K.pneumoniae	*Klebsiella pneumoniae*
kDa	Kilo dalton
LBP	Lipopolysaccharide binding protein
LEV	Levinthals
LPLUNC1	Long palate lung and nasal epithelium clone 1
LPS	Lipopolysaccharide
LUNX	Lung associated protein X
M.cattarhalis	*Moraxella cattarhalis*
M.pneumoniae	*Mycoplasma pneumoniae*
MAP	Mitogen activated protein
MIP	Macrophage inhibitory protein
mMECs	Mouse middle ear epithelial cells
MMEEC	Mouse middle ear epithelial cell line
mMMCs	Mouse middle ear mucosal cells
MMP-2	matrix mettaloproteinase-2
mNECs	Mouse nasal epithelial cells
MOI	Multiplicity of infection
MRC	Medical Research Council
MRSA	Methicillin resistant *Staphalococcus aureus*
MS	Mass Spectrometry
mTECs	Mouse tracheal epithelial cells
MUC	Mucin
NAD	Nicotineamide dinucleotide
NFκB	Nuclear factor kappa β
NHMEEC	Normal human middle ear epithelial cell line
NLR	Nucleotide-binding oligomerization domain-like receptor
NogoB	Neurite outgrowth inhibitor B
NP	Nasopharynx
NSCLC	non-small cell lung carcinoma
NT*Hi*	non-typeable *Haemophilus influenzae*
OM	Otitis media
P	Post-natal
P.aeruginosa	*Pseudomonas aeruginosa*
p63	Transformation-related protein 63
PAMP	Pathogen associated molelular pattern
PCD	Primary ciliary dyskinesia
PCR	polymerase chain reaction
PCV-7	Pneumococcal conjugate vaccine
PD	Population doubling time
PLTP	Phospholipid transfer protein

PLUNC	Palate lung and nasal epithelium clone
PRR	Pattern recognition receptor
qRT-PCR	Quantitatve real time PCR (for genotyping)
rAOM	Recurrent acute otitis media
Reg3$^{\gamma}$	Regenerating islet-derived protein 3 gamma
RLR	RIG-I-like receptors
ROCKi	Rho-kinase inhibitor
RQ	Relative quantification
RSV	Respiratory synctial virus
RT-PCR	Endpoint reverse transcription PCR
RT-qPCR	Quantitatve reverse transcription polymerase chain reaction
S.pneumoniae	*Streptococcus pneumoniae*
SEM	Scanning electron microscopy
SNP	Single nucleotide polymorphism
SP	Surfactant protein
SPF	Specific pathogen free
SPLUNC1	Short palate lung and nasal epithelium clone 1
SPURT	Secretory protein in upper respiratory tracts
Stfpd	Surfactant protein D gene
TBE cells	Tracheobronchial epithelial cells
TEM	transmission electron microscopy
TGF	Transforming growth factor
TGIF1	Transforming growth inhibitory factor 1
TLR	Toll-like receptor
Tm	Tympanic membrane
TNF	Tumor necrosis factor
URT	Upper respiratory tract
VEGF	Vascular endothelial grwith factor
WFDC	WAP four-disulfide core domain protein
Wt	Wild type
ZnF	Zinc finger
Zo-1	Zona occludens
αSMA	alpha smooth muscle actin

TABLE OF CONTENTS

TABLE OF FIGURES

TABLE OF TABLES

CHAPTER 1: GENERAL INTRODUCTION

1.1 Structure and function of the ear

The mammalian ear is the sensory organ of hearing and balance. Different parts of the ear co-ordinate to convert sound waves from the external environment into the electrical impulses transmitted to the brain. The ear can be divided into three parts: the external or outer ear, the middle ear and the inner ear (Fig 1.1). The outer ear is composed of the pinna, which gathers environmental sounds and the ear canal, which funnels them towards the eardrum or the tympanic membrane (Tm) of the middle ear. The sound waves hit the Tm and cause it to vibrate (Carola et al 1992).

The middle ear is an air-filled chamber, with an average volume of $2cm^3$ in humans. It contains a chain of 3 ossicles or auditory bones called malleus, incus and stapes, extending from the Tm to the oval window of the inner ear. The mechanical energy of the vibrations from the comparatively large area of the Tm is transmitted to the first ossicle, the malleus, followed by the incus and finally concentrated at the small footplate of the last ossicle, the stapes, which presses against the oval window of the inner ear. This results in an increase in the energy of the waves transmitted from the outer ear to the inner ear. The middle ear cavity is also connected to the Nasopharynx (NP) through a narrow tube called the Eustachian tube (ET) that opens intermittently to maintain atmospheric pressure within the middle ear cavity. Maintenance of optimal pressure within the middle ear ensures maximal vibration of the Tm (Emanuel et al 2009, Straetemans et al 2001).

The inner ear is the final part of the ear and is made up of a fluid-filled bony structure called the labyrinth. Pressure transferred from the stapes onto the round window displaces the fluid inside the cochlea, the auditory component of the labyrinth. This causes deflection of the stereocilia of the sensory cells or hair cells that line the cochlear membrane and generation of electrical impulses, which are transmitted to and recognised by the brain.

The inner ear also contains the vestibular system, which is maintains equilibrium and spatial orientation (Carola et al 1992, Emanuel et al 2009).

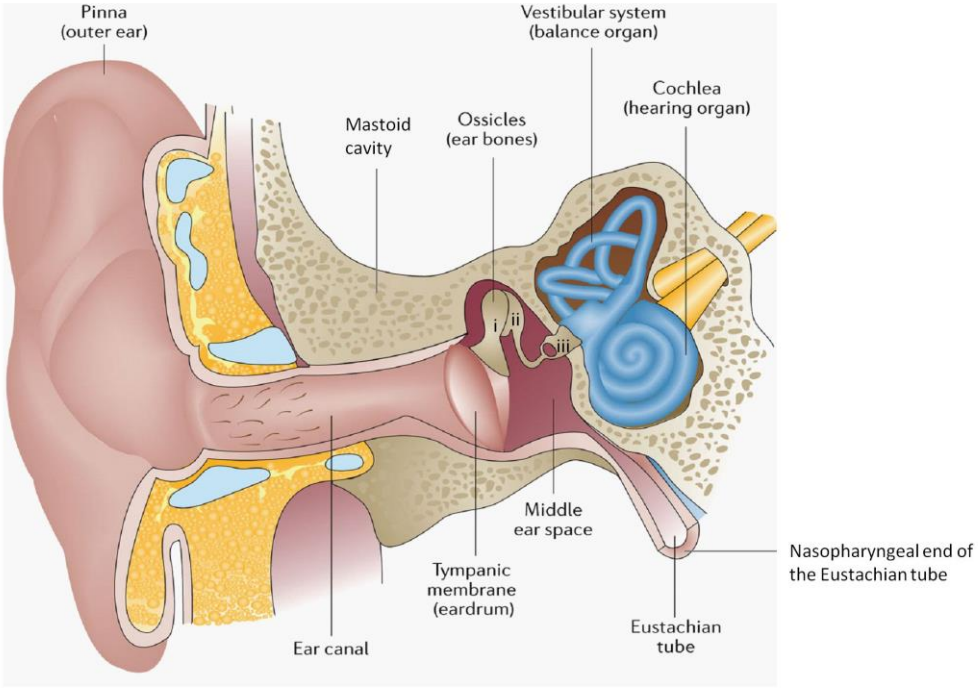

Figure 1.1 Structure of the ear
The ear is divided into three main parts: the outer ear, middle ear and the inner ear. The middle ear cavity comprises of the three ossicles, the (i) malleus, (ii) incus and (iii) stapes. The Tm separates the outer ear from the middle ear cavity. The ET connects the middle ear to the nasopharynx. Image reused with permission from (Schilder et al 2016), copyright 2016 Nature publishing group.

1.2 The burden of hearing loss

Around 360 million people globally suffer from partial or complete deafness, making hearing loss the most common sensory disorder (WHO 2015). Within the UK, more than 11 million people are affected by disabling hearing loss and this number has been estimated to reach 14.5 million by 2035 (Action On Hearing Loss 2015). Hearing loss can result due to various factors such as ototoxic drugs, genetic defects, persistent ear infections or exposure to loud noises. Hearing loss resulting from defects in or damage to the inner ear hair cells is termed as sensorineural hearing loss. Age related hearing loss is known as

presbycusis, whereas loss of hearing due to reduced transmission of sound through the outer and middle ear is called conductive hearing loss.

One of the major common causes of conductive hearing loss is Otitis Media (OM) or inflammation of the middle ear. It is the most prevalent childhood disease and the most common cause of paediatric deafness, surgery and antibiotic prescription in developed countries (Monasta et al 2012). 80% children suffer from at least one episode of OM by three years of age (Bakaletz 2010, Woodfield & Dugdale 2008). Severe and recurrent forms of the disease can cause perforation of the Tm and more than 50% of the affected children are at a risk of suffering from conductive hearing loss (Monasta et al 2012). OM is an enormous socio-economic burden. In the United States of America, annual diagnosis and management costs account for 2.3 billion dollars (Streubel & Ross 2013). Moreover, paediatric deafness hampers behaviour, language development and communication abilities and thus affects educational and social development (Rye et al 2011a). OM can also lead to life threatening complications such as brain abscesses, mastoiditis and bacterial meningitis (Geyik et al 2002, Schilder et al 2016) with an estimated paediatric mortality rate of 21,000 reported deaths per year (Monasta et al 2012).

1.3 Otitis media – a spectrum of middle ear diseases

OM is the most prevalent cause of paediatric surgery (insertion of tympanosomy tubes or grommets in the Tm) and conductive hearing loss in children. OM is often a combination of overlapping conditions, which are classified in the following categories, based on their symptoms and chronicity:

1.3.1 Acute suppurative Otitis media (ASOM) or acute Otitis media (AOM)

This is the most prevalent type of OM with over 709 million cases of AOM reported per year (Monasta et al 2012). It is characterised by rapid onset of symptoms such as otalgia (ear pain), otorrhea (discharge of pus or fluid from the ear), irritability and fever (Bakaletz 2010). It is sometimes associated with bulging of the tympanum and cholesteatoma. OM is classified as rAOM when the child suffers from AOM more than three times in 6 months or more than 4 times a year (Rye et al 2011a).

1.3.2 Otitis Media with Effusion (OME)

OME is usually sequelae of AOM and presents with ottorhea, without the signs of inflammation and through an intact Tm. It is often attributed to ET dysfunction and is also commonly known as 'glue ear' (Bakaletz 2010). When chronic, OME is termed as Chronic Otitis media with effusion (COME) (Rye et al 2011a).

1.3.3 Chronic suppurative Otitis media (CSOM)

If untreated, rAOM and COME can lead to development of CSOM, which is characterized by persistent inflammation, perforation of the Tm and continuous ear discharge for over 2 weeks (Bluestone 1998). CSOM can reduce hearing capacity by up to 30 decibels (db) and thus cause conductive hearing loss (Straetemans et al 2001).

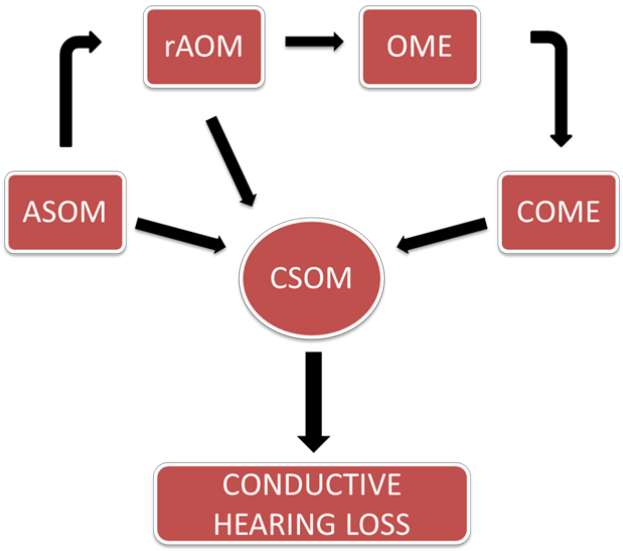

Figure 1.2 Interplay between types of OM
AOM, the commonest form of OM can lead to the development of rAOM as well as CSOM. Recurrent episodes of OM can cause OME, which in turn gives rise to its chronic form, COME. The persistence of rAOM and COME for long periods leads to perforation of the tympanum and development of CSOM. CSOM leads to conductive hearing loss.

1.4 The aetiology of OM

The upper airways consist of the trachea, NP, ET, middle ear and mastoid cells surrounding the middle ear. The middle ear epithelium is continuous throughout the upper airways (Fireman 1997). Therefore, the physiology and immune defences of the upper respiratory tract (URT) are very similar to that of middle ear and ET.

The middle ear is relatively sterile and this sterility is conferred as a combined result of the structure and physiology of the ET, and the immunological defence mechanisms of the mucociliary lining (Straetemans et al 2001).

1.4.1 Structure and function of the Eustachian tube

The middle ear is an isolated organ, separated from the outer ear by the Tm on one end and connected to the NP via the ET at the other end. The mucociliary epithelium of the middle ear and the ET comprises of, secretory, goblet and ciliated cells, plasma cells, blood vessels, and mast cells. (Ishii et al 1980). Both the middle ear and ET are involved in the development of OM. The ET plays an analogous role in relation to the NP and the middle ear as the bronchial tree performs in relation to the lung and the upper airways (Fireman 1997).

The ET performs three main functions: protection, ventilation and clearance.

Protection: The nasopharyngeal end of the ET is closed at rest, thus preventing the pathogens present the nasal secretions from entering into the middle ear cavity. It opens actively during actions like swallowing, sneezing, and yawning. Goblet cells of the mucociliary epithelium secrete a viscous substance called mucus which obscures epithelial attachment sites for bacteria, preventing bacterial colonization and thus protecting the middle ear from infections (Kubba et al 2000). The ET in children is narrower, shorter and more horizontal being inclined at an angle of 10° in children as compared to 45° in adults (Corbeel 2007). It is also more compliant (Bakaletz 2010) and sometimes patent i.e. more open (Straetemans et al 2001). Therefore, children are more prone to ET dysfunction.

Ventilation: Ventilation is provided due to intermittent opening of the ET. Surfactant components present in the ET lower the surface tension and aid in its opening (McGuire 2002). This facilitates equilibration of pressure between the middle ear and NP. Defects in the opening mechanism of the ET or its physical obstruction, can cause negative pressure to develop in the middle ear in comparison to the nasopharynx and leads to aspiration of nasal fluid (Robinson et al 1992, Straetemans et al 2001). Also, gaseous exchange between the middle ear and surrounding mastoid cells creates hypoxic conditions in the middle ear. Opening of the ET restores oxygen levels in the middle ear (Corbeel 2007).

Clearance: The goblet cells of the mucociliary epithelium continuously secrete mucus and the ciliated cells beat in a unidirectional manner, transporting this mucus from the middle ear into the NP, through the Eustachian tube. As a result, nasopharyngeal pathogens are physically prevented from ascending into the middle ear (Sade 1967).

1.4.2 Pathogens involved in OM

The three most commonly isolated pathogens from middle ear effusions of OM patients are *Streptococcus pneumoniae* (*S.pneumoniae*), non-typeable *Haemophilus influenzae* (NT*Hi*), and *Moraxella catarrhalis* (*M.catarrhalis*) (Faden 2001). Of these, *S.pneumoniae* is more commonly associated with AOM, while NT*Hi* is more commonly associated with the chronic forms. Apart from the 3 major bacterial species, other bacteria in middle ear effusions include *Alloiococcus otitidis, Pseudomonas aeruginosa* (*P.aeruginosa*), *Streptococcus pyogenes, Staphylococcus aureus, Klebsiella pneumoniae* (*K. pneumoniae*) and *Escherichia coli* (Ngo et al 2016). Most of these bacteria are a part of the normal flora of the NP and upper airways. AOM is often preceded by a viral URT infection, which compromises local immunity, increases the cell surface receptors for bacterial adhesion and increases the possibility of secondary infection by the normal flora of the NP (Bakaletz 2010). For example, infection by Respiratory Syncytial Virus (RSV) is shown to promote ascending infection of the middle ear by *M. catarrhalis* in chinchilla models of OM (Brockson et al 2012). The most common viral species causing URT infections include RSV, influenza, rhinovirus, coronavirus and adenovirus. 5% of middle ear effusions from AOM patients contain virus alone (Schilder et al 2016).

This thesis focuses on the role of NT*Hi* in the pathogenesis of OM. NT*Hi* is a Gram-negative non-encapsulated bacterium commensal to the NP. Globally, it is responsible for 25%-30% cases of AOM and is the most commonly isolated pathogen in COME (Giebink 1991). Colonisation of the URT with NT*Hi* during the first year of life increases the chances of OM

development four fold (Faden 2001). A study monitoring colonisation of the NP by NT*Hi* in children for the first two years of life showed that acquisition of this bacterial species was higher in the first year. Children carried one strain of NT*Hi* at a time but were colonised by up to 7 different strains, distinguished by changes in the outer membrane protein of NT*Hi* (Faden et al 1996). Currently a conjugate vaccine against 7 serotypes of *S.pneumoniae* (PCV7) is commonly administered to children (Shinefield et al 2002). The advent of this pneumococcal vaccine has caused a shift in the frequency of detection of NT*Hi* in AOM patients, with the frequency surpassing that of *S.pneumoniae* in developed countries (Ngo et al 2016). Thus, NT*Hi* is gaining more importance as the causative pathogen in OM.

1.4.3 Immunological defence mechanisms of the middle ear

Immunological defense is a key factor in maintaining sterility of the middle ear. Immunity is classified as innate immunity and adaptive immunity. Adaptive immunity requires prior sensitization of lymphocytes (B cells, T cells and natural killer cells) in order to elicit an antibody- and T-cell mediated response. Since the healthy middle ear does not harbor many lymphocytes, a well-developed innate immune system is essential in preventing infection and promoting resolution (Leichtle et al 2011).

Innate immunity does not require prior contact with antigenic epitopes. It provides the first line of defense against invading pathogens and in the ear, is comprised of the middle ear epithelium which acts as a physical barrier, epithelial secretions and resident macrophages, mast cells and dendritic cells in the peripheral tissue. The goblet cells of the mucociliary epithelium secrete high molecular glycoproteins called mucins which increase the viscosity of epithelial secretions and are important in trapping pathogens. MUC5AC and MUC5B are the major secreted gel forming mucins in the human middle ear (Kerschner et al 2010b, Lin et al 2001) and OM is associated with upregulation of these two proteins (Kerschner et al 2010b, Preciado et al 2010). The middle ear epithelium also produces antimicrobial

molecules such as Lysozyme, Lactotransferrin, components of complement system (Jeep 1990, Lim et al 2000) and broad-spectrum bactericidal molecules called β-defensins (Mittal et al 2014). β-defensins are involved in bactericidal activities like perforation of bacterial membranes, inhibition of bacteriotoxins, and promotion of inflammation. (Bakaletz 2009, Underwood & Bakaletz 2011). Moreover, surfactant proteins secreted by the mucosal lining of the ET and the middle ear and phosphatidylcholine promote dispersal of bacterial biofilms (McGuire 2002). It has recently been shown that the middle ear epithelium also secretes BPIFA1, a putative multifunctional host defense protein of the URT (Bartlett et al 2011).

The epithelial cells and sentinel cells such as dendritic cells and macrophages express receptors, known as pattern recognition receptors (PRRs), that recognize the invariant features of microbes known as pathogen associated molecular markers (PAMPs). PAMPs include characteristics such as flagella, Lipopolysaccharide (LPS) of Gram-negative bacteria and Lipotechoic acid of Gram-positive organisms, that are common to multiple organisms (Iwasaki & Medzhitov 2010). PRRs include Toll like receptors (TLRs), Retinoic acid inducible gene I like receptors (RLRs) and Nucleotide-binding oligomerization domain (NODs) (Mittal et al 2014). Of these, TLRs are the most widely studied. Thirteen TLRs are present in mammals, of which TLR2 and TLR4 have the best studied roles in OM pathogenesis. Upon ligand recognition, most TLRs activate the nuclear factor kappa-light-chain-enhancer of activated B cells (NFκβ). NFκβ signaling triggers the release of chemokines such as such as macrophage inflammatory protein 1α (MIP1α)/CCL3 and macrophage inflammatory protein 2 (MIP 2)/CXCL2 and pro-inflammatory cytokines, such as Interleukin (IL) 1β (IL1β), IL10, IL6, IL8, and Tumor necrosis factor α (TNFα) (Juhn et al 2008, Leichtle et al 2011). A concentration gradient of TLR4 expression exists in the ET with a higher concentration towards the middle ear cavity and a lower concentration towards the nasopharynx (Akashi-Takamura & Miyake 2008). Since, the nasopharynx is home to a wide range of normal flora,

low numbers of TLRs near the nasopharynx avert unnecessary elicitation of immune response whereas the higher concentration near the middle ear facilitates stringent control of immune response in the event of infection (Bakaletz 2010).

Middle ear fluids also show presence of antibodies such as antigen specific IgG and IgA. T-cells may also play a role in middle ear inflammation, however further research is warranted to fully explore the role of adaptive immunity in the aetiology of OM (Schilder et al 2016).

1.5 A model for the pathophysiology of OM

Failure of the structural defense mechanisms, such as ET dysfunction, coupled with impairment of the mucociliary apparatus, or failure of the innate immune system to prevent an infection or clear pathogens leads to the development of OM (Casselbrant & Mandel 2001). A pre-requisite in the disease pathogenesis is presence of bacteria in the nasopharynx. A preceding viral infection compromises the immunity of the URT, modifies the mucosa and enables greater adhesion of bacteria leading to colonization. It also induces a pro-inflammatory response, impairing mucociliary clearance which leads to ET dysfunction and development of negative pressure in the middle ear cavity (Schilder et al 2016). This in turn facilitates ascent of the normal flora of the NP into the middle ear (Bakaletz 2010).

The pathogens in the middle ear cavity are detected by TLRs, which trigger production of cytokines chemokines and antimicrobial peptides. Inflammatory cells such as neutrophils and macrophages infiltrate the middle ear cavity and add to the production of the inflammatory mediators (Leichtle et al 2011). Mounting such an inflammatory response is crucial for clearance of invading pathogens. However, persistent inflammation can have pathological implications as seen in chronic forms of OM. Over production of cytokines up regulates mucin genes, leading to excessive production of mucus, which obstructs the

movement of cilia (Hunter et al 1999). The inflammatory fluid is therefore retained in the middle ear cavity and also blocks the ET. This enhances inflammation further and leads to epithelial tissue remodeling, often characterized by a reduction in the number of ciliated cells, increases in the number of secretory or goblet cells (goblet cell hyperplasia) and conversion of other cell types to goblet cells (goblet cell metaplasia) (Straetemans et al 2001). The mucosal epithelium thickens and the single layer of squamous epithelium is converted into multiple layers of pseudostratified respiratory epithelium with copious amounts of underlying stroma. The oxygen requirements of bacteria and inflammatory cells, along with reduced ventilation in the middle ear, leads to development of hypoxia, which activates the Hypoxia inducible factor (HIFα). HIFα induces angiogenesis and activates other genes, which help in restoring homeostasis in the hypoxic tissues. However, prolonged activity of HIFα leads to further tissue remodeling and overactive inflammation. (Cheeseman et al 2011). Consequently, a vicious cycle of inflammation, mucus production and decreased ciliary function commences, which if persistent for extended periods of time, can lead to major complications like Mastoiditis - spread of infection to the temporal bone and damage to the Tm leading to conductive hearing loss (Schilder et al 2016).

Thus, the pathophysiology of OM is highly complex and a wide variety of factors may contribute to disease development (Fig 1.3).

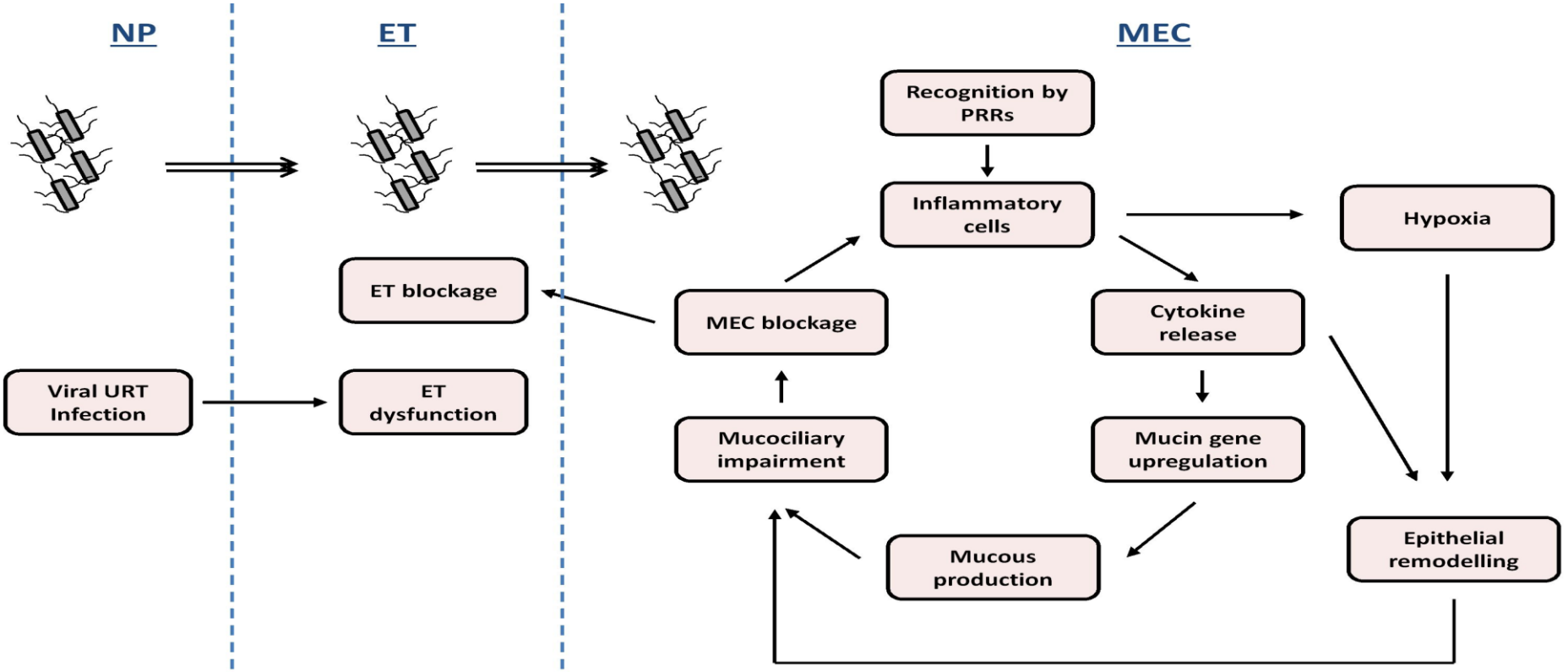

Figure 1.3 Pathophysiology of OM

Viral infection of the URT predisposes secondary infection by the normal flora of the NP and leads to ET dysfunction. Bacteria migrate from the NP through the ET and enter the middle ear cavity (MEC) where they activate PRRs such as TLRs. This causes recruitment of inflammatory cells and release of inflammatory mediators, like cytokines which subsequently up regulates mucous production. The viscous mucous contributes to ciliary dysfunction, leading to blocking of the MEC and ET. As a result, ET dysfunction increases and leads to further inflammation and epithelial remodeling. Hypoxia also contributes to epithelial remodeling. Thus, a vicious cycle sets in leading to the development of chronic OM.

1.6 Risk factors and candidate genes for OM

Epidemiological studies indicate that race is an important susceptibility factor for development of OM. Prevalence of OM is more common in American Indians and Australian aborigines. The occurrence of OM amongst Caucasians is relatively low (Bluestone 1998). Many other factors such as the male sex, lack of breast feeding, attendance at day care centres, immaturity of the immune system, prolonged URT inflammation, presence of affected siblings, exposure to cigarette smoke also. increase susceptibility to OM (Schilder et al 2016, Straetemans et al 2001).

Although OM is largely perceived as an infectious disease, the fact that some children suffer from these infections more frequently and some fail to resolve it in comparison to others, suggest a strong genetic basis, especially for rAOM, CSOM and COME (Parkinson et al 2006). Twin and triplet studies suggested that the children with siblings having a history of rAOM and COME demonstrated 1.6-4.2 higher fold higher susceptibility to the disease (Rasmussen 1993, Sipila et al 1988, Teele et al 1989). Based on these studies, it was determined that the genetic contribution to OM is between 45% - 75% (Casselbrant et al 2004). Two genome wide linkage studies (GWLS) have been performed to date (Casselbrant et al 2009, Daly et al 2004). Both studies have identified several susceptibility loci for OM including chemokine genes, surfactant genes, inflammasome genes and genes involved in allergy. However the studies were confounded by large size of the linkage loci, low statistical power and discrepancy between OM phenotypes recruited and the specific genes were not mapped (Casselbrant et al 2009, Daly et al 2004).

However, several other studies have identified candidate genes for susceptibility to OM. Majority of these genes are associated with dysfunction of the ET and other craniofacial structures, impairment of mucociliary defence or the innate immune system (Rye et al 2011a). For example, OM occurs in 92- 97% children with cleft palate, due to abnormally

structured ETs (Robinson et al 1992) and children with, Primary Ciliary Dyskinesia (PCD), which results in abnormal functioning cilia (leading to failure of mucociliary clearance, are also predisposed to OM (Campbell et al 2009). Mice deficient in Myd88 (a key regulatory innate defence protein) have delayed recruitment of inflammatory cells and more persistent OM (Hernandez et al 2008). Polymorphisms in *TLR2, TLR4, TLR9, PA11, EVI1, FBXO11,* mucin genes *(MUC2, MUC5B, MUC5AC)* as well as various cytokine genes (including interleukins, TNFα and Transforming growth factorβ (TGFβ), have also been linked to OM susceptibility (Patel et al 2006, Roy et al 2014, Rye et al 2012a, Schilder et al 2016, Segade et al 2006).

The largest GWAS study to date identified *BPIFA1 and BPIFA3* on chromosome 20q11 and *CALPN14* and *GALNT14* on chromosome 2p23 as the top candidate genes for OM susceptibility (Rye et al 2012b). Interestingly, loss of *Bpifa1* has recently been shown to increase OM susceptibility in aged mice (Bartlett et al 2015)

As outlined above, OM is a multifactorial; polymicrobial disease associated with a large number of susceptibility genes. Identifying genes involved in the development of the OM is key to the better understanding of its complex etiology and for the development of therapeutic approaches. Innate immunity is of particular importance in OM pathophysiology. In this thesis, I have investigated a role for the putative URT innate immunity gene, *BPIFA1* in the development of OM.

1.7 An introduction to PLUNCS or BPIF proteins

The Palate Lung and Nasal Epithelial Clone (*Plunc*) gene was first identified whilst studying proteins participating in closure of the embryonic mouse palate (Weston et al 1999). Whole mount *in situ* hybridisation showed that the gene was highly expressed during embryonic development of murine nasal epithelium. In adult mice, the gene was strongly expressed in the nasal passages and proximal trachea, but expression decreased towards the bifurcation

of the bronchi and disappeared in the peripheral lung. (Weston et al 1999). Following this study, multiple human *PLUNC* genes were soon identified on chromosome 20q11 using sequence analysis and bioinformatics approaches (Bingle & Bingle 2000, Bingle & Craven 2002, LeClair et al 2001).

1.7.1 Nomenclature and types of PLUNCS/BPIF proteins

PLUNCS have been previously known by various names, such as Secretory protein in the upper respiratory tract (Spurt*),* Lung specific X protein (Lunx) and YY1 (Barnes et al 2008, He et al 2000). Modelling studies suggest that PLUNC proteins are structurally similar to the antimicrobial and anti-inflammatory Bacterial permeability increasing protein (BPI), which is composed of two domains connected by a β sheet (Bingle & Craven 2002). BPI is also similar in structure to Lipopolysaccharide binding protein (LBP), Phospholipid transfer protein (PLTP) and, Cholesterol ester transfer protein (CETP), together forming the BPI/LBP superfamily (Bingle & Craven 2004). PLUNCS belong to, and form the largest branch of, the BPI/LBP superfamily and therefore were recently renamed as BPI-Fold containing proteins or BPIF proteins. This nomenclature was based on phylogenetic analysis of 102 sequences across different species and has been approved by the HUGO Gene Nomenclature Committee. Under the new system, PLUNC proteins containing a single BPI structural domain (previously known as SPLUNCs) have been renamed BPI fold containing A proteins (BPIFA) and PLUNC proteins containing structural similarity to both domains of BPI (previously known as LPLUNCs) have been renamed BPI fold containing B proteins (BPIFB) (Bingle et al 2011b).

BPIF orthologs are present in all air-breathing vertebrates and their gene loci have been characterised in mice (on chromosome 2) rats (on chromosome 3), cattle (on chromosome 13) and chickens (on chromosome 20) (Bingle et al 2004, Chiang et al 2011, Wheeler et al 2011). *BPIF* genes form a cluster in a 200-300kb region on the genome, and currently consist of 11 members in humans, and 14 in mice, including a number of pseudogenes (Fig

1.4) (Bingle et al 2011a). These adjacent genes, which are also positioned in close proximity to BPI and LBP, are suggested to have evolved through a number of duplication events (Bingle & Craven 2002, Bingle et al 2004).

Among the different BPIF proteins, BPIFA1 and BPIFB1 are the most expressed proteins within the upper respiratory tract. This thesis focuses on the role of BPIFA1 in development of OM.

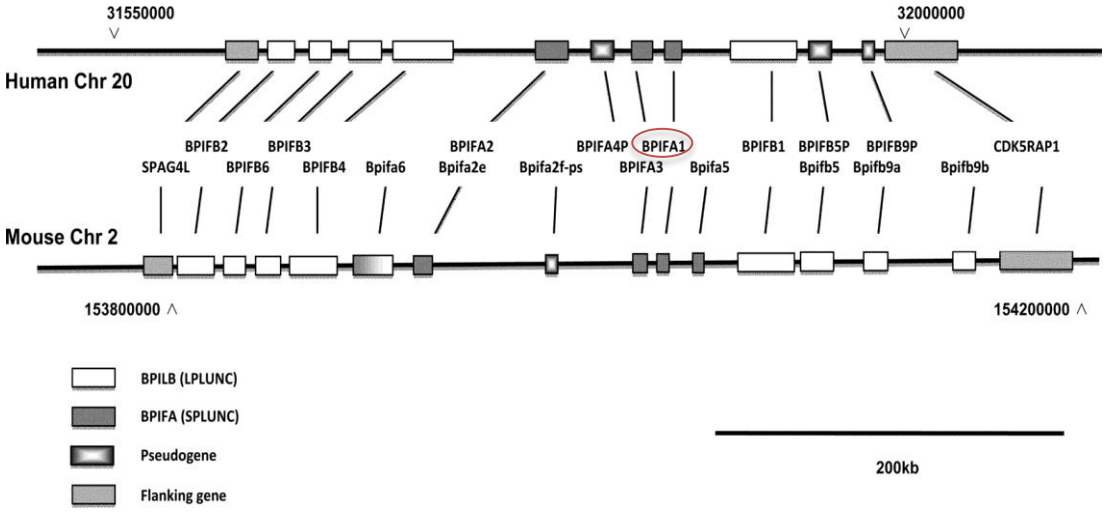

Figure1.4 Genomic organisation of the human and mouse BPIF genes
Human BPIF cluster is located on chromosome 20 (top) and mouse cluster on chromosome 2 (bottom). Arrows indicate orthologs for individual genes. The position of the locus on the chromosome (Chr) is indicated by the arrowheads. *BPIFA* (*SPLUNC*) genes are shown as grey boxes, *BPIFB* (*LPLUNC*) genes are shown as white boxes and pseudogenes are shown as shaded boxes. *SPA4L* and *CDK5RAP1* are unrelated genes flanking the locus. Our gene of interest, *BPIFA1* is circled in red. Scale bar, 200 kb. Image reused with permission from (Bingle et al 2011a), copyright 2011 Portland press.

1.8. Normal expression and localisation of BPIFA1

BPIFA1 is the founding member of the *BPIF* family, originally identified as "*Plunc*" in embryonic mouse palate (Weston et al 1999) and is the most extensively studied family member. The sequence identities between the mouse and human BPIFA1 orthologs is 72% (Britto & Cohn 2015). The product of the *BPIFA1* gene is a secreted protein with a mass of 28.6kDa in mice and 26.6 kDa in humans (Britto & Cohn 2015, Chu et al 2007). The crystal structure of BPIFA1 was recently published by two independent groups (Garland et al 2013,

Ning et al 2014). As predicted by modelling studies, both studies reveal a 256 amino acid monomer, consisting of 6 alpha helices (α1-6), flanking a central beta sheet and together enclosing a leucine rich hydrophobic core. The structure of BPIFA1 is largely homologous to the N-terminal domain of BPI except for the 2 helices, α4 and α6 (Fig 1.5). BPIFA1 is also structurally similar to the single domain proteins, equine surfactant Latherin and dust mite allergen Derp7 (Garland et al 2013, Ning et al 2014, Walton et al 2016).

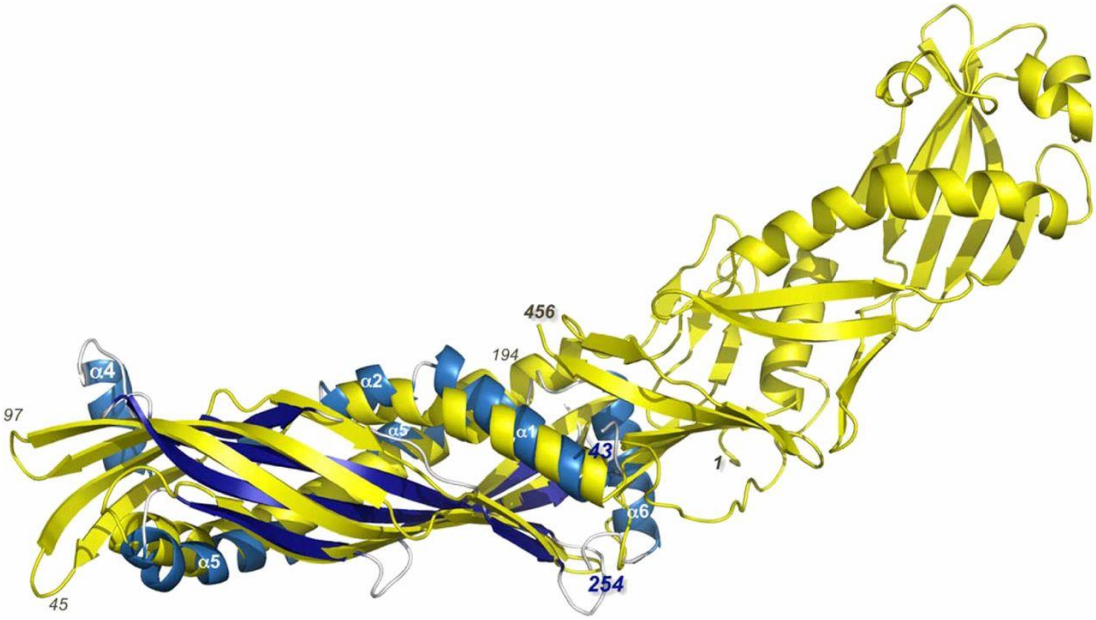

Figure1.5 Crystal structure of BPIFA1 showing structural homology to BPI
Human BPIFA1 (blue) demonstrates structural homology with the N-terminal domain of BPI (yellow). Residues 43–254 of BPIFA1 were superimposed on residues 1–194 of BPI and share only 12% sequence identity. The labelling is shown for the 6 α-helices of BPIFA1. Image reused with permission from (Garland et al 2013), copyright 2013 by National Academy of Sciences

1.8.1 Normal Expression and localisation of BPIFA1 in the upper airways and oral cavities

The expression of *BPIFA1* is highly tissue specific. *BPIFA1* is mainly expressed in the epithelium of nasal passages, oropharynx, trachea and bronchi (Bingle & Bingle 2000, Bingle & Bingle 2011). BPIFA1 localises to non-goblet, non-ciliated population of secretory cells of the upper airways (Bingle et al 2005). In humans, it is found also the minor glands of the nose, tongue, tonsils and sinuses (Barnes et al 2008, Bingle et al 2005) as well as in the

mucous cells of the sub-mucosal, sub-lingual and sub-mandibular glands (Bingle & Bingle 2011). In mice, expression of *Bpifa1* is largely restricted to the oral, nasopharyngeal and respiratory tissue. This expression pattern is shown by the murine tissue microarray expression dataset on the BioGPS data portal (http://biogps.org (Su et al 2004)), which shows expression of *Bpifa1* at high levels in the parts of the nasal passages and trachea and to a lower extent in the lung (Fig 1.6).

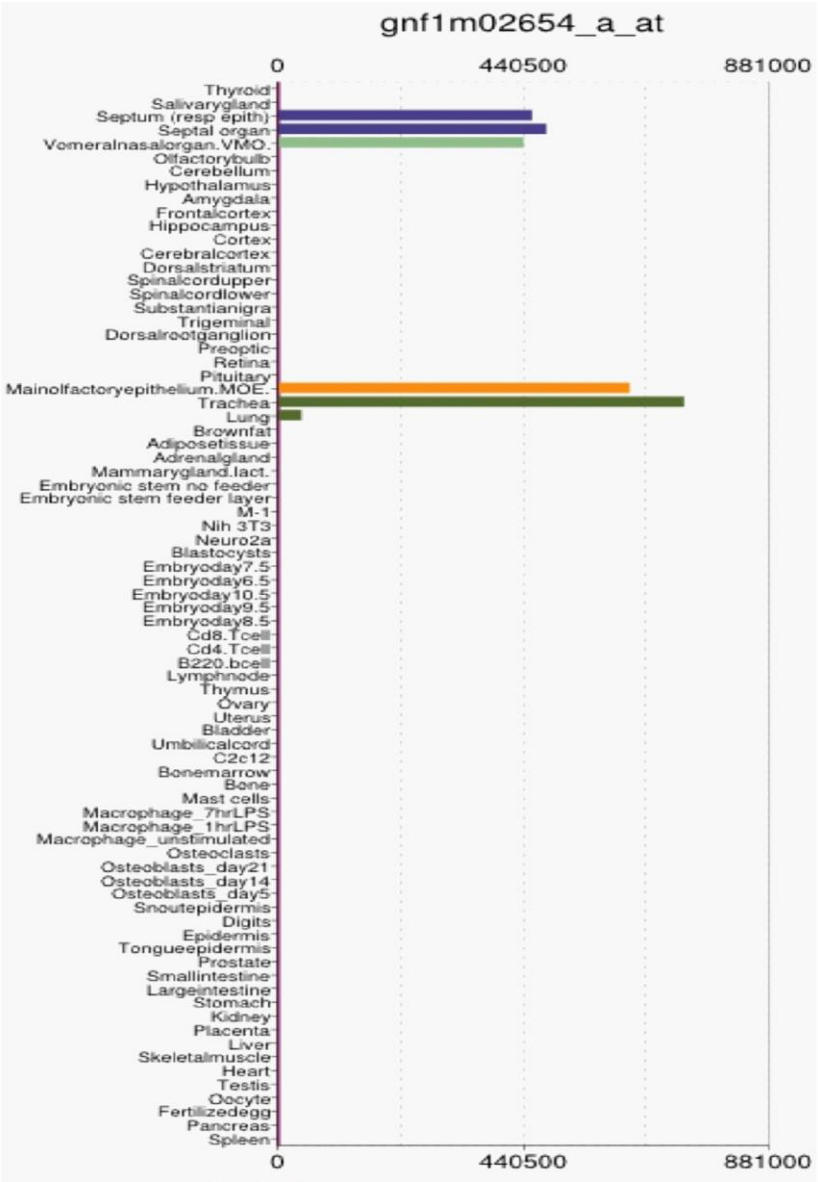

Figure 1.6 Tissue restricted expression of BPIFA1
Adult mouse tissue microarray data of *Bpifa1* demonstrated restricted sites of expression. *Bpifa1* expression was restricted to parts of the nasal cavity, trachea and lung (upper airways). The image was recovered from the BioGPS portal and is based on data from (Su et al 2004)

A previous study for our lab extensively studied localisation of BPIFA1 in coronal sections of the adult mouse head (Musa et al 2012). BPIFA1 was shown to localised to the non-ciliated cells of the respiratory epithelium in various parts of the nasal cavity. Additionally, it was present in the Bowman's glands and gland ducts. BPIFA1 staining was also seen in the sub-mucosal cells of the ducts in the larynx but unlike humans, BPIFA1 was absent in the parotid and submandibular salivary glands (Musa et al 2012). Glycosylated forms of secreted BPIFA1 can be identified in nasal lavage, saliva, sputum and Bronchi alveolar lavage (BAL). They are also secreted in large quantities into the apical surface lining fluid from air liquid interface (ALI) cultures of differentiated tracheobronchial epithelial (TBE) cells (Britto & Cohn 2015, Campos et al 2004)

There are limited reports of presence of human and mouse BPIFA1 outside the respiratory tract for example in the kidney, colon and stomach (Garcia-Caballero et al 2009, Hou et al 2004, LeClair et al 2004, Sentani et al 2008). However other reports, including studies from own lab failed to detect expression at these sites (Bingle & Bingle 2000, Gally et al 2011, Liu et al 2013b, Musa et al 2012). Indeed, extensive analysis of tissues from the GI tract and renal system failed to show the protein in any of these tissues (Musa et al 2012).

1.8.2 Normal expression of BPIFA1 in the middle ear

Since, the middle ear is an extension of the URT, in a preliminary study I investigated the localisation of the protein in the middle ear cavity of adult mice (Mulay MSc thesis 2011). I observed abundant staining for BPIFA1 along the middle ear epithelium and occasionally, in the layer of Tm facing the middle ear cavity (Fig 1.7). Subsequently, a report was published showing the presence of BPIFA1 in the murine middle ear as well as its involvement in OM (Bartlett et al 2015). BPIFA1 has also been reported to be present in the middle ears of

chinchillas (McGillivary & Bakaletz 2010) and in middle ear effusion of OM patients (Preciado et al 2010, Val et al 2016).

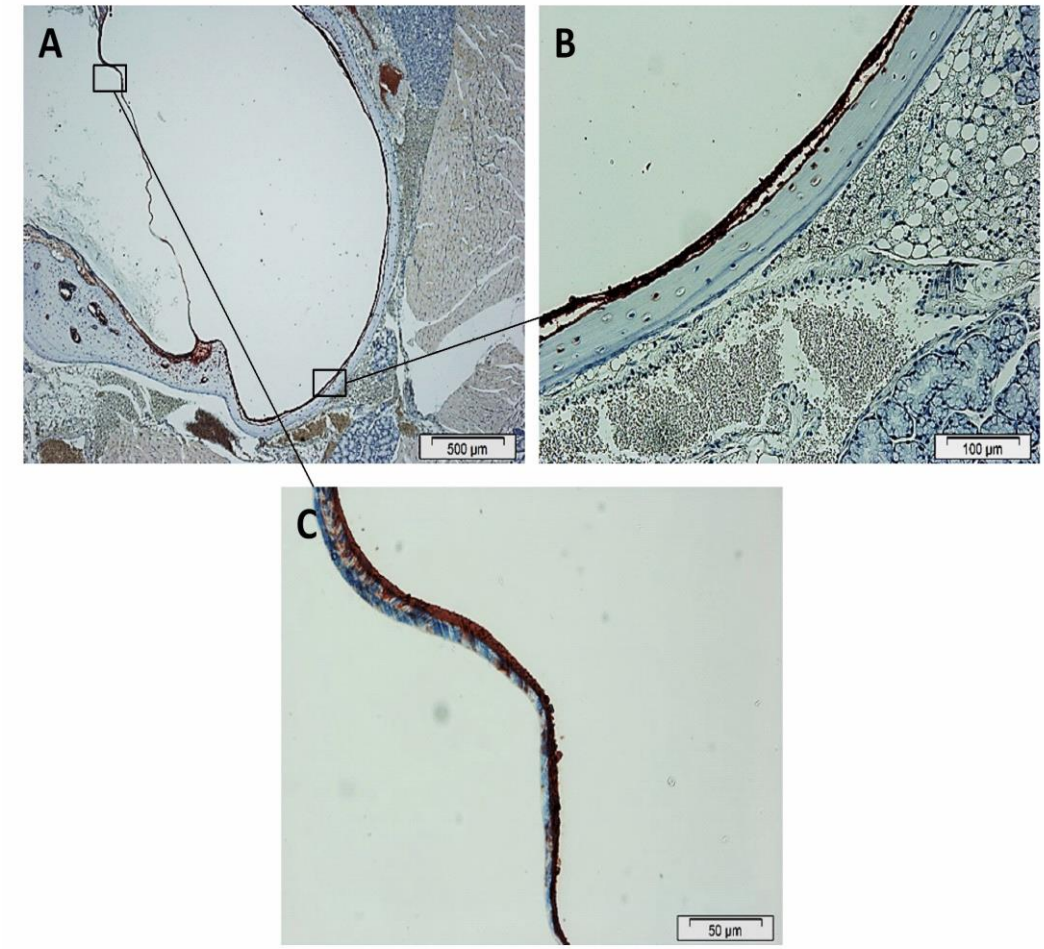

Figure 1.7 Expression of BPIFA1 in the *Wt* middle ear
Low magnification (A) and high magnification (B) images showing strong staining for BPIFA1 in the middle ear epithelium. BPIFA1 also occasionally localised to cells of the Tm towards the middle ear cavity. n=3. Image taken from (Mulay MSc thesis 2011).

1.9 BPIFA1 is a multifunctional host defence protein

BPIF genes and particularly the *BPIFA* subfamily of genes are amongst the most rapidly evolving mammalian genes and have undergone various duplication and deletion events over the course of evolution (Bingle et al 2011a). This has led to the development of a large number of orthologues and paralogues with low sequence similarities (an average of 16-28% for paralogues and 45-76% for orthologues), a feature that is typical of genes involved in host defence (Bingle & Craven 2003, Emes et al 2003). Moreover due to its structural

similarity with BPI and LBP and its expression at sites of immediate pathogen interaction, BPIFA1 has been published to be an innate immunity protein (Bingle & Craven 2004, Bingle et al 2011b). The literature suggests an antimicrobial, surfactant and immunomodulatory role for BPIFA1, as well as a role an involvement in regulation of the airway surface liquid (ASL) (Britto & Cohn 2015). However, despite an increasing number of published studies, mechanistic evidence to validate these functions has only recently started to arise. Following the solving of the crystal structure of BPIFA1, site-specific mutations in the protein have indicated that specific structural components of BPIFA1 may be responsible for specific host pathogen functions of the protein (Walton et al 2016).

1.9.1 Antimicrobial role

The most widely studied function of BPIFA1 is its antimicrobial role against Gram-negative respiratory bacteria. Both *in vitro* and *in vivo* studies have shown that BPIFA1 demonstrates an antimicrobial activity against Gram-negative bacteria such as *K. pneumoniae*, *P. aeruginosa,* NT*Hi* and more recently, *Burkholderia cepacia* (*B.cepacia*)(Ahmad et al 2016, Liu et al 2013a, Liu et al 2013b, Lukinskiene et al 2011, McGillivary & Bakaletz 2010, Sayeed et al 2013, Walton et al 2016). For example, silencing or ablation of *Bpifa1* in mice has been associated with increased susceptibility and higher pulmonary bacterial counts upon challenge with *K.pneumoniae* and *P.aeruginosa* (Liu et al 2013a, Liu et al 2013b). On the other hand, transgenic mice overexpressing BPIFA1 showed improved pulmonary bacterial clearance (Lukinskiene et al 2011). In another study, recombinant chinchilla BPIFA1 showed increased killing activity against NT*Hi* (McGillivary & Bakaletz 2010). However, some studies have suggested that BPIFA1 inhibits the growth of *P.aeruginosa* and *B.cepacia* and is thus bacteriostatic rather than bactericidal (Ahmad et al 2016, Sayeed et al 2013).

The mechanism proposed for the antimicrobial activity of BPIFA1 against Gram-negative bacteria is through binding and neutralising the endotoxin, LPS in a manner similar to BPI

(Chu et al 2010). However, the evidence regarding direct binding of BPIFA1 with LPS, is conflicting. Some groups reported binding whereas others reported either a lack of direct binding or a lack of competition with LBP (Britto & Cohn 2015, Campos et al 2004, Di 2011, Ning et al 2014, Sayeed et al 2013). However, a recent study have suggested that the α4 helix of BPIFA1 is responsible for binding to LPS and the bacteriostatic activity against *P.aeruginosa* and *B.cepacia* (Ahmad et al 2016, Walton et al 2016).

Besides, Gram-negative bacteria, BPFIA1 was also shown to inhibit growth and decrease susceptibility to pulmonary infections by the atypical bacterium, *Mycoplasma pneumoniae (M.pneumoniae*) (Chu et al 2007, Gally et al 2011) and also to inhibit replication of *Epstein-Barr* virus (Zhou et al 2008).

1.9.2 Surfactant role

Another proposed function for BPIFA1 is the ability to act as a surfactant. The surfactant role of BPIFA1 was first suggested by Gakhar and colleagues when they identified sequence homology between BPIFA1 and the equine surfactant protein, Latherin. Using *in vitro* assays they showed that BPIFA1 reduced the surface tension at the air liquid interface (ALI) and disrupted biofilm formation by *P. aeruginosa* (Gakhar et al 2010). Subsequently, two other studies demonstrated that ALI TBE cultures from *Bpifa1*$^{-/-}$ mice showed increased biofilm formation by *P. aeruginosa* and *K. pneumoniae* (Liu et al 2013a, Liu et al 2013b). Moreover, knocking down *Bpifa1 in vitro* in chinchillas led to impaired mucociliary clearance through the ET, indicating a reduction in surface tension affecting the water content in the ASL (McGillivary & Bakaletz 2010). A recently published study shows the leucine residues of the α4 helix of BPIFA1 are essential for it to function as a surfactant but not for biofilm disruption in *P. aeruginosa* and *B.cepacia* (Walton et al 2016). However, another group that studied the potential lipid ligands of BPIFA1 demonstrated that the protein binds pulmonary surfactants such as dipalmitoylphosphatidylcholine (DPPC) (Ning

et al 2014). Thus it is possible that BPIFA1 functions to sequester surfactants rather than act as a surfactant itself and thus, works in concert with other host defence components of the ASL in order to prevent fluid accumulation and to disperse bacterial biofilms.

1.9.3 Immunomodulatory role

Serum LBP (predominantly produced by the liver) binds to LPS to transfer it to Cluster of differentiation (CD)-14, in turn activating TLRs and a pro-inflammatory response whereas BPI (secreted by the neutrophils), binds to LPS at the site of infection and plays an anti-inflammatory role by making it unavailable for LBP (Weiss 2003). Due to its structural similarity with BPI and LBP, BPIFA1 was initially suggested to play either a pro-inflammatory or an anti-inflammatory role in response to pathogens (LeClair 2003).

Loss of *Bpifa1* was also associated with increased infiltration of inflammatory cells and expression of pro-inflammatory mediators compared to controls in *P.aeruginosa* and LPS induced pulmonary inflammation in mice (Di 2011, Lukinskiene et al 2011), whereas overexpression of the protein attenuated the pro-inflammatory response (Di 2011). This indicates an anti-inflammatory role for BPIFA1 in inflammation induced by Gram-negative bacteria. BPIFA1 deficient mice demonstrated higher levels of T_H2 cytokines and increased eosinophilic inflammation in an allergic model of inflammation compared to *Wt* mice. On the other hand, over expression of BPIFA1 complimented this effect, thus indicating an anti-inflammatory role for BPIFA1 in allergic inflammation (Wright et al 2010). In contrast, BPIFA1 demonstrated a pro-inflammatory function in the case of non-infectious inflammation induced by inhaled sterile carbon nanotubules. Here, transgenic mice overexpressing BPIFA1 showed increase in pulmonary neutrophil infiltration and up regulation of pro-inflammatory mediators (Di et al 2013).

1.9.4 Role in airway surface liquid regulation

The surface of the airway epithelium is lined by the ASL. ASL consists of a periciliary fluid layer which underlies the mucous layer, and consists of antimicrobial proteins such as lysozyme, proteases and protease inhibitors as well as BPIFA1 (Tarran 2004). The ASL covers cilia and adequate ASL height is essential for effective mucociliary clearance. The epithelial sodium channel, ENaC is a heterotrimer of the α, β and γ subunits and is activated by proteolytic cleavage by epithelial and inflammatory proteases leading to increased absorption of sodium and resorption of water by the epithelium (Tarran & Redinbo 2014). BPIFA1 was shown to act as a negative regulator of ENaC, thus contributing to the maintenance of ASL height (Garcia-Caballero et al 2009). The proposed mechanism for BPIFA1 mediated inhibition of ENAC function is through the extracellular binding to ENaC and prevention its cleavage by proteases (Garcia-Caballero et al 2009, Garland et al 2013, Hobbs et al 2013). A sequence of 18 amino acids (S18 peptide) at the N-terminus of BPIFA1 is responsible for ENaC binding (Hobbs et al 2013). The recent crystal structure of BPIFA1 has enabled site-specific mutagenesis studies, which demonstrated that the ENaC-regulatory motif (S18) is functionally independent of the surfactant and anti-biofilm motif (α4 helix) (Ahmad et al 2016, Walton et al 2016). It is also suggested that BPIFA1 regulates ENaC activity by maintenance of ENaC in a low opening state (Hobbs et al 2013) and reduction of ENaC expression on the epithelium (Rollins et al 2010).

Regulation of ASL volume is particularly important in pulmonary diseases such as Cystic fibrosis (CF), where dehydration of the mucosa leads to mucostasis and impaired mucociliary clearance. It has been shown that the ability of BPIFA1 to inhibit ENaC is impaired in the acidic microenvironment of CF lungs, resulting in mucosal hyper-absorption and depletion of the ASL, whereas addition of the S18 peptide increased ASL height (Garland et al 2013). Thus a loss of BPIFA1 function may contribute to CF development.

1.10 Alteration of BPIFA1 during infections and diseases of the URT

BPIFA1 is expressed at high concentrations in the steady state. *BPIFA1* is tightly regulation by both pathogens and inflammation and the direction of alteration depends upon the stimulus. For example, *Bpifa1* was reported to be down regulated in a study of acute murine pulmonary infection with *P.aeruginosa*, *Influenza A* and *S.pneumoniae* (Britto et al 2013) whereas, other studies reported an upregulation in *Bpifa1* expression upon infection with *K.pneumoniae* and *M.pneumoniae. Bpifa1* was downregulated in mice following treatment with cytokines IFNγ and in mouse tracheal epithelial cells (mTECs) upon treatment with TNFα and IL1β whereas, IL13 upregulated *Bpifa1* expression in mTECs (Britto & Cohn 2015, Britto et al 2013).

BPFIA1 is also altered in various inflammatory diseases of the URT. For example, BPIFA1 levels were reduced in subjects with perennial rhinitis and in nasal polyp tissues of patients with chronic rhinosinusitis compared to healthy controls (Irander et al 2014, Seshadri et al 2012). The expression of BPIFA1 in Chronic obstructive pulmonary disease (COPD) was variable and the studies were confounded by the relatively small number of subjects. The levels of BPIFA1 were reduced, elevated or unaffected in different studies that employed different sampling locations (Bingle et al 2007, Britto & Cohn 2015, Di et al 2003). BPIFA1 was elevated in CF lungs (Bingle et al 2007). As mentioned before, elevation in levels of BPIFA1 may serve as a defence mechanism to rehydrate the airway mucosa and assist in clearance of bacteria. However this function of BPIFA1 may be hampered due the low pH and increased proteolytic enzymes in the CF lungs (Garland et al 2013).

In addition, changes in expression levels of *BPIFA1* have also been implicated in head and neck cancers. BPIFA1 may serve as a marker for non-small cell lung carcinoma (NSCLC) (Bingle et al 2005, Vargas et al 2008). Levels of *BPIFA1* are also altered in adenocarcinoma, nasopharyngeal cancer, mucoepidermoid carcinoma, salivary gland tumours, bronchoalveolar carcinoma, etc. (Bingle & Bingle 2011).

Thus, it is evident that BPIFA1 is involved in several diseases of the URT.

1.11 Evidence for involvement of BPIFA1 in Pathogenesis of OM

As described above, BPIFA1 is highly expressed in the epithelium of the URT of both humans and mice (Bingle & Bingle 2011, Musa et al 2012) and has a proposed role in the immune defence mechanisms at these sites (Barnes et al 2008). The middle ear epithelium is a continuation of the URT epithelium and therefore the physiology of the middle ear is comparable to that of the URT. Thus, BPIFA1 may also serve as innate immunity molecule in the middle ear. OM is commonly preceded by an URT infection and is characterized by epithelial remodelling. Therefore, it can be postulated that OM is accompanied and affected by alterations in the levels of BPIFA1. Indeed, evidence regarding expression of BPIFA1 in the middle ear and its role in OM pathogenesis has started to emerge. A study in chinchillas showed that knocking down *Bpifa1 in vivo* using siRNA led to impaired mucociliary clearance, due to reduction in the surface tension of the tubotympanum, plausibly affecting the ASL water content and ion transport and thereby contributing to the pathogenesis of OM (McGillivary & Bakaletz 2010). A more compelling indication of the involvement of *BPIFA1* in OM is the Western Australian GWAS which identified *BPIFA1* gene as one of the top candidate genes associated with OM susceptibility (Rye et al 2012b). A recently published report also shows that aged *Bpifa1*$^{-/-}$ mice show increased susceptibility to OM (Bartlett et al 2015). Thus, recent literature has identified BPIFA1 as a strong determinant for predisposition to OM.

1.12 Mouse models for OM

One of the ways to better understand the pathogenesis of OM *in vivo* is to study the disease in an animal model which exhibits the OM phenotype. The mouse serves as a classic model for various human diseases. Mice can be bred in large numbers and have a

relatively short lifespan of 2 years in laboratory conditions. The sequence of the entire mouse genome is known since the Mouse Genome Consortium, 2002 and 90% of the genes are conserved between humans and mice (Waterston et al 2002). It is also comparatively easy to manipulate genes in mice. The advent of the clustered regularly interspaced short palindromic repeats (CRISPR) gene editing technology has further reduced the time required for generating mouse mutants considerably (Yin et al 2014).

The mouse is an excellent model of OM owing to significant functional and anatomical similarity between the ears of humans and mice (Brown et al 2008). Several disease susceptibility genes, thought to be involved in OM have been disrupted in mice, in an attempt to study their role in the pathogenesis of the disease. Table 1.1 gives a summary of some of the mouse models of OM. The two major approaches adopted to develop murine models of OM as follows:

- Targeted genes are disrupted to produce gene driven models
- Random mutations are induced to develop phenotype driven models (Rye et al 2011a).

Table 1.1 Mouse models of Otitis media.
This table has been adopted and modified by permission from (Rye et al 2011a), copyright Springer 2010

Gene mutated	Chromosome	phenotypic alterations	Type of OM	Reference
Tlr2	3	Immune deficiencies	AOM (induced)	(Leichtle et al 2009)
Tlr4	4	Immune deficiencies	AOM (induced)	(Hirano et al 2007)
Evi1	3	Rhinitis, presence of extra digits on both limbs	CSOM (spontaneous)	(Parkinson et al 2006)
Fbxo11	17	Bent ET, craniofacial abnormalities, deafness	COME (spontaneous)	(Hardisty et al 2003, Hardisty-Hughes et al 2006)
MyD88	9	Immune deficiencies	AOM (induced)	(Hernandez et al 2008)
Tgif	17	Craniofacial defects, placental defects	CSOM (spontaneous)	(Tateossian et al 2013)
Fas	19	Autoimmune syndrome	AOM (Induced)	(Rivkin et al 2005)
Dnahc5	15	Immotile cilia, early death	CSOM. AOM (spontaneous)	(Ibanez-Tallon et al 2002)
Cby1	15	Lack of motile cilia	CSOM (spontaneous)	(Voronina et al 2009)
Plg	17	Fibrin deposition across wide range of organs	CSOM (spontaneous)	(Eriksson et al 1995)

1.12.1 *Junbo* mouse- a model of chronic OM

This thesis utilises the *Junbo* mouse model of chronic OM.

1.12.1.1 Generation of Junbo mice

Junbo is a phenotype driven mouse model identified through a large scale N-Ethyl Nitrosourea (ENU) mutagenesis screen at the Medical Research Council (MRC), Harwell (Parkinson et al 2006). ENU is a powerful chemical mutagen that introduces random point mutations in the genome by transferring its ethyl group to the oxygen or nitrogen radicals of DNA (Noveroske et al 2000). To perform this screen, spermatogonial stem cells of *BALB/c* males were mutagenized and the mice mated with female C3H/HeH mice. Dominant phenotypes were identified by screening of generation 1 (G1) progeny, whereas recessive phenotypes were identified by screening the G3 progeny. G1 *Junbo* heterozygotes had elevated hearing thresholds. A more detailed analysis of the phenotype revealed that these mice suffer from conductive hearing loss due to development of OM (Parkinson et al 2006).

1.12.1.2 OM development in Junbo mice

The *Junbo* mouse is a model of conductive hearing loss following development of spontaneous, chronic OM. Heterozygote *Junbo* (*Evi1*$^{Jbo/+}$) mice develop OM after birth, which transforms into CSOM by post-natal day 28 (P28) in specific pathogen free conditions. *Evi1*$^{Jbo/+}$ mice also develop OM in germ free conditions by P54, indicating a genetic predisposition to OM development (Rye et al 2011a). *Evi1*$^{Jbo/+}$ middle ears are characterised by development of cellular fluid and thickening of the mucoperiosteum (Fig 1.8) (Parkinson et al 2006). Recent studies in our lab have also shown that both the mucoperiosteum and middle ear fluid of *Evi1*$^{Jbo/+}$ mice are markedly hypoxic (Fig 1.9) compared to *Wt* mice (Cheeseman et al 2011). OM development in *Evi1*$^{Jbo/+}$ mice is non-

syndromic i.e. there is an absence of phenotype outside the middle ear and no systemic immune defects (Parkinson et al 2006). Moreover, intranasal (IN) inoculation of *Evi1*$^{Jbo/+}$ mice with the otopathogen, NT*Hi* leads to high rates of middle colonisation by the bacterium (Hood et al 2016) Therefore, *Evi1*$^{Jbo/+}$ is a good model of OM development in humans.

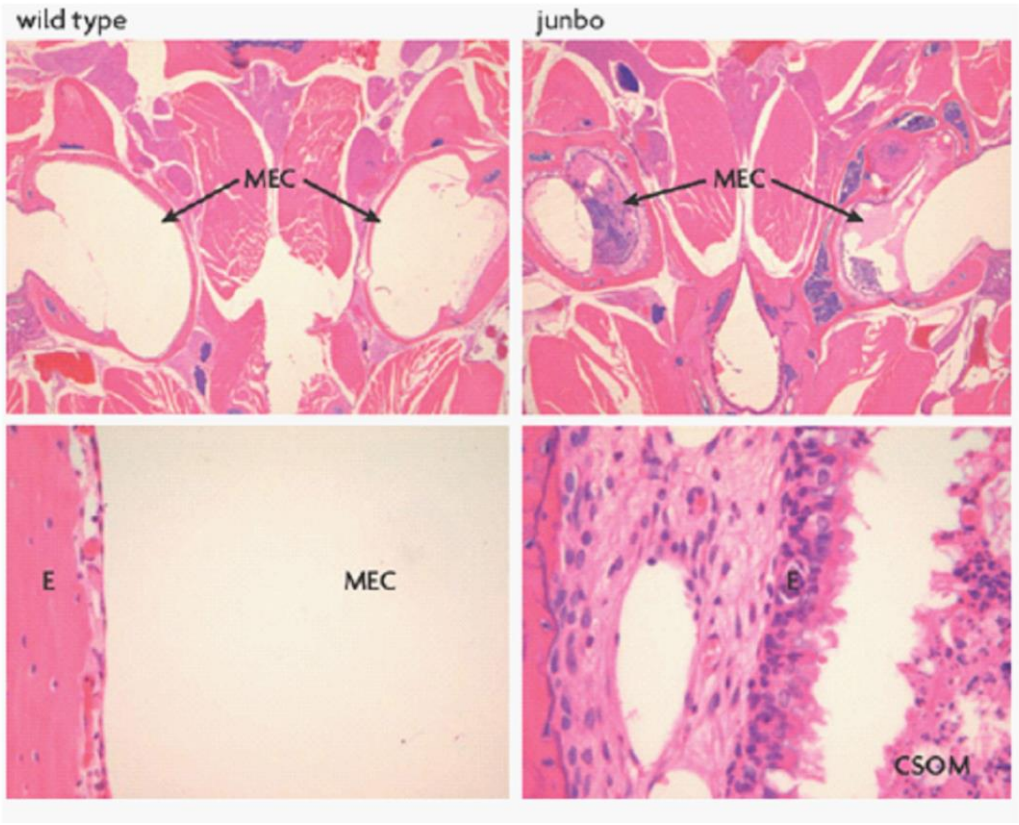

Figure 1.8 OM phenotype in *Evi1*$^{Jbo/+}$ mice
Images on the left show clear middle ear cavities (MEC) of *Wt* mice and a thin layer of the epithelium (E). *Evi1*$^{Jbo/+}$ mice (right) develop CSOM marked by build-up of inflammatory exudate in the MEC and thickening of the middle ear epithelium. Image reused with permission from (Brown et al 2008), copyright 2008 Nature publishing group

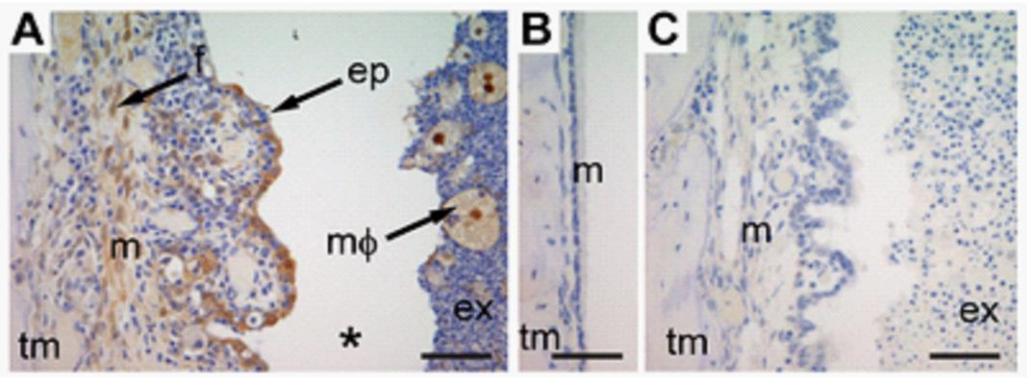

Figure 1.9 Middle ears of *Evi1*$^{Jbo/+}$ mice are hypoxic
Thickened mucosa and foamy macrophages in *Evi1*$^{Jbo/+}$ middle ears stained positive for the hypoxia marker, Pimonidazole, PIMO (A). *Wt* mice did not demonstrate mucosal thickening or hypoxia (B) Negative control for *Evi1*$^{Jbo/+}$ middle ear (C) ex: exudate, tm: temporomandibular bone; ep: epithelial cells, mφ: macrophage, m= mucosa, * histological artifact. Image reused with permission from (Cheeseman et al 2011), copyright 2011 Plos genetics.

The causative mutation in *Evi1*$^{Jbo/+}$ mice is a single nucleotide polymorphism (SNP) in the *ecotropic viral integration site-1* (*Evi1)* gene, also known as MECOM, located on chromosome 3, which encodes a 145 kDa transcription factor. Homozygote *Junbo* (*Evi1*$^{Jbo/Jbo}$*)* mutation is post-natal lethal (Parkinson et al 2006). *EVI1* plays a role in normal development and overexpression of the gene due to chromosomal rearrangements in humans is implicated in myeloid leukaemia (Goyama & Kurokawa 2010, Hirai 1999, Kurokawa et al 2000). EVI1 is made up of 2 Zinc Finger (ZnF) domains connected by a proline rich repressor domain and also consists of a C-terminus acidic region. The first ZnF domain contains 7 ZnF motifs and the second ZnF domain contains 3 ZnF motifs (Goyama & Kurokawa 2009). The first ZnF domain directly binds and regulates GATA2 promoter, a gene critically involved in proliferation of definitive haematopoietic stem cells (Yuasa et al 2005). The genes directly regulated by the second domain if EVI1 have not yet been identified. However, each domain interacts of EVI1 has been shown to interact with different co-repressors and co-activators and form larger regulatory complexes (Goyama & Kurokawa 2010). The *Evi1*$^{Jbo/+}$ mutation is in the second motif of the second ZnF domain and is three

amino acids away from a conserved contact residue. It causes an adenine to thymidine transversion, changing the 763rd amino from asparagine to isoleucine. Previous studies have shown that alterations in any of the contact residues led to total loss of the DNA binding capacity of the transcription factor. It is not known whether the *Evi1*$^{Jbo/+}$ mutation can alters the binding capacity of the first ZnF domain (Parkinson et al 2006).

The first ZnF domain of EVI1 directly binds to and inactivates SMAD3, a key signalling molecule of the TGFβ signalling pathway. Quenching of SMAD3 prevents the SMAD3/ SMAD4 complex from activating transcription of target genes and leads to inhibition of the anti-proliferative effect of the TGFβ signalling pathway (Kurokawa et al 1998a, Kurokawa et al 1998b, Sood et al 1999). In addition, the proline rich repressor domain, immediately preceding the second ZnF domain of EVI1 is involved in recruitment of C-terminal binding protein (CtBP), a co-repressor of TGFβ signalling (Izutsu et al 2001). The first ZnF domain of EVI1 also directly binds to and inactivates phosphorylated c-Jun N-terminal kinase (JNK), a subtype of mitogen-activated protein (MAP) kinases which plays a role in cellular response to environmental stress. Binding of EVI1 to JNK prevents phosphorylation of its target, c-JUN and the activation of genes involved in stress induced apoptosis (Kurokawa et al 2000). Thus, normally functional EVI1 is involved in repression of cellular hyper-proliferation and in cell survival.

The second ZnF domain of EVI1 trans-activates *cFOS* and increases activity of the transcription factor, Activator protein 1 (AP-1). AP-1 is a homodimer of cFOS or a heterodimer of cFOS/cJUN and converts extracellular signals into changes in gene expression. Changes in AP-1 activity are associated cellular proliferation and differentiation (Tanaka et al 1994). More recently, the second ZnF domain of EVI1 has also been shown to be involved in inflammation through negative feedback regulation of NFκβ signalling pathway (Xu et al 2012). This study showed that the otopathogen, NT*Hi* and the pro-inflammatory cytokine, TNFα induced expression of *EVI1*. EVI1 directly binds to the p65

subunit of transcription factor, NFκβ and inhibits its acetylation. This results in a decrease in the biological activity of NFκβ and inhibition of expression of subsequent inflammatory mediators and adhesion molecules. The study also shows that NT*Hi* infection of *Evi1*$^{Jbo/+}$ mice results in a pulmonary inflammatory phenotype. Thus, the second ZnF domain of EVI1 is involved in cellular proliferation and differentiation as well as prevention an overactive inflammatory response. Fig 1.10 summarises the biological functions of the different EVI1 domains.

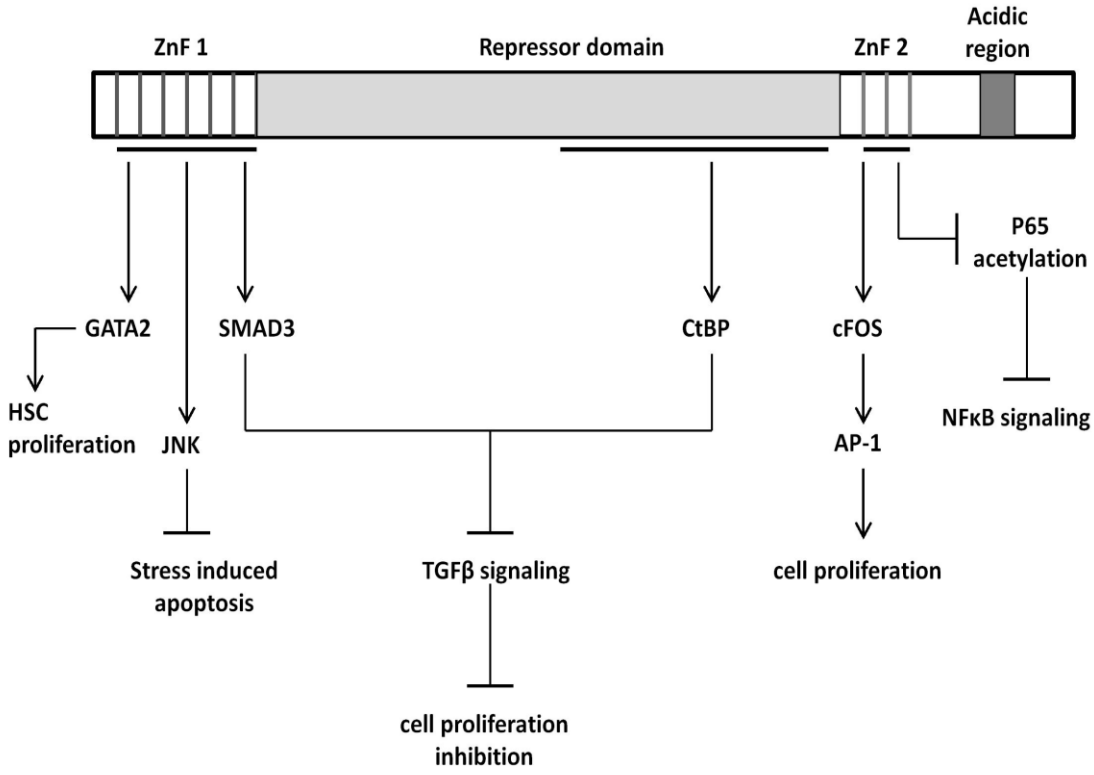

Figure 1.10 Biological functions of EVI1
The first ZnF domain of EVI1 directly binds to GATA2 promoter and activates proliferation of haematopoietic stem cells (HSCs). It is also involved in repression of the anti-proliferative properties of the TGFβ signalling pathway and inhibiting stressed induced apoptosis through the JNK pathway. The repressor domain also participates in blocking TGFβ signalling. The second domain of ZnF activates AP-1 and promotes cellular proliferation. It is also a negative regulator of the NFκβ signalling pathway. There is no known role for the acidic domain.

EVI1 is involved in control of inflammatory responses through repression of both TGFβ and NFκβ signalling pathways. These pathways interact with one another and regulate mucin production (Jono et al 2002, Jono et al 2003), a key-contributing factor to the pathophysiology of OM. Moreover, recent studies in our lab have shown that hypoxia plays an important role in the development of OM in *Evi1*$^{Jbo/+}$ mice (Cheeseman et al 2011). There is significant crosstalk between TGFβ signalling pathway and hypoxia signalling (Sanchez-Elsner et al 2001). The interaction between different pathways and their potential role of EVI1 in their regulation has been described in further detail in Chapter 5.

Polymorphisms in human *EVI1* have not been identified in OM association studies; however, the current evidence suggests that *EVI1* may be involved in OM development through an effect on regulation of mucin production as well as on cellular inflammation, proliferation and differentiation.

In this project, I chose to utilise *Evi1*$^{Jbo/+}$ mice as a model for OM because it is one of the most well characterised mouse models of non-syndromic OM i.e. these mice develop OM without any major phenotype outside the middle ear and without any systemic immune defects (Parkinson et al 2006). The network of inflammatory and hypoxia induced genes upregulated in the *Evi1*$^{Jbo/+}$ exudates (Cheeseman et al 2011) are very similar to those effusions from chronic OM patients (Mood et al, Low oxygen in OM study, unpublished). Thus *Evi1*$^{Jbo/+}$ mice closely mimic the human OM phenotype.

1.12.2 Other mouse models of Otitis media at MRC Harwell

1.12.2.1 Jeff mouse

The *Jeff* mouse was also identified through the Harwell ENU mutagenesis scheme. Heterozygote *Jeff* mice (*Fbxo11*$^{Jf/+}$) develop COME by P28 and demonstrate craniofacial abnormalities like facial contortions, a narrower and bent ET, collapsed middle ear cavity,

and cleft palate (Hardisty et al 2003). *Fbxo11*$^{Jf/Jf}$ mice have defects in eyelid, lung and palate development. The causative mutation is a SNP in the *Fbxo11* gene which encodes a member of the F-box family of proteins. Polymorphisms in human FBXO11 have been associated with human OM (Rye et al 2011b, Segade et al 2006). FBXO11 is implicated in TGFβ/SMAD signalling through its ability to regulate of phosphoSmad2 in epithelial cells of airways, palatal shelves and eyelids (Rye et al 2011b, Tateossian et al 2015)**.** Moreover, OM development in *Fbxo11*$^{Jf/+}$ middle ears is characterised by development of hypoxia, similar to *Evi1*$^{Jbo/+}$ mice (Cheeseman et al 2011, Tateossian et al 2015).

1.12.2.2 Tgif mice

The most recent mouse mutant studied at MRC Harwell was the *Tgif*$^{-/-}$ model (Tateossian et al 2013), a knockout mouse model for the *Transforming growth inhibitory factor 1 (TGIF)* gene which is a known regulator of the TGFβ signalling pathway through inhibition of SMAD2 activity (Melhuish & Wotton 2000, Seo et al 2004). *Tgif*$^{-/-}$ mice are characterised by middle ear mucosal inflammation, middle ear effusion and elevated hearing thresholds from P21. *Tgif*$^{-/-}$ middle ears also demonstrated goblet cell hyperplasia, presence of hypoxia and elevation in pro-inflammatory cytokines (Tateossian et al 2013).

The *Evi1*$^{Jbo/+}$, *Fbxo11*$^{Jf/+}$ and *Tgif*$^{-/-}$ models highlight the involvement of the TGFβ signalling pathway in OM susceptibility.

1.13 Preliminary studies from our lab showing involvement of BPIFA1 in OM development

During my Masters project, I performed preliminary experiments in order to characterise alterations in the levels of BPIFA1 during the development of OM in *Evi1*$^{Jbo/+}$ mice (Mulay MSc thesis 2011). Using IHC, I found that the intensity of BPIFA1 staining was reduced in the middle ear epithelium of *Evi1*$^{Jbo/+}$ mice compared to their age matched *Wt* littermate controls (Fig 1.11). Also, the intensity appeared to reduce with OM progression in *Evi1*$^{Jbo/+}$

mice from P21 to P56, but BPIFA1 localised to the inflammatory ear exudate in these mice (Fig 1.12).

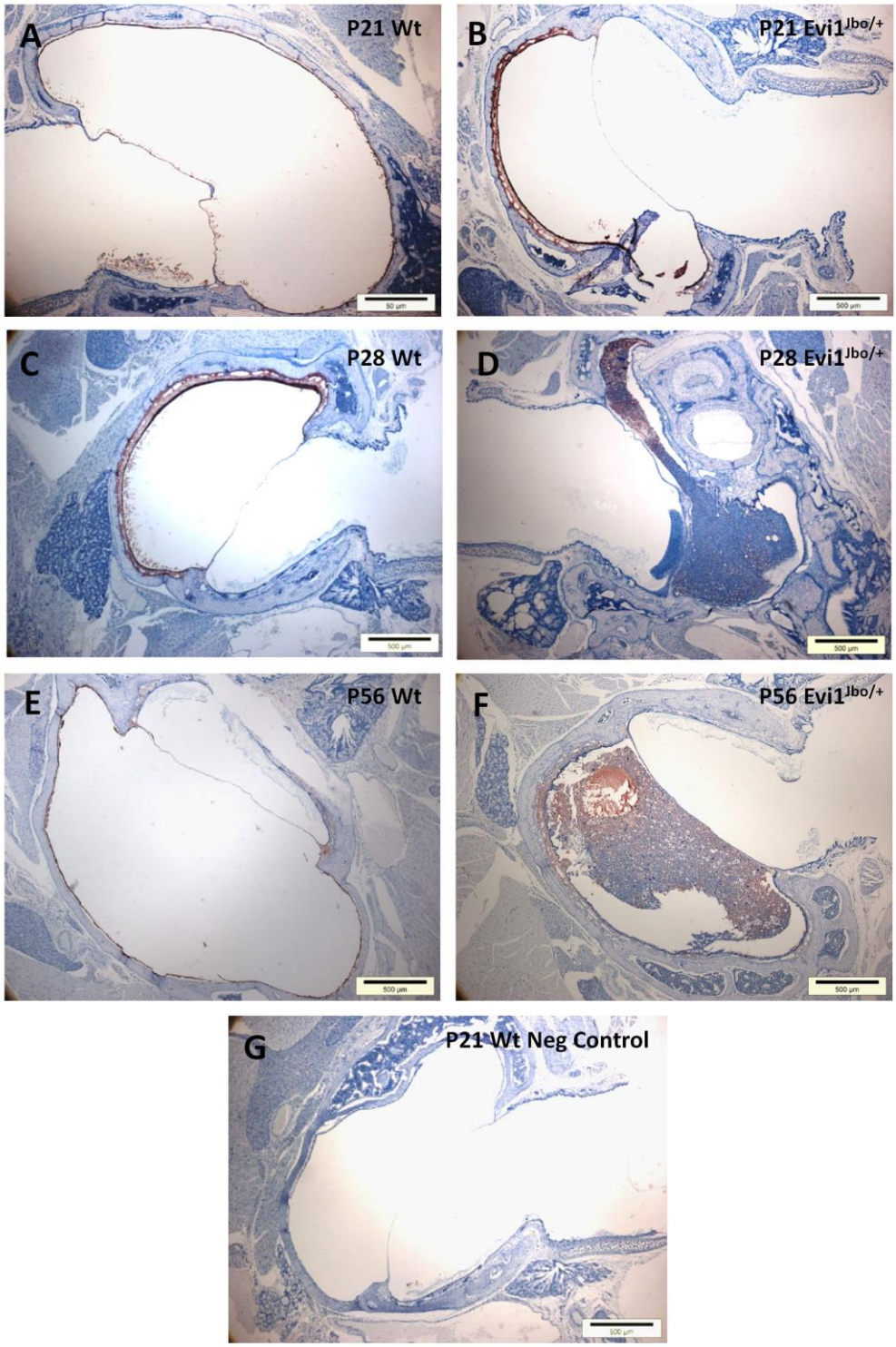

Figure 1.11 BPIFA1 staining in *Evi1*$^{Jbo/+}$ middle ears is reduced compared to Wt mice
Immunohistochemistry for P21, P28 and P56 Wt (A, C, E) and *Evi1*$^{Jbo/+}$ (B, D, F) middle ears shows lower intensity of staining in *Evi1*$^{Jbo/+}$ mice compared to age matched *Wt* mice. BPIFA1 staining also localises to the inflammatory exudates of *Evi1*$^{Jbo/+}$ mice. Wt Negative control is BPIFA1 negative (G). Scale bar 100µM. Image taken from (Mulay MSc thesis 2011).

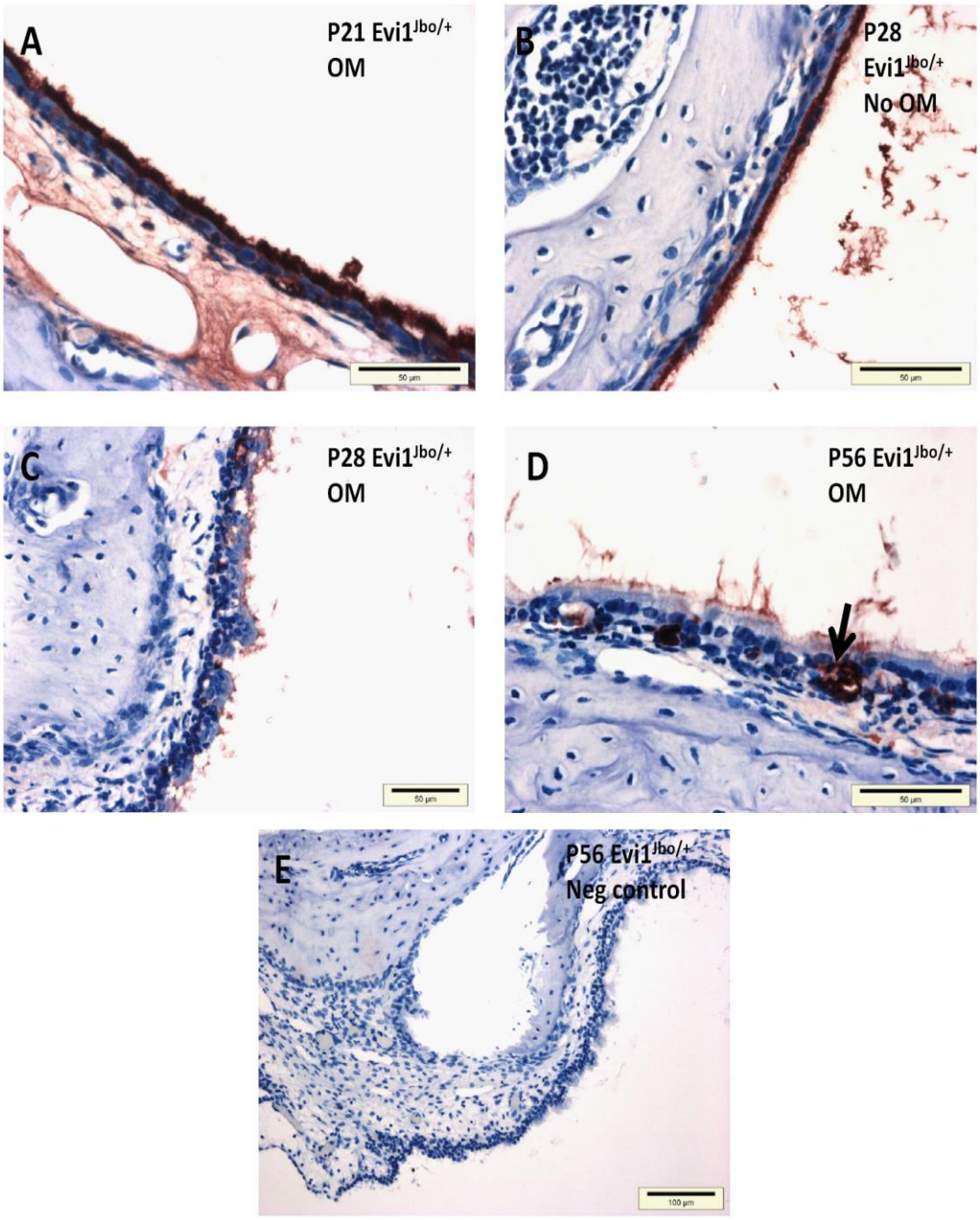

Figure 1.12 BPIFA1 staining reduces with OM progression in *Evi1*$^{Jbo/+}$ mice

Immunohistochemistry for BPIFA1 indicates intense staining in P21DAB *Evi1*$^{Jbo/+}$ mice (A) and P28 *Evi1*$^{Jbo/+}$ with unilateral OM (ear without OM, B). However staining intensity reduces in P28 *Evi1*$^{Jbo/+}$ mice with bilateral OM (C) and 56DAB *Evi1*$^{Jbo/+}$ mice with OM progression (D) Scale bar =50µM Negative control is clear of staining (E) Image taken from (Mulay MSc thesis 2011).

Using western blots, I identified abundant BPIFA1 (25kDa) in *Evi1*$^{Jbo/+}$ exudates. However, smaller bands suggested a partial degradation of the protein (Fig 1.13). These observations indicated that decrease levels of BPIFA1 or a loss of its function due to proteolytic degradation might contribute to OM pathogenesis.

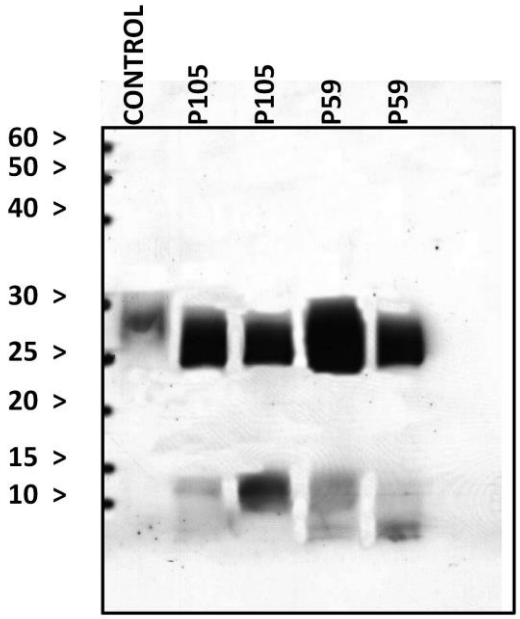

Figure 1.13 Detection of Bpifa1 in ear exudates of *Evi1*$^{Jbo/+}$ mice
Western Blots readily detected BPIFA1 in ear effusions of *Evi1*$^{Jbo/+}$ mice. Ear exudates from two different P105 and P59 animals showed presence of the full-length protein (25kDa) along partially degraded peptides. The control (BAL fluid from transgenic mice) showed presence of only the full-length proteins. Image taken from (Mulay MSc thesis 2011)

1.14 Hypothesis

BPIFA1 is one of the most abundant secretory proteins in the upper airways. It appears to possess pleiotropic roles in innate immune defence of the URT through its antimicrobial, surfactant and immunomodulatory functions as well by regulation of ASL height, thus ensuring efficient mucociliary clearance. The middle ear epithelium is a continuation of the upper airways and shares many physiological and immunological mechanisms with the URT. Otitis media is a disease with a complex pathophysiology, that is characterised by severe epithelial remodelling. SNPs in *BPIFA1* have been associated with OM. Preliminary data from my Masters project has shown that BPIFA1 is robustly expressed in middle ears of *Wt* mice and its expression decreases with OM development in the *Evi1*$^{Jbo+/-}$ mouse model of chronic OM. Based on this evidence, it can be hypothesized that BPIFA1 plays a role in the protection of the middle ear and the loss of BPIFA1 is associated with OM development.

1.15 Aims and objectives

The overall aim of this thesis was to characterize a role for BPIFA1 in the middle ear and study the effect of its loss on the development of OM as well as in middle ear infection by the human otopathogen, NT*Hi in vivo,* using mouse models and *in vitro,* using a novel system for culture of primary middle ear epithelial cells.

In order to achieve this aim *Bpifa1*$^{-/-}$ mice and *Bpifa1*$^{-/-}$*Evi1*$^{Jbo+/-}$ compound mice were generated. Also, a novel *in vitro* model of murine middle ear epithelium was developed.

More specifically, the objectives of this thesis were as follows:

1. To determine whether deletion of *Bpifa1* leads to spontaneous development of OM.
2. To determine whether deletion of *Bpifa1* causes increased carriage of the human otopathogen, NT*Hi* from the NP into the middle ear.
3. To develop a novel *in vitro* model of the murine middle ear epithelium and systematically characterise the epithelial sub-populations.
4. To utilise the *in vitro* culture system to study the effect of loss of *Bpifa1* on cellular differentiation and infection by NT*Hi.*
5. To investigate whether *Bpifa1* deletion exacerbates the OM phenotype in *Evi1*$^{Jbo+/-}$ mice.
6. To recapitulate the OM phenotype of *Evi1*$^{Jbo+/-}$ mice using the novel *in vitro* culture system.

CHAPTER 2: MATERIALS AND METHODS

2.1 Mouse lines

2.1.1 Maintenance of mouse stock

This project involves the use of 3 main mouse lines:

1) *Bpifa1*$^{-/-}$ line: Straight knockouts for *Bpifa1* wherein exons 2 and 3 of the *Bpifa1* gene have been deleted. *Bpifa1*$^{-/-}$ mice were originally obtained from University of Hawaii on a C57BL/6J background and re-derived at MRC Harwell. Generation of these mice is detailed in Section 2.1.2
2) *Evi1*$^{Jbo/+}$ line: *Junbo* heterozygotes, wherein the *Evi1* gene contains a SNP as mentioned before (Section 1.12.1). *Evi1*$^{Jbo/+}$ mice were identified through the Harwell ENU mutagenesis program and were maintained on a C3H/HeH background.
3) *Bpifa1*$^{-/-}$*Evi1*$^{Jbo/+}$ line: Compound mutants, which bear mutations both from the straight knockouts as well as Junbo heterozygotes. In order to generate compound mutants with *Evi1*$^{Jbo/+}$ mice, *Bpifa1*$^{-/-}$ mice were transferred onto the C3H/HeH background, in addition to being maintained on the original C57BL/6J background. The breeding strategy is discussed in depth in Section 2.1.3

All mice were housed in individually ventilated cages (Techniplast UK Ltd.) in specific pathogen free (SPF) conditions. Mice were fed on an irradiated diet (Special Diets Service, UK) and water containing 25-ppm chlorine. The cages were supplied with grade 6 sawdust bedding (Datesand, UK Ltd.) and maintained in a 12-hour light/dark cycle at 21°C (±2°C) and 55% (±10%) humidity. Mice were inspected daily and all animal procedures were carried out in accordance to the 'Responsibility in the Use of Animals for Medical Research (July 2003)', issued by the Medical Research Council, adhering to the procedures enlisted under the Home Office project and personal licenses.

2.1.2 Generation of transgenic mice deficient in *Bpifa1*

Bpifa1$^{-/-}$ mice were generated at University of Hawaii by Professor Ralph Shohet. These mice are unpublished A conditional targeting vector for *Bpifa1,* used for the transfection of C57BL/6J mouse embryonic stem cells was constructed by InGenious Targeting Laboratory Inc. (Ronkonkoma, NY). The targeted region on the *Bpifa1* gene includes exons 2-3 (Fig 2.1). Confirmed targeted embryonic stem cells were microinjected into BALB/c blastocysts. Resulting chimeras with a high percentage black coat colour were mated to wild-type C57BL/6J mice to generate F1 heterozygous offspring. Correctly targeted F1 mice contained a Neo-selection cassette, three lox-P sites and two FRT sites. Deletion of the Neo-cassette was achieved by breeding with a heterozygous C57BL/6J *FLP*$^{+/-}$ mouse (Jackson Lab, stock# 003800). Since these *FLP* mice are heterozygotes (homozygotes are embryonic lethal), the resulting F2 mosaic mice were screened for presence of the *FLP* transgene and deletion of the Neo cassette (Neo$^{-/-}$). After breeding with C57BL/6J mice, the resulting F3 generation was screened for absence of *FLP* transgene as well as deletion of the Neo cassette and such a mouse was bred with another heterozygous *FLP*$^{+/-}$ and *Neo*$^{-/-}$ F3 offspring to produce a homozygously floxed F4 mouse without the *FLP* transgene and without the Neo cassette (*Bpifa1*^{loxP}).

To generate a systemic, straight *Bpifa1* knockout mouse *(Bpifa1*$^{-/-}$), *Bpifa1*^{loxP} mice were mated with a mouse containing the *Cre-recombinase* transgene under the control of hCMV IE promoter (CMV-Cre, formally B6.C-Tg (Tg (CMV-cre)1Cgn/J; Jackson Lab Stock No: 006054).

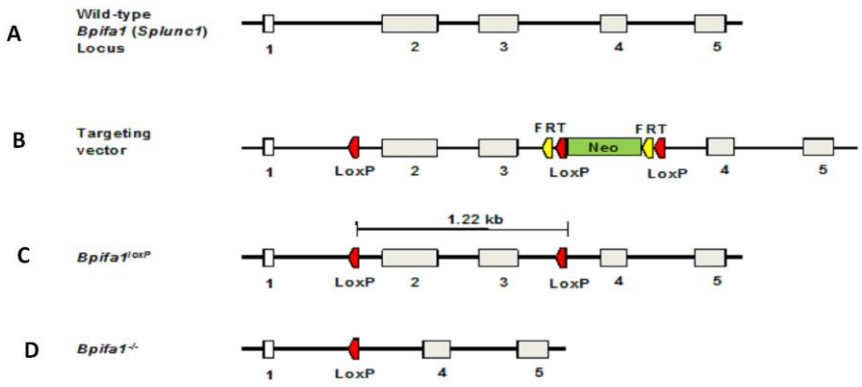

Figure 2.1(Parkinson et al 2006) Generation of *Bpifa1*$^{-/-}$ mice
The targeted region on wild type *Bpifa1* locus containing exon 2 and 3 (A) Mice were targeted with a vector containing a loxP site upstream of exon 2 and a neomycin resistance cassette flanked by a loxP site and an FRT region, downstream of exon 3 (B) *Bpifa1*^{loxP} *mice were generated through FLP-mediated deletion of the neomycin resistance cassette.* (C) Straight *Bpifa1*$^{-/-}$ mice were generated by mating the floxed mice with *C57BL/6J*$^{Cre+/-}$ mice to delete exons 2 and 3 (D).

2.1.3 Breeding strategy

Previous studies in our lab have revealed that *Evi1*$^{Jbo/+}$ mice exhibit strain variability in the severity of OM. The phenotype is most severe in C57BL/6J strain, followed by C3H/HeH and then the BALB/c strain. Due to better viability ratios on the C3H/HeH background *Evi1*$^{Jbo/+}$ have been maintained on this background (Tyrer PhD thesis 2013). Hence, in order to generate *Bpifa1*$^{-/-}$*Evi1*$^{Jbo/+}$ compound mutants, the founder C57BL/6J *Bpifa1*$^{-/-}$ mice were transferred to a C3H/HeH background. This was achieved by backcrossing *Bpifa1*$^{+/-}$ heterozygotes at each generation with wildtype (*Wt*) C3H/HeH females until generation 6 (G6), at which point their genome is estimated to be 96.9% C3H/HeH. *Bpifa1*$^{+/-}$ females were outcrossed with *Evi1*$^{Jbo/+}$ males to generate double heterozygotes in which one allele of the *Bpifa1* gene was deleted and one copy of the *Evi1* gene was mutated (*Bpifa1*$^{+/-}$ *Evi1*$^{Jbo/+}$) in a proportion of the progeny. This was because *Evi1*$^{Jbo/+}$ females have a high rate of abortion (Parkinson et al 2006). *Bpifa1*$^{+/-}$*Evi1*$^{Jbo/+}$ mice were then backcrossed with *Bpifa1*$^{+/-}$ to generate the compound mutants *Bpifa1*$^{-/-}$*Evi1*$^{Jbo/+}$ in which both alleles of *Bpifa1*

were deleted and one copy of the *Evi1* gene was mutated and other control genotypes. The breeding strategy is depicted in Figure 2.2

Backcrossing to congenicity is a lengthy process. Therefore, the initial experiments performed with *Bpifa1*$^{-/-}$ mice on a C57BL/6 background well as *Bpifa1*$^{-/-}$ mice on a mixed C57BL/6J-C3H/HeH background (intercrossed at Backcross 2). The strains are mentioned where relevant throughout the thesis.

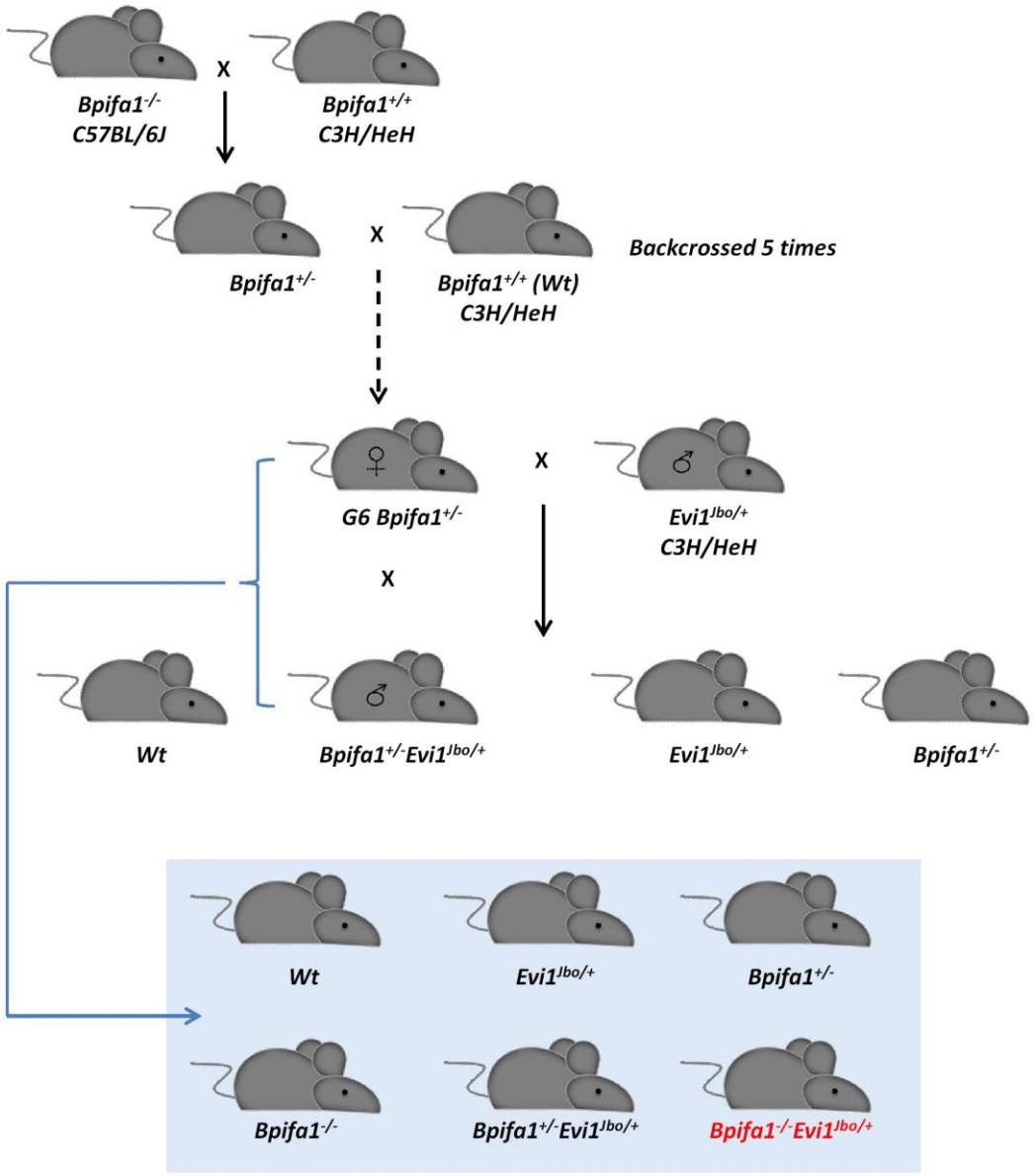

Figure 2.2 Breeding strategy for generation of compound mutants
Bpifa1$^{-/-}$ mice on a C57BL/6J re-derived at MRC Harwell were mated with *Wt* C3H/HeH mice to produce *Bpifa1*$^{+/-}$ progeny, which were repeatedly backcrossed with *Wt* C3H/HeH mice. G6 *Bpifa1*$^{+/-}$ females were mated with *Evi1*$^{Jbo/+}$ males to generate four different genotypes: *Bpifa1*$^{+/+}$*Evi1*$^{+/+}$ *(Wt), Bpifa1*$^{+/-}$*Evi1*$^{Jbo/+}$, *Evi1*$^{Jbo/+}$ and *Bpifa1*$^{+/-}$. *Bpifa1*$^{+/-}$*Evi1*$^{Jbo/+}$ males were subsequently backcrossed to *Bpifa1*$^{+/-}$ females (blue arrow) to generate the six experimental genotypes (blue box): test genotype, *Bpifa1*$^{-/-}$*Evi1*$^{Jbo/+}$ *(red)* and *the* control genotypes *Bpifa1*$^{-/-}$, *Wt, Bpifa1*$^{+/-}$*Evi1*$^{Jbo/+}$, *Evi1*$^{Jbo/+}$ and *Bpifa1*$^{+/-}$.

2.2 Genotyping

2.2.1 DNA Extraction Using Qiagen DNeasy Blood and Tissue Kit

DNA for the gel based genotyping assay was extracted using the Dneasy Blood and Tissue Kit (Qiagen). Ear biopsies were incubated overnight at 56°C in 20µL Proteinase K and 180µL buffer ATL. The following day, samples were vortexed and a mixture of 200µL Buffer AL and 200µL of absolute ethanol was added to each sample. Samples were thoroughly vortexed and centrifuged through a DNeasy mini spin column fitted in a 2ml collection tube at 8000 rpm for a minute to bind the DNA to the column. The column was transferred to a new collection tube, 500µL Buffer AW1 was added to it and centrifuged for 1 minute at 8000rpm. The column was again transferred to a new collection tube, 500µL Buffer AW2 was added to it and spun at 14,000 rpm for 3 minutes. The column was then placed into a fresh 1.5ml eppendorf and incubated with 100µL of Buffer AE for 1 minute. DNA was eluted in the flow-through by spinning the column at 8000 rpm for a minute and either used directly for gel based genotyping or stored at -20°C for long term use.

2.2.2 DNA Extraction Using Sample-to-SNP Kit

DNA for qPCR and Light scanner based genotyping assays was extracted using the TaqMan Sample-to-SNP Kit (Applied Biosystems). 50µL lysis solution from the kit was added to the ear biopsies contained in 96 well micro titre plates (one biopsy per well). Plates were sealed with transparent plastic PCR plate lids (Thermoscientific), centrifuged briefly at 2000 rpm to ensure that all samples were submerged in the solution and incubated at 95°C using G-storm thermocycler (GRI) for 3 minutes. Samples were cooled to room temperature, 50µL stabilising solution was added to each well and centrifuged briefly at 2000 rpm to give the crude lysate. 1:10 dilution of the crude lysate was used for genotyping.

2.2.3 Polymerase Chain reaction

The next step in genotyping the different lines was amplification of the extracted genomic DNA using a polymerase chain reaction (PCR). Details of the primer sequences for the gel based assay and the primer and probe sequences used for quantitative PCR (qPCR) and LightScanner assays are given in Table 2.1.

For gel-based genotyping, PCR was carried out in 96 well PCR plates (Thermoscientific) in a total volume of 10.5µL using the BioRad tetrad thermocycler and the Qiagen multiplex PCR kit master mix (Table 2.2A). For qPCR based genotyping, the reaction was carried out in a total volume of 10µL in 96 well PCR plates (Thermoscientific) using the 7500 Fast Q-PCR cycler (Applied Biosystems) and GTX Taqman master mix (Applied Biosystems) (Table 2.2B). For LightScanner based genotyping, a 10µL reaction (Idaho technologies) (Table 2.2C) was overlaid with 20µL of mineral oil (Sigma) was run in Frame Star plates (Client Life Science) using a G-Storm thermocycler (GRI). Full details of the different PCR master mix contents are given in in Tables 2.2A, B and C. Cycling conditions used for the various assays are mentioned in Table 2.3

Table 2.1 Primer sequences for gel based, LightScanner and qPCR based genotyping assays

Genotyping Assay	Primer type	Sequence 5'-3'
Agarose gel assay	Forward	CATGATGGCCTGAAAACAGA
	Reverse	CTCAGGCTTGGGTATGTGGT
LightScanner assay	Forward	ACTGTGATAGATCATTCAGCATTTC
	Reverse	CTTCAGGTGTCTGTCAAGATT
	Probe	GCTTCTCCTTGTTGTGGATGATGCG
WT qPCR assay	Forward	GGCCTGCTGGGAAAACTGA
	Reverse	GCTGCCTAGGACTTCTGTTGTTAG
	FAM labelled Probe	CGTCATCAGTTCCTCTCCTGAACAACA
KO Mutant qPCR assay	Forward	ACCGGTACCTGCAGAATTCATG
	Reverse	CTCAGGCACAGGTGATACAGA
	FAM labelled Probe	CGTTCTTCGGACGCCTCGTCAA
Internal control qPCR assay	Forward	TAGTTGGCATCCTTATGCTTCATC
	Reverse	GCCCCAGCACGACCATT
	VIC labelled Probe	CCAGCTCTCAAGTCG

Table 2.2A PCR master mix details for gel based genotyping

Gel based PCR Master mix components	Volume (µl)
Hotstart Master Mix	5
Q-Solution	2
Forward primer (10 µM)	0.5
Reverse primer (10 µM)	0.5
Nuclease free H2O	1.5
DNA (Qiagen Blood & Tissue Kit)	1

Table 2.2B PCR master mix details for qPCR based genotyping

qPCR Master mix components	Volume (µl)
GTX Taqman master mix	5
Primers Dot1L_2F (20uM)	0.225
Primers Dot1L_R (20uM)	0.225
Probe DotL_2M (5µM)	0.2
Biosearch *Wt*/ Mutant FAM Assay (Probe at 5µM & primers at 15µM each)	0.3
Nuclease free H2O	1.55
DNA (1:10 dilution of the ABI Sample-to-SNP crude lysate)	2.5

Table 2.2C PCR master mix details for LightScanner based genotyping

LightScanner PCR Master mix components	Volume (µl)
HotShot master mix	5
LC Green dye	1
Forward primer (20uM)	0.5
Reverse primer(20uM)	0.1
Probe	0.5
Nuclease free H2O	0.9
DNA (1:10 dilution of the ABI Sample-to-SNP crude lysate)	2

Table 2.3 PCR cycling conditions for genotyping of *Bpifa1*$^{-/-}$ line using gel based and qPCR assays and *Evi1*$^{Jbo/+}$ line using LightScanner assay

	Gel based assay		qPCR assay		LightScanner assay	
Step	**Temperature**	**Time**	**Temperature**	**Time**	**Temperature**	**Time**
1	95°C	15 min	95°C	20 secs	95°C	2 mins
2	94°C	1 min	95°C	30 secs	95°C	30 secs
3	60°C	1.30 min	60°C	30 sec	60°C	30 sec
4	72°C	3 min	72°C	3 min	72°C	3 min
5	72°C	10 min			95°C	30 secs
6	18°C	hold			25°C	30 secs
7					15°C	30 secs

x 40 (Gel based assay, step 2–4)

x 40 (qPCR assay, step 2–4)

x 44 (LightScanner assay, step 2–4)

2.2.4 Agarose gel based genotyping assay

To begin with, an agarose gel based genotyping assay was set up to differentiate between *Wt* and *Bpifa1*$^{+/-}$ mice during the initial backcrossing period. Post PCR, plates were briefly centrifuged and 2µl Orange-G loading dye was added to each sample. The plates were sealed and re-centrifuged to mix the dye well. 1% Agarose gel was prepared using 1 gm

Agarose powder (Sigma, UK Ltd.) in 100ml of 1% Tris- acetate- EDTA (TAE) buffer and 1mg/ml of Ethidium Bromide. 10µl of the PCR product was loaded in each well against a standard marker (100bp ladder- New England Bioloabs Ltd.). The gel was run at 150V for 30 mins and visualised using the Bio-Rad UV Illuminator and Quantity One v7-6.3 software.

The genotyping strategy was based on the principle that using a single set of primers, the *Wt* and mutant sequences yielded two different sized products on the agarose gel. The *Wt* sequence yielded a single band larger than 1kb while the *Bpifa1*$^{+/-}$ sequence showed two bands: a higher band corresponding to the Wt allele of >1kb and a lower corresponding to the mutant allele of 500bps, due to the loss of exons 2 and 3 from the sequence. An example of a gel for genotyping *Wt* and *Bpifa1*$^{+/-}$ animals is shown in Figure 2.3. A *Bpifa1*$^{-/-}$ sequence would have an expected single band at 500bps. However, the gel based assay was used in the initial stages of back crossing when no *Bpifa1*$^{-/-}$ mice had yet been generated.

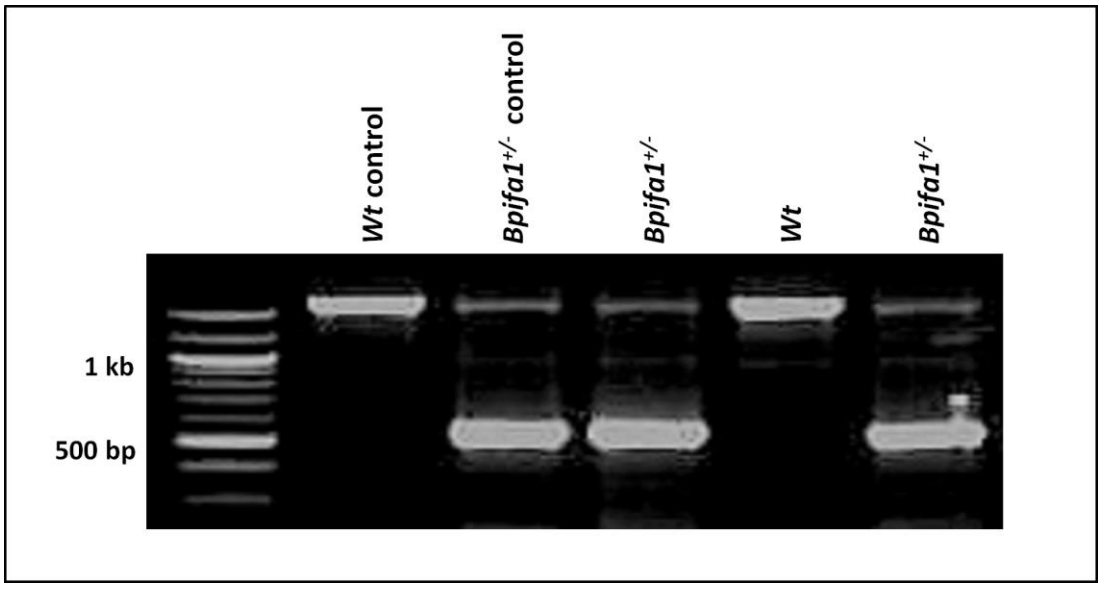

Figure 2.3: Gel based genotyping for *Wt* and *Bpifa1*$^{+/-}$ *mice*
The above image represents the results for the gel based genotyping assay used to differentiate *Bpifa1*$^{+/-}$ mice and *Wts*. A single higher band indicates a *Wt* animal whereas, a sample showing both higher and lower bands indicate a *Bpifa1*$^{+/-}$ mouse. The *Wt* control is mouse a random line *Wt* for the *Bpifa1* gene and the *Bpifa1*$^{+/-}$ control is the G1 mouse from the cross between the founder *Bpifa1*$^{-/-}$ male and a *Wt* female.

2.2.5 Quantitative PCR based genotyping

In order to facilitate genotyping of a large number of ear biopsies in a single run, the genotyping of the *Bpifa1*$^{-/-}$ line was transferred to a qPCR system. The qPCR assay was designed with the help of Adele Austin in the Genotyping Core facility (GEMS) at MRC Harwell. qPCR is a modification of the standard PCR method to continually monitor the progression of the reaction. It employs the use of a TaqMan probe complementary to a sequence between the forward and reverse primers. The probe is attached with a fluorescent reporter at its 5' end and a quencher at its 3' end. As long as they remain in close association, the emitted fluorescence is quenched. As the forward primer extends and reaches the probe, the reporter is cleaved and moves away from the quencher and the emitted fluorescence is detected and quantified by the qPCR software. The CT value of the product (the number of cycles required to reach a set threshold) is indicative of and inversely correlated to the amount of template DNA present in the sample. The CT value can also be used to determine the number of copies of a particular allele present in a sample.

Two separate assays were designed for the *Wt* and mutant *Bpifa1* sequence and each sample was run twice, once with the *Wt* assay and once with the mutant assay, thus allowing reconfirmation of the genotype. A representative graph showing the results from a genotyping experiment analysed using the ABI copy-caller software is shown in Figure 2.4. The *Bpifa1*$^{-/-}$ samples showed two copies of the mutant allele while the *Wt* samples showed two copies of the *Wt* allele. *Bpifa1*$^{+/-}$ samples demonstrated a copy number of one for both the *Wt* and the mutant sequence. A *Wt* copy number of 2 corresponded with a mutant copy number of 0 and vice-versa thus validating the results.

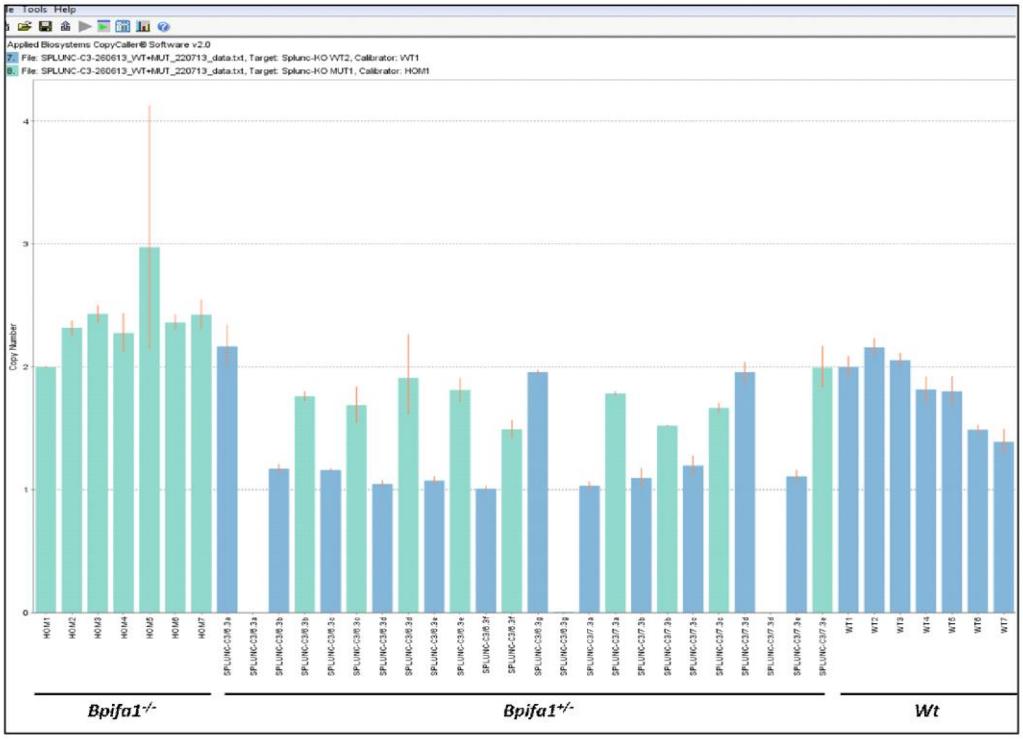

Figure 2.4: qPCR genotyping for the *Bpifa1*$^{-/-}$ line
The figure is an example of a qPCR assay performed for genotyping the *Bpifa1*$^{-/-}$ line. Each sample was run twice, once for the *Wt* assay and once for the mutant assay and the results for the two assays are shown adjacently for each sample. Green bars with a copy number of 2 denote *Bpifa1*$^{-/-}$ mice whereas the blue bars with a copy number of 2 denote *Wts*. For each *Bpifa1*$^{-/-}$ sample, the *Wt* copy number is 0 and vice-versa. *Bpifa1*$^{+/-}$ mice are denoted by 1 copy of both the *Wt* and the mutant allele.

2.2.6 LightScanner genotyping

A LightScanner assay was used for genotyping of the *Evi1*$^{Jbo/+}$ line and was developed by Deen Quwailid, GEMS core at MRC Harwell. Post PCR, the plates were centrifuged for 3 minutes at 1700 xg and analysed using the LightScanner HR/96 (Idaho Technology) along with the LightScanner Call-It software v2.0. This genotyping strategy exploits the variability in the melting temperatures of different DNA sequences to differentiate between various amplicons. The LC green dye in the master mix binds to the double stranded PCR product. During the final hybridisation step, this double stranded DNA is heated causing melting of the DNA and consequent release of the fluorescent dye which is detected by the system.

The method also uses a small probe that spans the SNP in the *Evi1*$^{Jbo/+}$ mutation. In the mutant allele (*Evi1*$^{Jbo/\ Jbo}$), the probe perfectly anneals to the SNP and emits the most fluorescence and does so at a higher temperature. The *Wt* allele has a mismatch between the probe and its complimentary DNA strand and thus emits less fluorescence. The melting profile for *Evi1*$^{Jbo/+}$ is intermediate between the two. This method was used to differentiate between *Wts* and *Evi1*$^{Jbo/+}$ mice *(Evi1*$^{Jbo/Jbo}$ mice are post-natal lethal*).* An example of the genotyping results is shown in Figure 2.5

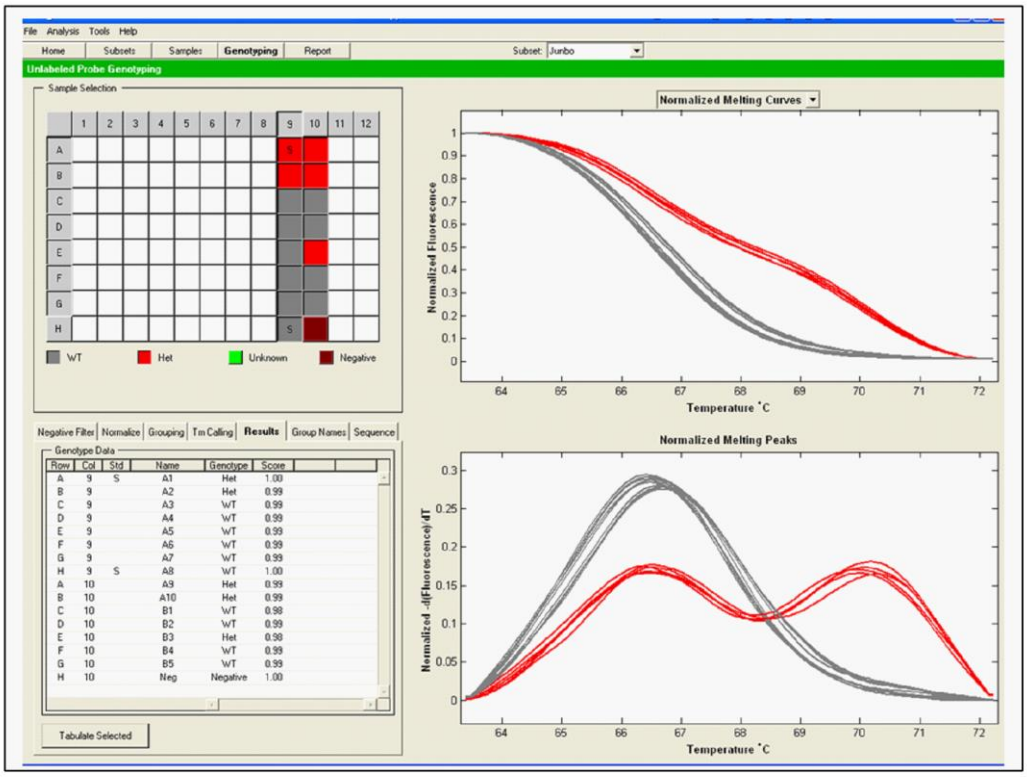

Figure 2.5: LightScanner genotyping for the *Evi1*$^{Jbo/+}$ line
The figure shows LightScanner analysis results for genotyping of the *Evi1*$^{Jbo/+}$ line. The melt profile for the *Wt* DNA strands is denoted in grey and that for the *Evi1*$^{Jbo/+}$ DNA strands is denoted in red. For genotyping the *Bpifa1*$^{-/-}$*Evi1*$^{Jbo/+}$ line, each DNA sample was analysed for the *Bpifa1*$^{-/-}$ allele using the qPCR assay and the *Evi1*$^{Jbo/+}$ allele using the LightScanner assay.

2.3 Auditory Brainstem response

Determination of Auditory Brainstem Response (ABR) thresholds is routinely used as a phenotypic test for identification of hearing loss in mice. In this study, the Click evoked ABR method was used in which a broad-spectrum sound of progressively reducing intensities from 70 decibels (dB) to 5 dB in decrements of 5 dB is played to the mouse's ear. Animals were weighed and intra-peritoneally injected with 1ml Ketamine (Ketaset®, Fort Dodge Animal Health) and 0.5 ml Xylazine (Sedaxylan®, Ceva Animal Health) in 8.5 ml sterile water (Dechra Veterinary products), at a dose of 0.1ml/10gm body weight using a 25-gauge syringe (Scientific Laboratory Supplies) and placed in a hot box at 35°C till deeply anaesthetised. Mice were then transferred onto a hot mat in a sound proof booth and a generous amount of Viscotears (Novartis AG) was applied to their eyes to avoid dehydration. Three electrodes were positioned sub-dermally in the following order: (a) The ground electrode behind the right mastoid (b) The reference (-) electrode at the midline or the cranial vertex and (c) the positive electrode behind the left mastoid. A sound emitting speaker was positioned 1.5 cm away from the pinna, directly facing the auditory canal. The booth was closed and a click stimulus was generated by TDT SigGen RP Software (TDT system III). The auditory response was recorded and analysed using the Intelligent Hearing Systems Opti amp 8002 software. The normal hearing response appears in the form of a graph trace with 5 peaks, each one indicating a different region of the auditory circuit. A typical ABR graph trace is shown in Figure 2.6. On completion of the test, mice were recovered in the hot box by subcutaneous administration of 0.1 ml/10gm body weight of the antidote, containing 0.1 ml Atipamezole hydrochloride (Antisedan, Pfizer Animal Health) in 9.9ml water. After full recovery the mice were returned to their home cages. For terminal ABRs, mice were culled according to Schedule 1 of the Home Office guidelines post ABR measurements and sent for histological analysis.

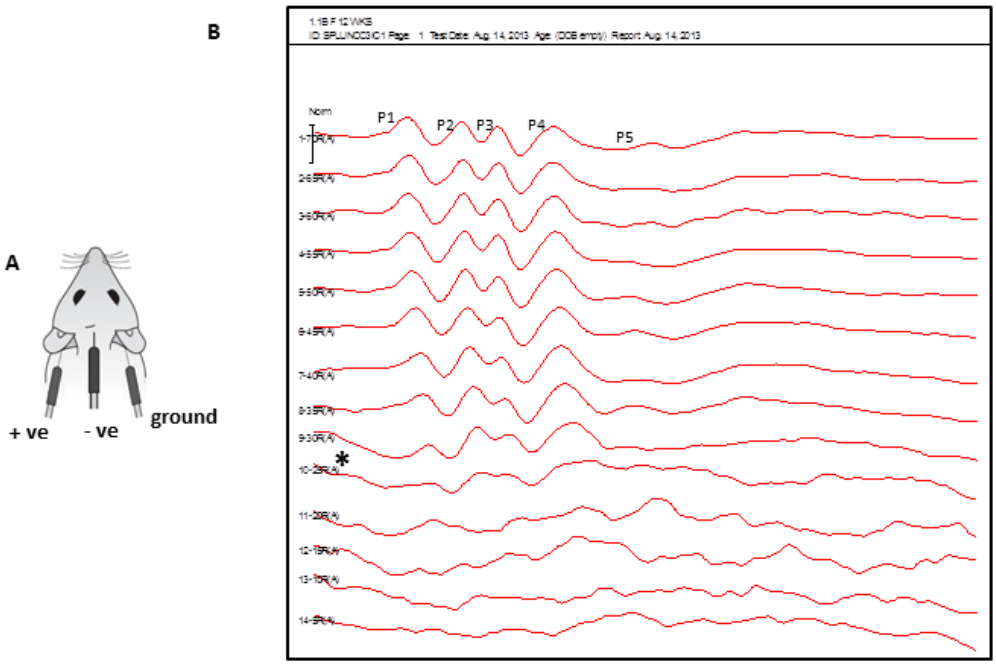

Figure 2.6: Auditory brainstem response measurement
The figure shows the measurement of ABR thresholds in mice. Sub dermal placement of electrodes – adapted from MLC standard operating procedure 1219 (A) A representative click-evoked ABR graph trace from a wild type mouse showing the 5 auditory peaks (P1- P5). Hearing threshold for the mouse was detected at 25dB (asterisk), which is the minimum intensity for which a reproducible graph trace can be obtained (B).

2.4 Histology

All samples unless otherwise mentioned were processed, embedded, sectioned and H&E stained by the necropsy and histology teams at MRC Harwell.

2.4.1 Decalcification, paraffin embedding and sectioning

Mice were culled by intraperitoneal overdose of sodium pentobarbital (Pentoject Animalcare, UK). Samples were fixed in 10% paraformaldehyde (Surgipath Europe) for 48 hours at room temperature and decalcified in Kristenson D.F.B agent (Pioneer Scientific) for 72 hours. Using the Shandon Pathcentre machine (Thermoscientific), samples were dehydrated through increasing concentrations of ethanol (70, 90 and 100%), cleared in Xylene and embedded in liquid paraffin wax and left to set. The paraffin blocks were cut

into 4µm transverse sections on the Finesse™ ME+ microtome (Thermoscientific), floated onto clean water to remove creases at 50°C and transferred to charged slides (Thermoscientific).

2.4.2 Haematoxylin and eosin staining

At least one paraffin embedded sections from each mouse was placed on Shandon Varistain 24 (Thermoscientific) for haematoxylin and eosin (H&E) staining. Sections were deparaffinised with Sub-X (a substitute for xylene), rehydrated through 100% and 70% isopropanol (Fischer Scientific) and rinsed under running water. The slides were then stained for 6 minutes with Haematoxylin (Shandon Gill 3, Thermo Scientific) which stains basophilic structures such as nuclei and differentiated in acid alcohol (hydrochloric acid diluted to 1% in 70% industrial methyl spirit) to clear background staining . Sections were then submerged in 1% lithium carbonate (Fischer Scientific), which makes nuclei appear blue and counter-stained for 3 minutes with Eosin (Thermoscientific) which stains eosinophilic structures such as the cytoplasm pink. The slides were rinsed briefly under running tap water between each step. Sections were finally dehydrated in 70% and 100% isopropanol and mounted with Clearium (Surgipath Europe). H&E stained sections were scanned using the NanoZoomer Digital Pathology system.

Bullae samples before and after pronase treatment were embedded, sectioned and H&E stained by the Histology core facility in the School of Clinical Dentistry at University of Sheffield.

2.5 Histological analysis of H&E sections

I accessed the scanned H&E stained sections of middle ears at Sheffield using Scan-srv NDP NanoZoomer software (Hamamatsu). Thickness of the middle ear mucosa was measured in

a defined 1mm area in the promontory region opposite the tympanic membrane. Average mucosal thickness was calculated using 5 measurements taken at a distance of 250 µM within this region.

Analysis of H&E slides of the tissue sections from the complete histology screen of *Bpifa1*$^{-/-}$ mice at 6 months of age was performed by Professor Michael Cheeseman at the Roslin Institute, Edinburgh. A total of 42 target tissues were analysed for morphological abnormalities.

2.6 Immunohistochemistry

2.6.1 Blocking and antigen retrieval

Tissue sections were deparaffinised and dewaxed by two 5 minute changes in 100% Xylene (Sigma) and rehydrated through 100% and 95% Ethanol (Fischer Scientific). Endogenous peroxidase activity was blocked with 0.3 % H_2O_2. Methanol (Fischer Scientific) for 20 minutes. High temperature antigen retrieval was performed for all primary antibodies except anti-BPIFA1 by microwaving the sections in 0.01M tribasic Sodium citrate (Sigma) for 8 minutes. This allows unmasking of antigens by breaking the methylene bridges or co-ordinate calcium bonds that are formed between some antigen peptides during the fixation process. Non-specific binding of secondary antibodies was blocked by incubating the sections in 100% normal serum from the animal used to raise the secondary antibody for 30 minutes at room temperature.

2.6.2 Detection and analysis

Sections were washed in PBS for 5 minutes and incubated overnight with the appropriate primary antibody in serum in a humified chamber at 4°C. Details of the antibodies used for Immunohistochemistry (IHC) are given in Table 2.4**.** For negative controls, no primary

antibody was added. The following day, sections were incubated in 0.5% biotinylated secondary antibody from the Vectastain® Elite® ABC kit for 30 minutes at room temperature. This was followed by incubation with the AB Complex (ABC) reagent for 30 minutes and brief incubation with NovaRed mixture from the VECTOR NovaRed kit (SK 4800) for colour development. Sections were washed twice in PBS for 5 minutes between each step. The ABC reagent is a pre-formed complex of the homotertramer, avidin and biotinylated horse radish peroxidase enzyme. The AB complex binds to the biotin of the secondary antibody. HRP oxidizes a chromogen in presence of H_2O_2, both of which are components of the NovaRed kit to form a dark red colour. Details for preparation of ABC reagent and Novared mixture are given in **Appendix I**. Sections were counterstained on the Leica ST4020 autostainer using Harris' haematoxylin (Thermoscientific), differentiated in acid alcohol, treated with Scott's tap water to change the colour of the nuclei to blue, dehydrated in 95 % to absolute ethanol and cleared in Xylene (Leica, Cat No- ST 4020). Sections were mounted using Di-N-Butyl Phthalate in Xylene (DPX, Leica Biosystems) and visualized and imaged using a light microscope (Olympus BX61) for analysis.

Table 2.4: Antibodies used for Immunohistochemistry (IHC)

Primary Antibody	Type	Dilution	Manufacturer
Anti- BPIFA1	Rabbit polyclonal	1:750	Prepared in lab (Musa et al 2012)
Anti- Lactotransferrin	Rabbit antisera	1:500	Milipore (07- 685)
Anti- αSMA	Rabbit polyclonal	1:200	Abcam (5694)

NB: IHC for comparison of protein expression between *Wt, Bpifa1*$^{-/-}$, *Evi1*$^{Jbo/+}$ and *Bpifa1*$^{-/-}$*Evi1*$^{Jbo/+}$ middle ears was performed by Catherine Russell, an undergraduate placement student in the lab

2.7 Collagen staining

Picrosirius red stain kit (Polysciences Inc) was used to chemically stain collagen I and III fibres in middle ear sections tissue sections. Picrosirius Red Stain binds to collagen fibrils of varying diameter. The kit contains 3 solutions: A (phosphomolybdic acid), B (Picrosirius red stain) and C (1N hydrochloric acid). Briefly, tissue sections were deparaffinised and dewaxed by two 5 minute changes in 100% Xylene (Sigma) and rehydrated through 100% and 95% Ethanol as mentioned in Section 2.6.1. 500µL of Weigert's haematoxylin (details in Appendix I) was added and the sections were stained for 8 minutes. Sections were briefly rinsed in distilled water and placed in solution A from the kit for 2 minutes. Sections were rinsed again with distilled water and stained with solution B for 60 minutes, followed by solution C for 2 minutes. Sections were placed in 70% ethanol for 45 seconds, dehydrated in 95 % to absolute ethanol, cleared in Xylene, mounted using DPX and visualised under Olympus BX61 light microscope as mentioned in Section 2.6.2.

2.8 Cell culture

2.8.1 Primary culture of mouse nasal and middle ear epithelial cells

I performed all cell culture work and subsequent treatments on cultured cells at University of Sheffield. The dissection of mouse nasal cavities, nasal septae and middle ears is detailed in Figure 2.7.

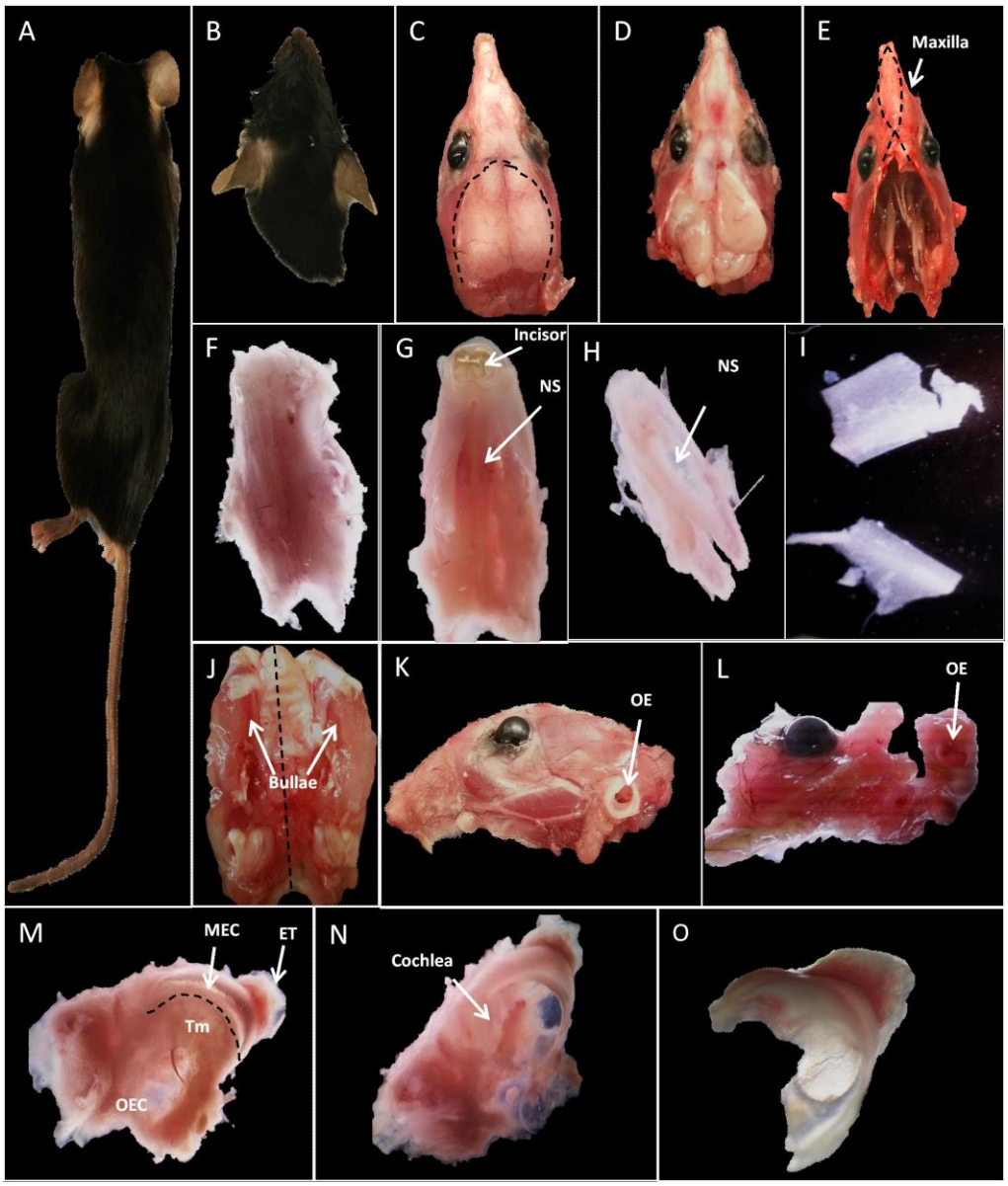

Figure 2.7 Dissection of mouse nasal cavity, nasal septum and middle ear cavity
Wild type C57BL/6J or C3HeH mice **(A)** were decapitated **(B).** The head was skinned **(C)** and skullcap removed **(D).** Dorsal view of the head after removing the brain. The nasal cavity was dissected along the dotted lines to separate it from the lateral maxillary walls **(E).** Dorsal **(F)** and ventral **(G)** view of the harvested nasal cavity, showing the nasal septum, NS. Under dissecting microscope, the nasal cavity was cleaned from the surrounding tissue **(H)**. The nasal septum was gripped and separated from the dorsal nasal bone **(I)**. Ventral aspect of the remaining head, after dissecting out the nasal cavity showing the bullae or middle ear cavities, MECs **(J).** Bisected head showing the outer ear, OE **(K).** Under dissecting microscope, the bullae were separated from surrounding tissue **(L).** The MEC is attached to the outer ear cavity, OEC, at the tympanic membrane, Tm and tapers towards the opening of the Eustachian tube, ET near its posterior end **(M)**. Removal of the OEC and the Tm along the dotted lines reveals the cochlea of the inner ear on the ventral side of the MEC **(N)** The cup shaped MEC was detached from the inner ear **(O)**

2.8.1.1 Harvesting of nasal cavities and nasal septae

Mice were euthanized by terminal intra-peritoneal injection of 100µL pentobarbital (50mg/ml, Henry Schein®) and exsanguinated by cutting the inferior vana cava. The method for dissection of nasal cavities and the nasal septum was adopted from (Woodworth et al 2007) and is shown in Figures (2.7A- 2.7I). Under direct visualization, mice were decapitated; the skin at the nape of the neck was incised, bisected anteriorly and removed entirely to expose the bony surface of the skull and the nose. The mandible was detached with a pair of blunt scissors. The head was placed under a dissecting microscope (Olympus SZx10), with the nares facing away and the skullcap was gently opened with a pair of fine forceps and the brain was removed. Removal of the brain exposes the anterior most part of the skull base, which is attached to the posterior most part of the nasal cavity (Figure 2.7E). In order to obtain entire nasal cavities, a pair of fine dissecting scissors was inserted at this boundary and nasal cavity was incised out bilaterally, along the dotted line (Figure 2.7E) to separate it from the lateral maxillary walls and the tip of the nose was severed (Figure 2.7F). The nasal cavity was inverted (Figure 2.7G); remnants of the upper palate were removed and any extraneous tissue and hairs were cleaned.

Inversion of the dissected nasal cavity enables clear visualization of the nasal septum (Figure 2.7H). Individual septae were harvested by grasping them with bent forceps, close to the floor of the nasal cavities to carefully pull them away from the nasal ridge bones (Figure 2.7I).

2.8.1.2 Harvesting of middle ear cavities

All initial steps including euthanisation of mice till the removal of brain from the skull cavity were performed as mentioned in section Section 2.8.1.1. The heads were then bisected at the midline (Figure 2.7J) and each half was oriented with the opening of the opening of the

ear facing upwards (Figure 2.7K) under a dissecting microscope (Olympus SZx10). Any muscle, soft tissue and remnant hair surrounding the ear were removed using fine dissecting scissors and forceps, leaving the middle ear cavity (bulla), still attached to the outer ear canal and the inner ear (IE; Figure 2.7L). The bony shell of the bulla was further cleaned free of any attached extraneous tissue. The Outer ear canal, which appears a shade lighter than the middle ear cavity, was gently broken away from the bulla using stork bill forceps (Figure 2.7M). The Tm and the ossicles usually detach from the bulla along with the outer ear canal. Alternatively, they were physically removed using fine stork bill forceps. Lastly, the cup-shaped bulla was carefully lifted away from the inner ear (Figure 2.7N and 2.7O).

2.8.1.3 Isolation of epithelial cells from the harvested tissue

The protocol for isolation, culture and differentiation of mouse middle ear epithelial cells (mMECs) and nasal epithelial cells (mNECs) was adapted from a method for isolation of mouse tracheal epithelial cells (mTECs) (You & Brody 2013, You et al 2002). For each batch of cells, harvested tissue (nasal cavities, nasal septae or bullae) from approximately six mice were pooled in a tube containing pronase (1.5 mg/ml) in *'mMEC basic media'*: DMEM/F-12 HAMs media (Life Technology) supplemented with penicillin (100 µg /ml) and streptomycin (100 µg/ml) (Life Technology) and subjected to overnight proteolysis at 4°C. The next day, the pronase was neutralised by the addition of 10% foetal bovine serum (FBS) and the samples were gently agitated by inverting the tube 25 times. The samples were then transferred to 2ml of fresh *mMEC basic 10% FBS media*, the tube was inverted again 25 times and this process was repeated 3 times. The combined proteolytic and mechanical actions led to dissociation of the epithelial cells from the tissue **(Figure 2.8).** Media from the three tubes was combined and centrifuged at 500 xg for 10 minutes at

10°C. The pelleted cells were re-suspended in 1ml of media containing 1 mg/ml bovine serum albumin (BSA) and 0.5 mg/ml DNase I (Sigma-Aldrich). Cell viability and number were assessed using trypan blue staining and a haemocytometer. Cells were centrifuged at 500 xg for 5 minutes at 10°C and the pellets re-suspended in 5ml of *mMEC basic 10% FBS media*. In order to remove contaminating fibroblasts from epithelial cells, a differential adherence step was performed by plating the cells on 60mm surface treated tissue culture dishes (Nunclon®, Sigma-Aldrich) at 37^0C in a 5% CO2 incubator for 3-4 hours. Fibroblasts attached to the plastic whilst the non-adherent epithelial cells were collected, centrifuged at 500g for 5 minutes at 10°C and re-suspended in 1ml of '*mMEC plus' media*: mMEC basic media supplemented with 5% FBS, 30 µg/ml bovine pituitary extract (Life Technology), 10 µg/ml of insulin (Sigma-Aldrich), 25 ng/ml of mouse epidermal growth factor (BD Biosciences), 5 µg/ml of transferrin (Sigma-Aldrich), 0.1 µg/ml of cholera toxin (Sigma-Aldrich) and 0.01 µM of freshly added retinoic acid (Sigma-Aldrich).

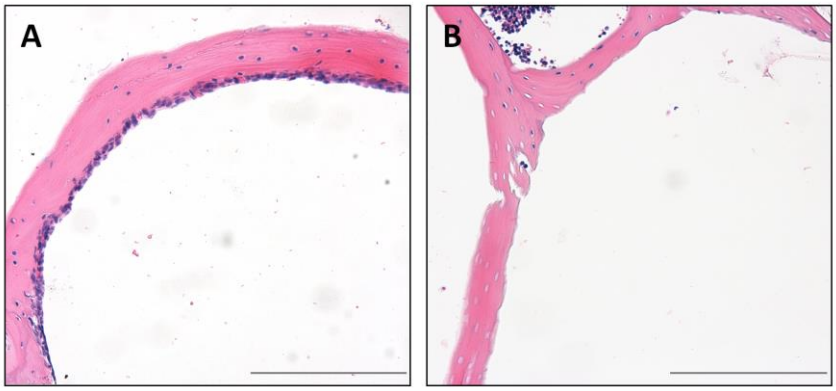

Figure 2.8 Effect of pronase treatment on middle ear epithelial cells
Haematoxylin and eosin staining of dissected middle ear cavities showing intact middle ear epithelium before proteolytic treatment with pronase **(A)** and loss of the epithelial lining after treatment with pronase and mechanical agitation **(B)** during the cell isolation process suggesting that our isolation protocol successfully dissociates middle ear epithelial cells for culture. Scale bar = 200 µm

2.8.1.4 Optimisation of culture conditions

For determination of optimal culture conditions for the growth of mMECs and mNECs and formation of a confluent monolayer, cells were plated on either tissue culture plastic (2.5 x 10^4cells/well) or sterile, 0.4µm pore sized transparent PET (Polyethylene Terephthalate) membranes coated with 150µL (50µg/ml) of rat-tail collagen type I (BD Biosciences) in a 24-well supported transwell format (Falcon) 1. On transwells, mMECs were seeded at an initial density of 1 x 10^4 and 2 x 10^4 cells/well in the presence or absence of 10 µM of Rho Kinase inhibitor Y-27632 dihydrochloride (ROCKi, Tocris bioscience) and 5 x 10^4 cells/well without ROCKi. mNECs obtained from whole nasal cavities were seeded at an initial density of 5 x 10^4 and 1 x 10^5 and 2 x 10^5 without ROCKi and at 3 x 10^4 cells/well with ROCKi. mNECs isolated from nasal septae were seeded at 5 x 10^4 cells/well without ROCKi.

The total number of cells obtained from the nasal septum was very low. Hence, all batches of mNECs described in this thesis were isolated from whole nasal cavities. A seeding density of 1 x 10^4 cells/well with ROCKi for mMECs and 3 x 10^4 cells/well with ROCKi for mNECs, both grown on transwell membranes was identified as optimum and therefore used for culturing all subsequent batches of cells.

2.8.1.5 Air liquid interface culture of mouse middle ear and nasal epithelial cells

mMEC and mNEC cells were plated on collagen coated transwell membranes placed in 24 well plates. Cells were initially cultured, submerged, in '*mMEC plus-proliferation media*' with 300 µL of media in the top chamber and 700 µL in the bottom chamber. Media was changed every 48 hours, until the cells were completely confluent, whereafter media from the top chamber was removed and media in the bottom chamber was replaced with *'mMEC SF- differentiation media'*: DMEM/F-12HAMs media supplemented with 1 mg/ml BSA (Life Technology), 5 µg/ml insulin, 30 µg/ml bovine pituitary extract, 5 µg/ml transferrin, 5 ng/ml mouse epidermal growth factor, 0.025 µg/ml cholera toxin and freshly

added 0.01 µM retinoic acid. This system of culture, with media in the bottom culture and apical surfaces of cells exposed to air is known as ALI (Air liquid interface) culture and it promotes maximal differentiation of cells by mimicking the *in vivo* physiology. Cells were grown at ALI for 14 days. Media was changed and apical surfaces of cells were washed with 200µL of sterile, warm HBSS every 48 hours to clear any cellular secretions and mucous deposition. Cells were lysed in 250 µL of Trizol reagent (Sigma- Aldrich) for RNA extraction and apical washes were collected in 200 µL of sterile HBSS at ALI Day 0 (submerged Day 10), Day 3, Day 7 and Day 14. **Figure 2.9** gives a brief summary of the cell culture system.

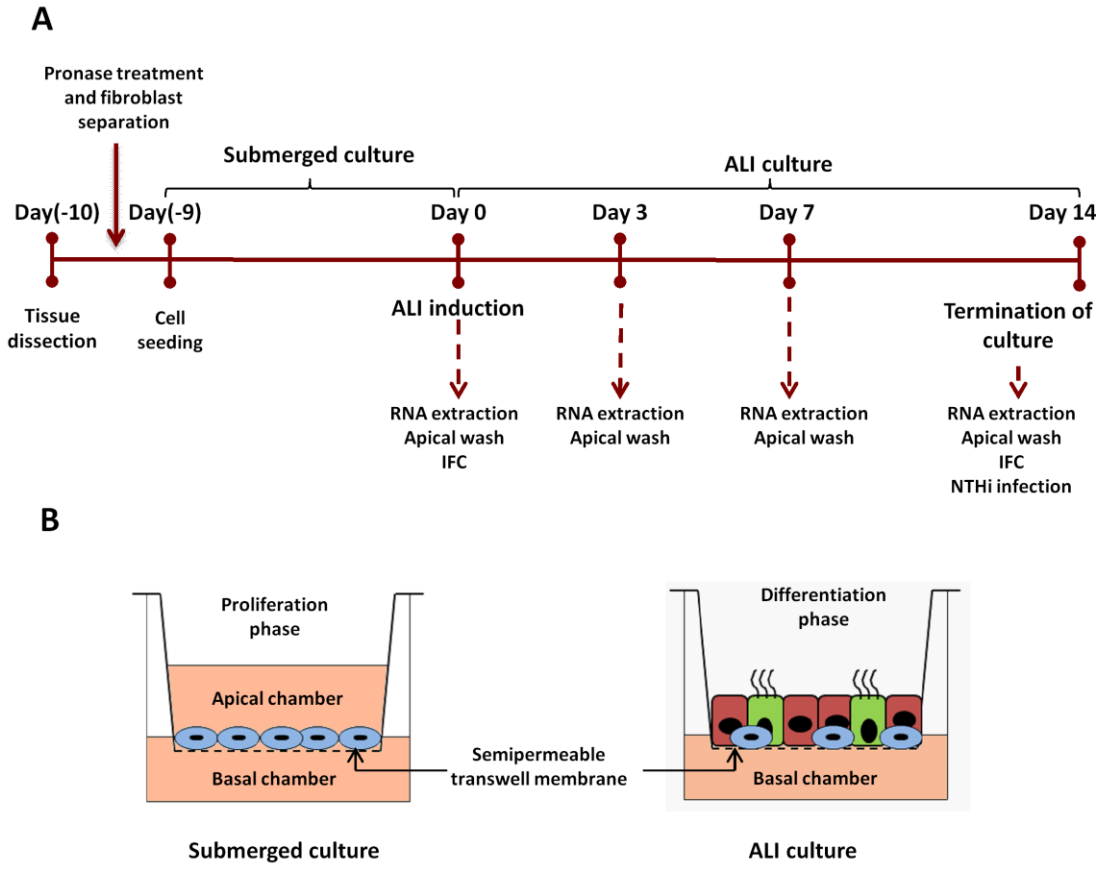

Figure 2.9 Timeline and method for ALI culture of mMEC and mNEC cells
Timeline for culture of mMECs and mNECs is shown above. Bullae were dissected, treated with pronase for dissociation of the middle ear epithelial cells and fibroblasts excluded from culture by differential adherence to plastic. ALI was induced upon confluence. Samples for transcriptional and proteomic analysis were collected at regular time points (A). Establishment of air liquid interface (ALI) cultures. Cells were initially grown in submerged culture on 0.4µM semipermeable transwell membranes up to confluence in a proliferation medium. Most cells are undifferentiated basal cells at this point (blue). At confluence, basal chamber is replenished with a differentiation medium and apical surface of cells is exposed to air. This promotes differentiation into ciliated cells (green) and various secretory cell types (red) (B)

2.8.2 Fibroblast culture

The principle of separation of fibroblasts from mMEC and mNEC cells using the differential adherence is explained in Section 2.8.1.3. Fibroblasts have higher affinity to plastic than epithelial cells and were separated by incubating the mixed population of epithelial cells plus fibroblasts on 60mm plastic petri dishes for 3-4 hours and collecting the non-adherant epithelial cells. Adherent fibroblasts were cultured by adding 5 ml of *mMEC basic 10% FBS media* to the tissue culture dish and incubating at 37^0C in a 5% CO2 incubator till confluent. Upon confluence, cells were washed with warm HBSS and sub cultured twice to obtain a pure fibroblast population. For passage 3, 3mls of Trypsin-EDTA solution (Sigma) was added to the dish and incubated in the incubator for a minute to dislodge the cells. Trypsin was neutralised by addition of 3ml neutralising medium (*mMEC basic 10% FBS*) and cells were centrifuged at 500 xg for 5 minutes. Cell pellets were resuspend in 5mls of fresh *mMEC basic 10% FBS* and split into 5 T25 flaks for expansion of the fibroblast cultures. 4 ml of media was added to each flask and cells were cultured 37^0C in a 5% CO2 till confluence. Confluent fibroblasts from 3 flasks were lysed in 250 µL TRI reagent each for RNA extraction.

2.8.3 Freezing down fibroblasts

Fibroblasts from the remaining two T25 flasks were dislodged by trypsinisation, pelleted at 500 xg for 5 minutes and resuspend in 1 ml of *mMEC plus* media +10% DMSO in cryovials. Cells were frozen at -80^0C overnight and then transferred to liquid nitrogen.

2.9 Calculation of population doubling time for mMECs and middle ear fibroblasts

For calculation of population doubling time (PD), mMECs were seeded at 5 x 10^4 cells/well in *mMEC- Plus media* without ROCKi in submerged culture. Middle ear fibroblasts were seeded at 5 x 10^4 cells/well in *mMEC basic 10% FBS media* in tissue culture grade 6 well plastic plates (Falcon). Media was changed every 48 hours. mMECs were harvested every 48 hours by trypsinisation and quantified using a haemocytometer from day 2 to day 10. Fibroblasts were harvested every 24 hours from days 1-3.

Population doubling time was determined using the formula:

$$PD = \frac{T\ X\ Log\ 2}{Log\ C2 - Log\ C1}$$

Where, PD = Population doubling, T= time (24 hours for fibroblasts and 48 hours for mMECs), Log =Log_{10}, C1 = initial cell count, C2 = final cell count].

2.10 Fluorescence Immunocytochemistry

Fluorescence Immunocytochemistry (IFC) was used for the localisation of proteins produced by mMECs and mNECs. Transwell membranes at ALI Day 0 and Day 14 were fixed with 10% phosphate buffered formalin at 37^0C for 30 minutes. Cells were permeabilised using 0.5% Triton X-100. Non-specific binding of the secondary antibodies was blocked using 10% normal serum from the animal used to raise the secondary antibody for 1 hour at 80rpm on an orbital shaker at room temperature. The membranes were washed 3 times with PBS for 5 minutes at 150 rpm and incubated with the appropriate primary antibody overnight at 4°C at 80rpm on the shaker. Details of the primary antibodies used are given in Table 2.5. For negative controls, no primary antibody was added. The following day, membranes were washed as previously described and bound primary antibodies detected using 1:200 dilutions of the appropriate fluorophore-tagged secondary antibody: 568 Goat anti-rabbit antibody or 488 Goat anti-mouse antibody (Alexa Fluor) and incubated for 1 hour at 80 rpm at room temperature in the dark. Excess antibody was removed by washing

the membrane 3 times in PBS. The membranes were carefully detached from the transwell support using a fine scalpel and placed on a glass microscope slide with the cells facing upwards. Nuclei were counterstained using Vectashield DAPI mounting medium (Vector laboratories) and the cells visualised and imaged using an Olympus Fluoview 1000 Confocal microscope.

Table 2.5 Antibody details for IFC

Primary Antibody	Type	Dilution	Manufacturer
Anti- BPIFA1	Rabbit polyclonal	1:200	Prepared in lab (Musa et al 2012)
Anti- FOXJ1	Mouse monoclonal	1:300	Affymetrix eBioscience (2A5)
Anti- MUC5B	Rabbit polyclonal	1:200	Santa Cruz Biotechnology (H-300)
Anti- P63	Mouse monoclonal	1:100	Santa Cruz Biotechnology (4A4)
Anti- Lactotransferrin	Rabbit antisera	1:200	Milipore (07- 685)
Anti- REG3γ	Rabbit polyclonal	1:200	Kindly provided by Professor Lora Hooper (Cash et al 2006)
Anti ZO-1	Rabbit polyclonal	1:100	Life Technologies (40-2200)

2.11 Quantification of intracellular localization of epithelial proteins

ALI Day 14 mMEC membranes immunostained for BPIFA1, FoxJ1 and MUC5B as mentioned in Section 2.10 were visualized using the Olympus Fluoview 1000 Confocal microscope. 8 – 10 adjacent fields at 20x magnification, spanning one half of the membrane were imaged. Z stacks were analysed and merged using Photoshop elements editor 8 to obtain a single image. The amount of protein expression in each field was quantified by measuring the mean integrated fluorescence using Image J software. The percentage of cells expressing a specific protein was quantified using Image J as follows:

$$\frac{number\ of\ cells\ expressing\ protein\ of\ interest}{Total\ number\ of\ cells\ stained\ by\ DAPI} X100$$

The amount of BPIFA1 expression post bacterial infection was quantified at 60x magnification by measuring the mean integrated intensity of 5 fields per membrane using Image J software. Three individual batches were analysed for all quantification.

2.12 Electron Microscopy

All post fixation processing for both scanning electron microscopy (SEM) and transmission electron microscopy (TEM) and imaging for TEM were performed by Dr Christopher Jill in the Department of Biomedical Science, University of Sheffield.

2.12.1 Sample preparation and fixation

For SEM and TEM of mMEC ALI cultures, media was removed from the bottom chamber of the transwells. Cells were washed 3 times with 200µl of warm sterile HBSS (Gibco) and the transwell membranes were transferred to a fresh 24 well plate. Membranes were immediately fixed by adding 3% Glutaraldehyde in 0.1M Sodium Cacodylate buffer to the top chamber and incubated overnight at 4°C. Following day, membranes were washed 2 times with 0.1M Cacodylate buffer for 5 minutes each and detached from their transwell support as mentioned before Section 2.10.

For SEM of native middle ear epithelium, whole bullae were dissected as mention in Section 2.8.1.2. Bullae were rinsed in in sterile HBSS and immediately fixed overnight in 3% Glutaraldehyde in 0.1M Sodium Cacodylate buffer at 4°C. The following day, bullae were washed in buffer as mentioned above.

2.12.2 Scanning electron microscopy

Samples were post fixed in 2% aqueous Osmium tetroxide for 2 hour at room temperature, washed 2 times with 0.1M Cacodylate buffer for 5 minutes each. Samples were then dehydrated by passing through a series of ethanols of increasing strength (75%, 95%, 100% and 100%) for 15 minutes each and then dried twice for 15 mins at room temperature in 100% ethanol over anhydrous Copper sulphate. Samples were placed in a 1:1 mixture of Hexamethyldisilazane (HEX) and absolute ethanol for 20 minutes before being finally

transferred to 100% HEX for 20 minutes and air dried overnight, in a fume hood. Samples were mounted onto a pin-stub using Leit-C sticky tabs and coated with gold using the Edwards sputter coater and examined using a Philips XL-20 SEM at 15kV operating voltage.

2.12.3 Transmission electron microscopy

Samples were post fixed in 2% Osmium Tetroxide, washed briefly in water and dehydrated through a graded series of ethanols as mentioned in Section 2.12.2. Samples were then cleared in two changes of Epoxypropane (EPP) for 15 minutes and infiltrated in 1:1 mixture of araldite resin and EPP overnight on a rotating mixture at room temperature. This mixture was replaced in two changes with full strength araldite resin over an 8 hour period, embedded in fresh resin and cured at 60°C in an oven for 48-72 hours. Ultrathin sections of the embedded samples (approximately 85nm thick) were cut on a Leica UC6 ultra-microtome onto 200 mesh copper grids, stained for 30 minutes with saturated aqueous Uranyl Acetate followed by Reynold's Lead Citrate for 5 minutes. Sections were examined using a FEI Tecnai Transmission Electron Microscope at an accelerating voltage of 80Kv. Electron micrographs were recorded using a Gatan Orius 1000 digital camera and Digital Micrograph.

2.13 Non Typeable Haemophilus influenzae challenge experiments

All *in vivo* challenge experiments with the human otopathogen, NT*Hi* were performed at MRC Harwell and all *in vitro* NT*Hi* challenge experiments on mMEC ALI cultures were performed at University of Sheffield.

2.13.1 NT*Hi* strains

For *in vivo* intranasal and baro-inoculation of mice, genomically sequenced, streptomycin resistant strains of (NT*Hi*) #162 (NT*Hi 162*^{SR}) and NT*Hi* #375 (NT*Hi375*^{SR}) were used. Both NT*Hi* #162 and #375 are clinical isolates from a Finnish pneumococcal vaccine study on children undergoing tympanocentesis during the year 1994-95 (Cody et al 2003). For NT*Hi* infection of mMECs, a GFP tagged strain of NT*Hi375*^{SR} (NT*Hi 375*$^{SR\text{-}GFP}$) was used. All streptomycin resistant strains were generated and supplied by Dr. Derek Hood, MRC Harwell.

2.13.2 Preparation of bacterial inoculums

For *in vivo* experiments, bacteria were grown from glycerol stocks on brain heart infusion (BHI) agar plates supplemented with Levinthals (LEV) and streptomycin sulphate (Melford Laboratories) (BHI-LEV). For *in vitro* experiments, bacteria were streaked onto BHI plates supplemented with 2µg/ml Nicotinamide adenine dinucleotide hydrate (NAD, Sigma Aldrich), 2µg/ml hemin (Sigma Aldrich) and 200µg/ml streptomycin sulphate (Melford Laboratories) (BHI-NAD-Hm). Plates were incubated at 37°C, 5% CO_2 overnight. The following day, a few colonies were transferred into BHI-LEV or BHI-NAD-Hm broth and incubated for 3 hr at 37°C, 5% CO_2, at 250 rpm. An optical density (OD_{490}) of 1ml liquid culture was spectrophotometrically determined (Jenway 6300) and calibrated against 1 ml of uninoculated broth. 1ml of the culture was centrifuged at 13,000 rpm for 2 minutes and resuspended in required volume of PBS to give an inoculum containing $1x10^{10}$ bacteria/ml, by using the equation (OD_{490}/0.4) x 2 $x10^9$. For *in vivo NTHi* challenge experiments, the PBS was supplemented with 1% gelatin to increase the viscosity of the inoculum. Purity and colony forming units (CFU)/ml of bacteria were checked by plating the inoculum on BHI-LEV or BHI-NAD-Hm plates before and after infection to ensure that bacteria remained viable through the infection process.

2.13.3 Intranasal inoculation of mice with NT*Hi*

Mice were removed from their home cage and placed into a gas anaesthetic chamber containing isoflurane. The isoflurane flow rate was set at 2.5- 3 litres/ min and oxygen flow rate at 2 litres/min. Once deeply anaesthetised, mice were removed from the chamber and 5µl of inoculum ($1x10^{10}$ CFU/ml) was placed into each nostril using a pipette tip, thus inoculating each mouse with a total of $1x10^{8}$ bacteria. Animals were returned to their cage to recover. Mice are obligate nose breathers, hence the inoculum entered their nasal passages as they sniffed during the recovery process.

2.13.4 Baro-inoculation of mice

2.13.4.1 Baro-inoculation pilot study

Baro-inoclutaion is a modification of the intranasal inoculation protocol in which mice are inoculated under the effect of increased pressure. In theory, this serves to open the ET and improves the efficiency of bacterial ascension from the nasopharynx into the middle ear cavity. The protocol was adapted from previously published studies in mice (Stol et al 2009) and rats (Tonnaer et al 2003). Since this was the first baro-inoculation experiment conducted at MRC Harwell, a pilot study was performed as proof of principle before inoculating mice with NT*Hi.* A pressure chamber was developed at the Scientific Workshop at MRC, Harwell. 2 *Wt* mice were anaesthetized and intranasally inoculated with 10µl of 0.1% Evans blue dye in 1% Methyl cellulose-PBS solution in manner similar to Section 2.13.3 and then placed in the pressure chamber on a cardboard bed on their backs and the lid was secured tightly. The entire process took about 30 secs. Immediately, the pressure in the baro-inoculation chamber was raised to approximately 1.4 pounds per square inch (Psi) by puffing air in through the inlet. Thereafter, the pressure was increased by approximately 0.7 PSI every 15 secs, such that a maximum pressure of 5.8 Psi was achieved by the end of 2 minutes. The pressure in the chamber was then decreased by puffing air out at an

interval of 30 secs to return it to atmospheric pressure. The mice were closely observed for 30 minutes to identify any adverse effects of the procedure, after which they sacrificed and their middle ears, nasal passages and lungs were analysed for traces of the blue dye. The middle ears and nasal passages were rinsed 3 times with 2µl PBS to recover any dye. This solution was diluted to 1 ml and its absorbance was compared with 1ml of 0.1% solution of the dye, to quantitate the amount of dye entering the MECs of mice. Even though the maximum translocation of the dye from the nasopharynx to the middle ear was found to be 0.3-0.9%, this ratio was deemed to be sufficient to cause colonisation of the middle ear with the routinely used live bacterial inoculum of $1x10^{10}$ CFU/ml. Hence, based on this pilot study Ethical Review Process (ERP) approval was obtained to carry out baro-inoculation with NT*Hi.*

2.13.4.2 Baroinoculation with NTHi

After receiving the ERP approval, mice were anaesthetised with isoflurane as mentioned in Section 2.13.3**.** Following this, mice were baroinocluated with 5 µl of $1x10^{10}$ CFU/ml NT*Hi* into each nostril in accordance to method described in 2.13.4.1**.** Animals were returned to their home cage after completion of the procedure.

2.13.5 Determination of NT*Hi* colonization of middle ears

At specific time points, intranasally or baroinoculated mice were sacrificed using an intraperitoneal overdose of Sodium pentobarbital. Mice were decapitated, their heads were skinned and mandibles detached. Their ears were examined under a dissecting microscope (Leica M50) to determine the appearance of the Tm. Clear ears without fluid have a transparent tympanum, where the malleus is easily visible whereas fluid filled ears have a cloudy tympanum where the malleus is not clearly visible. Previous studies in our lab have shown that clear ears rinsed with PBS do not culture positive for NT*Hi* and

therefore no clear ears were plated. Cloudy TMs were gently pierced and the ossicles were removed with fine forceps. 0.5µl of ear fluid was collected and added to 500 µl of sterile PBS, at a time. Each fluid containing bulla was collected as a separate sample. Samples were thoroughly vortexed to obtain a homogenous solution and then the sample was diluted 10-fold twice. 50µl of the dilutions were plated on streptomycin containing BHI-LEV plates. Plates were incubated overnight at 37°C, 5% CO_2. Following day, plates were examined for NT*Hi* growth and the number of colonies was counted. The presence of NT*Hi* was confirmed by examining wet mounts of representative colonies in PBS by phase contrast microscopy at 100x magnification using an oil immersion lens.

2.13.6 NT*Hi* infection of mMEC cultures *in vitro*

mMECs were cultured in antibiotic free *mMEC-SF* media for 48 hours prior to infection. The number of mMECs at ALI Day 14 was determined by trypsining the membrane and counting the cells on a haemocytometer (n=3*).* NT*Hi*$^{375SR\text{-}GFP}$ inoculum was prepared as mentioned in 2.13.2**.** An appropriate amount of the bacterial inoculum in antibiotic free *mMEC-SF* media was added to the apical chamber of ALI Day 14 mMEC cultures such that the membranes were infected at a multiplicity of infection (MOI) of 1:100 and 1:1000 (mMECs: bacteria). An equal volume of sterile PBS was added instead of the bacterial cultures to generate MOCK infected controls. The membranes were incubated at 37°C, 5% CO_2 for 1 hr and washed 3 times with sterile HBSS to remove non-adherent bacteria. Media was replaced in the basal chamber and the cultures were incubated at 37°C, 5% CO_2 for 4, 24, 48 and 72 hours post infection (hpi). At the desired time points, apical washes were collected in 200µl sterile HBSS, cells were lysed in Trizol reagent for gene expression studies and membranes were fixed for IFC as previously described.

2.13.7 Determination of infection of mMECs by NT*Hi*

Two approaches were utilised for determination and quantification of infection of mMECs by NT*Hi.*

2.13.7.1 Quantification of infection using IFC

ALI Day 14 mMEC membranes infected with NT*Hi*$^{375SR\text{-}GFP}$ for 24, 48 and 72 hpi at MOI 100 and MOI 1000 were visualized using the Olympus Fluoview 1000 Confocal microscope along with their MOCK infected controls. Four central fields on every membrane were imaged at 10x magnification at each time point to define a constant area for quantification. The amount of infection in this area was quantified by measuring the mean integrated intensity for green using Image J software.

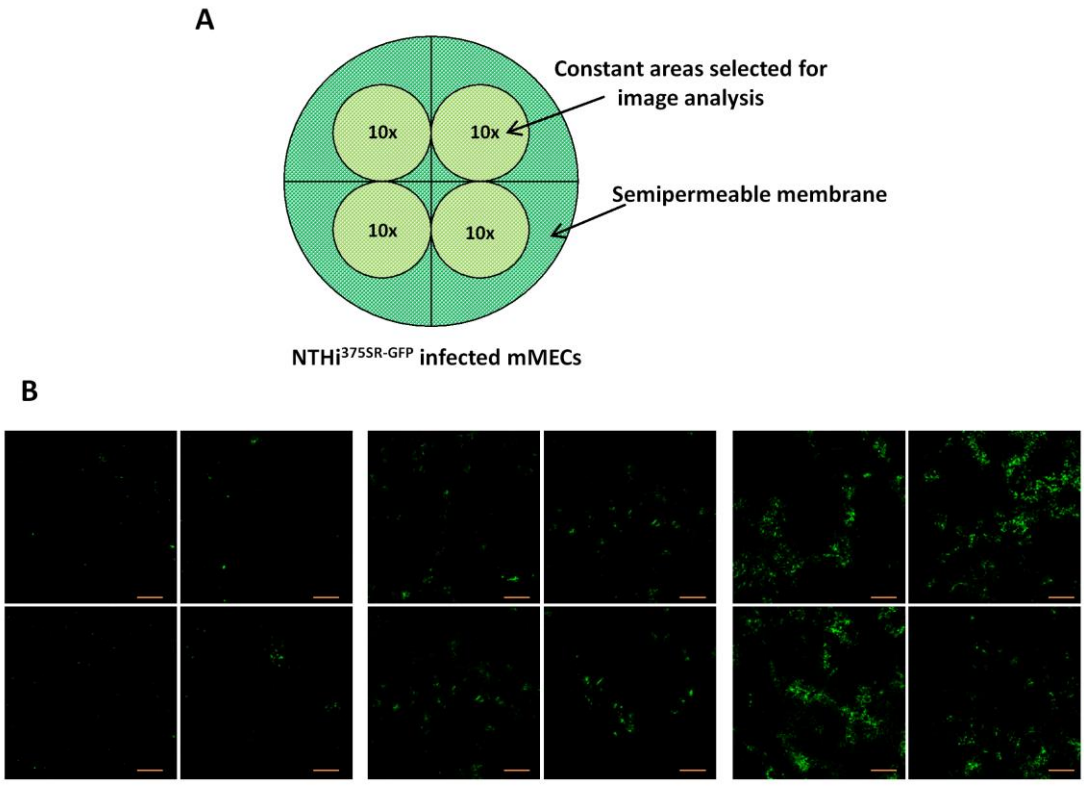

Figure 2.10 Quantification of NTHi infection in mMEC cultures using IFC
Selection of 4 central 10x fields on each ALI Day 14 mMEC cells infected NTHI-375$^{SR\text{-}GFP}$ to define a constant area for quantification of infection, spanning approximately 50% of the membrane (A). A representative image showing progression of *NTHi* infection in the selected fields at 24 hpi, 48hpi and 72 hpi (B). The amount of infection at each time point was quantified as a measure of the mean integrated intensity for green fluorescence in these panels from 3 independent batches of infections.

2.13.7.2 Quantification of infection using bacterial viable counts

ALI Day 14 mMEC cultures were infected with NT*Hi*$^{375SR\text{-}GFP}$ for 48 and 72 hpi at MOI 100 as described in Section 2.13.6**.** At the desired time point, 250µl of 2% Saponin (Sigma Aldrich) was added to the apical chambers of 3 MOCK and 3 infected wells and the cells incubated for 12 minutes at 37°C, 5% CO_2. Following incubation, cells were lysed by vigorously scraping the membrane and repeatedly pipetting up and down. The volume was made up to 1ml with sterile PBS, serially diluted and required dilutions were plated on BHI-NAD-Hm plates using the Miles Misra technique (Miles et al 1938). The plates were incubated overnight at 37°C, 5% CO_2 and the numbers of colonies were enumerated the following day.

2.14 Bacterial Association Assay

ALI Day 14 mMEC cultures were infected with NT*Hi*$^{375SR\text{-}GFP}$ at MOI 100 for 1 hr as described in **Section 2.13.6**. Cells were washed 3 times with sterile PBS to remove unbound bacteria. 200µl of 1% Saponin was added to the top chamber and cells incubated at 37^0C, 5% CO_2 for 10 minutes. Cells were lysed by vigorously scraping the membrane and repeatedly pipetting up and down, serially diluted and plated on BHI-NAD-Hm agar plates using the Miles Misra method. The plates were incubated overnight at 37°C, 5% CO_2 and the numbers of bacteria were enumerated the following day. Association of bacteria to mMEC cultures was calculated as follows:

$$\% \text{ Association} = \frac{\text{CFU/ml of NT}Hi \text{ associated after 1 hour}}{\text{CFU/ml of NT}Hi \text{ in the original inoculum}} x\ 100$$

2.15 Secretome analysis of mMEC cultures by Mass Spectrometry

Mass Spectrometry (MS) was performed on apical wash secretions pooled from 6 batches of ALI Day 14 mMEC cultures by Stuart Armstrong at the Institute of Infection and Global Health, University of Liverpool, Liverpool, UK.

2.15.1 Sample preparation for Mass Spectrometry

50 µg of soluble proteins were precipitated by adding an equal volume of ice-cold 30% (w/v) TCA in acetone and incubating for 2 hours at -20°C. Proteins were pelleted at 12,000 xg for 10 minutes at 4°C; pellets washed 3 times with ice-cold acetone, air dried and re-suspended in 50 mM ammonium bicarbonate, 0.1% (w/v) RapiGest SF (waters). Samples were heated at 80°C for 10 minutes, reduced with 3 mM DTT at 60°C for 10 minutes, cooled and alkylated with 9 mM iodoacetamide (Sigma) for 30 minutes. All steps were performed with intermittent vortexing. Proteomic-grade trypsin (Sigma) was added at a 50:1 ratio of protein: trypsin and incubated at 37°C overnight. Samples were precipitated using 1% TFA at 37°C for 2 hr to remove and centrifuged at 12,000 g for 1 hr at 4°C to remove RapiGest SF. The peptide supernatant was desalted using C_{18} reverse-phase stage tips (Thermo Scientific Pierce) according to the manufacturer's instructions, dried and re-suspended in 3% (v/v) acetonitrile, 0.1% (v/v) TFA for analysis by MS.

2.15.2 NanoLC-MS ESI MS/MS analysis

Peptides were analysed by on-line nanoflow LC using the Thermo EASY-nLC 1000 LC system (ThermoFisher Scientific) coupled with Q-Exactive mass spectrometer (ThermoFisher Scientific). Samples were loaded onto an Easy-Spray C_{18} column (50cm, i.d. 75 µm), fused to a silica nano-electrospray emitter (ThermoFisher Scientific). Chromatography was performed at 35°C using a buffer system consisting of 0.1 % formic acid (buffer A) and 80%

acetonitrile in 0.1 % formic acid (buffer B). The peptides were separated over a 97-minute linear gradient of 3.8-50% buffer B at a flow rate of 300nl/min. The Q-Exactive was operated in data-dependent mode with dynamic exclusion (20s) and survey scans acquired at a resolution of 70,000. Up to 10 of the most abundant isotope patterns with charge states +2, +3 and/or +4 from the survey scan were selected with an isolation window of 2.0Th and fragmented by higher energy collisional dissociation with normalized collision energies of 30. The maximum ion injection times for the survey scan and the MS/MS scans were 250 and 100ms, respectively, and the ion target value was set to 1E6 for survey scans and 1E4 for the MS/MS scans.

2.15.3 Protein Identification and Quantification

Thermo RAW files were imported into Progenesis LC–MS (version 4.1, Nonlinear Dynamics) and only peaks with a charge state between +2 and +7 were picked. Spectral data converted into mascot generic files (.mgf) and exported for peptide identification using the Mascot (version 2.3.02, Matrix Science) search engine. Tandem MS data were searched against translated ORFs from the mouse genome (Uniprot release 2015_02; 16,868 sequences; 9,451,355 residues). The search parameters were as follows: precursor mass tolerance was set to 10 ppm and fragment mass tolerance was set to 0.8 or 0.01Da and two missed tryptic cleavages were permitted. Carbamidomethylation (cysteine) was set as a fixed modification and oxidation (methionine) set as variable modification. Mascot search results were further validated using the machine-learning algorithm Percolator embedded within Mascot. The Mascot decoy database function was utilised and the false discovery rate was <1%, while individual percolator ion scores> 13 indicated identities or extensive homology ($p < 0.05$). Mascot search results were imported into Progenesis LC–MS as XML files for relative quantification using non- conflicting peptides.

2.16 Western blotting

Two types of samples were used for Western blotting:

1. Apical washes from uninfected mMEC and mNEC ALI cultures.
2. Apical washes from NT*Hi* infected mMEC ALI cultures

2.16.1 Protein quantification using Bradford assay

Total protein concentrations of apical washes from NT*Hi* infected mMEC ALI cultures were determined using the Bradford assay (Sigma Aldrich) in accordance to the manufacturer's guidelines. Briefly, bovine serum albumin (BSA) standards were prepared in the dilution range of 1.4mg/ml to 0.0625mg/ml. 5 µl of all standards and samples was added to 250µl

of the Bradford reagent in 96 well micro-titre plates in triplicates. Samples were incubated for 1 minute at room temperature. Protein concentrations of samples were determined by measurement of absorbance at 595nm on a plate reader.

2.16.2 Sodium Dodecyl Sulphate Polyacrylamide Gel Electrophoresis (SDS-PAGE)

Appropriate percentage resolving gels (12% or 15%, depending on the band size of the protein) of interest were poured and allowed to set, followed by 4% stacking gels. 300ng of total protein from NT*Hi* infected mMEC apical washes was combined with an appropriate amount of 2X SDS lysis buffer and the volume was made up to 40 µL. For all other studies, where the main purpose of western blotting was to detect proteins rather than quantification of their amount across samples, equal amounts of sample and 2X SDS lysis buffer was loaded onto the gels. Samples were denatured at 90˚C for 5 minutes and run alongside 10µl of marker (New England BioLabs #P7711S) in 1X Running Buffer at 150 Volts (for approximately 1 hour), till the dye reached the bottom on the gel.

2.16.3 Transfer of proteins

Stacking gels were discarded and resolving gels were placed in 1X Transfer Buffer. A transfer cassette was prepared by placing the various components in the following order from the cathode to the anode of the semi dry blotting system (Biorad Trans-blot turbo): 3 layers of Whatmann paper; resolving gel; methanol activated PVDF membrane; 3 layers Whatmann paper. All components were soaked in 1X Transfer buffer before assembly. Excess buffer was squeezed out and air bubbles were eliminated from the cassette using a plastic roller. Proteins were transferred at 25V for 12 minutes.

2.16.4 Immuno- detection of proteins

PVDF membranes were blocked using 5% Marvel in 1X Tris Buffered Saline-TWEEN (TBS-TWEEN) for 1 hour on an orbital shaker. Membranes were washed for 5 minutes in 1X TBS and probed with the appropriate primary antibody diluted in 5ml blocking buffer overnight, at 4˚C on a rolling platform. The primary antibodies and their concentrations used for Western blotting are given in Table 2.6. The following day, membranes were washed 3 times in 1X TBS-TWEEN for 5 minutes each. The primary antibody was detected using a polyclonal goat anti-rabbit secondary antibody (Dako P0448) conjugated with HRP (1:2000) for 1 hour at room temperature on a rolling platform. The membranes were washed 1X TBS-TWEEN as described before. The enhanced chemiluminescence (ECL) western blotting detection kit (Geneflow) was used to detect the secondary antibody. Membranes were placed in a plastic sleeve and 1 ml of ECL solution, prepared by mixing equal volumes of solution A (contains the substrate, luminol) and solution B (contains H_2O_2) was added to them. The plastic sleeve was sealed and placed in a light-proof cassette. Photographic X-ray films (GE Healthcare) were exposed to the membranes for an appropriate period of time in a dark room. In presence of H_2O_2, luminol is oxidised by HRP its electrons and transferred to an excited state. When the luminol electrons return to the ground state they emit light as a by-product which is captured by the Xray film. The films were developed, rinsed under tap water and fixed.

Preparation of all stock solutions used for Western blotting are detailed in **Appendix I**.

Table 2.6 Antibodies used for Western blotting

Primary Antibody	Type	Dilution	Manufacturer
Anti- BPIFA1	Rabbit polyclonal	1:200	Prepared in lab (Musa et al 2012)
Anti- Lactotransferrin	Rabbit antisera	1:2000	Milipore (07- 685)
Anti- Reg3γ	Rabbit polyclonal	1:5000	Kindly provided by Professor Lora Hooper (Cash et al 2006)

NB: Hannah Armes, a summer student in the lab, performed western blotting for Lactotransferrin and Reg3γ.

2.16.5 Quantification of western blots by Densitometry

For quantification of secreted BPIFA1 in apical washes from NT*Hi* infected mMEC cultures, western blot bands were quantified using Image J software. The intensity of the infected bands was compared to that of the MOCK infected bands. Statistics was performed using a two tailed students t-test and p values <0.05 were considered significant.

2.17 RNA extraction

Total RNA was extracted from cells using Trizol reagent (Sigma- Aldrich), in accordance to the manufacturer's guidelines. Briefly, cells were lysed in 250µl of TRI reagent. 50µl Chloroform (Fisher Scientific) was added to the lysate, vortexed vigorously for 15 secs and incubated at room temperature for 15 minutes. Samples were spun at 13,000 rpm at 8˚C for 15 minutes to enable phase separation. The top aqueous phase containing RNA was transferred to a fresh Eppendorf. 125µl of Isopropanol (Fisher Scientific) and 1µl of Glycoblue dye (Ambion) were added to the tube. Glycoblue increases the visibility of RNA pellets during the later steps. Samples were left to stand at room temperature for 10 minutes and then centrifuged at 13,000 rpm at 8˚C for 10 minutes to obtain RNA pellets. The pellets were washed with 75% ethanol (Fisher Scientific) and centrifuged again as mentioned previously. The ethanol was removed, pellets were air dried and re-suspended in 20µl of nuclease free water. RNA samples were stored at -20˚C.

2.18 End Point Reverse Transcription PCR (RT-PCR)

2.18.1 RNA quantification and DNAse I treatment

RNA concentration and quality were determined by measurement of absorbance of 1µl of the extracted RNA (Section 2.17) using NanoDrop ND-1000 (Thermoscientific). The 260nm:

280nm ratio was > 1.7 in all cases. Any residual genomic DNA was digested by DNase I treatment (Promega). Briefly, 1µl each of RQ1 RNase free 10x Reaction Buffer and RQ1 RNase free DNase enzyme from the kit were added to 200 ng of extracted RNA and the total reaction volume was made up to 10µl with nuclease free water. Samples were incubated at 37˚C for 30 mins. The reaction was terminated by addition of 1µl of RQ1 DNase Stop Solution and incubation at 65˚C for 10 minutes using a thermal cycler (MJ Research PTC-200).

2.18.2 cDNA synthesis

RNA was reverse transcribed into complementary DNA (cDNA) using the AMV Reverse Transcriptase kit (Promega). 0.5µl each of OligoDT (Sigma) and random primers (Promega) were added to the DNase digested RNA solution (Section 2.18.1)**.** The total volume was made up to 19µl with nuclease free water and samples were heated at 70˚C for 5 minutes. 6µl of master mix containing 5x AMV buffer, 100µM dNTPs, 0.25µl AMV RT enzyme and 0.25µl RNasin was added to the samples and cDNA was synthesised on the thermal cycler according to the recommended program: 42˚C for 1 hour; 95˚C for 5 minutes. Samples were either used immediately for RT-PCR or stored long term at -20˚C.

2.18.3 RT- PCR

End-point RT-PCR was performed to detect the expression of various genes. 1µl of template cDNA was amplified using Maxima Hot Start Green PCR Master Mix (ThermoFisher Scientific). Information regarding primer pairs used for RT-PCR is described in **Table 2.7** and details of the master mix contents and cycling conditions for the reactions are mentioned in **Table 2.8**. The reaction was run for 35 cycles for all genes

expect *Bpifa1* (25 cycles). *Oaz1* was used as the endogenous control for all end point RT-PCR experiments.

Table 2.7 Primer sequences and amplicon sizes for end point RT- PCR

Assay	Primer type	Sequence (5'-3')	Product size (bp)
Bpifa1	Forward	ACAGAGGAGCCGACGTCTAA	127
	Reverse	CCAAGAAAGCTGAAGGTTC	
Tekt1	Forward	CAGTGCGAAGTGGTAGACG	373
	Reverse	TTCACCTGGATTTCCTCCTG	
Muc5B	Forward	ATGGTGACCAAGAGCCAAAA	178
	Reverse	CAGGACTGTTCACCCAGGTT	
Muc5AC	Forward	GCACCAAAGACAGCAGATCA	167
	Reverse	CTGAGAGGTTTGCAGCTCCT	
Lactotransferrin	Forward	TCTGTCCCTGTGTATTGGT	237
	Reverse	GTTTCCGGGTGTCATCAAGG	
Sftpd	Forward	AAGCAGGGGAACATAGGACC	109
	Reverse	GCCTTTTGCCCCTGTAGATC	
Bpifb1	Forward	CCCTGACCAAGATCCTTGAA	148
	Reverse	GAGGCTGGAGTGAGCTTGAG	
Keratin 5	Forward	ACCTTCGAAACACCAAGCAC	337
	Reverse	TGACTGGTCCAACTCCTTCC	
Vimentin	Forward	CAAGCAGGAGTCAAACGAG	273
	Reverse	CCTGTAGGTGGCGATCTCAA	
Reg3$^{\gamma}$	Forward	CCTGTCCTCCATGATCAAAGC	250
	Reverse	GCAGACATAGGGTAACTCTAAGT	
Oaz1	Forward	ACAGAGGAGCCGACGTCTAA	274
	Reverse	CCAAGAAAGCTGAAGGTTC	

Table 2.8 Master Mix details and cycling conditions for end point RT-PCR

RT-PCR master mix (Total volume 20 µl)		RT-PCR cycling conditions		
Reagent	**Volume (µl)**	**Step**	**Temperature**	**Time**
Maxima hot start mix (5x)	10	Hot start	95^{0}C	5
Nuclease H_2O	7	Denaturation	94^{0}C	1 min
Forward primer (10 µM)	1	Annealing	60^{0}C	1 min
Reverse primer 10 µM	1	Extension	72^{0}C	1 min
Template cDNA	1	Final	72^{0}C	7

x 35

2.18.4 Agarose gel electrophoresis

The amplified PCR products were run on a 2% agarose gel containing 0.5µg/ml ethidium bromide at 80V (Dutscher scientific) and bands were visualised using Biorad ChemiDoc™ XRS+ alongside a 100 base pair ladder (Bioline).

2.19 Quantitative Reverse Transcription PCR

Quantitative Reverse Transcription PCR (RT-qPCR) was used to study relative gene expression using a variety of samples. I performed the following steps with the help of Dr. Debbie Williams at GEMS, MRC Harwell.

2.19.1 RNA clean-up

RNA extracted using Trizol (Section 2.17) was found to be contaminated with components from the TRI reagent such as phenol and guanidine salts as indicated by the low 260:230nm absorbance ratio. Therefore, RNA was treated with the Ambion DNA-*free*™ kit (Applied Biosystems) to reduce these contaminants and eliminate any residual genomic DNA. 12µl master mix containing 1x DNase I buffer, 1µl DNase I enzyme and nuclease free water was added to 18µl of total RNA. Samples were incubated at 37˚C for 30 minutes on a heat block. 0.1 volume of DNase I inactivation reagent was added and samples were mixed by gently flicking the tubes. The inactivation reagent contains beads that bind the degraded DNA and contaminants. Samples were centrifuged at 10,000 xg for 1.5 minutes to pellet the beads. The supernatant containing the RNA was transferred to a fresh eppendorf.

2.19.2 RNA quantity and quality assessment

The concentration of cleaned RNA samples was determined by measurement of absorbance on NanoDrop ND-8000 (Thermoscientific). RNA quality and integrity were

checked on a Bioanalyzer 2100 instrument with the RNA 6000 Nano kit (both Agilent), using 1µl (1:2 diluted) RNA which had been denatured at 70°C for 2 minutes. This instrument provides information about the RNA integrity number (RIN), absorbance ratios as well as produces RNA gel-like electropherograms showing the integrity of the 28s and 18s rRNA subunits.

2.19.3 cDNA synthesis

240- 500ng of total RNA was reverse transcribed into cDNA in 20µl reaction volume using the Superscript™ III First Strand Synthesis kit (Invitrogen), in accordance to manufacturer's guidelines. Briefly, 12µl of master mix containing 2x RT reaction mix and 2µl of RT enzyme mix was added to the RNA samples. Samples were run on the thermal cycler according to the recommended program: 25˚C for 10 minutes; 50˚C for 30 minutes and 85˚C for 5 minutes. Samples were chilled on ice; 1µl of RNase H was added to the tubes and incubated at 37˚C for 20 minutes on the thermal cycler. RT^{-ve} samples were generated using all components of the master mix expect the RT enzyme mix. The cDNA was either used immediately or stored at -20˚C.

2.19.4 Determination of appropriate endogenous controls for RT-qPCR

2.19.4.1 The Primerdesign geNorm™ assay

For accurate measurement of gene expression, it was necessary to normalise quantitative real time PCR results to reference genes (endogenous controls) which did not vary with the experimental conditions such as genotype or NT*Hi* infection of cells. The routinely used endogenous controls, GAPDH and β-actin, and the endogenous control used for end point RT-PCR, *Oaz1,* did not show stable expression across samples for the required experimental conditions (data not shown). Therefore, the geNorm™ Reference Gene Selection Kit

(Primerdesign) was used to establish the optimal endogenous controls for use. This kit contained primer sets for 12 murine candidate reference genes **(Table 2.9)** *Rpl13a* from the geNormTM kit was replaced with TaqMan® gene expression assay for *Ppia* (Peptidylprolyl isomerase A), because this gene has previously been used as an endogenous control for studying hypoxia signalling in the mouse middle ear by our lab (Cheeseman et al 2011). Individual reactions were set up in MicroAmpR Fast Optical 96 well reaction plates with 10 ng cDNA from representative samples to be used for each experimental condition. 2x TaqMan® Fast Universal PCR Master mix (Applied Biosystems, contents detailed in Table 2.10) was added to each well and the final reaction volume was made up to 20µl with nuclease free water. Each sample was run in triplicates for each assay. cDNA was amplified on the 7900HT Fast Real-Time PCR System (Applied Biosystems) using the Fast program. Cycling conditions are detailed in Table 2.10.

Table 2.9 List of candidate reference genes assayed using the geNorm™ Reference Gene Selection Kit

Gene Name	Gene symbol
Actin, beta, cytoplasmic	*Actb*
Glyceraldehyde-3-phosphate dehydrogenase	*Gapdh*
Ubiquitin C	*UbC*
Beta-2 microglobulin	*B2m*
Phospholipase A2	*Ywhaz*
Ribosomal protein L13a	*Rpl13a*
Calnexin	*Canx*
Cytochrome c-1	*Cyc1*
Succinate dehydrogenase complex, subunit A	*Sdha*
18S rRNA	*18S*
Eukaryotic translation initiation factor 4A2	*Eif4a2*
ATP synthase subunit	*ATP5B*

NB: *Rpl13a* from the geNorm™ kit was replaced with TaqMan® gene expression assay for *Ppia* (Mm02342429_g1)

2.19.4.2 geNorm™ assay analysis

For selection of the best reference genes, data was analysed using the geNorm module on the RT-qPCR software, qBase^{Plus} which ranks the candidate reference genes according to the stability of their expression across all samples. The software generates two types of graphs:

a) **The geNorm M** plot indicates the average expression stability value (M) of the reference genes across samples at each step and arranges the least stably expressed gene on the left and the most stably expressed gene on the right.

b) **The geNorm V** plot helps to determine the ideal number of reference genes that should be used for normalisation of target genes. It measures a factor called pairwise variation, *V(n/n+1)* which indicates the successive addition of each reference gene beginning with the 2 most stably expressed genes as identified by the geNorm M plot and the inclusion of successive genes moving right across the plot. The ideal number of reference genes (n) is obtained when the value of *V(n/n+1)* drops below the threshold of 0.15.

Separate geNorm™ assays were performed to identify optimal reference genes to study relative gene expression for each experimental condition in this thesis i.e. for original middle ear mucosal cells isolated from bullae from mice of different genotypes, for mMECs cultured at ALI from different genotypes and cultured mMECs infected with NT*Hi*. An example of geNorm analysis is shown in Figures 2.11 and 2.12.

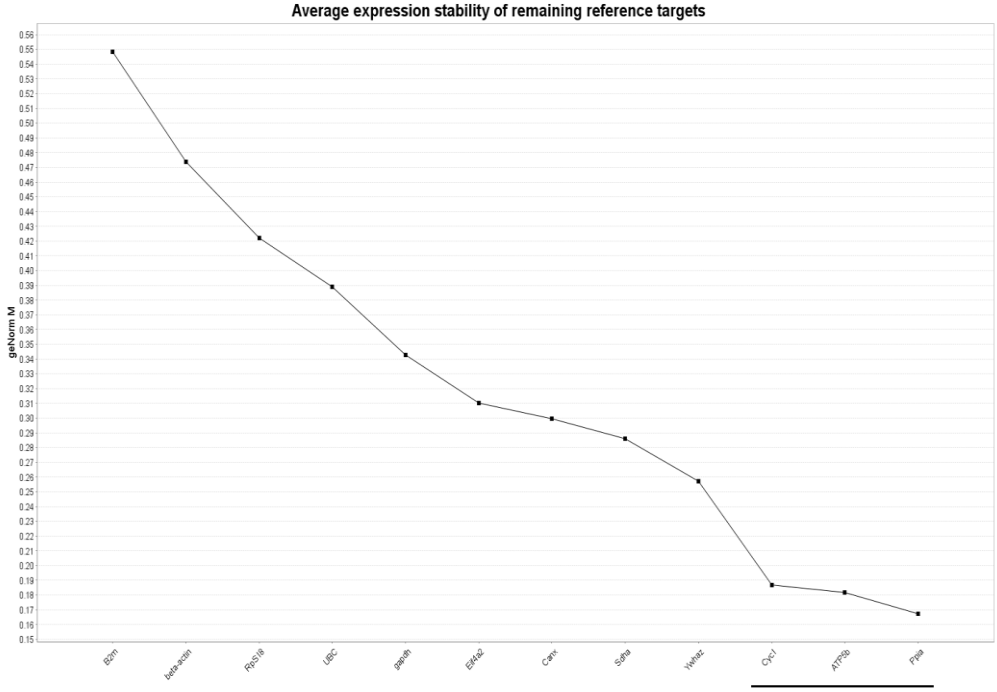

Figure 2.11 geNorm M plot for selection of ideal endogenous controls
The above figure shows a representative Primerdesign geNorm™ M plot for reference gene selection. In this case, the plot indicates that *Ppia* was the most stably expressed reference gene across *NTHi* infected and Mock infected ALI Day 14 mMECs at various time points, followed by *ATP5b* and *Cyc1.*

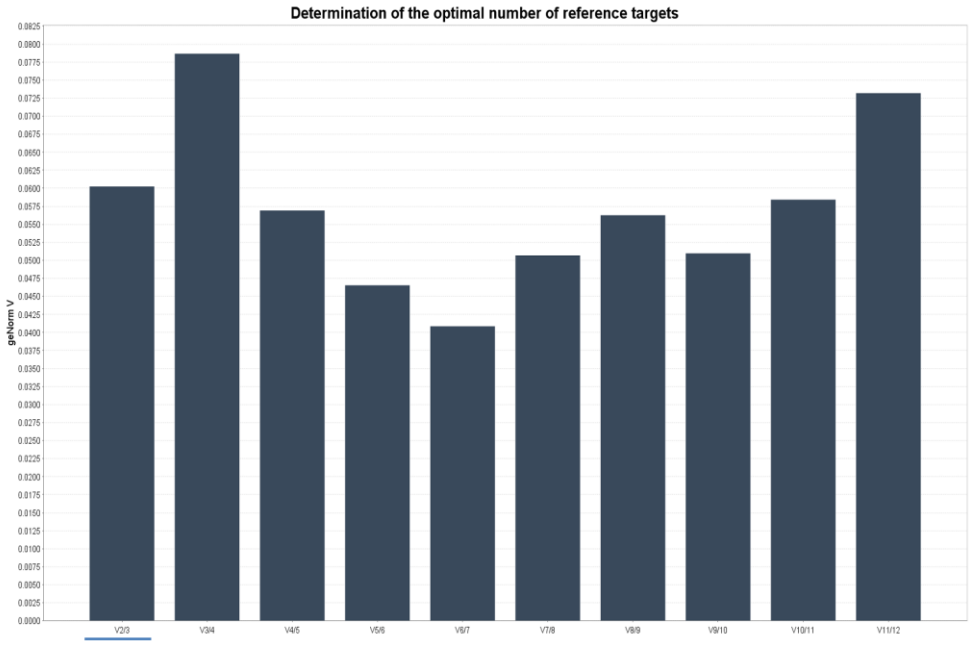

Figure 2.12 geNorm V plot for determination of the ideal number of endogenous controls for normalisation of target gene expression
The above figure is a Primerdesign geNorm™ V plot, used in this case, to determine the optimal number of endogenous controls (ECs) required for normalisation of target genes in NT*Hi* infected and MOCK infected mMEC samples. The plot suggests the use of 2/3 ECs since the pairwise variation value is below the minimum threshold of 0.15. Therefore, 3 reference genes, *Ppia, ATP5b and Cyc1* were selected for normalisation or target genes in this study.

2.19.5 Quantitative real time PCR (RT-qPCR) using mouse TaqMan® assays

RT-qPCR was performed using Applied Biosystems TaqMan® gene expression assays. As mentioned above, 10 ng cDNA was used per well. Master Mix and cycling conditions used for RT-qPCR were the same as that used for geNorm assay (Section 2.19.4.1). 15µl of 2x TaqMan® Fast Universal PCR Master mix (Applied Biosystems) was added to each well. The final reaction volume was made up to 20µl with nuclease free water. Plates were sealed using MicroAmp optical adhesive films (Applied Biosystems). Reactions were carried out in triplicates for each assay and each sample on the 7500 Fast Real Time PCR system (Applied

Biosystems) in the Fast mode. Details of the master mix and cycling conditions are outlined in Table 2.10**.** TaqMan assays used for RT-qPCR are mentioned in Table 2.11.

Table 2.10 2x TaqMan® Fast Universal PCR Master mix details and cycling conditions for quantitative RT-PCR and geNorm assay

RT-qPCR master mix (Total volume 20 µl)		**RT-qPCR cycling conditions**		
Reagent	**Volume(µl)**	**Step**	**Temperature**	**Time**
2x TaqMan® Fast Universal PCR	10	Hot start	95^0C	20secs
Nuclease H_2O	4	Denaturation	95^0C	3 secs
20x TaqMan assay	1	Annealing and extension	60^0C	30 secs
Diluted cDNA (10ng/well)	5			

x 40

NB: Primerdesign geNorm™ primer mix was used instead of 20x TaqMan® assay for the geNorm analysis

2.19.6 RT-qPCR analysis

Each TaqMan® assay consisted of a primer pair for cDNA amplification and a probe complementary to a sequence between the two primers, with a FAM fluorophore on the 5' end and a quencher on the 3' end. During RT-qPCR, the endogenous 5' nuclease activity of the Taq polymerase cleaves the fluorophore, separating it from the quencher. This results in emission of fluorescence which is detected and quantified by the software and is directly proportional to the amount of cDNA present in the sample. Cycle threshold (CT) value is the number of cycles required for this fluorescent signal to reach the threshold level set by the software. Samples with more cDNA for a particular gene reach the threshold faster and thus, have lower CT values.

Results were analysed on the SDS software v2.2 (Applied Biosystems) using the 'Comparative CT (ΔΔCT)' method where,

- $\Delta CT = CT_{\text{Target gene}} - CT_{\text{Endogenous control}}$

Gene expression of targets was normalised against that of endogenous controls selected using the geNorm™ Reference Gene Selection Kit as mentioned in Section 2.19.4.

- $\Delta\Delta CT = \Delta CT_{\text{Experimental sample}} - \Delta CT_{\text{Calibrator sample}}$

Relative quantification (RQ) or fold change was calculated using the formula,

- $RQ = 2^{-\Delta\Delta CT}$

Error bars were calculated as RQ_{min} and RQ_{max} by the software which is based on the calculation of the standard error of mean for each ΔCT value using an automated algorithm. However, error bars for individual data points have been calculated manually as individual RQ value for each biological replicate ±SEM and this has been mentioned where relevant. Statistical analysis was performed using ΔCT values of each biological replicate.

Table 2.11 TaqMan® gene expression assays used for quantitative real time PCR experiments

Gene	TaqMan® Gene Expression Assay ID
BPI fold containing family A, member 1 (*Bpifa1*)	Mm00465064_m1
Chemokine (C-X-C motif) ligand 2 (*Cxcl2*)	Mm00436450_m1
EVI1 complex locus (*Evi1*)	Mm00491303_m1
Forkhead box J1 (FoxJ1)	Mm01267279_m1
Interleukin 6 (*IL6*)	Mm99999064_m1
Mucin 5, subtype B (*Muc5B*)	Mm00466391_m1
Mucin 5, subtypes A and C(*Muc5AC*)	Mm01276718_m1
Transformation related protein 63 (*p63*)	Mm00495793_m1
Transforming growth factor, beta (*TGFβ*)	Mm01178820_m1
Tumor necrosis factor alpha (*TNFα*)	Mm99999068_m1
Vascular endothelial growth factor A (*Vegfa*)	Mm00437304_m1

2.20 Cytocentrifugation and staining of middle ear fluids

Middle ear fluids from *Evi1*$^{Jbo/+}$ and *Bpifa1*$^{-/-}$*Evi1*$^{Jbo/+}$ mice were sampled and diluted in PBS as mentioned in Section 2.13.5. 80µl of the sample containing 1- 2 X10^{6} cells were mixed with 20µl of 10%FBS, vortexed and transferred to clip-slide-filter-chambers/cytospins in duplicates. The cells were placed on the slides by centrifugation in Shandon Cytocentrifuge (Shandon Cytospin 3, Thermo Scientific) at 300x g for 3 minutes. Cells were air dried briefly and fixed on the slides with a drop of 100% methanol. Cells were stained by placing the slides in diff quick stain I (orange dye) (Gentaur) for 1 minute, followed by transfer to diff quick stain II (blue dye) (Thermo Fisher Scientific) for 2-3 minutes. Cells were washed briefly, dried and mounted in a drop of distrene-80 plasticiser xylene (DPX) (Fisher

Scientific). The slides were observed by using Zeiss Axioplan microscope with X100 oil immersion lens.

2.21 Statistics

Variance of experimental groups and parametricity was determined by performing Levene's test prior to the statistical analysis. GraphPad Prism (version 6.0) was used to perform all statistical tests. 2 tailed students *t*-test was used to compare two groups. One way or two-way analysis of variance (ANOVA) with Tukey's posthoc test was used to compare more than two groups, for parametric data. Fisher's exact test was used for analysing frequency data such as presence or absence of middle ear fluids or genotype ratios (Chi squared analysis if there were more than 3 groups). Significance threshold was set at $p < 0.05$. Data are presented as the mean +/- standard error of the mean (SEM) unless otherwise stated. Significance levels represented on graphs are as follows: ns = not significant; * = $p \leq 0.05$; ** = $p \leq 0.01$; *** = $p \leq 0.001$; **** = $p \leq 0.0001$.

CHAPTER 3: ASSESSMENT OF THE EFFECT OF *BPIFA1* DELETION ON DEVELOPMENT OF OM

3.1.1 Introduction

Otitis media is an opportunistic infection of the middle ear caused by transfer of the indigenous nasopharyngeal microflora into the middle ear. Some mice with craniofacial abnormalities and defects in innate immunity genes are predisposed to OM, leading to the generation of several mouse models of spontaneous OM (Rye et al 2011a). Preliminary IHC studies in our lab have shown abundant staining for BPIFA1 in the *Wt* middle ear epithelium and there was a decrease in the staining intensity with progression of OM in the *Evi1*$^{Jbo/+}$ mice, a model of spontaneous, chronic OM (Sections 1.8.2 and 1.13). Owing to the abundant expression of this putative innate host defence gene in the middle ear, I postulated that deletion of *Bpifa1* might result in spontaneous development of OM. This hypothesis is supported by a GWAS study showing association of SNPs in BPIFA1 with OM (Rye et al 2012b) and the more recent report suggesting that aged *Bpifa1*$^{-/-}$ mice show increased susceptibility to OM development (Bartlett et al 2015).

OM can also be induced in animal models by infection with otopathogens. NT*Hi* is one of the most common causative organisms of both AOM and COM, responsible for 25- 30% of the cases (Giebink 1991). Since the advent of pneumococcal vaccines, it has become the most common pathogen in OM (Casey & Pichichero 2004). The chinchilla is the most commonly used *in vivo* model for the study of NT*Hi* induced OM, primarily due to the large size and easy accessibility of its middle ear cavity (Bakaletz 2009). However, there has been an increase in the number of mouse models of induced OM in the recent years (Ryan et al 2006, Sabirov & Metzger 2008). The two routes used for induction of OM in animal models using bacteria are, direct injection into the middle ear cavity and IN inoculation. IN inoculation mimics the natural route of OM pathogenesis, starting with initial colonisation of the NP, followed by transfer of bacteria through the ET and leading to a subsequent middle ear infection.

BPIFA1 is abundantly expressed in various parts of the nasal passages (Musa et al 2012) along with the middle ear epithelium. Several studies advocate a surfactant function for BPIFA1 (Bartlett et al 2011, Gakhar et al 2010, Liu et al 2013a, Walton et al 2016). Surfactants in the middle ear and ET are important in modulating optimal functioning of the ET and promoting mucociliary clearance (McGuire 2002). A previous study in chinchillas showed that down regulation of *Bpifa1 in vivo* leads to ET dysfunction (McGillivary & Bakaletz 2010). Moreover, based on its structural homology to BPI, an antimicrobial function was originally suggested for BPIFA1 (Bingle & Craven 2002). Mice in which *Bpifa1* was either silenced or ablated, show increased susceptibility and higher pulmonary bacterial counts when challenged with *K.pneumoniae*, *P.aeruginosa*, and *M.pneumoniae* (Chu et al 2007, Gally et al 2011, Liu et al 2013a, Liu et al 2013b).

Therefore, owing to its surfactant and antimicrobial properties, I proposed that IN challenge of *Bpifa1*$^{-/-}$ mice might lead to an increased ascension of bacteria from the NP into the middle ear, resulting in induction of OM.

3.1.2 Aims of this study

The first aim of this study was to assess spontaneous development of OM in *Bpifa1*$^{-/-}$ mice. The second aim was to study the effect of the loss of *Bpifa1* on the nasopharyngeal carriage of the human otopathogen NT*Hi.*

3.1.3 Study design

Figure 3.1 gives a brief study plan for this chapter. Post-natal localisation of BPIFA1 protein in the *Wt* developing middle ear cavity was studied (Section 3.2.1) and deletion of the gene was confirmed in *Bpifa1*$^{-/-}$ mice using IHC (Section 3.2.2). *Bpifa1*$^{-/-}$ mice were systematically, phenotypically characterised for variety of features such as viability, weight, general

behaviour (Section 3.2.2) and organ morphology (Section 3.2.4). Auditory threshold measurements and histological analysis were performed to identify signs of early and late onset OM in these mice (Section 3.2.3). Transfer of NT*Hi* from the NP to the ME was evaluated using two different strains of bacteria and using IN inoculation and baroinoculation techniques (Section 3.2.5). Experiments for this chapter were performed in the initial period of the breeding pipeline (Section 2.1.3, Fig 2.2). Hence, either *Bpifa1*$^{-/-}$ mice on a C57BL/6 background or on a mixed C57BL/6-C3H/HeH background (inter-crossed at Backcross 2) were used throughout this chapter. The strains are mentioned where relevant.

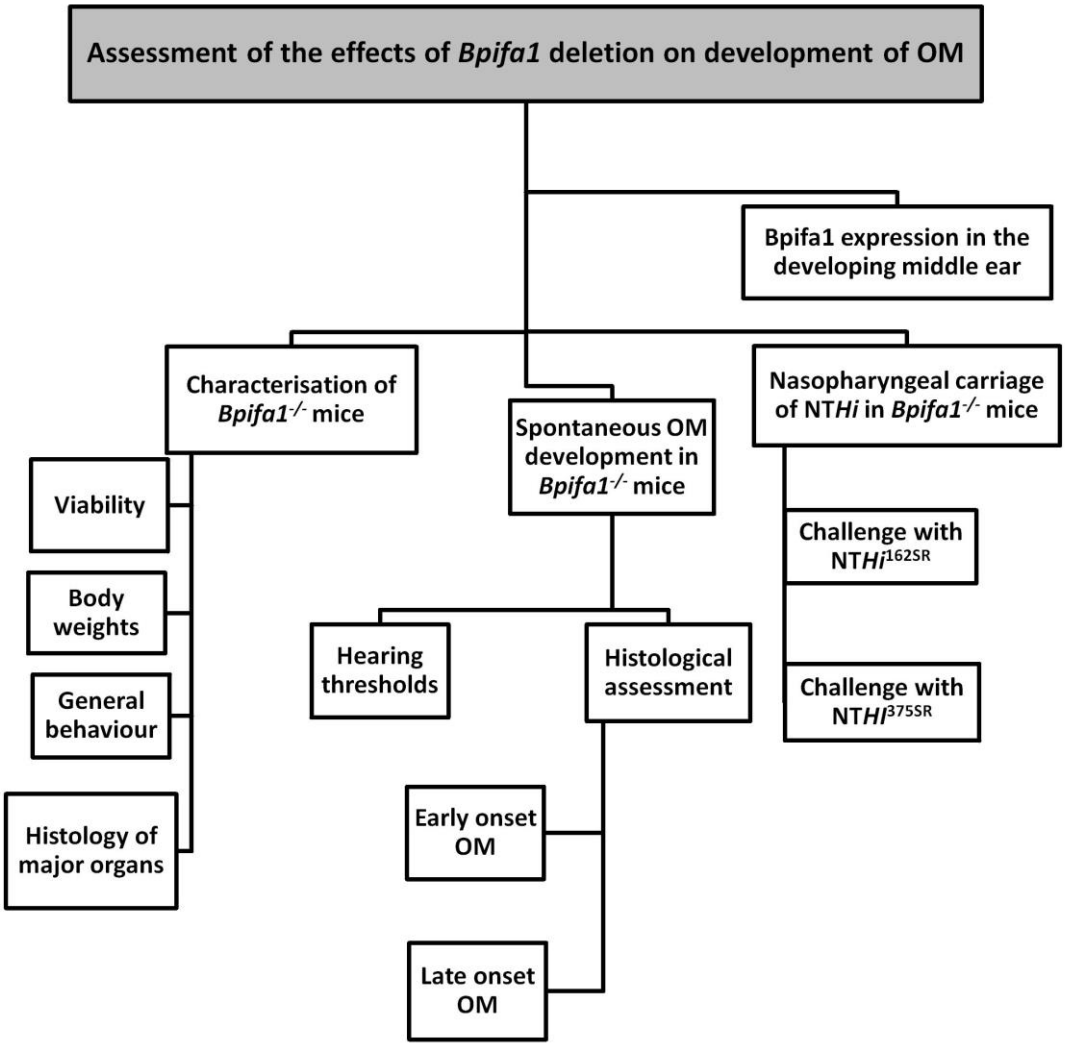

Figure 3.1: Major steps in planning this chapter.

3.2 Results

3.2.1 BPIFA1 is expressed in the post-natal developing mouse middle ear cavity

Preliminary IHC studies in our lab had shown that BPIFA1 localised to the *Wt* middle ear epithelium from P21 to P56 and the intensity of staining decreases with progression of OM in *Evi1*$^{Jbo/+}$ mice during this time period (Section 1.13). In order to evaluate the onset of BPIFA1 production during the post-natal development of the middle ear cavity, I performed IHC on middle ear sections of C3H/HeH mice from the day of birth (P0) to P30 at regular intervals of 5 days. BPIFA1 staining was seen in the middle ear epithelium throughout this

developmental period. In neonates, from P0 to P10, the middle ear space was packed with mesenchymal material. BPIFA1 staining was visible in the epithelial cells and submucosal glands enclosing this mesenchyme-filled space, in the region where the mesenchyme pulled away from the underlying epithelium (Fig 3.2A-C). Occasionally, the mesenchyme itself stained positive for BPIFA1 (Fig 3.2C). Retraction of the mesenchyme from the epithelium began at P5, starting ventrally and continued towards the attic, until an air filled cavity was formed by P15 (Fig 3.2 B-D). Occasionally, the layer of the Tm facing the middle ear cavity also stained positive for BPIFA1 (Fig 3.2D). At P15, the middle ear cavity demonstrated its adult shape. BPIFA1 was localised to the non-ciliated cells and submucosal glands throughout the middle ear epithelium from P15 to P30 (Fig3.2 E-G). It must be noted the changes in the staining intensity for BPIFA1 were not quantified during this developmental period and no assessment was made for the number of ciliated cells. Hence, no assumptions can be made regarding the changes occurring in the cell types from the histology sections.

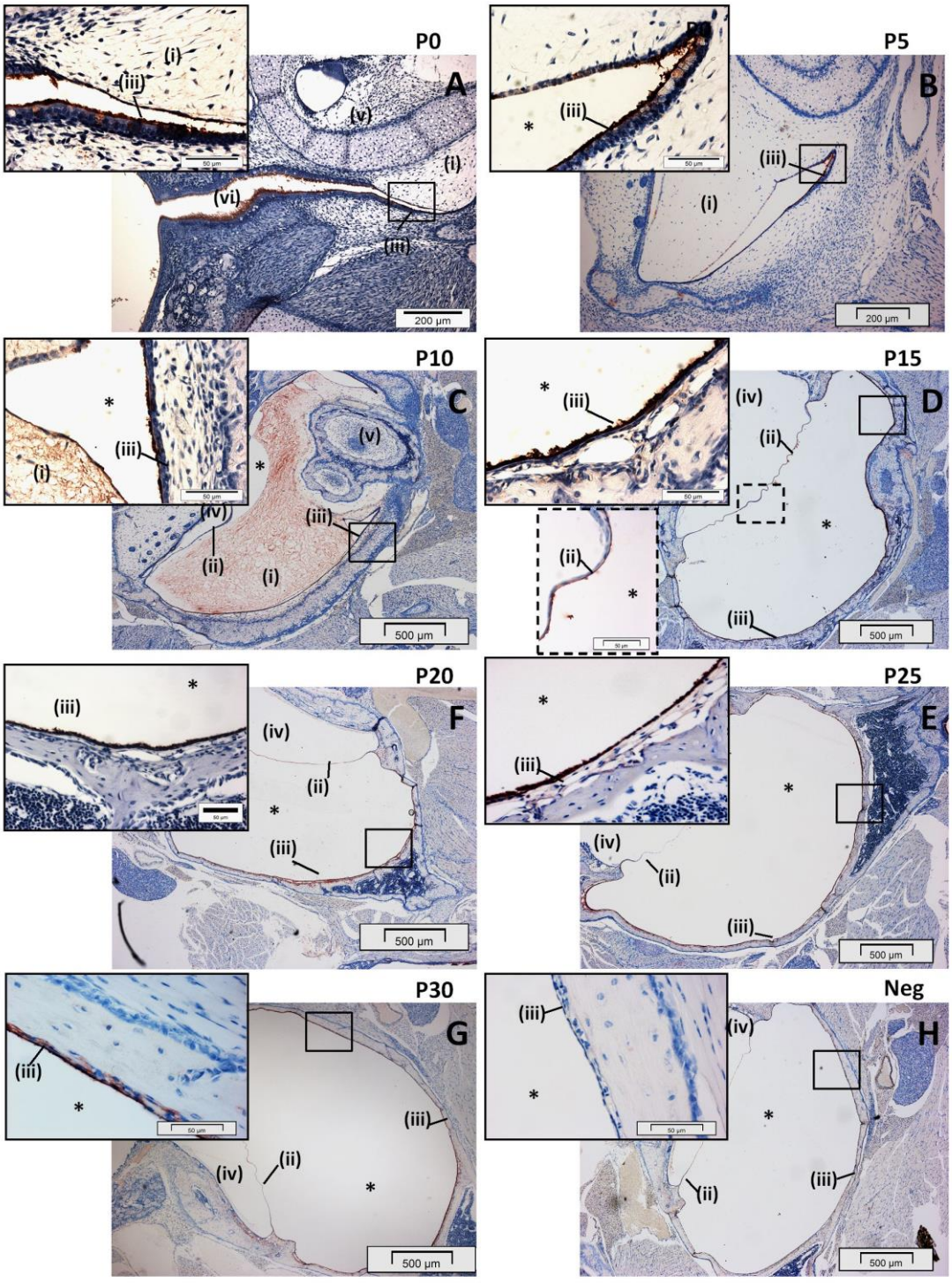

Figure 3.2 Localisation of BPIFA1 in the post-natal middle ear cavity

Low and high magnification images showing IHC for BPIFA1 in the developing middle ear cavity from P0 to P30. All sections are orientated with the OEC towards the left-hand side (Iv) and the MEC towards the right hand side (i), separated by the Tm (iii). BPIFA1 localises to the non-ciliated epithelial cells and submucosal glands (A-G). Middle ear space is filled with mesenchymal material until P10 which resorbes to form a fully air filled cavity by P15 (A-D). Negative control for BPIFA1 (H). Mesenchymal material (i); Tm (ii); middle ear epithelium (iii); outer ear space (iv); cochlea (v); middle ear cavity (asterisk). Images representative of n=3 mice at each time point. Scale bar 500µm for 4x images and 50µm for 60x images.

3.2.2 Characterisation of *Bpifa1*$^{-/-}$ mice

All mice were inspected daily by ward technicians and no abnormalities were seen in the gross anatomy and overt behaviour of *Bpifa1*$^{-/-}$ mice. Successful ablation of *Bpifa1* was confirmed by IHC of P28 middle ear cavities. As described above BPIFA1 was localised to the non-ciliated cells of the *Wt* middle ear epithelium and it coated the surfaces of cilia. However, staining was completely absent in the middle ear epithelium of the *Bpifa1*$^{-/-}$ littermate controls (Fig 3.3).

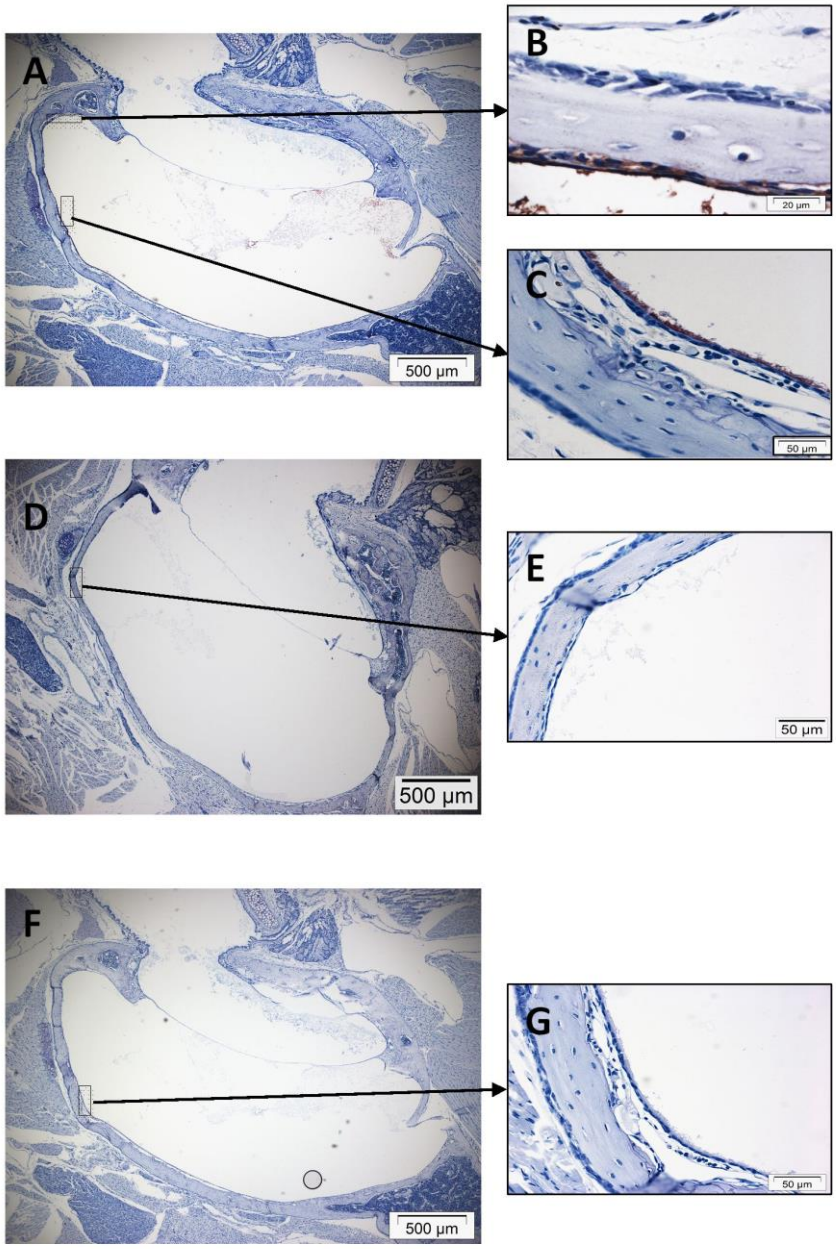

Figure 3.3 Localisation of BPIFA1 in *Wt* and knockout middle ear cavities
BPIFA1 expression was detected in the *Wt* mouse middle ear using IHC. Low magnification image of *Wt* mouse middle ear showing localisation of BPIFA1 along the middle ear epithelium (A). High magnification images showing that BPIFA1 is produced by non-ciliated cells of the middle ear epithelium (B), but coats the surface of the cilia (C). BPIFA1 staining is absent in the *Bpifa1*$^{-/-}$ middle ear (D, E) and the negative control (F, G). Data is representative of n=3 mice for both genotypes. Scale bar 500µm for 4x images and 50µm for 60x images. All 4x images are orientated with the OEC towards the upper side and the MEC towards the lower side, separated by the Tm.

3.2.2.1 Analysis of genotypic ratios

The viability of the *Bpifa1*$^{-/-}$ line was assessed on the original C57BL/6 background (Table 3.1) and after transfer to C3H/HeH background (Table 3.2) by analysing genotype ratios of the progeny obtained from *Bpifa1*$^{+/-}$ x *Bpifa1*$^{+/-}$ intercrosses (Fishers exact test). On both backgrounds, normal Mendelian ratios were observed at weaning age (P21).

Table 3.1: Numbers of live mice for *Bpifa1*$^{-/-}$ line on the C57BL/6 background

Genotype	Observed numbers	% Observed	Expected numbers	% Expected	P-value
***Bpifa1*$^{-/-}$**	60	22.38	67	25	0.172045
***Bpifa1*$^{+/-}$**	120	44.74	134	50	
Wt	88	32.83	67	25	
Total	268	100	268	100	

Table 3.2: Numbers of live mice for *Bpifa1*$^{-/-}$ line on the C3H/HeH background

Genotype	Observed numbers	% Observed	Expected numbers	% Expected	P-value
***Bpifa1*$^{-/-}$**	59	25	59	25	0.657047
***Bpifa1*$^{+/-}$**	126	53.3	118	50	
Wt	51	21.6	59	25	
Total	236	100	236	100	

3.2.2.2 Analysis of body weights

Body weights of C57BL/6-C3H/HeH *Bpifa1*$^{-/-}$ and *Bpifa1*$^{+/-}$ mice were compared to their *Wt* littermate controls. As expected males weighed more than females. No significant differences were found between the three genotypes for either males or females at 8 weeks (Fig 3.4A) and 12 weeks of age (Fig 3.4B).

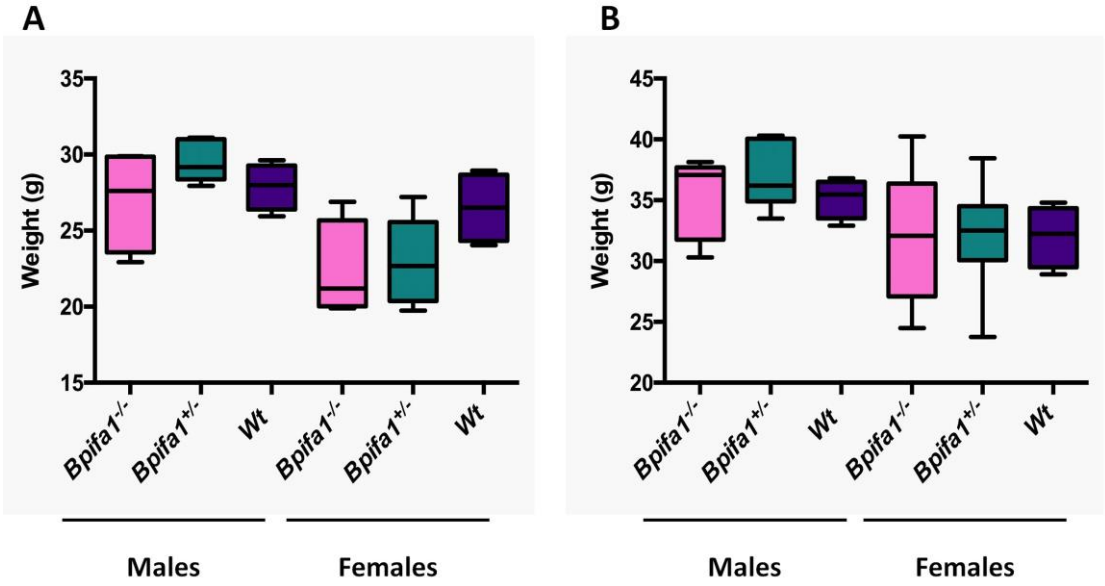

Figure 3.4 Body weight analysis of *Bpifa1*$^{-/-}$ mice
The figure shows that there is no significant difference between mean body weights of male and female *Bpifa1*$^{-/-}$ compared to their *Bpifa1*$^{+/-}$ and *Wt* littermate controls at 8 weeks (A) and 12 weeks (B). Data presented as box and whisker plots demonstrating minimum to maximum weights and horizontal line indicates median weight. Male *Bpifa1*$^{-/-}$ n=4; male *Bpifa1*$^{+/-}$ n=5; male *Wt* n=4; female *Bpifa1*$^{-/-}$ n=4; female *Bpifa1*$^{+/-}$ n=10; female *Wt* n=4. p values for all inter-genotype comparisons analysed using One-way ANOVA with Tukey's posthoc test >0.05

3.2.3 *Bpifa1*$^{-/-}$ mice do not spontaneously develop OM

3.2.3.1 Bpifa1$^{-/-}$ *mice do not demonstrate altered auditory thresholds*

The first test I used to identify whether the loss of *Bpifa1* leads to an OM phenotype, was measurement of the ABR thresholds in 8 week (Fig3.5A) and 12 week old (Fig3.5B) *Bpifa1*$^{-/-}$ mice and their littermate controls. Previous studies in our lab have shown that these time points can be used to accurately identify early onset OM (Hardisty et al 2003, Parkinson et al 2006, Tateossian et al 2013). Hearing thresholds of *Bpifa1*$^{-/-}$ and *Bpifa1*$^{+/-}$ mice were within the normal *Wt* range of 20-30dB and did not differ significantly between the three groups at either time point.

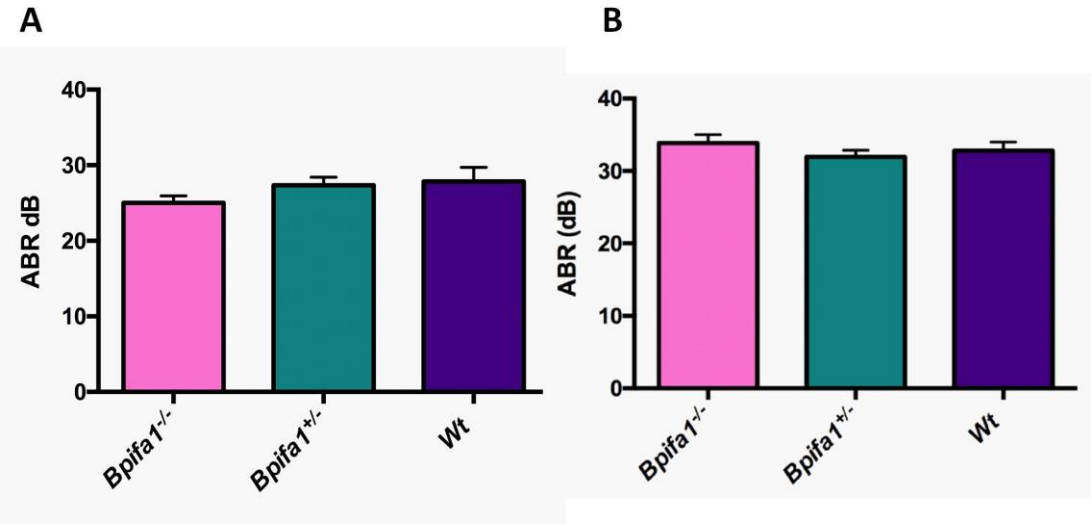

Figure 3.5 Hearing thresholds of *Bpifa1*$^{-/-}$ mice
Hearing thresholds for *Bpifa1*$^{-/-}$ (n=8) and *Bpifa1*$^{+/-}$ (n=15) do not differ significantly from those of *Wt* mice (n=7) at 8 weeks of age (A). Hearing thresholds for *Bpifa1*$^{-/-}$ (n=13) and *Bpifa1*$^{+/-}$ (n=18) do not differ significantly from those of *Wt* mice (n=9) at 12 weeks of age (B). p>0.05 for One-way ANOVA with Tukey's posthoc test.

3.2.3.2 Bpifa1-/- mice do not exhibit histological signs of early OM development

In addition to the ABR measurements, OM phenotype was also evaluated by histological assessment of middle ear sections (Fig 3.6). Deletion of one or both alleles of *Bpifa1* did not lead to any morphological signs of OM development at 12 weeks (n=8). Similar to their *Wt* controls, *Bpifa1* mutants on the C57BL/6-C3H/HeH background demonstrated a thin mucosal epithelium and no middle ear fluid build-up (Fig 3.6A-C). Additionally, no recognizable morphological differences were noted in the nasal passages, trachea and lung, the primary sites of BPIFA1 expression at this age (Fig3.6D-I).

3.2.3.3 Bpifa1$^{-/-}$ *mice do not exhibit histological signs of late onset OM*

Middle ear sections from *Bpifa1*$^{-/-}$ mice aged to 6 months were also examined to identify signs of late onset OM. Out of the 24 middle ears analyzed, 3 had a small amount of

eosinophilic material but lacked any inflammatory cell components in the middle ear cavity. Also, no mucosal thickening was observed in any of the sections assessed (Fig 3.6J). These changes were therefore interpreted as an incidental occurring rather than an OM phenotype. Moreover, no morphological abnormalities were seen in the nasal passages, lungs and trachea at this time point (Fig3.6K-L, Appendix II).

Taken together, my data suggests that ablation of *Bpifa1* does not lead to spontaneous development of OM in naïve mice on the C57BL/6-C3H/HeH genetic background.

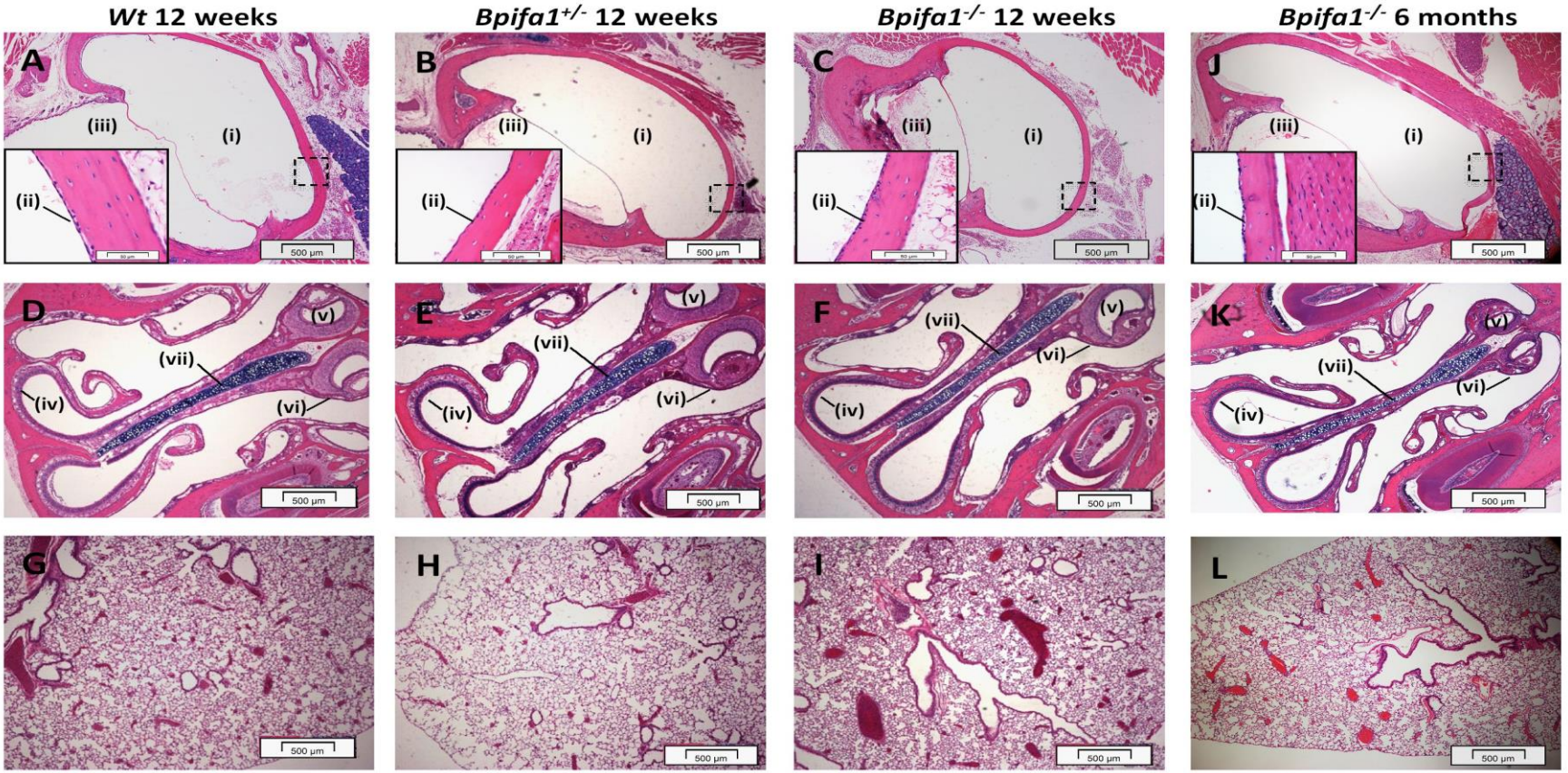

Figure 3.6 Histological analyses of 12 weeks and 6 month old *Bpifa1*$^{-/-}$ mice

H&E sections from middle ear (A-C), rostral nasal passages (D-F) and lung (G-I) from *Wt, Bpifa1*$^{+/-}$ and *Bpifa1*$^{-/-}$ mice show no histological abnormalities at 12 weeks (n=8) of age. H&E sections from middle ear (J), rostral nasal passages (K) and lung (L) from n=13 *Bpifa1*$^{-/-}$ mice show no histological abnormalities at 6 months of age. Middle ear cavity (i); middle ear epithelium (ii); outer ear canal (iii), olfactory epithelium (iv) vomeronasal organ (v); respiratory epithelium (vi); nasal septum (vii). Scale bar 500µm for 4x images and 50µm for 60x images.

3.2.4 Detailed histological analysis of *Bpifa1*$^{-/-}$ mice

Comprehensive histological screening of *Bpifa1*$^{-/-}$ mice at 6 months of age was undertaken by Professor Michael Cheeseman. H&E stained sections from n=13 (9 female and 4 male) mice were analysed to assess the morphology of the major organs including the brain, kidney, liver, spleen, heart, ovaries etc. Appendix II gives the details of the full histology screen. Overall, no major pathological changes were observed in any of the 42 target tissues analysed.

3.2.5 *Bpifa1* mutants do not demonstrate increased nasopharyngeal NT*Hi* carriage

As *Bpifa1* mutants did not develop OM spontaneously, I was interested in studying the effect of *Bpifa1* deletion on the induction of OM by IN inoculation with the otopathogen, NT*Hi*. Mice between 8-10 weeks of age were used for all bacterial challenge experiments.

3.2.5.1 Challenge with NTHi^{162SR}

Initially, *Wt* *Bpifa1*$^{+/-}$ and *Bpifa1*$^{-/-}$ mice on a C57BL/6-C3H/HeH background were baroinoculated with NT*Hi*^{162SR}. The streptomycin resistant version of NT*Hi*^{162} was used in order to avoid overgrowth of *Proteus,* which confounds studies of NT*Hi* growth. *Proteus* is a bacterial species commensal to the nasal passages and is routinely found in a proportion of mice maintained under SPF conditions at MRC Harwell (Fray et al 2008). Theoretically, the baroinoculation method serves to enhance ascending nasal infection into the middle ear (Stol et al 2009). The baroinoculation chamber used in these experiments was built at MRC, Harwell and the methodology was optimised as described in Section 2.13.4. OM induction was assessed on the basis of the appearance of the Tm and presence of middle ear fluids at

day 7-post baroinoculation. Serially diluted middle ear fluids and PBS washes from clear ears were incubated on agar plates to evaluate culture positivity. The sampling time point was selected based on detailed studies performed with *Evi1*$^{Jbo/+}$ mice (Hood et al 2016). Only 2/30 *Bpifa1*$^{-/-}$ ears, and no *Bpifa1*$^{+/-}$ (n= 30) or *Wt (n=30)* ears showed the presence of fluid in the middle ears (Fig 3.7A). 1 of the 2 fluid filled *Bpifa1*$^{-/-}$ ears cultured positive for NT*Hi,* whereas none of the clear washes showed any bacterial growth (Fig 3.7B).

I postulated that the lack of middle ear fluid and bacteria at day 7 was perhaps due to resolution of any infection and perhaps the lack of effectiveness of the baroinnoculation method in these mice. Therefore C57BL/6-C3H/HeH *Wt* (n=5), *Bpifa1*$^{+/-}$ (n=9) and *Bpifa1*$^{-/-}$ (n=10) mice were directly intranasally challenged with NT*Hi*^{162SR} and OM development was assessed after 3 days. However, irrespective of the genotype of the animals, none of the mice in this study showed ear fluids or cultured positive for NT*Hi* (Fig 3.7 C, D).

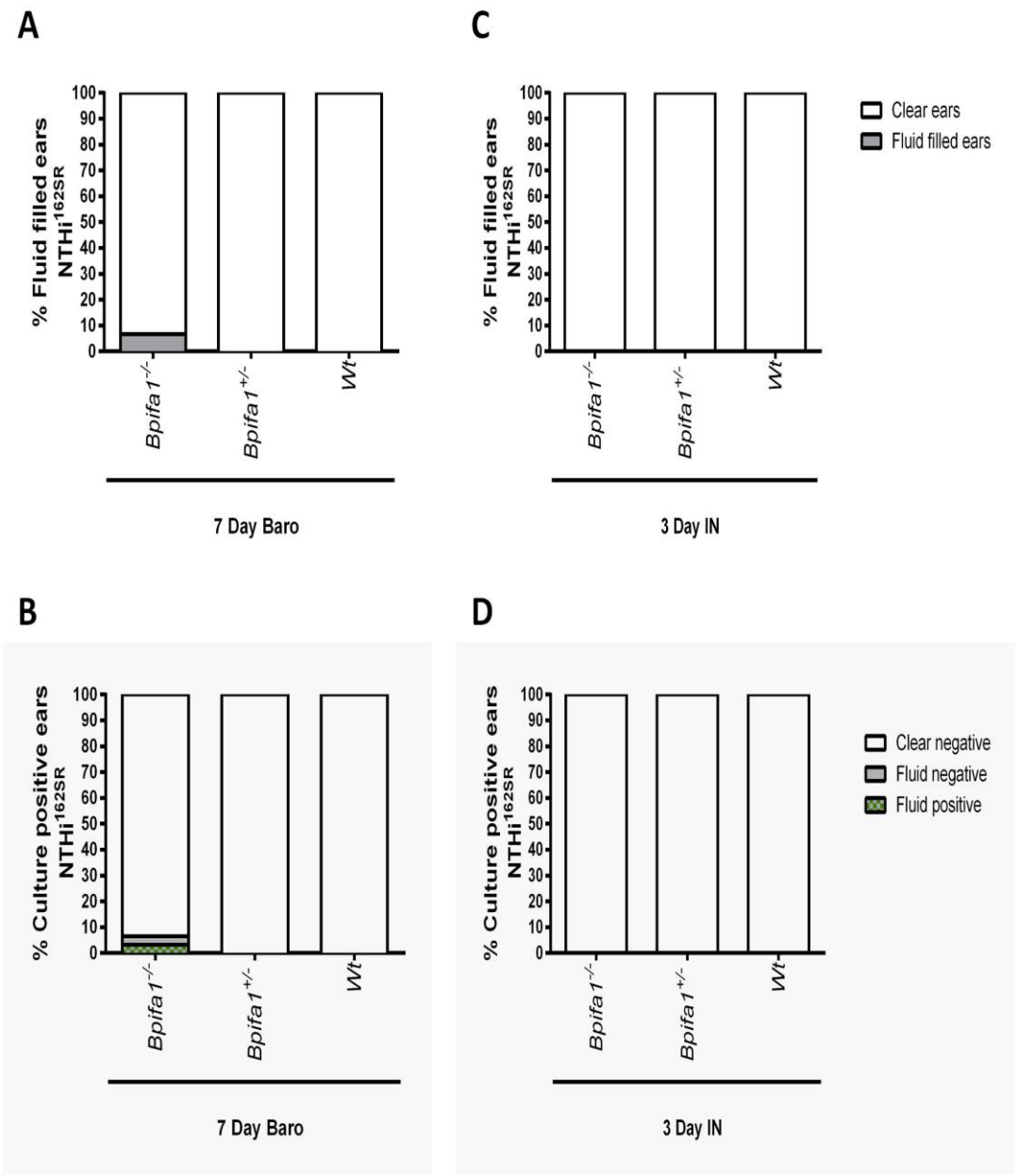

Figure 3.7 Challenge of mice with NT*Hi*^{162SR}

Histograms showing the percentage *Wt*, *Bpifa1*$^{+/-}$ and *Bpifa1*$^{-/-}$ middle ears with fluid build-up (A) and NT*Hi* positive or negative middle ears (B) sampled at day 7-post baroinoculation with NT*Hi*^{162SR}; n=30 for each genotype. None of the Wt (n=5), *Bpifa1*$^{+/-}$ (n=9) and *Bpifa1*$^{-/-}$ (n=10) middle ears showed fluid build-up (C) and NT*Hi* positivity (D) when sampled at day 3-post IN inoculation with NT*Hi*^{162SR}.

3.2.5.2 Challenge with NTHi^{375SR}

Due to the very low efficiency of infection observed with NT*Hi*^{162SR}, mice were challenged with an alternative strain, NT*Hi*^{375SR} which bears a slight modification in the LPS side chain compared to the former. Middle ear fluids were sampled at day 1 and day 3-post IN inoculation and plated to evaluate NT*Hi* growth. To compare efficiency of baroinoclutaion, fluids were also sampled at day 3-post baroinoculation with the same bacterial strain. PBS washes from clear ears were also plated. These earlier time points were chosen to increase the probability of isolating bacteria and observing fluid development in the ears.

Percentage of OM development was measured in terms of the numbers of ears demonstrating fluid build-up (Fig 3.8). At day 1 post IN inoculation, there was no significant difference between the proportions of *Wt* (6/24), *Bpifa1*$^{+/-}$ (4/24) and *Bpifa1*$^{-/-}$ (8/24) ears with middle ear fluids. At day 3 post IN inoculation, 2/12 *Bpifa1*$^{-/-}$ and 2/8 *Bpifa1*$^{+/-}$ ears, but none of the *Wt* ears (0/16) retained the middle ear fluid. Baroinoculation did not show a significant difference between the number of fluid filled *Bpifa1*$^{-/-}$ (6/24), *Bpifa1*$^{+/-}$ (4/20) *Bpifa1*$^{+/-}$ and *Wt* (2/22) ears at day 3.

The percentage of fluid filled ears between the *Wts, Bpifa1*$^{-/-}$ and *Bpifa1*$^{+/-}$ mice did not differ significantly at a particular time point using either inoculation technique (IN or baroinoculation at day 3). However, the decrease in the percentage of fluid filled ears from day 1 to day 3 following IN inoculation (which indicates resolution of OM/ bacterial clearance) was significant in the *Wts* ($p = 0.035$) but not in *Bpifa1*$^{-/-}$ and *Bpifa1*$^{+/-}$ mice.

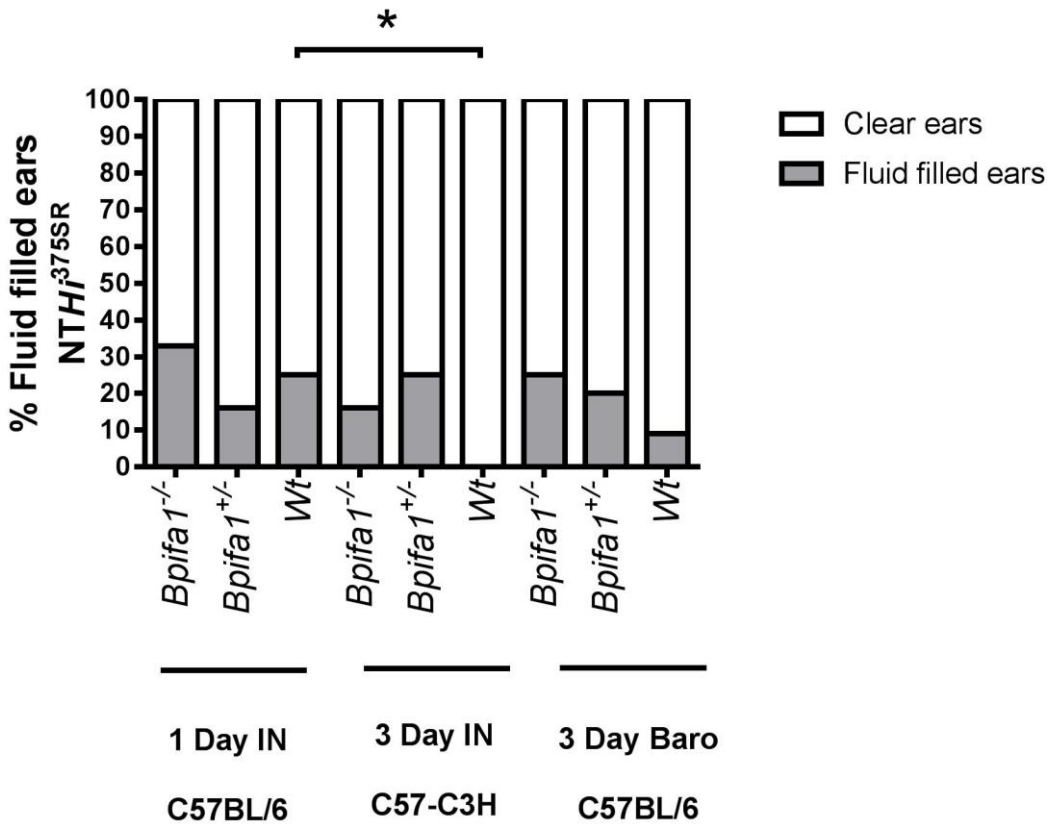

Figure 3.8 Percentage of fluid filled ears on challenge of mice with NT*Hi*^{375SR}
Comparison of the percentage of ears with fluid build-up, sampled at day 1-post IN inoculation (*Wt* n=12, *Bpifa1*$^{+/-}$ n= 12 and *Bpifa1*$^{-/-}$ n=12), day 3 post IN inoculation (*Wt* n=16, mutants, 8 *Bpifa1*$^{+/-}$ n=8 *Bpifa1*$^{-/-}$ n=12) and day 3 post baroinoculation with NT*Hi*^{375SR} (*Wt* n=12, *Bpifa1*$^{+/-}$ n=12, *Bpifa1*$^{-/-}$ n=12). Fishers exact test, *p<0.05

Fig 3.9 describes the percentage of middle ears producing culturable NT*Hi*. At day 1 post IN inoculation 6/24 Wt ears and 4/24 *Bpifa1*$^{-/-}$ ears and 5/24 *Bpifa1*$^{+/-}$ ears cultured positive and these included washes from some clear ears. At day 3, baroincoluation 2/24 *Bpifa1*$^{-/-}$ and 1/20 *Bpifa1*$^{+/-}$ ears were positive. At day 3 post IN inoculations 4/12 *Bpifa1*$^{-/-}$ ears were culture positive of which 2 were washes from clear ears and only 1/8 *Bpifa1*$^{+/-}$ ears was culture positive. However, *Wt* mice never produced culturable NT*Hi* at this time point using either IN or baroinoculation. The number of fluid positive ears positive for NT*Hi* growth was too low to perform a statistical comparison of CFU counts between genotypes.

This data suggests that there was no significant difference in the number of culture positive ears between *Wt, Bpifa1*$^{-/-}$ and *Bpifa1*$^{+/-}$ ears, at a specific time point (at day 1 or day 3 individually) and between the two bacterial challenge methods (IN and baroinoculation at day 3). However, comparison of the two time points after IN inoculation indicated that at day 1 bacteria got into the middle ear cavities of both *Wt* mice and *Bpifa1* deficient mice at similar rates but they were cleared more effectively in *Wts* (p=0.004) than in the *Bpifa1*$^{-/-}$ and *Bpifa1*$^{+/-}$ mice (p>0.05) by day 3.

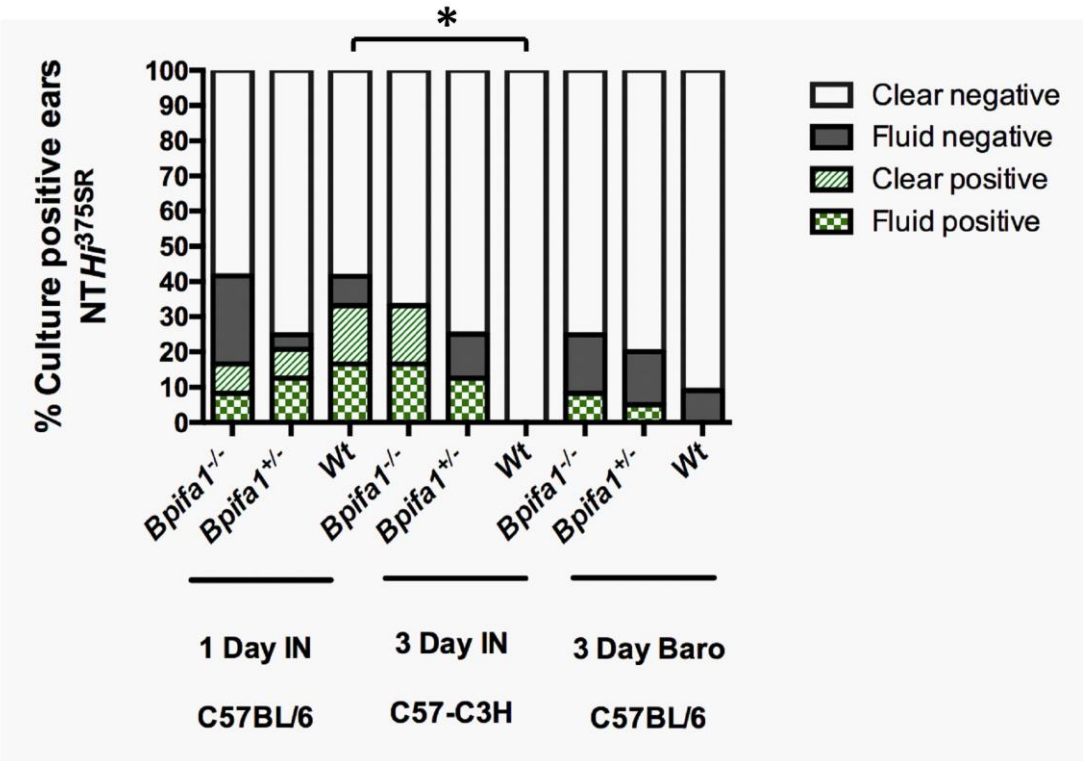

Figure 3.9 Percentage of culture positive ears on challenge of mice with NT*Hi*^{375SR}
Comparison of the percentage ears with culture positivity sampled at day 1-post IN inoculation (n=12 *Wt* , n= 12 *Bpifa1*$^{+/-}$ and n=12 *Bpifa1*$^{-/-}$), day 3 post IN inoculation (n=16 *Wt* n=: 8 *Bpifa1*$^{+/-}$ and n= 12 *Bpifa1*$^{-/-}$) and day 3 post baroinoculation with NT*Hi*^{375SR} (n=12 *Wt* n=12, n=24 n=12 *Bpifa1*$^{+/-}$ n= 2 *Bpifa1*$^{-/-}$). Fishers exact test, *p<0.05

3.3 Discussion:

This chapter describes the *in vivo* effects of *Bpifa1* deletion with regards to spontaneous development of OM in *Bpifa1*$^{-/-}$ mice and induction of OM in *Bpifa1* mutants by intranasal challenge with the human otopathogen, NT*Hi.*

3.3.1 Localisation of BPIFA1 in the developing middle ear

Prior to undertaking this work I had shown that BPIFA1 is produced at high basal levels in the adult middle ear epithelium (Mulay MSc thesis 2011). It was important to identify the point of onset of BPIFA1 expression in the neonatal middle ear. Examination of *Wt* sections of the developing middle ear cavity from P0 to P30 confirmed that the middle ear space is initially filled with a loose mesenchymal material and cavitates around P15. This developmental anatomy has been described previously suggesting that a tubotympanic recess is formed by the extension of the first pharyngeal pouch during gestation (Huangfu & Saunders 1983). The endoderm of the first pharyngeal pouch then breaks down filling the middle ear space with mesenchyme. The mesenchyme may play a role in epithelial differentiation and is slowly resorbed post-natally by day 11 (Huangfu & Saunders 1983, Thompson & Tucker 2013). Intriguingly, I detected BPIFA1 staining in the middle ear epithelial cells and submucosal glands from the day of birth and staining was abundant until the furthest time point which was tested (P56). A previous report has demonstrated that ciliated cells, secretory cells and glands develop in the middle ear space between embryonic day (e)16 -e18, suggesting that the mucociliary defence system is established during foetal growth and ready for use immediately after birth (Lim et al 1973). Interestingly, it has previously been noted that *Bpifa1* gene expression is seen in the mouse nasal passages from e14.5 (LeClair et al 2001, Weston et al 1999) whereas expression in the

respiratory tract begins around the time of birth (LeClair et al 2001). The reasons for these temporal differences in expression are unresolved.

3.3.2 *Bpifa1*$^{-/-}$ mice exhibit no phenotypic abnormalities

The *Bpifa1* gene in mice is 7.3kb in length and is composed of 9 exons (LeClair et al 2001). Previously, two other groups have generated *Bpifa1*$^{-/-}$ mice. One of these is an ENU mutant on a C3HeB/FeJ background, bearing a point mutation in exon 2 of the *Bpifa1* gene (Bartlett et al 2015, Liu et al 2013a); while the other is a deletion mutant on a C57BL/6J background, generated by removal of exons 2-8 (Gally et al 2011). *Bpifa1*$^{-/-}$ mice used for this study were generated by deleting exons 2 and 3.

Bpifa1 expression is highly tissue specific. The nasal passages, oropharynx, trachea and large airways of the lung are the sites of BPIFA1 protein localisation (Bingle & Bingle 2000, Di et al 2003). The previous two studies with *Bpifa1*$^{-/-}$ models did not report abnormalities in the overt appearance and lung histopathology (Gally et al 2011, Liu et al 2013a). *Bpifa1* mRNA has also been reported to be expressed in the kidney and colon, where it has been suggested to play a role in the regulation of ENaC (Garcia-Caballero et al 2009). However reports from several labs including our own have shown that *Bpifa1* is not expressed at these sites in humans or mice (Bingle & Bingle 2000, Gally et al 2011, Liu et al 2013a, Musa et al 2012). A comprehensive histology screen of *Bpifa1*$^{-/-}$ mice at 6 months of age spanning 42 tissues did not detect any specific alterations in the morphology of the major organs, viability, body weights and behaviour. This analysis included both kidney and colon.

3.3.3 Loss of *Bpifa1* does lead to spontaneous development of OM.

In this study the loss of *Bpifa1* did not lead to the development of OM. Deletion of *Bpifa1* had no effect on click ABR thresholds and did not lead to mucosal thickening and middle

ear fluid build-up in 8 and 12-week-old mice, a standard time point used to study OM development (Hardisty et al 2003, Parkinson et al 2006, Tateossian et al 2013). To extend this study further and to look at an age related effect of *Bpifa1* deletion; *Bpifa1*$^{-/-}$ mice were aged to 6 months. Again, comprehensive histological analysis did not uncover evidence of later onset OM. During the course of these investigations, a study was published identifying an increased susceptibility of aged *Bpifa1*$^{-/-}$ mice to OM (Bartlett et al 2015). Although this study differs from my data, there are some key points that must be considered. Firstly, OM being a paediatric disease is typically studied at an early age in mouse models. The *Bpifa1*$^{-/-}$ mice used by the researchers were between 10-18 months of age (Bartlett et al 2015), rather late in the timeline of a paediatric disease. The mice exhibited a low penetrance phenotype with only 30% of the mice developing OM. Secondly; in the study susceptibility to OM was measured on the basis of a histological scoring system suggesting an increased trend in the presence of inflammatory cells and cell debris in the middle ear cavity and thickened mucosa in the *Bpifa1*$^{-/-}$ mice compared to *Wt* mice. However, the number of mice developing overt OM (30%) was not significantly higher compared to *Wt* (5%) mice. Lastly, middle ear fluids from the mice affected with OM did not show presence of bacteria indicating a sterile inflammation. Studies in our lab have shown that *Evi1*$^{Jbo/+}$ mice develop OM spontaneously in germ free conditions (Hood et al 2016), possibly due to allergic response to environmental stimuli such as bedding material. BPIFA1 has been previously implicated in inflammatory responses to airway allergens such as cigarette smoke as well as to sterile carbon nanotubules (Britto & Cohn 2015, Di et al 2013). Therefore, the development of a low penetrance OM phenotype in these mice may be the result of a cumulative effect of loss of *Bpifa1* along with an overall compromised immune response due to increased age, rather than a specific effect of *Bpifa1* deletion alone. Due to lack of time, I was unable to set up more matings to age mice longer than 6 months of age. However, in future, this aspect needs to be explored on further detail.

3.3.4 Intranasal NT*Hi* challenge does not lead to induction of OM in *Bpifa1*$^{-/-}$ mice.

NT*Hi* is a common pathogen, isolated from AOM as well as COME patients (Giebink 1991). This thesis is the first report to investigate the effect of bacterial infection on OM development in *Bpifa1*$^{-/-}$ mice. NT*Hi*^{162SR} and NT*Hi*^{375SR} are clinical isolates from a Finnish pneumococcal vaccine study and differ in the structure of their LPS side-chain structure (Cody et al 2003, Hood et al 1999). A screen of 7 NT*Hi* strains previously performed in our lab, identified NT*Hi*^{162SR} and NT*Hi*^{375SR} as the most efficient strains for intranasal infection of *Evi1*$^{Jbo/+}$ mice. (Hood et al 2016). In this study, challenge with NT*Hi*^{162SR} led to no OM development in *Bpifa1* mutant mice. Infection with NT*Hi*^{375SR} did not lead to a significant difference in the frequency of OM or NT*Hi* positive middle ears between *Wt, Bpifa1*$^{-/-}$ and *Bpifa1*$^{+/-}$ mice at individual time points. However, the percentage of fluid filled ears and NT*Hi* positive ears significantly decreased in the *Wts* from day 1 to day 3 but not in the mutants. The data suggests that bacteria arrived in the middle ear cavities of both *Wt* and *Bpifa1* mutant mice at day 1 leading to fluid build-up, but were cleared more effectively in *Wts* compared to *Bpifa1* mutants. This suggests a diminished resolution of infection in *Bpifa1*$^{-/-}$ mice, perhaps due to dampened mucociliary clearance. Indeed, in vivo downregulation of chinchilla *Bpifa1* using siRNA was shown to alter middle ear pressure and cause ET dysfunction during NT*Hi* induced OM. (McGillivary & Bakaletz 2010). Thus, BPIFA1 may be involved in maintaining the stability of the epithelium through its surfactant properties and its loss may affect mucociliary clearance upon bacterial insult. There was no clear effect of haploinsufficiency of BPIFA1 in the heterozygote mice.

However, it must be noted that this difference in clearance of bacteria between *Wts* and *Bpifa1*$^{-/-}$ mice cannot be conclusively interpreted as biologically significant in this context. This is because mice sampled on day 1-post IN inoculation and on day 3-post

baroinoculation were on a C57BL/6 background, whereas those sampled on day 3-post IN inoculation were on a C57BL/6-C3H/HeH background. It is known that OM phenotype is influenced by background strain (Melhus & Ryan 2003, Tyrer PhD thesis 2013). Therefore, an accurate comparison cannot be made between time points. This discrepancy in genotypes was simply owing to the availability of mice at this early stage in the breeding pipeline. Also, due to the insufficient numbers of culture positive ears for individual genotypes, I could not estimate differences in bacterial titers following infection. The bacterial challenge experiments were performed with a relatively large number of mice (maximum of 12 mice per genotype) because of the low infection rates observed. It was therefore not deemed ethically appropriate to perform more experiments in order to standardize the variables.

The low infection rates in *Bpifa1*$^{-/-}$ mice can be explained based on recent data from our lab showing that the presence of fluid is a prerequisite for bacterial infection of the middle ear. Assessment of OM in a large number of mice at day 7 after NT*Hi* challenge showed that *Wt* mice almost never showed ear fluids and PBS washes from *Wt* middle ears were culture negative. On the other hand, the different mouse models of spontaneous OM, *Evi1*$^{Jbo/+}$, *Fbxo11*$^{Jf/+}$ and *Tgif*$^{-/-}$, all of which show pre-existing inflammation and middle ear fluids facilitated access of NT*Hi* into the middle ears (Hood et al 2016). Also NT*Hi* infection did not alter OM frequency in challenged *Evi1*$^{Jbo/+}$ mice when compared to unchallenged *Evi1*$^{Jbo/+}$mice. The hypoxic, inflamed environment containing suppurative fluid in the middle ears of the OM models, may promote the entry, colonisation and survival of bacteria (Cheeseman et al 2011, Hood et al 2016). This notion is supported by studies which showed that a single dose of intranasally inoculated bacteria did not cause middle ear infection in chinchillas (Bakaletz 2009) and caused only sporadic infection in mice (Ryan et al 2006). However co-infection with respiratory viruses (Bakaletz 2009, Giebink 1981, Short et al 2013) or use of baroinoculation (Giebink et al 1979, Stol et al 2009) promoted middle ear

infection in both species. In this study, an increased effect of baroinoculation on efficiency of NT*Hi* infection was not observed. However, repeated bacterial inoculation or a coincident viral infection in future may provide a more biologically relevant set up to investigate NT*Hi* induced OM development in *Bpifa1*$^{-/-}$ mice.

Another important argument that my observations raise is with respect to the variability in disease susceptibility of *Bpifa1*$^{-/-}$ mice to different NT*Hi* strains with modifications in their LPS structures. BPIFA1 is structurally similar to LBP and BPI, both of which bind LPS. There is conflicting evidence on binding activity of BPIFA1 to LPS, where some studies showed that it bound LPS but others showed that it does not compete for binding with LBP (Ahmad et al 2016, Campos et al 2004, Ning et al 2014, Walton et al 2016). Perhaps a more systematic study to identify the optimal strain for infection would yield higher infection rates.

Analysis of middle ear fluids does not provide information on bacteria associated with the middle ear epithelium. *In vitro* culture of middle ear epithelial cells would enable assessment of a controlled dose of NT*Hi* infection, directly on middle ear cells. It will also help to explore the antimicrobial and immunoregulatory roles of BPIFA1 in further detail. The development of an *in vitro* system of middle ear epithelial cells and its utilisation to study NT*Hi* infection has been described in **Chapter 4.**

Overall, the data from this chapter indicates that loss of *Bpifa1* alone does not increase susceptibility to spontaneous or NT*Hi* induced OM development. However, upon bacterial infection, absence of *Bpifa1* may affect the phenotype of the middle ear epithelium, leading to altered mucociliary clearance and delayed resolution of infection.

3.4 Key experimental conclusions

- BPIFA1 localises to the non-ciliated epithelial cells and sub-mucosal glands in the *Wt* middle ear since the day of birth.
- *Bpifa1*$^{-/-}$ mice exhibit no differences between viability, body weights, morphology and overt phenotype compared to *Wt* mice.
- Loss of *Bpifa1* does not alter the auditory function of *Bpifa1*$^{-/-}$ mice.
- *Bpifa1*$^{-/-}$ mice do not demonstrate histological signs of spontaneous OM development, at least up to 6 months of age.
- Challenge of *Bpifa1*$^{-/-}$ mice with the human otopathogen, NT*Hi* demonstrates a trend towards decreased clearance of bacteria from the middle ear cavity compared to *Wt* mice, suggestive of altered mucociliary clearance. However, deficiency *of Bpifa1* does not increase nasopharyngeal carriage of NT*Hi* and induction of OM.

CHAPTER 4: DEVELOPMENT OF A NOVEL MODEL OF THE MURINE MIDDLE EAR EPITHELIUM AND ITS USE TO STUDY THE EFFECT OF LOSS OF *BPIFA1*

4.1.1 Introduction

The middle ear epithelium is similar to the respiratory epithelium and is composed of ciliated cells, secretory cells, non-secretory cells and basal cells. Secretory cells are responsible for the production of mucins and various anti-microbial proteins such as lactotransferrin, lysozyme, defensins and surfactants (Lim et al 2000, McGuire 2002). The epithelium, along with its secretions, is involved in maintaining homeostasis and sterility within the middle ear cavity. Epithelial remodelling, characterised by mucociliary metaplasia and infiltration of the middle ear cavity with inflammatory cells, is a common feature of OM (Straetemans et al 2001).

In most animals, the middle ear is a relatively inaccessible organ lined by a thin mucociliary epithelium and sampling of the mucosa is a terminal procedure. Human middle ear tissue can be acquired only during surgical procedures and this limits the amount of sample available for study of OM. Culturing of middle ear cells *in vitro* enables maximisation of the available material, allows the effect of modifying culture conditions to be studied more easily and also enables studies of host pathogen interactions. Previously, attempts have been made to culture middle ear epithelial cells from a number of organisms including rats (Toyama et al 2004, Ueyama et al 2001, Vanblitterswijk et al 1986), mice (Tsuchiya et al 2005), chinchillas (Amesara et al 1992, Nakamura et al 1991), gerbils (Herman et al 1992, Portier et al 2005, Takeno 1990), rabbits (Schousboe et al 1995) and humans (Choi et al 2002, Chun et al 2002, Moon et al 2000). These studies have included organ and explant cultures, primary cell cultures and development of middle ear cell lines.

However, there remains a lack of a robust *in vitro* middle ear epithelial model that differentiates into the different epithelial cell types of the middle ear and is free of fibroblast contamination. This has greatly restricted the ability to identify the function of

different cell types and their products within the middle ear and limits our understanding of the pathophysiology of OM.

Pulmonary research has been revolutionised by use of the ALI system for culture of TBE cells. The exposure of apical cell surfaces to air and the supply of nutrients from the basal compartment mimic the *in situ* arrangement and promote maximal differentiation. ALI cultures of TBE cells have been generated from several species (Clarke et al 1992, Davidson et al 2000, Yamaya et al 1992, You et al 2002). More recently, this system has been applied to the culture of murine nasal epithelial cells, recapitulating the characteristics of the respiratory epithelium of the nasal passages (Woodworth et al 2007). Studies employing ALI cultures of TBE and nasal epithelial cells have enhanced our knowledge of airway epithelial biology tremendously, by shedding light on various aspects such as cellular differentiation and secretion, (Kim et al 2000, Pillai et al 2014), cell-cell communication (Yeh et al 2007) inflammatory signalling (Krunkosky et al 2003) and pathogenesis of infections (Kesimer et al 2009, Lopez-Souza et al 2009, Wu et al 2005). Applications of these cultures have furthered our understanding of drug transport and delivery to these sites (Dimova et al 2005, Lee et al 2005), effects of environmental and occupational pollutants (Auger et al 2006, Johnson et al 2007) and genetic disorders such as CF (Matsui et al 1998) and PCD (Hirst et al 2014).

The middle ear epithelium can be considered to be an anatomical extension of these conductive epithelia by the means of the ET. Therefore, using the ALI system I developed a novel *in vitro* model of the murine middle ear epithelial cells, with the view of systematically characterising the different cell types present in the middle ear and studying the effect of loss of *Bpifa1* in culture.

4.1.2 Aims of this study

This chapter addresses two major aims:

1. The foremost aim of this chapter was to develop a novel *in vitro* model of the mouse middle ear epithelium and to methodically characterise the different epithelial sub-populations in the middle ear.
2. The second aim of this chapter was to utilise the model to assess the effect of loss of *Bpifa1* on uninfected middle ear cells and also following infection with NT*Hi*. In Chapter 3, I have shown that intranasal carriage of NT*Hi* is not affected by loss of *Bpifa1*. The goal of this chapter was to identify the more subtle effects of NT*Hi* infection, specifically on the middle ear epithelial cells.

4.1.3 Study design

Figure 4.1 gives a summary of the study design for this chapter. 8- 10 week old *Bpifa1*$^{-/-}$ mice on the C57BL/6J background were used for all experiments in this chapter unless otherwise mentioned. Briefly, an *in vitro* model of primary mouse middle ear epithelial cells (mMECs) was developed using the ALI culture system. Mouse nasal epithelial cells (mNECs) were grown in a similar manner as a comparator due to the similarities between the markers of the URT and middle ear (Section 2.8). Prior to performing any major experiments, culture conditions were optimised and the characteristic features of cell growth were evaluated (Sections 4.2.1 and 4.2.2). For validation of the model and systematic characterisation of cell types, mMECs were compared to native mouse middle ear epithelium using a variety of approaches. Light microscopy and electron microscopy were used for morphological characterisation of mMECs (Section 4.2.3). The expression of a selected panel of known and novel airway epithelial genes was analysed using RT-PCR (Section 4.2.4). MS was employed to perform a global proteomic analysis of the mMEC

secretome. Western blotting and RT-PCR were used to confirm some of the most highly expressed proteins detected by the MS analysis (Section 4.2.5).

The validated model was first utilised to evaluate differences in the expression of selected epithelial markers between uninfected *Wt* and *Bpifa1*$^{-/-}$ cultures (Sections 4.2.8 and 4.2.9). Next, differentiated mMEC cultures were infected with NT*Hi*$^{375SR\text{-}GFP}$, to compare the susceptibility of *Bpifa1*$^{-/-}$ mMECs to *Wt* cells (Sections 4.2.12). Lastly, RT-qPCR was used to study the pleotropic effect of *Bpifa1*$^{-/-}$ deletion on levels of various inflammatory and epithelial markers during the course of infection (Sections 4.2.15).

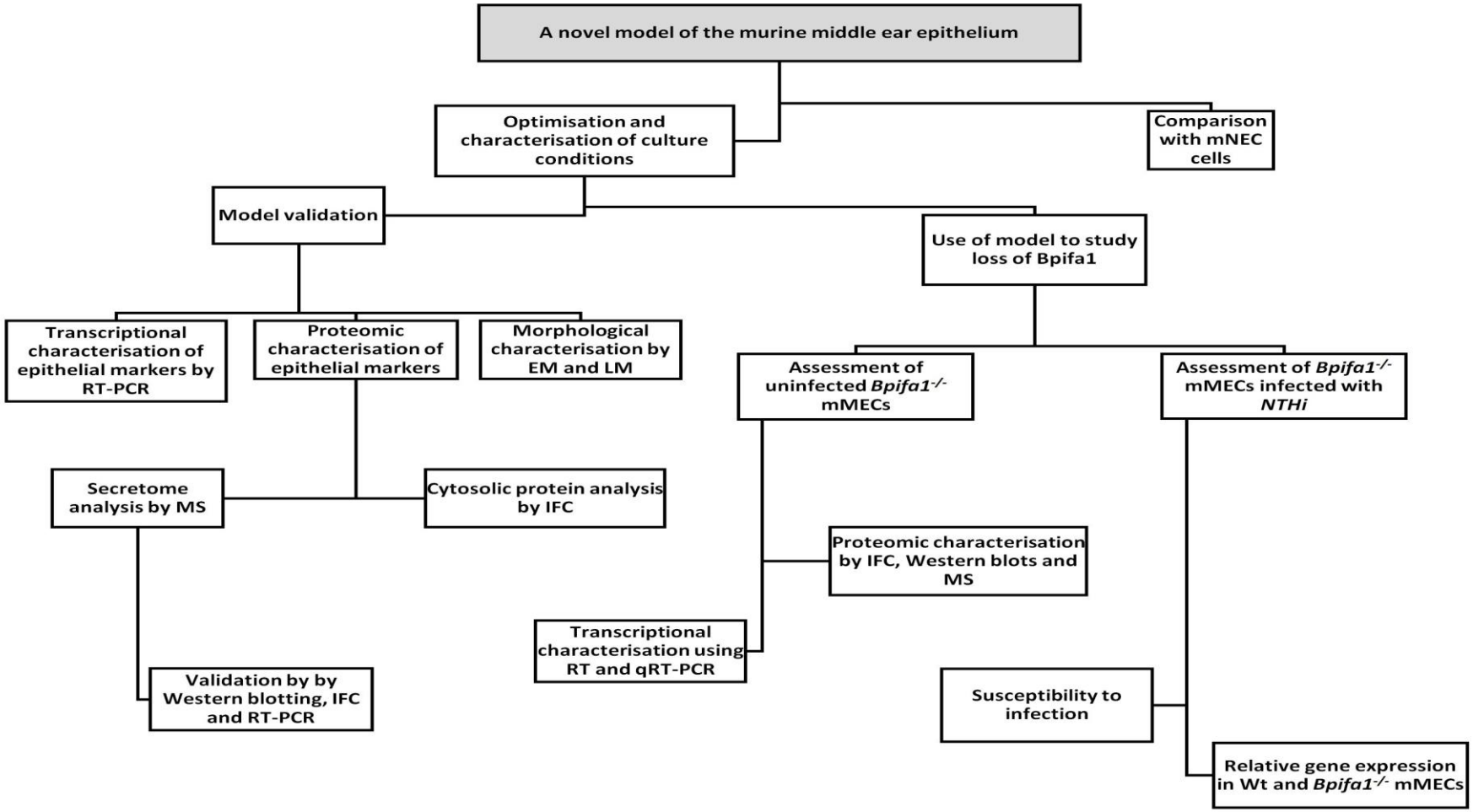

Figure 4.1 Study design for this chapter

4.2 Results

4.2.1 Determination of optimal culture conditions for mMECs and mNECs

Formation of a confluent monolayer during the initial submerged culture is a pre-requisite for establishing an ALI. Hence, I seeded *Wt* mMECs and mNECs at a variety of initial seeding densities. I also tested the effect of addition of ROCKi in order to facilitate the use of the lowest possible seeding density to form a monolayer. In addition, I evaluated the use of plastic and collagen coated semipermeable transwell membranes as grow*t*h substrates for mMECs.

The average number of mMECs isolated was 74,667±10,621/bulla (n=12 *Wt* batches). When grown on plastic (2.5 x10^4 cells/ well), both in absence (Fig 4.2 A) and presence (Fig 4.2 B) of ROCKi, mMECs did not exhibit the typical epithelial morphology in culture, started forming vacuoles, detached from the surface and did not achieve confluence. On transwell membranes, in the absence of ROCKi, at 1 x10^4 cells/ well (Fig 4.2 C) cells grew in small epithelial clusters but did not form a confluent monolayer. At 2 x10^4 cells/ well (Fig4.2 D), a proportion of wells formed a confluent monolayer at submerged Day 15 and at 5 x10^4 cells/well (Fig 4.2 E) cells formed a confluent monolayer around submerged Day 9. By addition of ROCKi, the formation of a confluent monolayer could be achieved within 9 -10 days of seeding at the lower initial seeding densities of 1 x10^4 cells/ well (Fig 4.2 F) and 2 x10^4 cells/ well (fig 4.2 G). A seeding density of 1 x10^4 mMECs/ well (Fig 4.2 F), in presence of ROCKi was selected in order to increase the number of wells from the small number of cells available from the middle ear cavities.

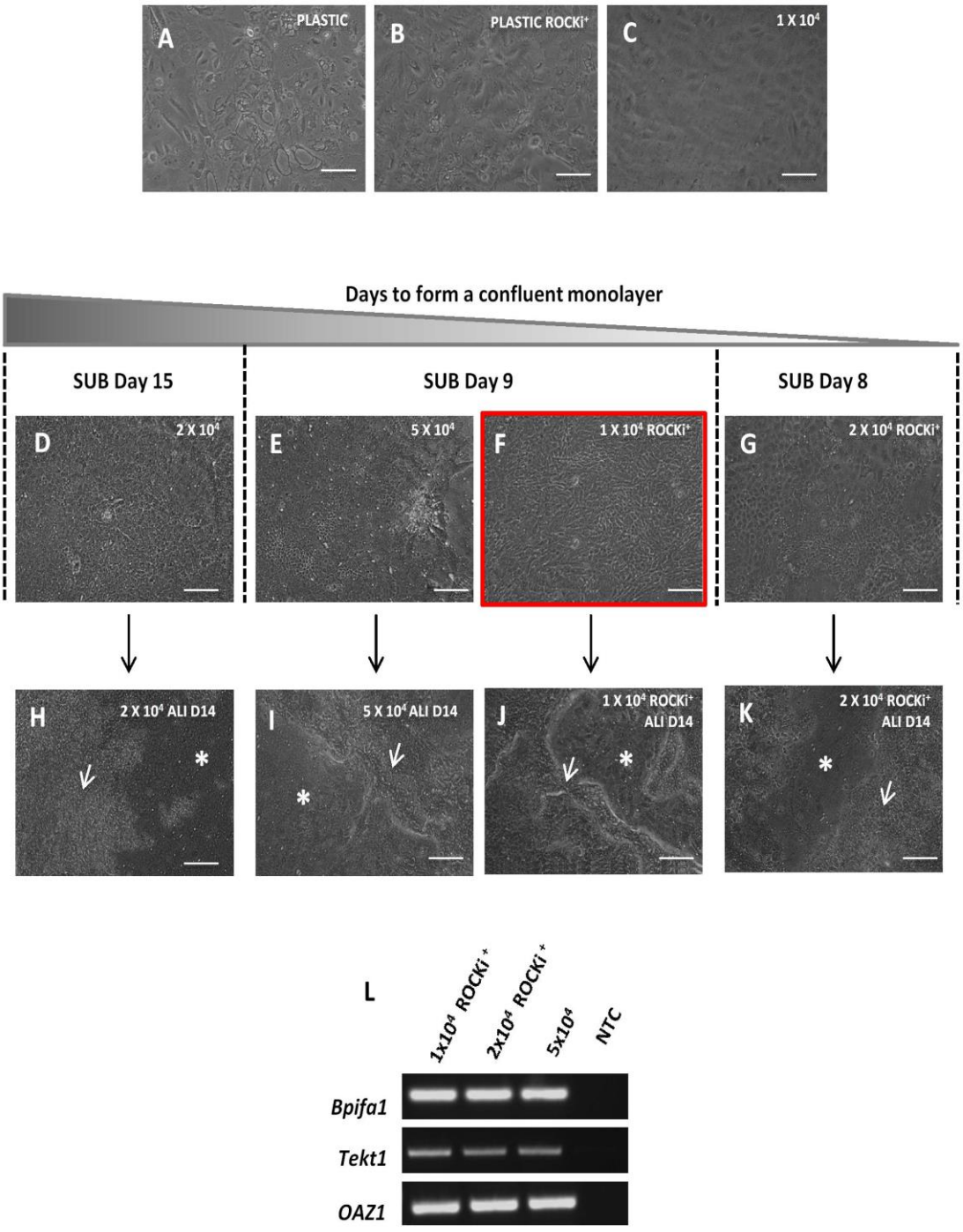

Figure 4.2 Optimisation of seeding density for mMEC culture

Cells did not form a confluent monolayer when grown on plastic, both in absence (A) and presence (B) of ROCKi and on transwell membranes at 1 x10^4 cells in absence of ROCKi (C). The number of days required to confluence when seeded on transwell membranes at initial densities of 2 x10^4 cells (D) and 5 x10^4 cells without ROCKi (E) and at 1x10^4 (F) and 2 x10^4 (G) with ROCKi. Formation of a confluent monolayer led to successful differentiation at ALI and a typical cobbled stone appearance, irrespective of the initial seeding density (H-K). Seeding density of 1 x10^4 cells/ well with ROCKi was selected (red box) Scale bar = 200 µm. White arrowheads indicate elevated clusters of cells with actively beating cilia and asterisk denote flatter polygonal cells. RT PCR of ALI Day 14 mMECs (L), demonstrating that adding ROCKi to the culture medium did not affect differentiation into secretory (*Bpifa1*) and ciliated (*Foxj1*) cell types

The average number of mNECs isolated from nasal cavities (233,517±27,575/NC; n=11 *Wt* batches) was 2.6 times higher than those isolated from nasal septae (88,333±20,000/NS; n=2 *Wt* batches). mNECs were seeded on collagen coated semipermeable transwell membranes. Cells isolated from the nasal septum, seeded at an initial density of 5 $x10^4$ cells/ well in the absence of ROCKi reached confluence at submerged Day 13 (Fig 4.3 A). Cells isolated from the nasal cavity took 10, 6 and 5 days to become confluent, when seeded at 5 $x10^4$ cells/ well (Fig 4.3 C), 1 $x10^5$ cells/ well (Fig 4.3 E) and 2 $x10^5$ cells/ well (Fig 4.3 F) respectively in absence of ROCKi. Addition of ROCKi enabled the formation of a confluent monolayer at submerged Day 7 at a lower initial seeding density of 3 $x10^4$ cells/ well (Fig 4.3 D). This seeding density in the presence of ROCKi was selected for culture of all mNEC batches from nasal cavities.

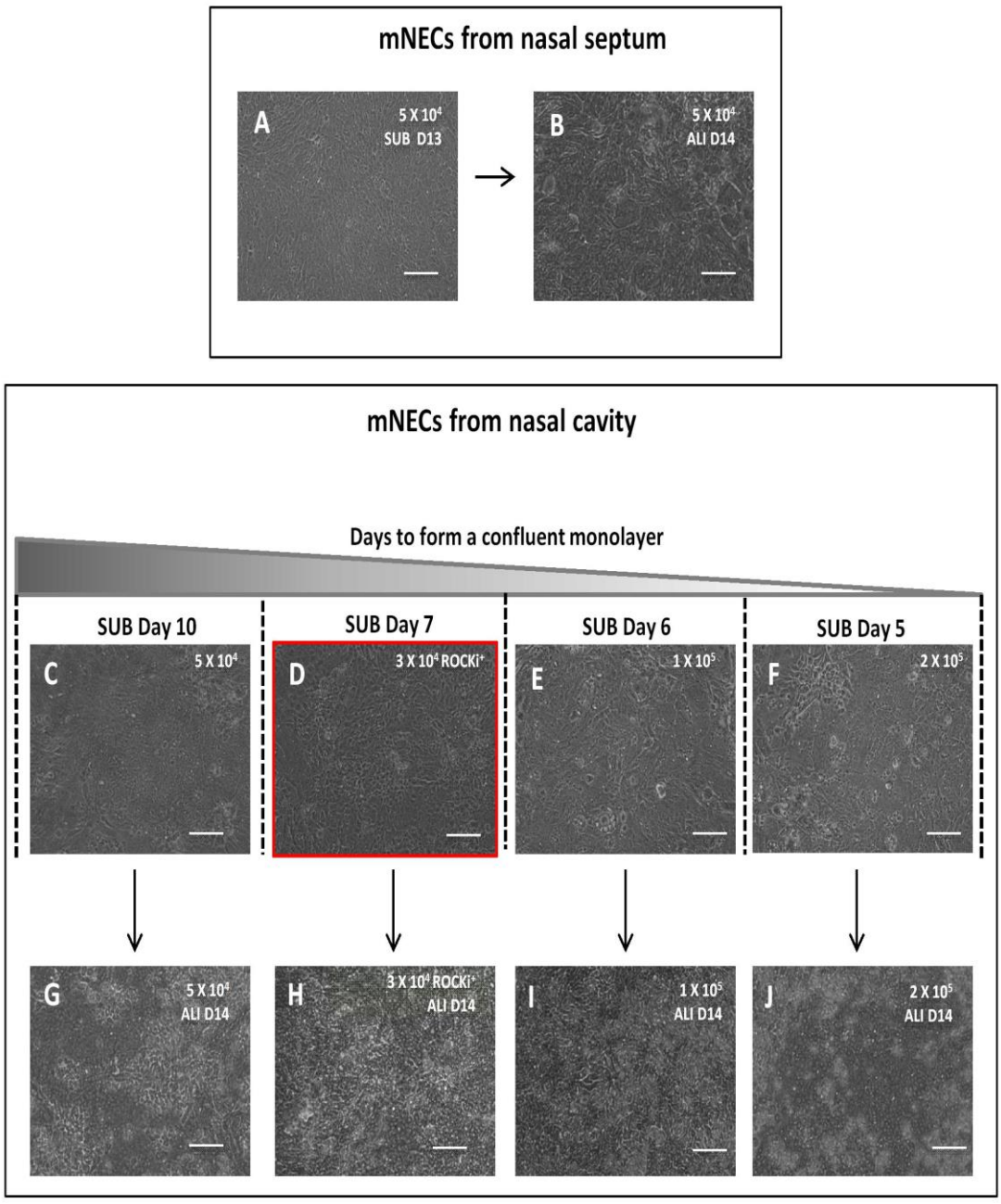

Figure 4.3 Optimisation of seeding density for mNEC culture

mNECs isolated from nasal septum took 13 days to reach confluence and differentiated within 14 days at the ALI (A, B). Number of days required for mNECs from nasal cavity to form a confluent monolayer when seeded on transwell membranes at initial densities of 5 $x10^4$ (C), 1 $x10^5$ cells (E), 2 $x10^5$ (F), without ROCKi and 3 $x10^4$ with ROCKi (D) Formation of a confluent monolayer led to successful differentiation at ALI and a typical cobbled stone appearance, irrespective of the initial seeding density (G-J). Seeding density of $3x10^4$ cells/ well with ROCKi was selected (red box). Scale bar = 200 µm. Cultures were homogenous with evenly distributed, actively beating cilia.

For both mMECs and mNECs, cells forming a confluent monolayer differentiated successfully at ALI and demonstrated a typical cobbled stone appearance, irrespective of the initial seeding density (Figures 4.2 H-K, 4.3 B, and G-J). Addition of ROCKi did not appear to alter differentiation of cells, as demonstrated by Figure 4.2 L

The growth characteristics of cells throughout the culture period are detailed the following section.

4.2.2 Culture characteristics

As described previously (Section 2.8.1.5), primary culture of mMECs and mNECs proceeded in two phases – a proliferative phase in submerged culture and a differentiation phase at air liquid interface (Figure 2.9).

4.2.2.1 Culture characteristics of mMECs

mMECs were seeded at a density of $1x10^4$ cells/ membrane and 3 days after seeding only 16.8±2.6% cells (n=3) adhered to the membrane and had started forming small epithelial islands (Figure 4.4A). The attached cells began to elongate to establish contact with neighbouring cells, and proliferated more rapidly from day 5 to day 7 (Figure 4.4B, C). Cells formed a confluent monolayer of flat, polygonal cells within 9 to 10 days in submerged culture (ALI Day 0) in the presence of ROCKi (Figure 4.4D). The morphology of the cells became more complex when transferred to the ALI. At ALI Day 3, cells started changing in size and shape (Figure 4.4E) and by ALI Day 7 two distinct sub populations of cells could be observed, the majority of which were flat polygonal cells, intersected with clusters of slightly elevated, more compactly arranged cells (Figure 4.4F). Around ALI Day 9, ciliary beating could be seen in these clusters under phase contrast microscope. ALI Day 14 cells ($1.2x10^5$cells/membrane; n=3) displayed a cobble-stone appearance with well-defined cell

boundaries; and were a combination of flat polygonal cells and compactly clustered elevated cells with actively beating ciliated cells. (Figure 4.4G).

There was no noticeable difference between the growth characteristics of *Wt* and *Bpifa1*$^{-/-}$ mMEC cultures (Table 4.1). ALI Day 14 *Bpifa1*$^{-/-}$ mMECs exhibited a similar heterogeneous population of flat polygonal cells and elevated cells with actively beating cilia (Fig 4.4H). No cells with fibroblasts-like morphology were seen in mMEC ALI cultures. However, fibroblasts isolated through the differential adherence treatment during the cell isolation process, were grown separately on plastic culture dishes to obtain pure mouse middle ear fibroblasts (Figure 4.4I), which were later utilised as negative controls for transcriptional analysis of epithelial markers (Section 4.2.4).

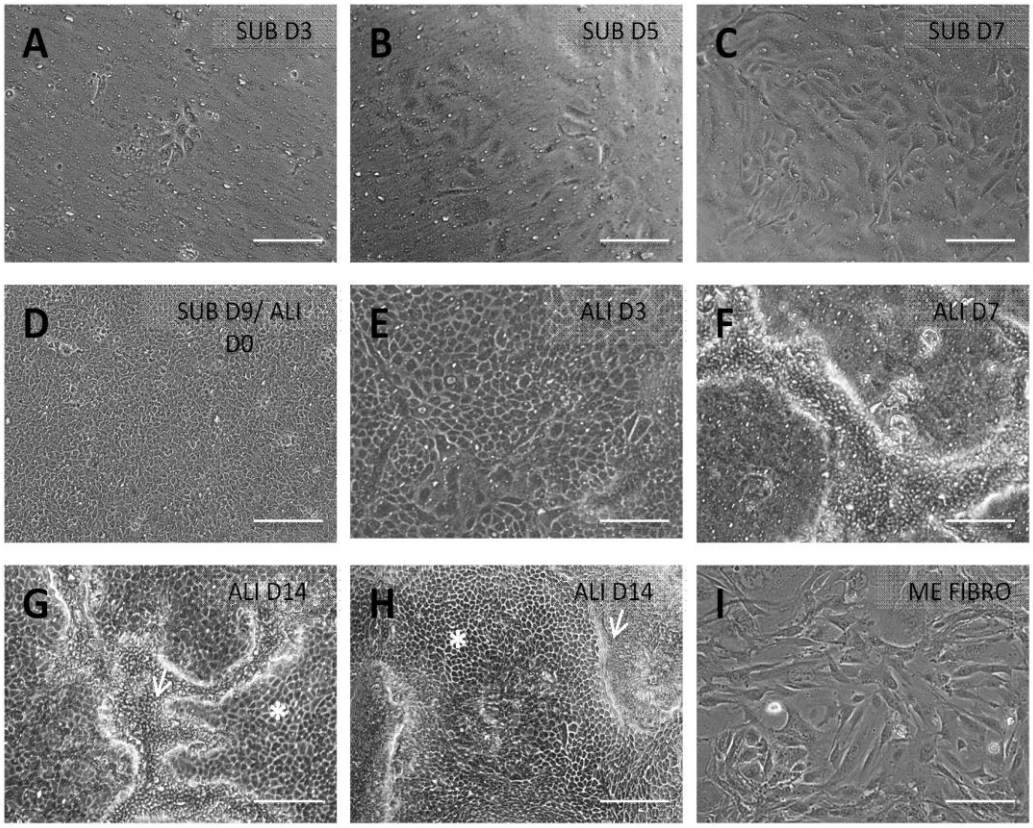

Figure 4.4 Growth characteristics of mMECs in culture.
Phase contrast images showing *Wt* mMECs in culture under 10x magnification (A-G). In the proliferative submerged conditions, a small number of cells attached to form epithelial islands 3 days after seeding (A) The cells proliferated faster from day 5 (B) through day 7 (C) and formed a confluent monolayer at day 9. This was termed as ALI Day 0 (D) Morphology of cells changed from ALI Day 3 (E) and clusters of compactly arranged cells started forming at ALI Day 7 (F). ALI Day 14 cultures were composed of flat polygonal and compactly clustered pseudo stratified cells with active cilia. *Bpifa1*$^{-/-}$ ALI Day 14 mMEC displayed a similar morphology (H). White arrowheads mark elevated ciliated cells and asterisk mark flatter polygonal cells. Fibroblasts cultured on plastic plates through differential adhesion method (I) Scale bar = 200 µm.

4.2.2.1 Culture characteristics of mNECs

mNECs were seeded at a density of 3x10^4 cells/ well in presence of ROCKi. After 3 days in submerged culture, clusters of epithelial cells attached to the membrane were observed (Figure 4.5A). Cells became elongated similar to mMEC cells by day 5 (Figure 4.5B) and rapidly proliferated to form a confluent monolayer of flat polygonal cells by day 7 (ALI Day 0, Figure 4.5C). At ALI Day 3, cells appeared more compactly arranged (Figure 4.4D). Ciliary

movement was detected around ALI Day 7 (Figure 4.5E). Unlike mMECs, ALI Day 14 mNECs ($1.5x10^5$cells/membrane) displayed a homogenous appearance with actively beating ciliated cells, interspersed throughout the culture under phase contrast microscope. Cells were polygonal, with well-defined cell boundaries, displaying a cobble-stone appearance characteristic of epithelial cells (Figure 4.5F). Nasal fibroblasts were cultured through differential adherence (Figure 4.5H).

There was no noticeable alteration in the growth characteristics and appearance of *Bpifa1*$^{-/-}$ mNEC cultures (Figure 4.5G, Table 4.1).

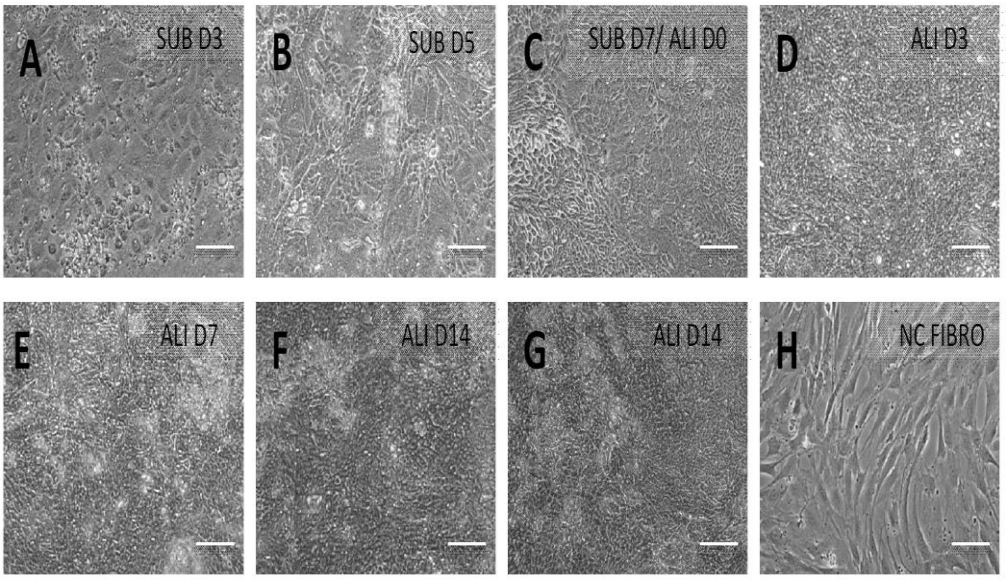

Figure 4.5 Growth characteristics of mNECs in culture.
Phase contrast images showing *Wt* mNECs in culture under 10x magnification (A-F). In the proliferative submerged conditions, a small number of cells attached to form epithelial islands 3 days after seeding (A) The cells proliferated rapidly through day 5 (B) and formed a confluent monolayer at day 9 (C). ALI Day 3 (D) and Day 7 (E) cells were more compactly arranged. ALI Day 14 cultures were composed of a homogenous layer of flat polygonal cells with active cilia (F). *Bpifa1*$^{-/-}$ ALI Day 14 mNEC displayed a similar morphology (G). Scale bar = 200 µm.

Table 4.1 Summary of culture characteristics of mMECs and mNECs

Characteristic feature	*Wt* mMECs n=12	KO mMECs n=8	*WT* mNECs n=11	KO mNECs n=6
No of cells isolated	74667±10621	80127±12439	233517±27574	195214±71773
% Viability of isolated cells before seeding	86.4% (n=3)	90.06% (n=3)	83% (n=3)	88.03% (n=3)
Optimised seeding density	1x 10^4 cells/ well + ROCKi	1x 10^4 cells/ well + ROCKi	3x 10^4 cells/ well + ROCKi	3x 10^4 cells/ well + ROCKi
Confluent monolayer formation	Submerged Day 9/10	Submerged Day 9/10	Submerged Day 7	Submerged Day 7
Ciliated cells appear	ALI Day 9	ALI Day 9	ALI Day 7	ALI Day 7
Cell morphology by LM	Cobbled stone appearance; combination of flat polygonal and tightly clustered elevated cells	Cobbled stone appearance; combination of flat polygonal and tightly clustered elevated cells	Homogenous cobbled-stone appearance	Homogenous cobbled-stone appearance

Following optimisation of seeding densities, I first validated *Wt* mMECs as a suitable model for the study of the cell biology of the middle ear epithelium and host pathogen interactions within the middle ear as described in Sections 4.2.3 to 4.2.7.

4.2.3 mMECs exhibit an epithelial morphology

Electron microscopy imaging of *Wt* ALI Day 14 mMECs revealed a morphology reminiscent of the upper airway epithelium (Figure 4.6). At ALI Day 0 (undifferentiated cells), SEM showed uniformly flat, large cells with microvilli on the apical surfaces (Figure 4.6A). At ALI Day 14, the cells exhibited a dome shaped appearance (Figure 4.6B), areas of flatter polygonal and secretory cells with microvilli on the apical surfaces and areas abundant in ciliated cells (Figure 4.6C). The morphology of the ALI Day 14 mMEC cultures resembled the

in vivo middle ear epithelium (Figure 4.6D). TEM revealed that ALI Day 14 cells were polarized with desmosomes on the baso-lateral surfaces suggesting the formation of tight junctions, another feature of epithelial cells (Figure 4.6E). The formation of tight junctions was further confirmed by uniform expression of zonna occludens, ZO-1 in the cell membrane (Figure 4.6F).

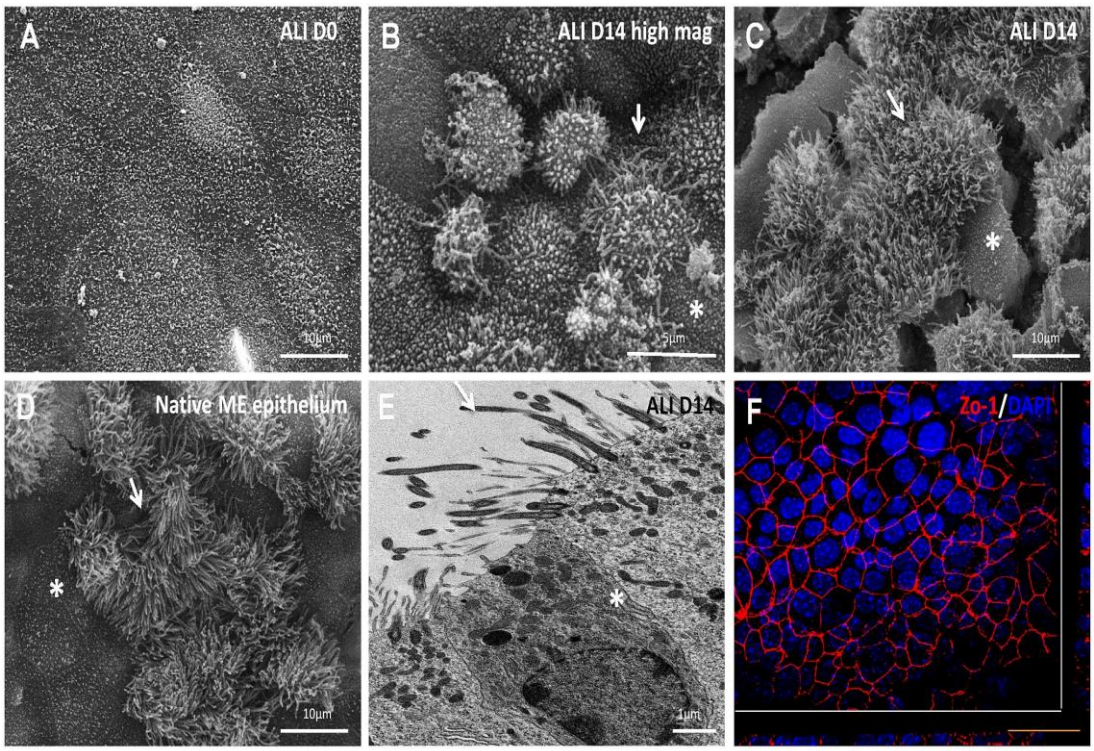

Figure 4.6 Morphology of mMEC cultures.
SEM of ALI Day 0 mMEC cultures showing large flat polygonal cells with apical microvilli (A) ALI Day 14 cultures showing dome shaped cells at higher magnification (B) and combination of interspersed flat polygonal and densely ciliated cell populations (C) resembling the morphology of native middle ear epithelium (D). Cracks in the membrane are due to processing of samples for SEM. White arrowheads mark elevated ciliated cells and asterix mark flatter polygonal cells. TEM of ALI Day 14 mMEC cultures showing adjacent ciliated and secretory cells and formation of tight junctions demonstrated by presence of desmosomes (asterisk). Arrow shows cilia (E). Immunoconfocal microscopy image showing formation of tight junctions marked by ZO1 positive staining. Area beyond white lines indicates a cross section through the membrane. (n=3) Scale bar =10 µm (A, C, D); 5 µm (B); 1 µm (E); 50 µm (F).

4.2.4 Expression of epithelial markers by *Wt* mMEC cultures

The expression of a selected panel of genes, known to be expressed by the middle ear epithelium and upper airways was assessed by RT- PCR of RNA from the original *Wt* mMECs before seeding (mMEC original) and compared to ALI Days 0 and 14 mMEC cells. Fibroblasts isolated by differential adherence were used as a negative control for epithelial markers (Figure 4.7A). *Bpifa1* was expressed strongly in the original and ALI Day 14 cells, but was lower in the undifferentiated ALI Day 0 cells. *Bpifb1* was detected only in the original cells, not in cultured cells. *Tekt1* (a marker of ciliated cells) was detected at ALI Day 14. Analysis of *Muc5ac* and *Muc5b* expression, markers of goblet cells, suggested that *Muc5ac* was weakly expressed in mMEC original cells but was not detectable in the cultured cells, whereas Muc5b was expressed more strongly in the original cells and maintained this expression to ALI Day 14. I also studied the mucosal innate immune genes *Lactotransferrin, Surfactant protein D (Stfpd)* and *Regenerating islet-derived protein 3 gamma (Reg3$^{\gamma}$),* which were identified through a proteomic study of the mMEC secretome, mentioned later in Section 4.2.5. *Lactotransferrin* and *Reg3$^{\gamma}$* were detected in the mMEC original cells and at ALI Days 0 and 14, whereas expression of *Stfpd* was seen in the cells during ALI differentiation. As expected, the expression of *Keratin5*, a marker of basal cells, was reduced as cells differentiated from ALI Day 0 to Day 14. The expression of these epithelial markers in the mMEC cultures indicated that the cells differentiated in culture from ALI Day 0 to ALI Day 14 and the pattern of expression in the differentiated cells was in line with that seen in the mMEC original cells isolated from the middle ear. *Vimentin* is a marker of fibroblasts and other mesenchymal cell types. The absence of *Vimentin* in ALI Day 14 cultures indicates that the mMEC cultures are devoid of potential fibroblast contamination. *Oaz1* was used as a housekeeping gene for all RT-PCR experiments.

4.2.5 Apical secretome of *Wt* mMECs

To complement the gene expression studies, I also performed a global proteomic analysis of apical ALI Day 14 secretions of *Wt* mMECs by Orbitrap MS. Table 4.2 lists the most abundant secreted proteins identified classified according to their emPAI score, which is the ratio of the number of peptides found for a protein divided by the predicted number of peptides that could be potentially seen in the sample. The most abundant secreted protein was Lactotransferrin, with Serotransferrin, Reg3$^{\gamma}$, Lipocalin2, Ceruloplasmin and BPIFA1 also being found at high levels. Multiple anti-proteinase and proteinase proteins were also found in the secretions including members of the WAP four-disulfide core domain protein (WFDC) family, WFDC2, SLPI (WFDC4) and WFDC18 (EXPI) as well as multiple cathepsins. I validated the secretion of BPIFA1, Lactotransferrin and Reg3$^{\gamma}$ in the apical washes from the differentiating mMEC cells using western blotting (Fig. 4.7 B, C, D). The list of top 500 proteins identified is given in Appendix III, Table S5.

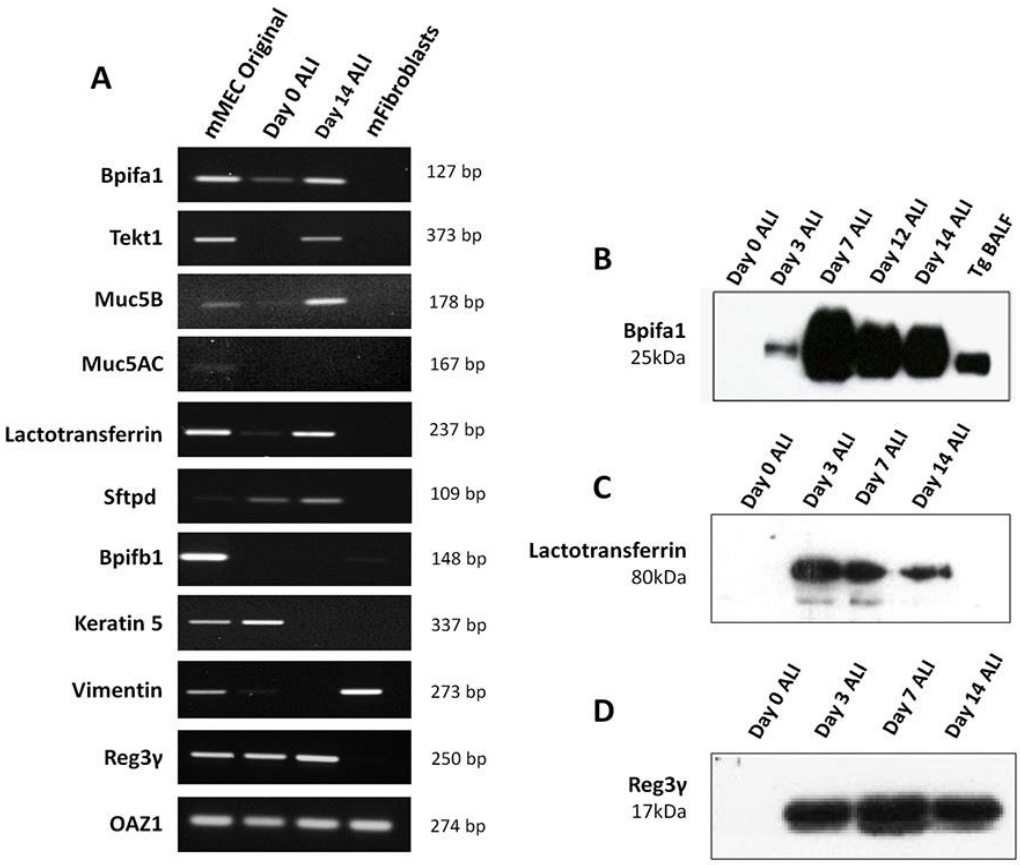

Figure 4.7 Expression of epithelial markers in mMEC cultures
End-point RT-PCR showing expression of a selected panel of upper airway associated genes in mMEC original cells isolated from the middle ear cavity, ALI D0 cells and ALI D14 cells. Expression profile of ALI Day 14 cells was similar to mMEC original cells isolated from the middle ear for most genes (A). Detection of BPIFA1 (B), Lactotransferrin (C) and Reg3Ɣ (D) in the apical washes from differentiating cells using the western blotting technique. Data is representative of results from three independent cultures.

Table 4.2: Most abundant secreted proteins identified in apical ALI Day 14 washes from *Wt* mMEC cultures

Accession Number	Protein	Peptide count	emPAI Score	Biological reference
P08071	Lactotransferrin	47	202.53	Anti-microbial iron chelation
Q921I1	Serotransferrin	40	29.58	Iron chelation, cell proliferation
O09049	Regenerating islet-derived protein 3-gamma	8	11.38	Anti-microbial
P11672	Neutrophil gelatinase-associated lipocalin	9	10.45	Iron trafficking, innate immunity
Q61147	Ceruloplasmin	55	10.1	Copper transport, antioxidant defense
P97361	BPI fold-containing family A member 1	9	4.74	Suggested role in innate immunity
P01027	Complement C3	111	4.68	Activates complement system
P06797	Cathepsin L1	12	3.11	Lysosomal protein degradation
Q61805	Lipopolysaccharide-binding protein	19	2.96	Antimicrobial activity through bacterial LPS binding
P10605	Cathepsin B	15	2.47	Intracellular protein degradation and turnover
Q61362	Chitinase-3-like protein 1	22	2.16	Tissue remodeling in response to environmental stress, activation of NfκB signaling pathway
P25785	Metalloproteinase inhibitor 2	14	2.08	Inactivates metalloenzymes
Q9CQV3	Serpin B11	24	1.97	Serine protease inhibitor
P18242	Cathepsin D	20	1.67	Intracellular protein breakdown
O88312	Anterior gradient protein 2 homolog	10	1.53	Regulates giblet cell differentiation and mucous secretion.
P50404	Pulmonary surfactant-associated protein D	23	1.5	Innate immunity response, respiratory gaseous exchange and homeostasis
P10810	Monocyte differentiation antigen CD14	16	1.41	TLR2 mediated innate immune and inflammatory response to bacterial LPS in concert with LBP
Q62426	Cystatin-B	6	1.24	Proteinase inhibitor
Q9ER10	Brain-specific serine protease 4	15	1.11	Protease activity
P08905	Lysozyme	10	1.05	Bacteriolytic activity
Q9DAU7	WAP four-disulfide core domain protein 2	6	0.91	Protease inhibitor
P11214	Tissue-type plasminogen activator	31	0.89	Tissue remodeling, cell migration
Q9WUU7	Cathepsin Z	14	0.89	Peptidase activity
O88593	Peptidoglycan recognition protein 1	10	0.81	Triggers apoptosis of Gram positive bacteria
Q60854	Serpin B6	23	0.81	Regulation of serine proteases
P34884	Macrophage migration inhibitory factor	5	0.61	Pro inflammatory cytokine involved in regulation o macrophage activity
Q9R118	Serine protease HTRA1	21	0.54	Cell proliferation and viral response
P12032	Metalloproteinase inhibitor 1	12	0.49	Cell differentiation and wound healing
P97430	Antileukoproteinase	11	0.49	Anti microbial host defense
P61939	Thyroxine-binding globulin	22	0.4	Thyroid hormone transport

P25085	Interleukin-1 receptor antagonist protein	7	0.35	Inhibits IL-1 activity
P70124	Serpin B5	22	0.35	Morphogenesis of epithelium
Q61703	Inter-alpha-trypsin inhibitor heavy chain H2	48	0.24	Hyaluronan metabolic process
P97290	Plasma protease C1 inhibitor	25	0.12	Blood coagulation, complement activation.

NB- Accession numbers and biological functions from the UniProt database

4.2.6 Cytosolic localisation of epithelial markers in *Wt* mMEC cultures

I used IFC microscopy to study the localisation of epithelial markers in *Wt* ALI Day 0 and ALI Day 14 cultures, in order confirm the differentiation process at the protein level. ALI Day 0 cultures showed abundant expression of transformation-related protein 63, p63 (basal cell marker), scanty expression of BPIFA1 (Figure 4.8A) and no expression of FOXJ1 (ciliated cells) and MUC5B (goblet cells) (Figure 4.8C). However, by ALI Day 14, the cells had differentiated into multiple cell types and expressed high levels of BPIFA1, reduced levels of p63 (Figure 4.8B) and were populated with ciliated and goblet cells (Figure 4.8D). BPIFA1 was localised to the non-ciliated population in differentiated mMECs, consistent with that seen in the *in vivo* middle ear epithelium (Section 3.2.2; Fig 3.3). In keeping with proteomic and RT-PCR data, I also detected abundant cytosolic staining of Lactotransferrin and Reg3$^{\gamma}$ in the ALI Day 14 cultures (Figures 4.8E, F). Staining of nuclei with DAPI and Z-slice imaging using confocal microscopy also demonstrated that the cells formed a flat monolayer at ALI Day 0, but showed a more complex reorganisation by ALI Day14 with a combination of flat and elevated cells showing 2 or 3 different layers, with nuclei further away from the base of the membrane (Figures 4.8G, H).

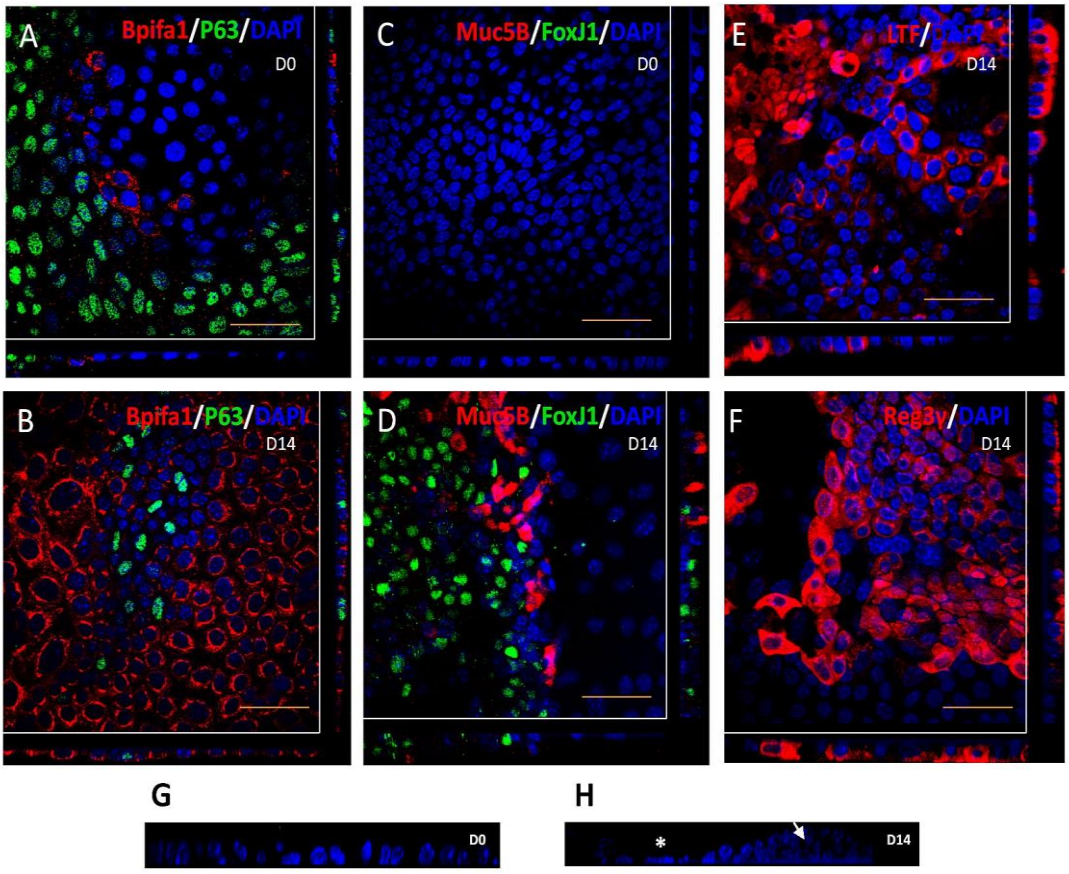

Figure 4.8 Localisation of epithelial markers in *Wt* mMEC cultures.
Immunofluorescence confocal images (representative of three independent batches) showing abundant expression of the basal cell marker, P63; limited expression of the secretory protein, BPIFA1 (A), no expression of goblet cell marker, MUC5B and the ciliated marker, FOXJ1 (C) in undifferentiated ALI Day 0 mMEC cultures (A and C). Differentiated mMEC ALI Day 14 (B, D, E, F) cultures showing expression of secretory cells positive for BPIFA1 (B), Lactotransferrin (E), Reg3γ (F), goblet cells positive for Muc5B and ciliated cells positive for FoxJ1 (D). Area beyond white lines indicates a cross section through the membrane. High magnification Z-stack cross sections of nuclei stained with DAPI shows that ALI Day 0 cells form a flat monolayer (G) whereas ALI Day 14 cells are a combination of pseudostratified elevated cells (arrowheads) and flatter cells (asterisk) (H). Scale bar =50µm.

4.2.7 Relative abundance of secretory, goblet and ciliated cells

mMEC cultures displayed a heterogeneous distribution of BPIFA1 positive cells and FOXJ1 positive ciliated cells. Staining for BPIFA1 was abundant in the cultures, whereas ciliated cells appeared in smaller clusters. Low powered phase contrast microscopy (Fig 4.9A) and SEM (Fig 4.9B) of mMEC cultures demonstrated that the ALI Day 14 cultures were composed of distinct anatomical areas of flat polygonal cells and patches of more elevated pseudostratified cells. I further analysed the localisation of secretory, goblet and ciliated

markers within the two regions of this cellular morphology. FOXJ1 positive ciliated cells and MUC5B positive goblet cells, were restricted to the elevated pseudostratified cell clusters, whilst BPIFA1 was more commonly seen in the flatter cells, although some staining was seen in the elevated cells, especially near the periphery (Fig. 4.9C, D). This was consistent with the observation that ciliated cells could be seen beating in the elevated clusters of cells under light microscopy. I also confirmed BPIFA1 and MUC5B positive cells were not ciliated (Fig. 4.9E, F).

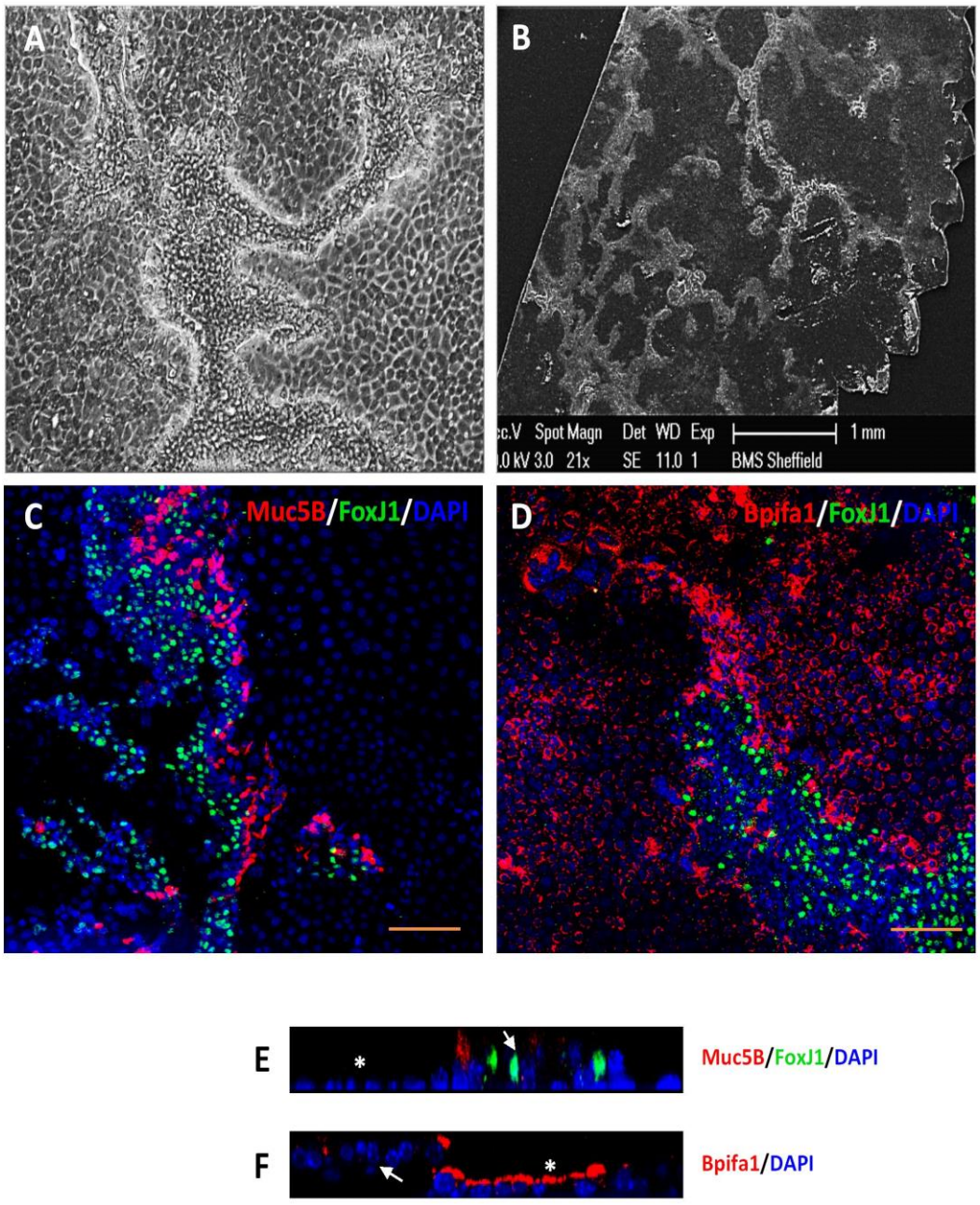

Figure 4.9 Distribution of cell types in mMEC cultures.
Phase contrast image at 10x magnification (A) and very low powered SEM image (B) reveal that ALI Day 14 mMEC cultured are composed of regions of flat and elevated cells. Immunofluorescence confocal images showing a similar pattern of flat cells elevated clusters cells at slightly different foci. Ciliated cells (FOXJ1) do not co-localise with and goblet cells (MUC5B) (C) and BPIFA1 expressing cells (D) High magnification (60x) cross section Z-stack confocal images showing that FOXJ1 and MUC5B expression is mostly restricted to the elevated cell types (arrowheads) (E) and BPIFA1 is predominantly expressed by flatter cells (asterisk) (F) Scale bar = 200µm (A) 100µm (C,D) 50µm (E,F). Images representative of 3 independent batches.

The native middle ear epithelium showed tracts of dense cilia near the ET (Figure 4.10A). The central part of the bulla however exhibited a combination of areas of ciliated clusters and non-ciliated cells and regions of only flat non-ciliated polygonal cells (Figure 4.10B, C), much like that shown for mMEC cultures previously (Fig 4.6B, C).

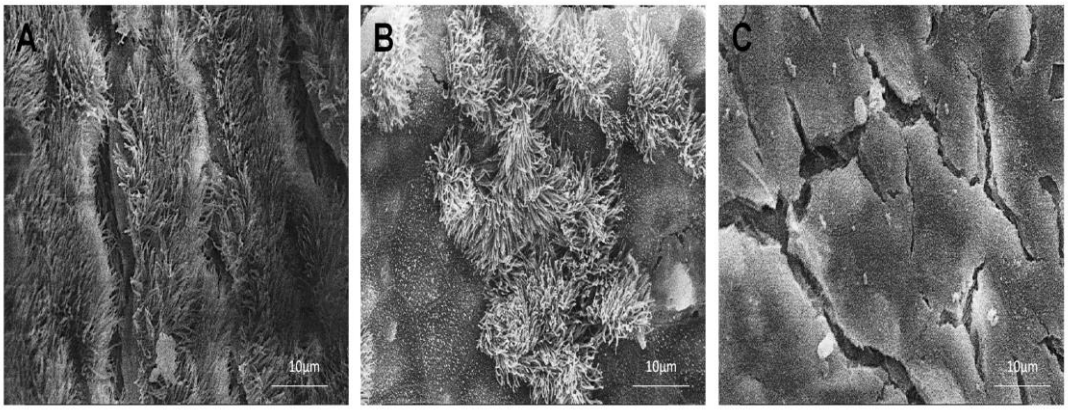

Figure 4.10 Distribution of ciliated cells in *WT* native mouse middle ear cavity
SEM images showing the distribution of ciliated cells in various parts of the native *Wt* middle ear cavity. Areas near the Eustachian tube were lined with tracts of dense ciliated cells (A). The central part of the middle consists of flat polygonal cells interspersed with clusters of short and long ciliated cells (B), similar to what is seen in mMEC cultures. Areas towards the Tm exhibit patches similar to central part of the middle ear as well as larger patches of flat polygonal cells with apical microvilli (C). Scale bar = 10 µm

The next step following the development of a model that mimicked the *in vivo* middle ear epithelium and the characterisation of the epithelial sub-populations in the middle ear was in order to utilise the mMEC culture system to evaluate the effect of *Bpifa1* deletion.

4.2.8 *Bpifa1*$^{-/-}$ mMECs retain the expression profile of epithelial markers

Using RT-PCR, expression of a subset of epithelial markers identified in (Section 4.2.4) was compared between three independent batches of *Wt* and *Bpifa1*$^{-/-}$ mMECs, at regular time points during differentiation. The rationale behind this experiment was to analyse the regulation of these genes from ALI Day 0 to 14, as well as to assess the result of loss of

Bpifa1 on expression of other epithelial markers. The genes selected for comparison included *Bpifa1* (secretory marker and the gene of interest), *Tekt1* (a ciliated marker) and *Muc5b* and *Muc5ac* (goblet cell markers). *Bpifa1* was either faintly detectable in *Wt* mMECs at ALI Day 0 as shown earlier in Fig 4.7A or at ALI Day 3 (Fig 4.11A). In both *Wt* and *Bpifa1*$^{-/-}$ mMEC cultures, *Muc5b* and *Tekt1* expression was switched on at ALI Day 3 and continued throughout the differentiation period, up to ALI Day 14. *Muc5ac* was faintly detected in the original cells and could not be detected at ALI Day 14 by using this technique (as also seen before in Fig 4.7A), but was detectable at ALI Day 7 (Fig 4.11A). Batch to batch variation in the intensity of gene expression was noticed at various time points for *Wt* as well as *Bpifa1*$^{-/-}$ mMECs. This inconsistency among batches may be indicative of the variability in the composition of cell types in the cultures.

IFC microscopy of ALI Day 0 and Day 14 *Bpifa1*$^{-/-}$ *mMECs* indicated successful differentiation of cells at the proteomic level. Ciliated cells (FOXJ1) and goblet cells (MUC5B) were absent in the undifferentiated cells at ALI Day 0 (Fig 4.11C, E), but seen in clusters in differentiated ALI Day 14 cells (Fig 4.11D, F). This heterogeneous pattern of localisation was similar to that described previously for the *Wt* mMECs (Section 4.2.6, Fig 4.8). Absence of secreted and cytosolic BPIFA1 confirmed effective deletion of the gene (Fig 4.11B, D)

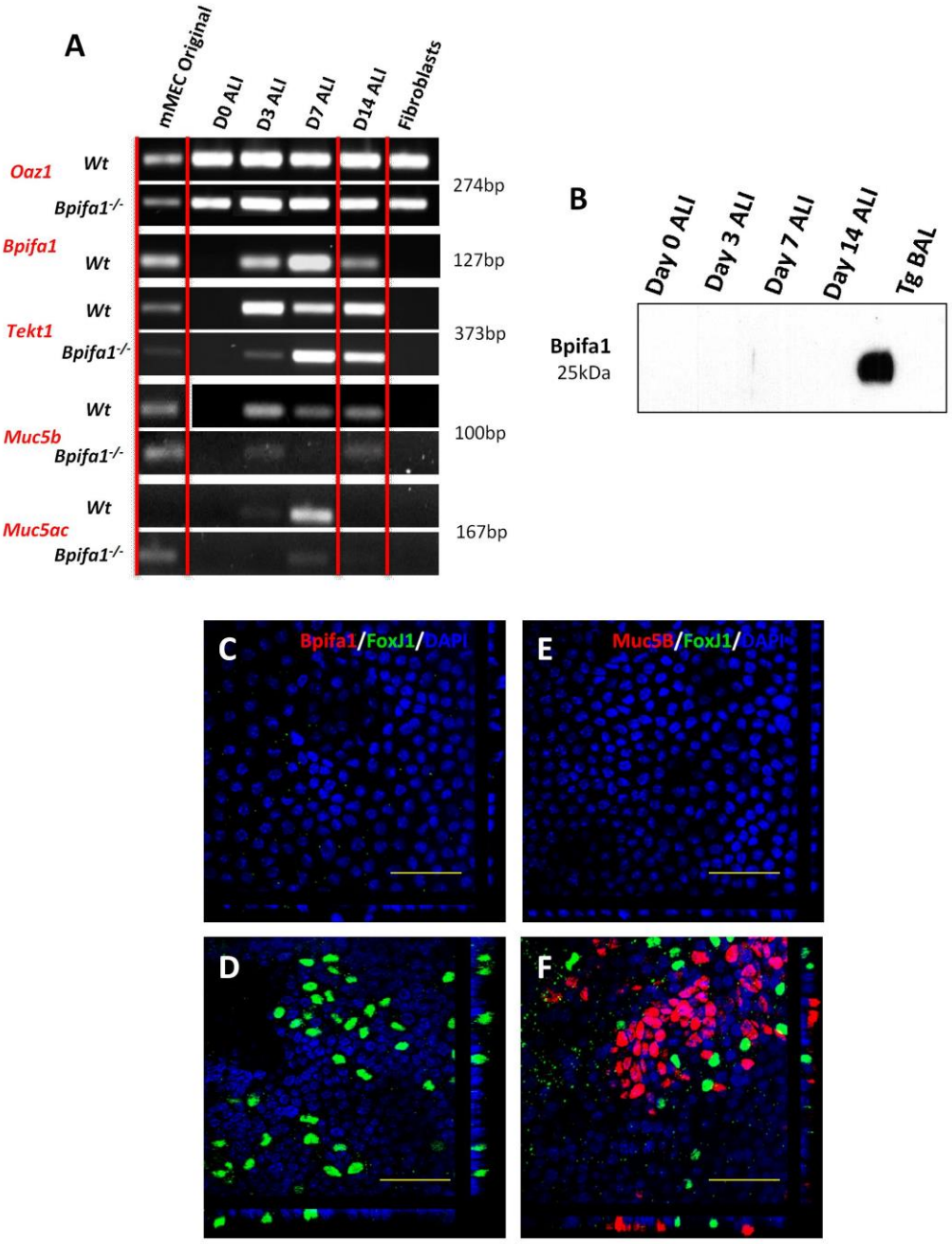

Figure 4.11 Pattern of expression of epithelial markers by *Bpifa1*$^{-/-}$ *mMECs*
End-point RT-PCR comparing expression of selected secretory, mucin and ciliated cell genes between *Wt* and *Bpifa1*$^{-/-}$ *mMECs.* Expression profile of ALI Day 14 cells was similar to mMEC original cells for most genes (A). Absence of BPIFA1 in apical washes from differentiating *Bpifa1*$^{-/-}$ *mMECs* using western blotting technique when compared with transgenic BAL fluid from mice overexpressing BPIFA1 as a positive control (B). IFC images showing no staining of BPIFA1, MUC5B and FOXJ1 in undifferentiated ALI Day 0 *Bpifa1*$^{-/-}$ mMEC cultures (C, E). Differentiated mMEC ALI Day 14 *Bpifa1*$^{-/-}$ (D, F) cultures showing staining of FOXJ1 and MUC5B indicating successful differentiation but no staining of BPIFA1 indicating successful gene knockout (D). Scale bar =50µm. Data are representative of 3 independent batches of culture.

4.2.9 *Bpifa1* deletion does not affect mRNA levels of other epithelial markers in differentiated mMEC cultures

Variability in expression of epithelial genes across batches made it difficult to compare differences in expression between *Wt* and *Bpifa1*$^{-/-}$ mMECs using endpoint RT-PCR (Section 4.2.8). To account for this and to detect lowly expressed genes such as *Muc5ac* with greater efficiency, quantification of epithelial gene expression at ALI Day 14 in *Wt* and *Bpifa1*$^{-/-}$ mMEC cultures was performed using RT-qPCR. Expression of target genes was normalized against three endogenous controls; *Atp5b, Ppia* and *Cyc1,* identified as the most stable controls for this experiments using the geNORM assay (Section 2.19.4). Data are presented as mean RQ± $RQ_{min/max}$ quantified by the ABI software.

Bpifa1 deletion could be confirmed in *Bpifa1*$^{-/-}$ mMECs by average down regulation of 24 fold (p=0.0004) compared to *Wt* mMECs. There was no difference in the expression of *FoxJ1* (p=0.55*)*, *Muc5b* (p=0.53), *Muc5ac* (p=0.64) *and p63* (p=0.73) between mMECs from the two genotypes. (Fig 4.12).

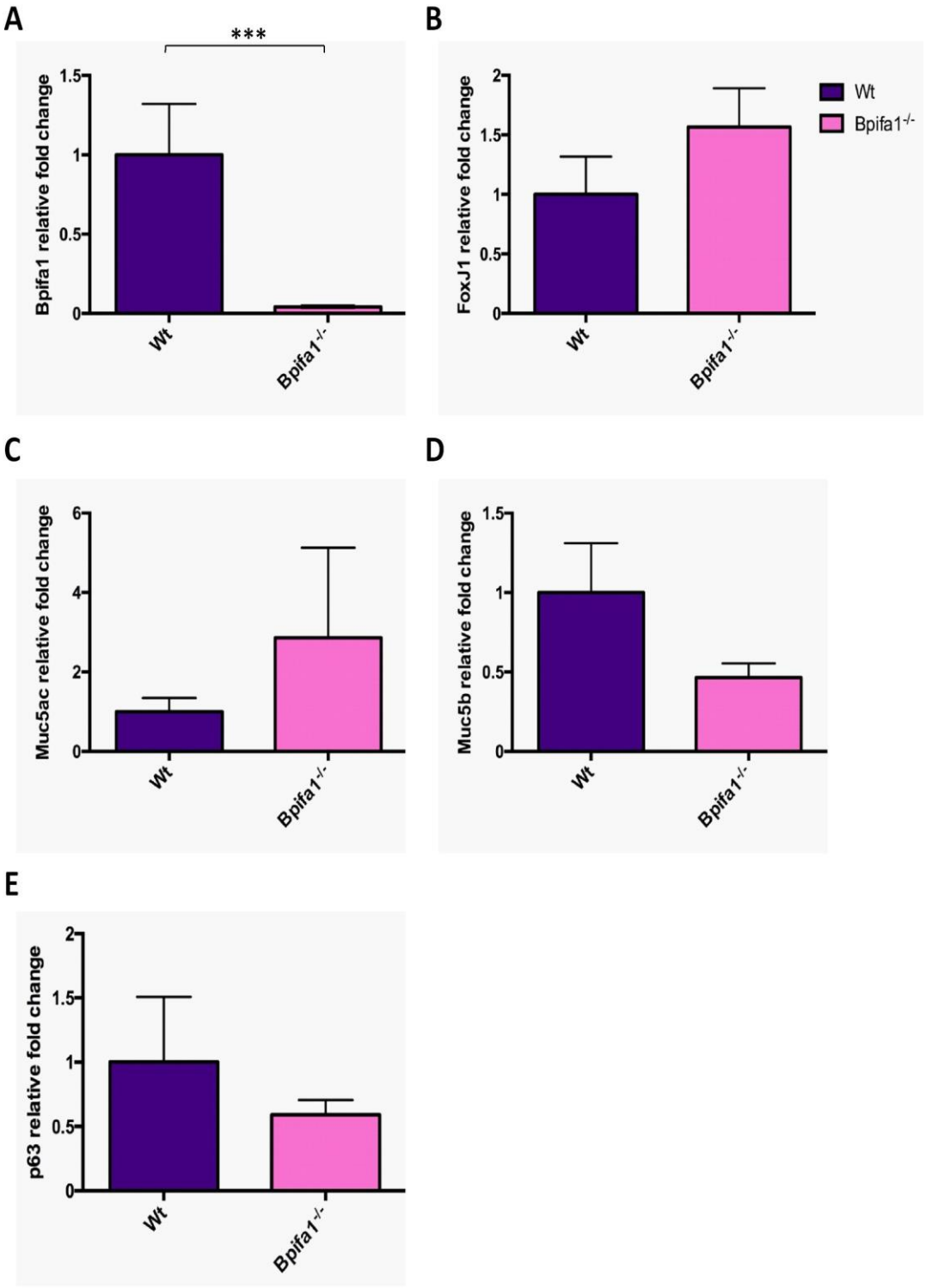

Figure 4.12 Relative gene expression of epithelial markers in ALI Day 14 *Bpifa1*$^{-/-}$ mMECs compared to *Wt* mMECs

Confirmation of *Bpifa1* gene deletion in *Bpifa1*$^{-/-}$ mMECs (A). *FoxJ1* expression (B), *Muc5ac* expression (C) *Muc5b* expression (D) and P63 expression (E) did not change significantly between genotypes ($p>0.05$). Data analysed using two tailed student's t-test and represented as mean relative quantification (RQ) ± $RQ_{min/max}$ for three independent batches of cultures. ***$p<0.005$

4.2.10 Apical secretome of *Bpifa1*$^{-/-}$ mMECs

Global proteomic analysis of apical ALI Day 14 secretions from *Bpifa1*$^{-/-}$ mMECs by Orbitrap MS, revealed a pattern very similar to that seen in *Wt* mMECs. Table 4.3 lists the 12 most abundant secreted proteins identified in apical washes from *Bpifa1*$^{-/-}$ mMECs, classified according to their emPAI score. Since this analysis was not performed at the same time as the *Wt* mMEC secretome analysis, comparisons between the levels of proteins expressed by the two cell types could not be quantified. However, the overall spectrum of proteins in the apical washes from the two genotypes was similar. The complete list of proteins identified is given in Appendix III, Table S6.

Table 4.3: Most abundant secreted proteins identified in apical ALI Day 14 washes from *Bpifa1*$^{-/-}$ mMEC cultures

Accession Number	Protein	Peptide count	emPAI Score
P08071	Lactotransferrin	47	247.93
Q921I1	Serotransferrin	40	13.69
O09049	Regenerating islet-derived protein 3-gamma	8	8.04
P11672	Neutrophil gelatinase-associated lipocalin	9	5.66
Q61147	Ceruloplasmin	55	4.58
P10605	Cathepsin B	15	1.94
Q61362	Chitinase-3-like protein 1	22	1.55
LG3BP	Galectin-3-binding protein	26	1.41
P01027	Complement C3	111	1.32
P50404	Pulmonary surfactant-associated protein D	23	1.3
P08905	Lysozyme C-2	10	0.2
Q9CQV3	Serpin B11	24	1.07

NB- Accession numbers and biological functions from the UniProt database

4.2.11 Expression of epithelial markers in *Wt* and *Bpifa1*$^{-/-}$ mNECs

As a comparison to mMECs, I simultaneously cultured and assessed the expression of a limited number of epithelial markers in mNEC cultures at a transcriptional and proteomic level. Since the focus of the chapter was to develop a model of the mouse middle ear

epithelium, culture of mNECs was only used as preliminary evaluation and to confirm the successful differentiation of murine cells.

Using RT-PCR, *Bpifa1* was detectable in mNECs from ALI Day 3. *Tekt1* and *Muc5ac* expression was delayed in *Wt* cultures (ALI Day 7) compared to knockout cultures (ALI Day 3), but this observation was not consistent across the different batches tested. Nonetheless, the data indicates that the cells differentiated in culture from ALI Day 0 to ALI Day 14 and the pattern of expression in the differentiated cells was comparable to that of the original cells isolated from the nasal cavity (Fig 4.13A).

This differentiation of *Wt* and *Bpifa1*$^{-/-}$ mNECs in culture was confirmed by IFC. Secretory cells (BPIFA1) and ciliated cells (FOXJ1) were absent in undifferentiated ALI Day 0 cultures (Fig4.13C, E). Differentiated ALI Day 14 mNECs cells showed a uniform distribution of cilia throughout the culture (Fig 4.13D, F), rather than clusters as described previously in mMECs. *Wt* ALI Day 14 mNECs stained positive for BPIFA1 (Fig 4.13D) and their abundance was lower than that seen in differentiated mMECs, although this was not quantified. Absence of secreted (Fig 4.13B) and intracellular (Fig 4.13F) BPIFA1 at ALI Day 14 again confirmed successful deletion of the gene.

Nuclear staining of cells with DAPI and Z-slice imaging using confocal microscopy demonstrated that mNECs formed a flat monolayer at ALI Day 0 (Fig 4.13G) and showed a homogenous organisation at ALI Day 14, with tightly organised single layer of cells (Fig 4.13H). This morphology was contrasting to the combination of flat and elevated pseudo stratified type morphology noticed in mMECs. (Figures 4.8G, H).

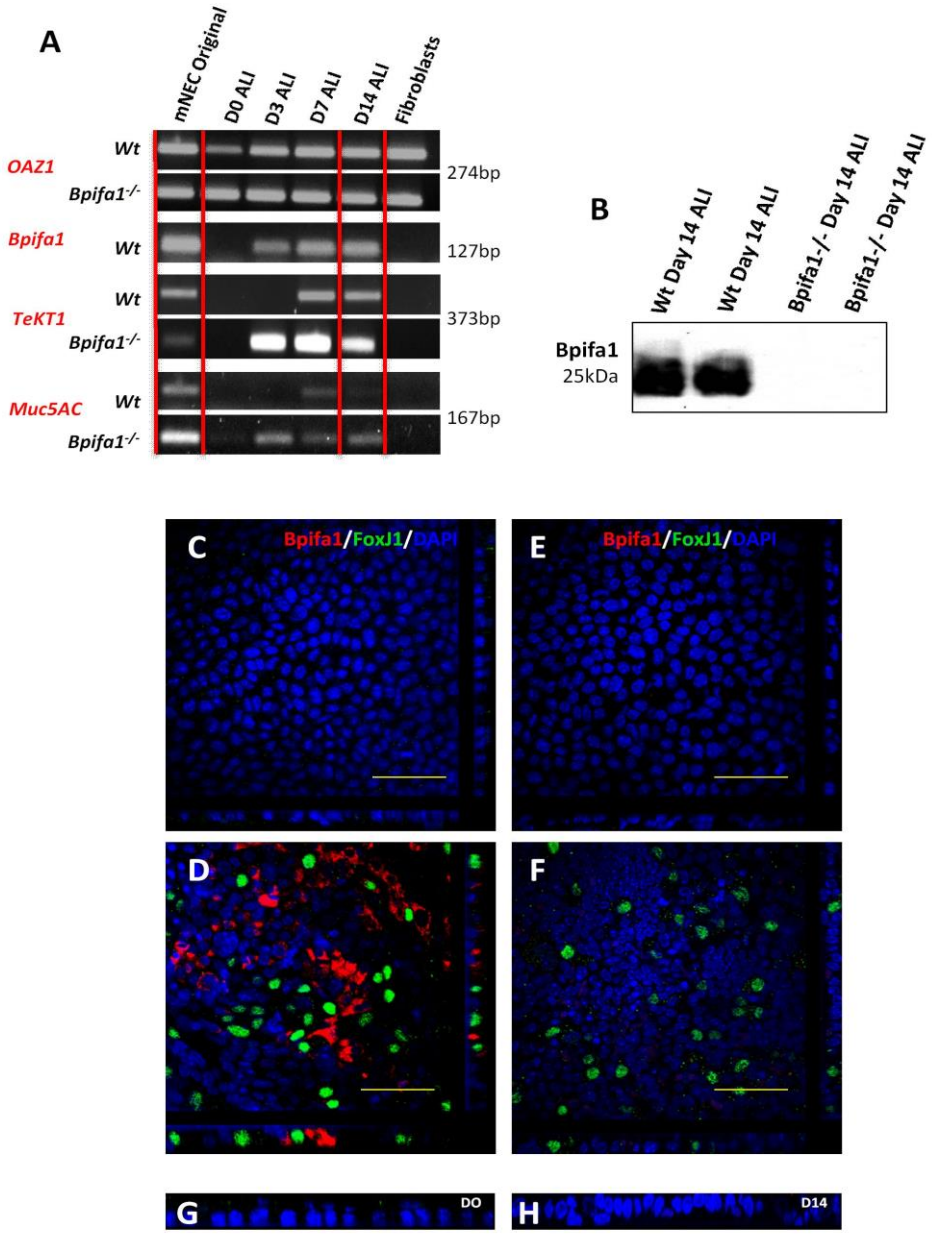

Figure 4.13 Expression of epithelial markers by *Bpifa1*$^{-/-}$ mNECs

End-point RT-PCR comparing expression of selected secretory, mucin and ciliated cell genes between *Wt* and *Bpifa1*$^{-/-}$ mNECs during differentiation. Expression profile of ALI Day 14 cells was similar to mNEC original cells for most genes (A). The absence of BPIFA1 in apical washes from 2 batches of ALI Day 14 *Bpifa1*$^{-/-}$ mNECs compared with 2 batches of ALI Day 14 *Wt* mNECs as a positive control (B). IFC images showing no expression of BPIFA1 and FOXJ1 in undifferentiated ALI Day 0 *Wt* (C) and *Bpifa1*$^{-/-}$ (E) mNECs. Differentiated mNEC ALI Day 14 *Wt* cells produces BPIFA1 and FOXJ1 (D) and *Bpifa1*$^{-/-}$ mNECs express FoxJ1 (F) indicating successful differentiation. Z-stack images of cross sections of nuclei stained with DAPI shows that ALI Day 0 and Day 14 cells form a relatively homogenous monolayer (G, H). Scale bar =50µm. Data are representative of 3 independent batches of culture.

The data up to this point indicate that I have developed an *in vitro* model of differentiated mouse middle ear cells that mimics the *in vivo* murine epithelium. *Bpifa1* deletion does not affect the morphology and expression of epithelial markers in culture. Similarly, mNECs mimic the murine nasal epithelium and share many common features with middle ear cells; reinforcing the view that middle ear is physiologically similar to that of the URT. The next step was to evaluate the utility of mMECs for the study of host pathogen interactions as well as to assess the effect of *Bpifa1* deletion on susceptibility to *NTHi* infection. Due to time constraints, comparison of the *in vitro* infections using mNECs was not performed.

4.2.12 Susceptibility of *Bpifa1*$^{-/-}$ and *Wt* mMECs to *NTHi* infection

4.2.12.1 Progression of infection

In order to test the ability of the mMEC model to support the growth of otopathogens, *Wt* and *Bpifa1*$^{-/-}$ ALI Day 14 mMECs were infected with NT*Hi*$^{375SR\text{-}GFP}$ at MOIs of 1:100 ($1.2x10^7$ bacteria/ membrane) and 1:1000 ($1.2x10^8$ bacteria/membrane). Quantification of infection in the four central 10x fields indicated that the amount of infection increased in a time dependent manner at both the MOIs. Only a few bacteria were visible at 24 hpi but by 48 hpi the infection rate had increased and the bacteria continued to spread laterally in culture, infecting the majority of cells by 72 hpi (Fig. 4.14 and 4.15). As expected, the amount of infection was higher for MOI 1:1000 (Fig. 4.15) compared to MOI 1:100 (Fig. 4.14). Moreover, there was a suggestion of a higher infection in *Bpifa1*$^{-/-}$ mMECs than *Wt* mMECS, especially at 48 and 72 hpi at both MOIs.

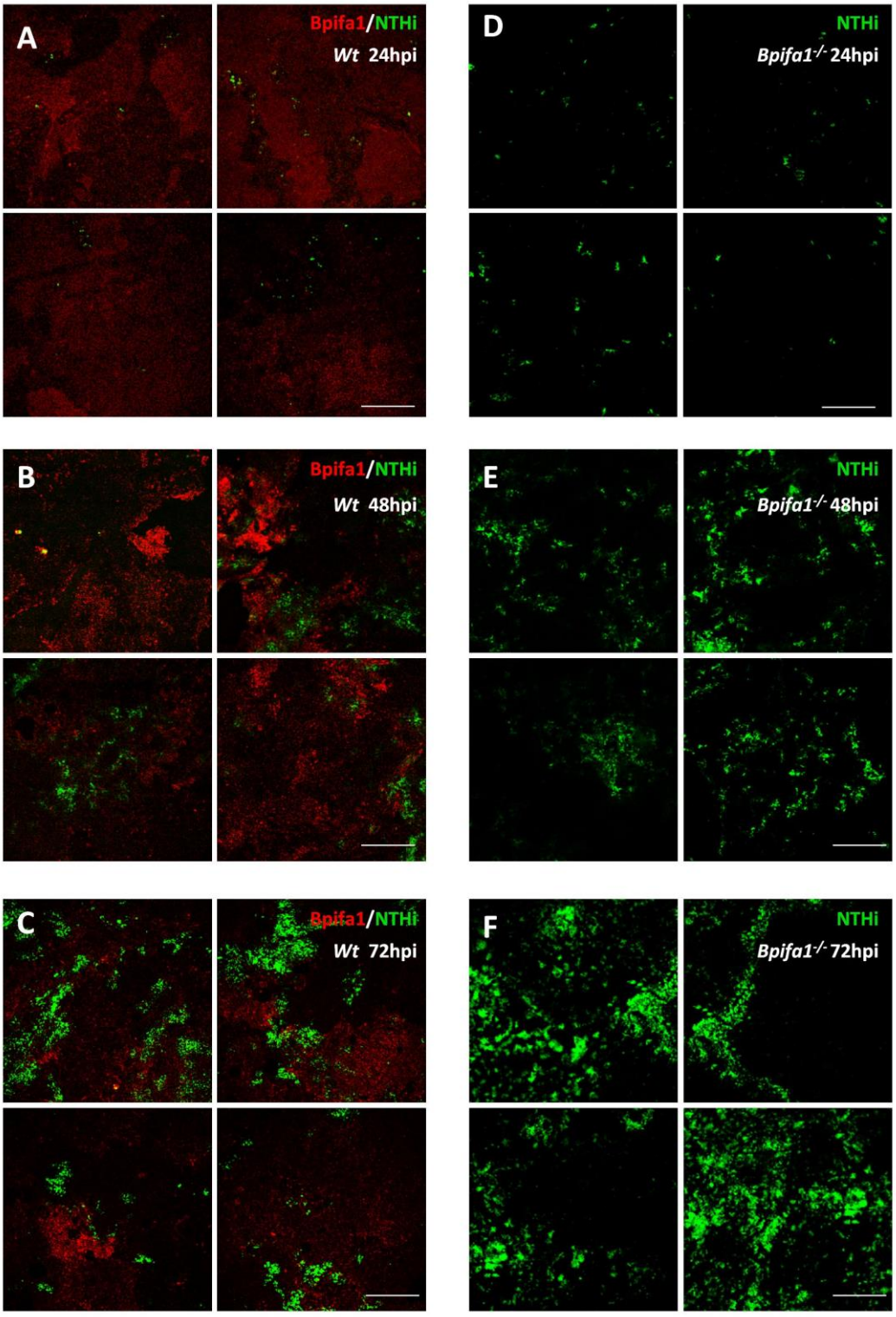

Figure 4.14: Progression of NT*Hi* infection at MOI 1: 100
Low power IFC images showing progression of NT*Hi*-375$^{SR\text{-}GFP}$ (MOI 1: 100) infection in ALI Day 14 *Wt* (A, B, C) and *Bpifa1*$^{-/-}$ (D, E, F) mMECs at 24 hpi (A, D), 48hpi (B, E) to 72 hpi (C, F). Each panel represents 4 central fields at 10x magnification spanning approximately 50% of the membrane. Amount of infection appears to be greater in *Bpifa1*$^{-/-}$ mMECs. Representative image for n=3 independent batches. Scale bar = 200µm

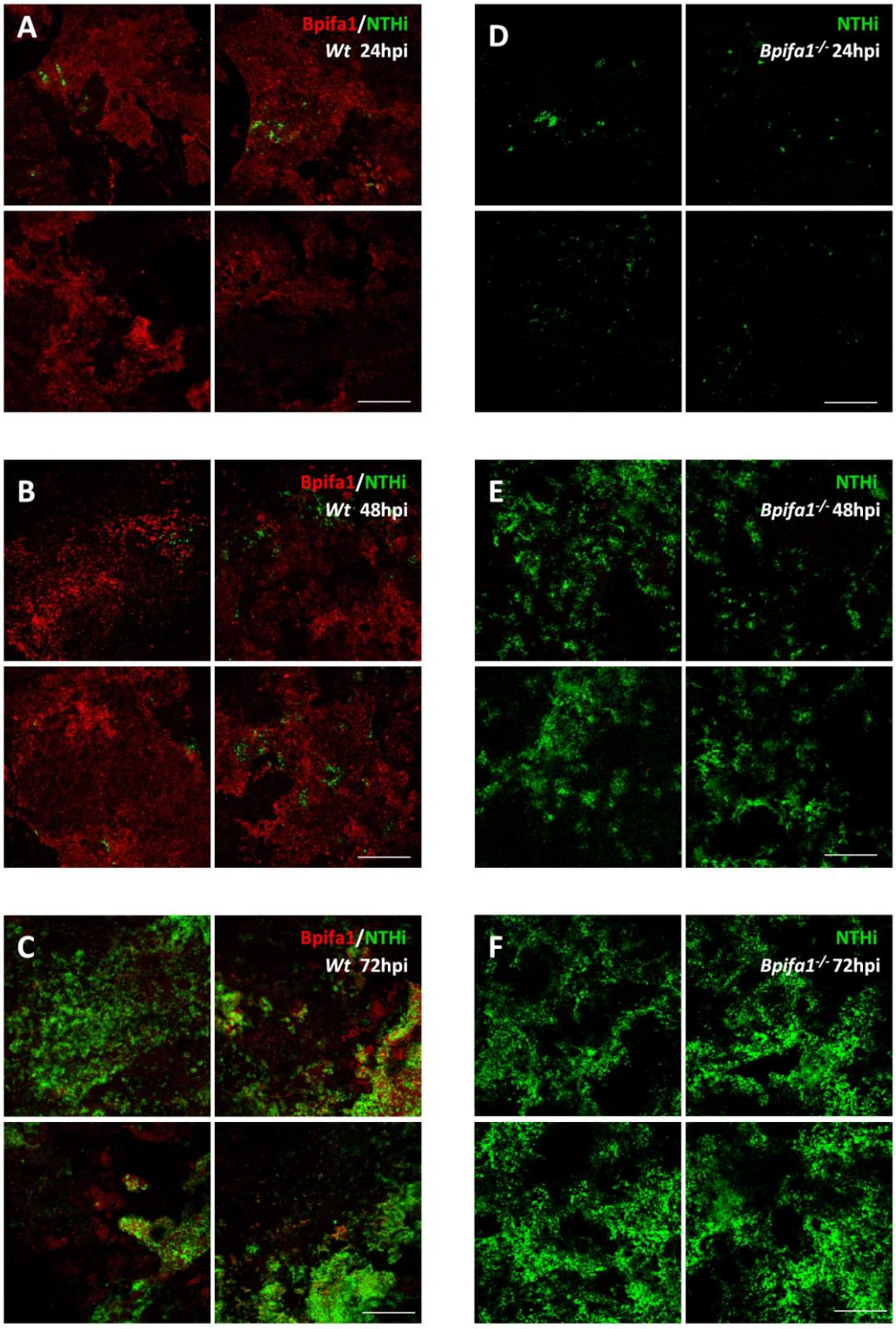

Figure 4.15 Progression of NT*Hi* infection at MOI 1: 1000
Low power IFC images showing progression of *NTHi*-375$^{SR\text{-}GFP}$ (MOI 1: 1000) infection in ALI Day 14 *Wt* (A, B, C) and *Bpifa1*$^{-/-}$ (D, E, F) mMECs at 24 hpi (A,D), 48hpi (B,E) to 72 hpi (C,F). Each panel represents 4 central fields at 10x magnification spanning approximately 50% of the membrane. Amount of infection appears to be higher in *Bpifa1*$^{-/-}$ mMECs. Representative image for n=3 independent batches. Scale bar = 200µm.

4.2.12.2 Cellular damage based on nuclear fragmentation

The pattern of infection was the same for both MOI 1:100 and MOI 1:1000. However, mMECs infected at MOI 1:1000 demonstrated high levels of cellular damage, indicated by nuclear fragmentation at 48 and 72 hpi compared to MOI 1:100. Here, the same batch of *Wt* mMECs infected at MOIs of 1:1000 (Fig 4.16A-F) and 1:100 (Fig 4.17A-F) respectively shows noticeably more nuclear disintegration for the higher dose, indicating more cell death. Therefore, M01 1:1000 was deemed too high a dose for infection studies and MOI of 1:100 was selected for all further infection experiments.

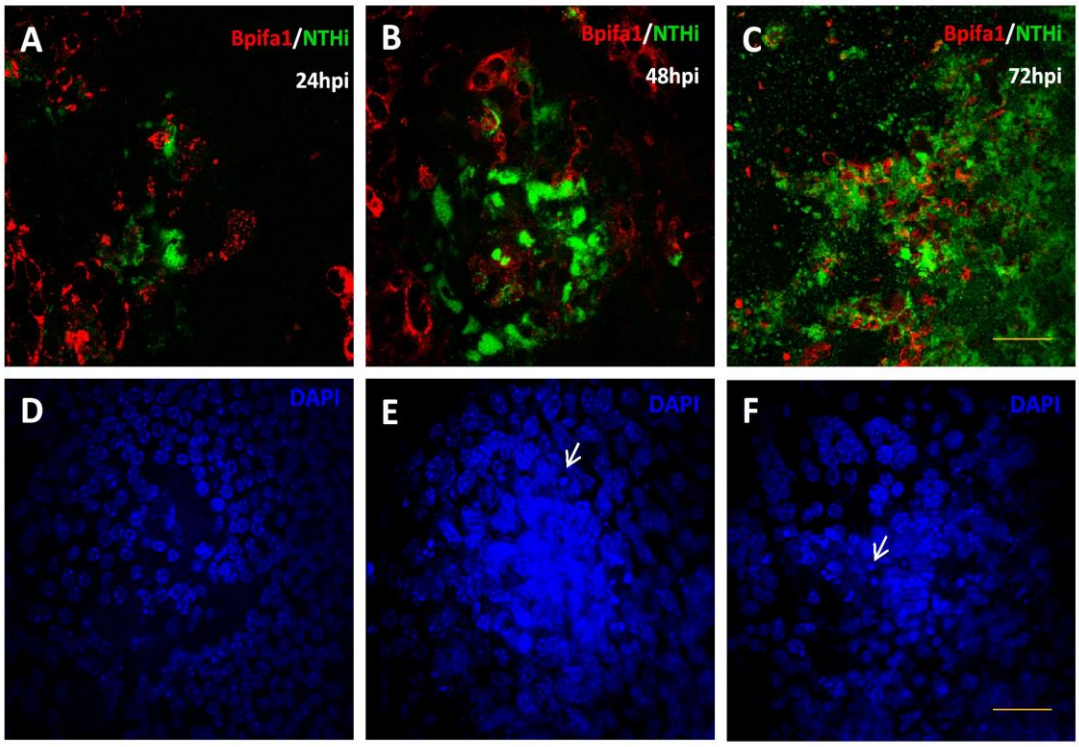

Figure 4.16 Nuclear fragmentation at MOI 1:1000
IFC of *NTHi* infected *Wt* mMECs at MOI 1000 shows increase in infection from 24hpi, 48hpi to 72 hpi (A, B, C). DAPI staining for the corresponding nuclear sections (D, E, F) shows severely fragmented nuclei at 48hpi and 72 hpi (E, F). Examples of fragmented nuclei are shown with white arrows. Scale bar = 50µm

A comparison between *Wt* and *Bpifa1*$^{-/-}$ mMECs at MOI 1:100, revealed intact nuclei at 24hpi (Fig 4.17D, J). However, at 48hpi and 72hpi, *Bpifa1*$^{-/-}$ mMECs showed greater nuclear fragmentation (Fig 4.17K, L) compared to *Wt*s (Fig 4.17E, F) indicating more severe infection and thus an enhanced susceptibility to NT*Hi*.

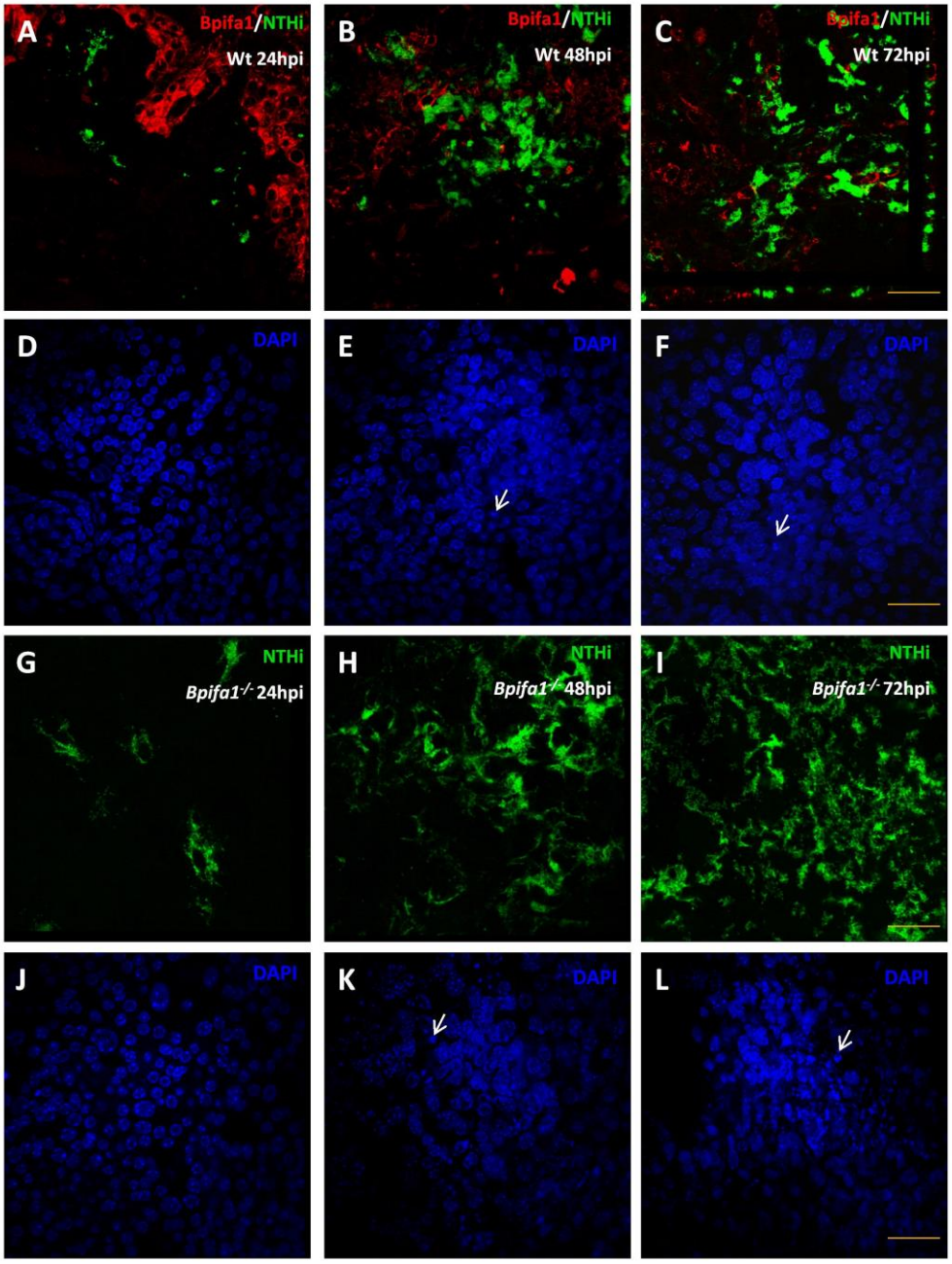

Figure 4.17 Nuclear fragmentation at MOI 1:100
IFC images NT*Hi* infected *Wt* mMECs infected at MOI 100 shows increase in infection from 24hpi, 48hpi to 72 hpi (A-C). *Bpifa1*$^{-/-}$ mMECs at MOI 100 also show progression in infection from 24hpi to 72 hpi (G-I). DAPI staining for *Wt* (D-F) and *Bpifa1*$^{-/-}$ (J-L) nuclear sections at corresponding time points shows fragmented nuclei at 48hpi and 72 hpi (E, F, K, L). However, amount of fragmentation appears higher in *Bpifa1*$^{-/-}$ mMECs compared to *Wt* mMECs. Examples of fragmented nuclei are shown with white arrows. Scale bar = 50µm

4.2.12.3 Quantification of NTHi infection in Bpifa1$^{-/-}$ and Wt mMECs

Thus, the data so far suggested a higher level of infection in *Bpifa1*$^{-/-}$ mMECs than *Wt* mMECs. In order to confirm this observation, the amount NT*Hi*$^{375SR\text{-}GFP}$ infection was quantified by measuring the green fluorescence in 3 individual batches of *Wt* and *Bpifa1*$^{-/-}$ mMECs. This indicated a clear progression of infection from 24hpi to 72hpi for both genotypes. The severity of infection was higher at 48 and 72 hpi in each batch of *Bpifa1*$^{-/-}$ mMECs compared to the corresponding batch of *Wt* mMECs. However, due to the variation in the intensity of infection between individual *Wt* and *Bpifa1*$^{-/-}$ batches, the difference in the mean fluorescence for the two genotypes did not reach statistical significance (Fig 4.18A).

In order to address this issue and obtain more tangible quantification data, I performed viable bacterial counts at 48 and 72hpi to determine the total number of bacteria associated with *Wt* and *Bpifa1*$^{-/-}$ mMECs. There was a significant increase in number of bacteria infecting *Wt* ($p=0.021$) as well as *Bpifa1*$^{-/-}$ ($p=0.029$) mMECs from 48hpi to 72 hpi, confirming progression of infection noted by IFC. However, there was no significant difference between the two genotypes (Fig 4.18B).

4.2.13 BPIFA1 expressing cells are resistant to initial *NTHi* infection

A more detailed analysis of multiple higher magnification images of infected ALI Day 14 *Wt* mMECs demonstrated a lack of co-localisation of NT*Hi* with BPIFA1 positive cells at the 24hpi time point. However, at 48hpi a few BPIFA1 positive cells were infected and by 72 hpi the infection spread laterally, affecting most cells including BPIFA1 expressing cells. Thus BPIFA1 positive cells appeared to be resistant to initial bacterial infection at 24hpi (Fig 4.18C).

Since BPIFA1 expressing cells appeared to be resistant to initial infection, I sought to investigate if loss of *Bpifa1* affects the initial association of NT*Hi* with mMECs. ALI Day 14 *Wt* and *Bpifa1*$^{-/-}$ mMECs were infected with NT*Hi*$^{375SR\text{-}GFP}$ at MOI 1:100. Bacterial association was evaluated by washing unbound bacteria 1 hour after infection, lysing cells and enumerating CFUs/ml of serial dilutions, as a percentage of the initial inoculum. However, there was no significant difference in the percentage of NT*Hi* adhering to *Wt* and *Bpifa1*$^{-/-}$ mMECs after 1 hour (Fig 4.18G).

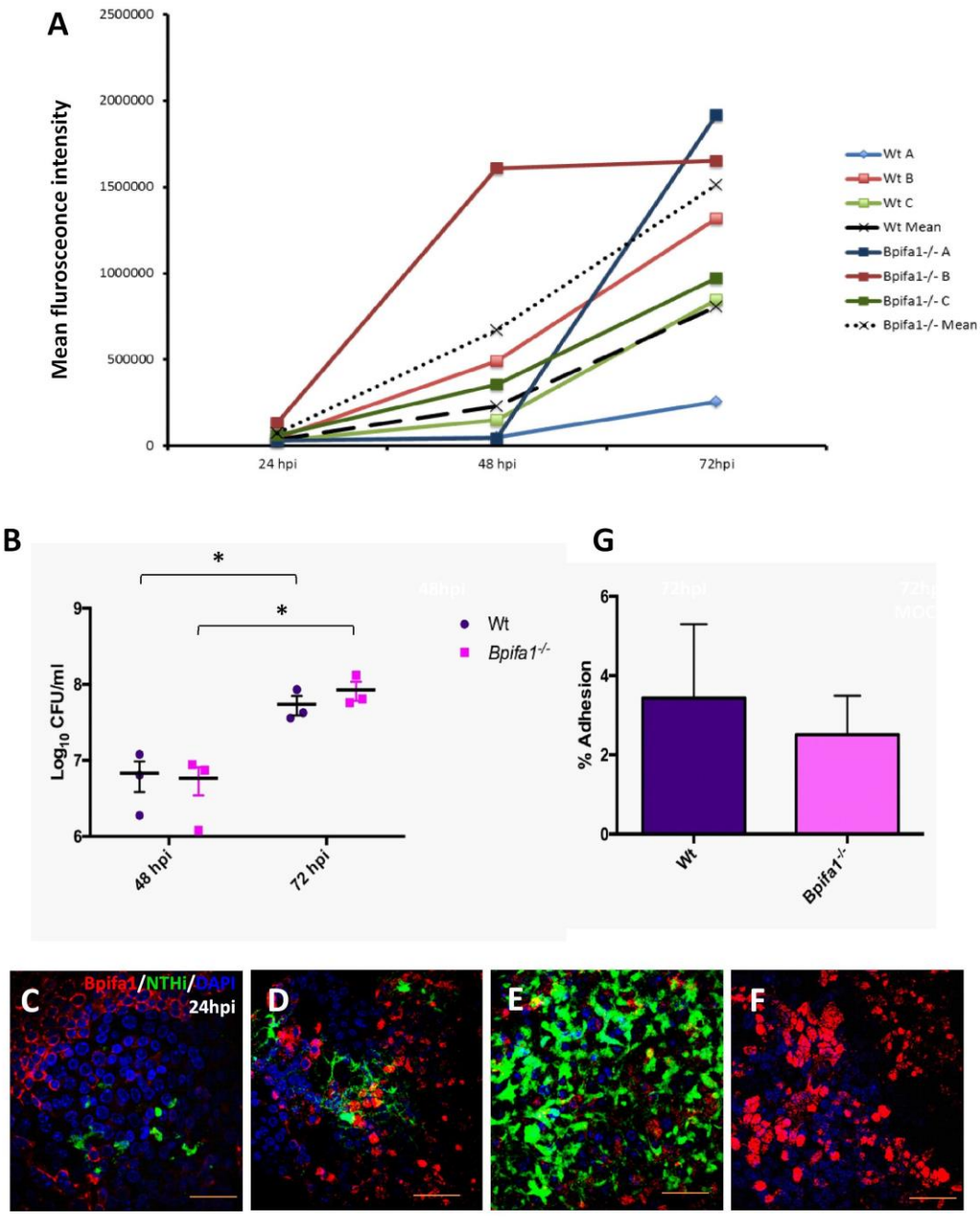

Figure 4.18 Quantification of *NTHi* infection in mMECs

Increase in mean green fluorescence intensity in *Wt* and *Bpifa1*$^{-/-}$ mMECs infected at MOI 1: 100 from 24hpi to 72hpi quantified using lower 10x IFC images. Each batch of *Bpifa1*$^{-/-}$ mMECs is infected at a higher rate that its corresponding *Wt* batch, infected at the same time. However, difference in mean infection intensity between *Wt* and *Bpifa1*$^{-/-}$ mMECs is not statistically significant (A). Viable counts show a significant increase in infection with time for both genotypes but no difference between genotypes (B). High magnification (60x) IFC images of *Wt* ALI Day 14 mMECs infected 24 (C), 48 (D) and 72 hpi (E) showing an apparent decrease in BPIFA1 staining with time. Co-localisation of bacteria with BPIFA1 expressing cells can be seen at 48 and 72 hpi but not at 24 hpi. Control *Wt* ALI Day 14 mMECs MOCK infected for 72 hpi (F) Scale bar =50µm. There is no significant different between initial association of bacteria with *Wt* and *Bpifa1*$^{-/-}$ mMECs (G) Data quantified using one-way ANOVA with Tukey's post hoc test (A) and two tailed students t-tests (B, G) *p<0.05 n=3 individual batches of culture.

4.2.14 BPIFA1 levels in *Wt* mMECs decreases following NT*Hi* infection

Along with a progression in infection (Sections 4.2.12.1 and 4.2.13), a decline in the amount of BPIFA1 staining was observed in NT*Hi* infected *Wt* mMECs (Fig 4.18C). Intensity of red fluorescence, indicative of cytosolic BPIFA1, was quantified in five 60x fields per membrane for 3 individual batches of *Wt* mMEcs. This decrease from 24hpi to 72 hpi was not statistically significant (Fig4.19A).

To investigate whether the apparent decrease in intracellular BPIFA1 with infection was due release of the protein, I examined the BPIFA1 levels in apical washes from infected mMECs and compared them to MOCK controls at the corresponding time point. Equal total protein concentrations tested using western blots revealed no difference at 24hpi, but the amount of BPIFA1 in the cell secretions was significantly lower in the infected washes at 48hpi ($p= 0.01$) and 72hpi ($p=0.006$) compared to the MOCK infected controls. (Fig 4.19 B, C).

To determine if the decrease in secreted BPIFA1 levels correlated with a decrease in *Bpifa1* mRNA levels, RT-qPCR was performed on NT*Hi* infected and MOCK infected *Wt* mMECs. In keeping with the western blot data, mean *Bpifa1* expression was lower in the infected samples than the MOCK samples (Fig 4.19D), particularly at 48hpi and 72hpi. The reduction in *Bpifa1* reached statistical significance at 48hpi ($p= 0.013$) but not at 72hpi. A more careful analysis revealed decreased expression of *Bpifa1* expression in each batch of infected sample compared to its respective MOCK sample, both at 48 and 72 hpi (Fig 4.19E). However, batch variation in the levels of *Bpifa1* expression was higher at 72hpi, thus affecting the overall significance levels. However, the data indicate that the expression of *Bpifa1* in *Wt* mMECs decreases upon *NTHi* infection.

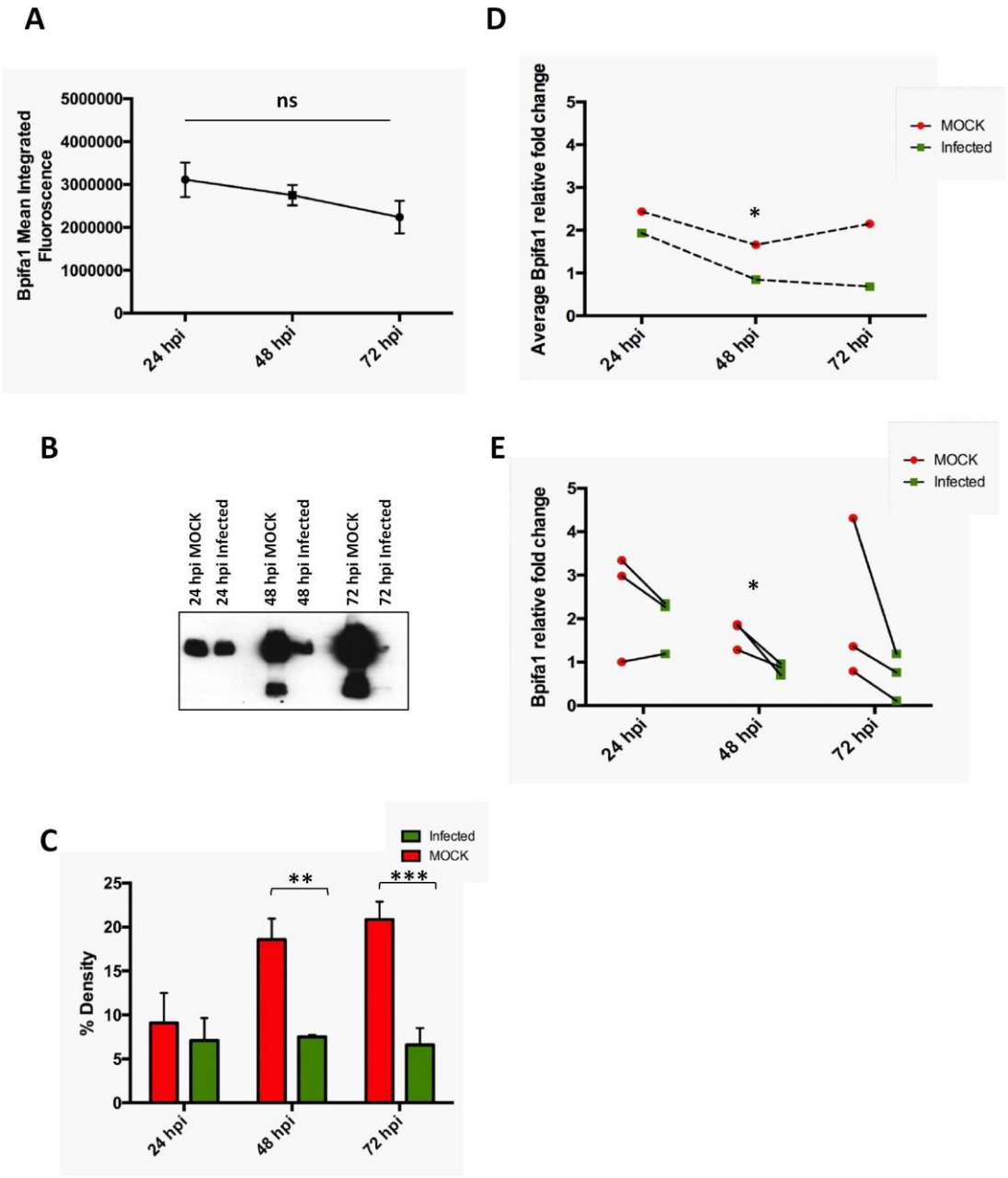

Figure 4.19 BPIFA1 decreases upon NT*Hi* infection of *Wt* mMECs

Decrease in mean fluorescence intensity of BPIFA1 staining following NT*Hi* infection of *Wt* mMECs was non-significant (A). Secreted BPIFA1 decreased at 48hpi (**p<0.01) and 72 hpi (***p<0.005) compared to corresponding MOCK infected controls as seen by western blotting (B) and its quantification by densitometry (C). Mean genetic expression of *Bpifa1* is significantly lower at 48hpi (*p<0.05) in infected samples compared to MOCK samples (D). Individual data points indicate reduction in *Bpifa1* gene expression in each batch of infected mMECs compared to MOCK mMECs at 48hpi and 72 hpi. Data presented at individual RQ values ± SEM (E). n=3 individual batches. Statistical significant measured using one-way ANOVA with Tukey's post hoc test (A) and two tailed students t-tests (C, D, E).

4.2.15 Expression of pro-inflammatory and epithelial genes in *Bpifa1*$^{-/-}$ mMECs following NT*Hi* infection.

Having established a novel mMEC culture model that supports otopathogenic infection, I evaluated if *Bpifa1* ablation resulted in an exacerbated pro-inflammatory response.

Gene expression analysis of the pro-inflammatory chemokine *Cxcl2/MIP2α* and cytokine *Tnfα* was performed using RT-qPCR during progression of infection at 24hpi to 48hpi. The 72hpi time point was excluded from this analysis due to the higher level of cellular damage and consequent RNA degradation. *Cxcl2* was up regulated 85 fold at 24hpi and 63 fold 48hpi in the infected *Wt* mMECs and 91 fold at 24 hpi and 158 fold in 48 hpi in infected *Bpifa1*$^{-/-}$ mMECs when compared to the respective MOCK samples at each time point (Fig 4.20A $p<0.0001$). *Tnfα* was up regulated with infection by 4.3 fold at 24 hpi and by 3.1 fold in *Wt* mMECs, yet these increases were not significant. However, in *Bpifa1*$^{-/-}$ mMECs *Tnfα* was up regulated significantly at 24hpi (4.4 fold, $p= 0.01$) and 48hpi (2.6 fold, $p= 0.05$). Again, the responses exhibited a wide variation between individual batches (Fig 4.20B). Nevertheless, the data confirms that the mMEC model is capable of eliciting an inflammatory response.

There was no difference between expression of *Cxcl2* and *Tnfα* between *Wt and Bpifa1*$^{-/-}$ mMECs at either time points. (Fig 4.20A, B)

I also analysed expression of the epithelial markers, *Foxj1*, *Muc5b* and *Muc5ac* in *Wt* and *Bpifa1*$^{-/-}$ mMECs following infection. Analysing this data was challenging due to the high level of batch variation in expression of these genes and no significant differences were seen either with genotype or infection (Fig 4.20C, D, E).

The expression of target genes was normalized to three endogenous controls; *Atp5b, Ppia* and *Cyc1* identified as most suitable controls for this experiment using the geNORM assay (Section 2.19.4). Here, I have presented all data as individual RQ values for each biological replicate ± SEM here in order to demonstrate the trend of upregulation of the pro-

inflammatory cytokines in the infected samples, the degree of batch variation and its effect on statistical significance of means.

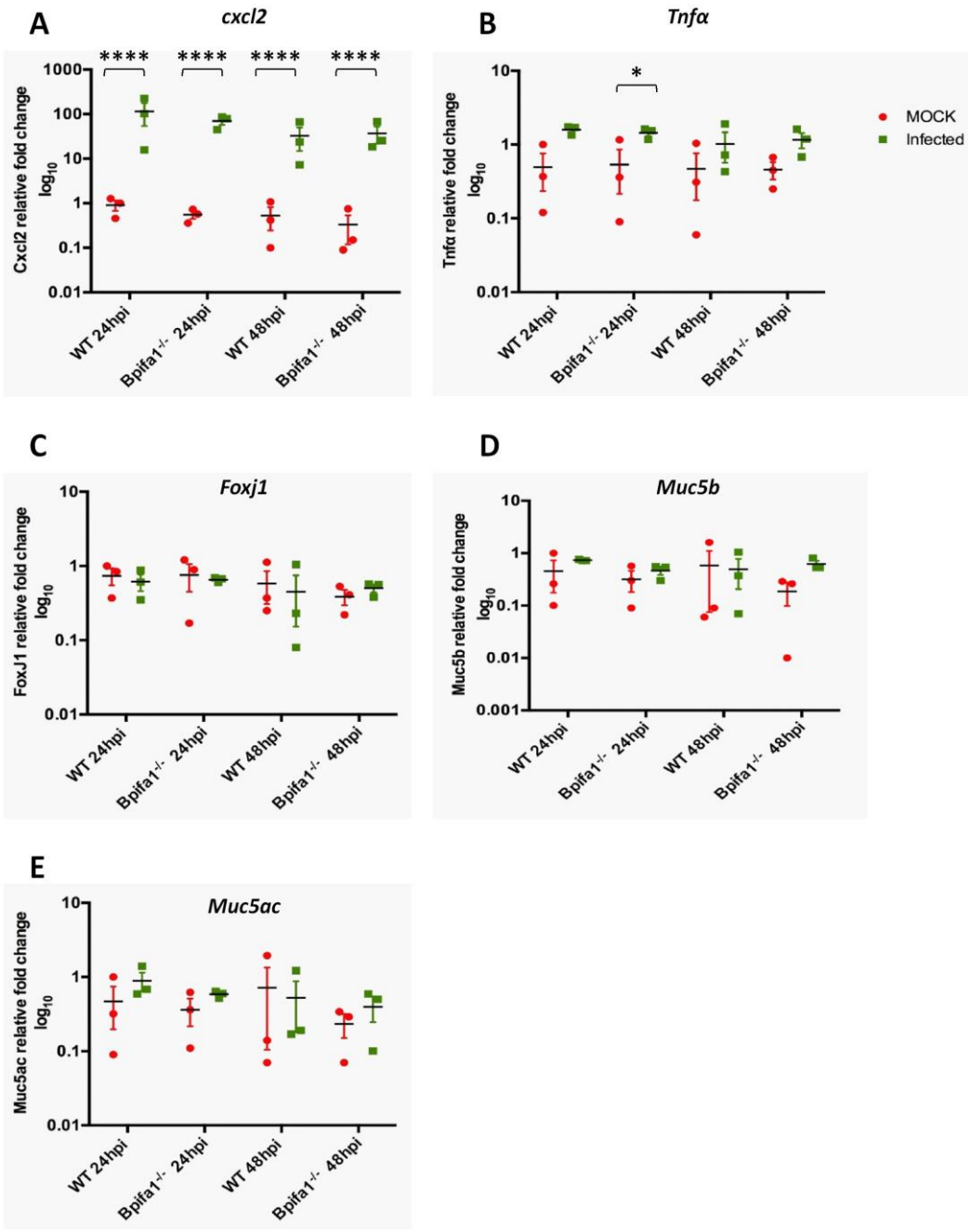

Figure 4.20 Relative gene expression of pro-inflammatory and epithelial markers in ALI Day 14 *Bpifa1*$^{-/-}$ *mMECs* compared to *Wt* mMECs

Significant up regulation of *Cxcl2* in infected samples compared to MOCK samples, but no difference between genotypes ***p<0.0001 (A). Up regulation in *Tnfα* expression was significant only at 24hpi in the *Bpifa1*$^{-/-}$ *mMECs* with infection and not with genotype. (B), *FoxJ1* expression (C) *Muc5b* expression (E) and *Mu5cac* expression (E) did not change significantly between with either infection or genotypes. Data were analysed using two-way ANOVA plus Tukey's post Hoc test and represented as mean individual RQ values ± SEM for three independent batches of cultures.

4.3 Discussion

4.3.1 Establishment of a novel model of the mouse middle ear epithelium

In this chapter I have described the development of a novel model of the murine middle ear epithelium. The culture method that I have established was adapted from methods used for the ALI culture of murine TBE cells (Clarke et al 1992, Davidson et al 2000, Yamaya et al 1992, You et al 2002) and murine nasal epithelial cells (Woodworth et al 2007). The media supplements, epidermal growth factor, insulin, transferrin and cholera toxin enhance cell proliferation and ciliogeneisis whereas retinoic acid is important for differentiation of mucous cells (Lechner et al 1982, Wu et al 1997, You & Brody 2013, You et al 2002). Moreover, the ALI culture system mimics the *in situ* organization of airway epithelial cells and further promotes their differentiation.

Normally, setting up ALI cultures requires a large number of animals in order to generate sufficient numbers of cells. The addition of ROCKi to the culture medium has been shown to enhance basal cell proliferation in airway epithelial cultures (Horani et al 2013). Using ROCKi, I could increase the number of transwell-cultures established from the limited number of cells isolated from the thin middle ear epithelium and nasal cavities without altering the ability of the cells to undergo differentiation; an observation that has been made in both human and mouse airway cells (Butler et al 2016, Horani et al 2013). Thus I was able to minimize the number of animals required and typically, 30 to 35 transwells were seeded from each batch of 6 mice.

4.3.1.1 mMECs are an epithelial system

mMEC cultures model the native middle ear epithelium as the cells exhibit characteristic epithelial features such as a cobble-stoned morphology, formation of tight junctions,

apical-basal polarisation, presence of desmosomes and apical microvilli. Following differentiation, the cultures contained a combination of single layered flatter polygonal cells and clusters of pseudostratified, dome shaped, elevated cells, with some of these demonstrating beating cilia. The dome shaped appearance of cells can be attributed to an active ion transport mechanism (Chun et al 2002, Nakamura et al 1991). An important and common problem identified in a number of previous attempts to grow middle ear epithelial cells was the contamination and overgrowth of fibroblasts in the cultures (Nakamura et al 1991, Tsuchiya et al 2005, Vanblitterswijk et al 1986). By adding a differential adherence step, in which fibroblasts adhered to plastic in preference to the epithelial cells, I was able to eliminate fibroblasts from the cultures, generating a pure epithelial population, as shown by a lack of expression of the fibroblast marker, *Vimentin*, in ALI Day 14 mMEC cultures.

4.3.1.2 mMECs express markers of the in vivo middle ear epithelium

Another major limitation of previous middle ear epithelial culture models has been the lack of differentiation into distinct epithelial cell types. The middle ear epithelium, like the epithelium of the upper airways, is composed of ciliated cells, basal cells, goblet cells and other secretory cells. Previous studies highlighted difficulties in maintaining ciliated cells in culture (Nakamura et al 1991, Ueyama et al 2001). To my knowledge, the development of ciliated cells has only been described in one other report of human middle ear cultures (Choi et al 2002), a study in which cells were also grown at the ALI. mMEC cultures clearly showed the presence of actively beating cilia and also stained for nuclear FoxJ1 protein, a marker of motile cilia. The distribution of cilia in mMEC cultures partially mimicked that seen in the native middle ear epithelium by SEM. Parts of the middle ear epithelium were populated with tracts of dense cilia, parts with interspersed ciliated and non-ciliated cells

and some parts with a simple epithelium composed of flat non-ciliated polygonal cells. This distribution of cell types within the middle ear cavity is supported by previous studies (Lim 1979, Thompson & Tucker 2013) which show that the native epithelium of the hypotympanum and towards the opening of the ET is densely packed with ciliated cells, whereas the mesotympanum contains ciliated islands amongst other non-ciliated cells. The epitympnaum is composed primarily of flat squamous cells, which may also contribute to the secretory defence system. On this basis, I believe that mMECs, which are a combination of flat non-ciliated, secretory and ciliated cells closely model the morphology of the native middle ear epithelium.

Mucins are products of goblet cells, unique to the mucosal epithelia, and are essential for the maintenance of mucosal innate defence. A number of attempts have been described to utilise the existing middle ear models in order to study mucin gene expression at the transcriptional level (Kerschner et al 2010a, Liu et al 2016, Moon et al 2000, Tsuchiya et al 2005). However, these studies were limited by the lack of production and localisation of detectable amounts of mucins at the protein level. Goblet cells (as shown by MUC5b positivity) were seen in the elevated pseudostratified clusters of ALI Day 14 mMEC cells, in close association with ciliated cells. It has previously been shown that in the native middle ear epithelium, the localisation of mucous secreting cells is in parallel to the distribution of ciliated cells, reiterating that the model mimics the *in vivo* middle ear epithelium (Lim et al 1973). MUC5B is the predominant mucin in COM effusions (Preciado et al 2010). It has been shown to be indispensable for airway mucocilliary clearance and maintenance of mucosal homeostasis and *Muc5b*$^{-/-}$ mice develop OM (Roy et al 2014). The identification of Muc5b at readily detectable levels as demonstrated by IFC enables the mMEC model to be potentially utilised for further study of the role of mucins in the middle ear epithelium. Moreover, treating primary tracheal and bronchial epithelial cells grown at ALI with IL13 has been shown to induce goblet cell hyperplasia (Atherton et al 2003, Kondo et al 2002).

The mMEC model therefore provides a platform to alter culture conditions to study middle ear mucous hypersecretory phenotypes of OM *in vitro.* The lack of MUC5AC or MUC5B detection in the MS analysis could be because of the loss of these high molecular weight glycoproteins during the sample processing and preparation.

In addition to ciliated and goblet cells, the mMEC cultures also produced a range of other secretory cell products. We have previously shown that BPIFA1 is expressed abundantly in the middle ear epithelium (Sections 1.8.2 and 3.2.1). BPIFA1 constitutes a major proportion of secretions from TBE cells grown at ALI (Campos et al 2004) and is also strongly detected in primary nasal epithelial cells (Bingle & Bingle 2000). BPIFA1 was readily detectable in mMEC cultures and apical secretions from the cells. It localised to non-ciliated cells in the cultures, which is consistent with studies from the respiratory tract (Barnes et al 2008, Kim et al 2006, Musa et al 2012). *Bpifb1* mRNA, on the other hand, was detectable in the original cells, but not in the ALI Day 14 cultures and was absent from the list of proteins identified in the proteomic analysis performed using MS. BPIFB1 protein localises to goblet cells and minor glands associated with the ET, but its expression is limited in the middle ear epithelium (Mulay MSc thesis 2011). This observation suggests that the mMEC cultures model the middle ear epithelium rather than the ET epithelium.

4.3.1.3 Evaluation of the mMEC secretome

Unbiased, label-free proteomic MS analysis was used to identify a number of secretory proteins in the apical washes from the cells. The most abundant proteins comprised a variety of secretory host defence proteins with anti-microbial roles, proteins involved in cellular proliferation, wound repair, stress response, compliment activity and maintenance of cellular homeostasis. It is notable that the MS data contained a number of proteins also identified in a proteomic analysis of ear exudates from chronic OM patients such as

Lactotransferrin, BPIFA1, Lipocalin, Lysozyme and various cathespins and complement proteins (Val et al 2016). Lactotransferrin was by far the most abundant protein identified in this study. It is an antimicrobial protein secreted by airway mucosal surfaces and has been shown to play a role in maintenance of middle ear immunity (Bernstei.Jm et al 1974, Lim et al 2000, Moon et al 2002). Lactotransferrin prevents colonisation of mucosal surfaces by scavenging environmental iron, thus limiting its availability for bacterial growth. Human milk Lactotransferrin has been shown to attenuate the pathogenic potential of *H.influenzae* by proteolytically cleaving two important colonisation factors found on the bacterial surface (Hendrixson et al 2003) and the administration of Apolactoferrin has been shown to reduce bacterial counts in chinchilla middle ears with pneumococcal induced OM (Schachern et al 2010). SP-D was originally identified as a lung surfactant associated protein but is also expressed in the middle ear and the ET and has a suggested role in enhancing opsonisation and phagocytosis of bacteria (Lim et al 2000, van Rozendaal et al 2001, Wright 1997). Reg3γ is C-type lectin produced by paneth cells and secreted into the intestinal lumen with a suggested bactericidal activity against Gram-positive bacteria by binding to peptidoglycan in the bacterial cell wall (Cash et al 2006). It has been shown to spatially regulate the separation of microbiota from the host small intestinal epithelium (Vaishnava et al 2011). *Reg3γ*$^{-/-}$ mice have an altered mucosal distribution and increased inflammatory response in the small intestine (Loonen et al 2014). *Reg3γ* has also been shown to be involved in pulmonary innate immunity as it is induced by *Stat3* during methicillin resistant *Staphalococcus aureus (MRSA)* infection in lung and inhibits *MRSA* growth *in vitro* (Choi et al 2013). This is the first study reporting the expression of this protein in the middle ear and it is possible that Reg3γ performs a similar function in the middle ear.

It was noticeable that the proteomic data unexpectedly contained many intracellular proteins. The presence of the membrane-tethered mucins Muc1, Muc4 and Muc18 was also detected (Table S1). These proteins can be reasoned to be the contents of secreted

exosomes or products released from damaged cells. Exosomes are small membrane bound units released by the fusion of endosomal microvesicular bodies with the apical plasma membrane. They have been suggested to be involved in stimulating immune responses, modulating secretory activities and engaging in cell communication by packaging and delivering microRNAs to other cells (Keller et al 2006, Valadi et al 2007). Exosomes are released by epithelial cells (Kapsogeorgou et al 2005, van Niel et al 2001), are found in BAL fluids (Admyre et al 2003) and are also present in the apical secretions from human TBE cultures (Kesimer et al 2009, Pillai et al 2014). The presence of exosome-associated proteins in the mMEC secretome further adds to the potential utility of this model to study the role of exosomes in middle ear biology and OM pathogenesis.

Thus I have developed a novel in vitro model that closely mimics the *in situ* middle ear epithelium and for the first time systematically characterised the epithelial cell types in the middle ear.

4.3.2 Effect of loss of *Bpifa1* on uninfected mMEC cultures

Since BPIFA1 was localised to a large number of secretory cells in the middle ear epithelium and mMEC cultures, it was of interest to determine whether the ablation of *Bpifa1* affected the morphology of mMECs or the expression of other epithelial markers. A study by (Liu et al 2013b) showed that *Bpifa1*$^{-/-}$ mice demonstrated decreased basal expression of *Muc5ac, Muc5b* and *FoxJ1* in the lung tissue. *Bpifa1*$^{-/-}$ mMECs were morphologically and physiologically similar to *Wt* mMECs. Differences in expression of the epithelial genes could not be conclusively deduced using end point RT-PCR due to batch variability and lack of sensitivity of the technique in detecting subtle changes in expression. However, RT-qPCR analysis showed that loss of *Bpifa1* did not affect the expression of any of the aforementioned genes in differentiated mMEC cultures. It is important to note that at this

point, I only quantified the expression levels of these markers in cultured cells but not in the original cells. Even though mMECs retain the characteristics of the native murine epithelium, there is a possibility that the culture conditions may modify the proportions of the different cell types. This issue is explored in detail in Chapter 5.

The spectrum of proteins detected by MS in the apical secretome of the *Bpifa1*$^{-/-}$ mMECs was largely similar to that of the *Wt* cultures. Since the proteomic studies on *Wt* and *Bpifa1*$^{-/-}$ washes were not conducted simultaneously, it was not ideal to quantify the magnitude of difference in protein levels identified in the two secretomes. In this study, pooled ALI apical washes from 6 batches were used for MS analysis, due to the limited availability of samples. In future, individual apical washes from multiple batches *Wt* and *Bpifa1*$^{-/-}$ mMEC should be analysed in order to quantify differences between the two secretomes.

4.3.3 mNECs are a comparator of the mMEC culture system

The intra-nasal route is the biological route for the entry of bacteria into the middle ear and nasopharyngeal infections often precede OM development. The nasal passages of all animals consist of 4 major types of epithelia – squamous epithelium, transitional epithelium, respiratory epithelium and olfactory epithelium. The location of these epithelia within the nasal passages is highly strategic in order to effectively prevent entry of pathogens and irritants. The respiratory epithelium covers 46% of the nasal passages in rodents (Harkema et al 2006) and is similar to the epithelium of the remaining conducting airways. Previous studies in our lab have shown that BPIFA1 localises to the non-ciliated epithelial cells, in the respiratory epithelium of the nasal passages (Musa et al 2012). The method adopted for dissection of the nasal cavities (Woodworth et al 2007) along with the

highly specific growth medium used (You et al 2002) promoted the growth of the respiratory nasal epithelial cells.

Since the middle ear can be considered to be an extension of the conducting airways, I postulated that mNECs are physiologically similar to mMECs and express common epithelial markers. Therefore, I cultured mNECs cells as a comparator cell type in order to ensure successful differentiation of mouse epithelial cells using the ALI technique. Similar to mMECs, mNECs displayed a cobble-stoned morphology, however the cultures appeared homogenous, with evenly distributed ciliated cells. *Wt* and *Bpifa1*$^{-/-}$ mNECs differentiated within 14 days at ALI, expressing ciliated and goblet cell markers and recapitulating the *in vivo* nasal epithelium. *Wt* mNECs demonstrated BPIFA1 staining in the non- ciliated cells consistent with the previously published *in situ* observations (Musa et al 2012). Thus, I have shown that middle ear cells and nasal respiratory cells express similar epithelial signatures. Due to time constraints I did not pursue further studies with mNEC cultures. However, the successful culture of this cell type *in vitro* at ALI provides an ideal platform to study cell biology of the nasal passages in conjunction with the middle ear, in order to develop a holistic understanding of the aetiology of OM.

4.3.4 mMECs are an ototpathogenic model

Since the advent of PCV-7 vaccine, N*THi* has become the most common pathogen identified in OM effusions (Casey & Pichichero 2004). First and foremost, infection of mMECs using the human otopathogen, NT*Hi* demonstrated that the mMEC culture system can be effectively utilised for the study of host pathogen interactions within the middle ear. NT*Hi* initially infected or was associated with a small number of cells in culture and the infection spread laterally over time, indicating that mMECs are infected in a time dependent manner. Secondly, an elevation in expression of the pro-inflammatory molecules *Cxcl2 and*

Tnfα indicated that the model was responsive to infection. Both these aspects are discussed below along with the effect of ablation of *Bpifa1* following infection.

4.3.4.1 Evaluating the antimicrobial role of BPIFA1

Based on the structural homology of BPIFA1 with BPI which binds LPS, and its expression in the proximal airways, an area of high pathogen contact, an antimicrobial role was originally suggested for this protein (Bingle & Craven 2002). As described in Chapter 3, a number of *in vivo* pulmonary infection models have suggested an increased susceptibility of *Bpifa1* deficient mice to bacterial challenges. In addition, a number of *in vitro* studies have highlighted the antimicrobial function of this protein. For example, *Bpifa1* reduced biofilms formation by *K.pneumoniae* and *P.aeruginosa* on polarized human airway epithelial cells and nasal cells by increasing the surface tension at ALI (Gakhar et al 2010, Liu et al 2013a). BPIFA1 exerted bacteriostatic effects on *B.cepacia and P.aeruginosa* and the suggested mechanism in the later is by formation of small pores in the bacterial cell wall (Sayeed et al 2013, Walton et al 2016). BPIFA1 inhibited growth of *M.pneumoniae* upon infection of HBE cells and has been suggested to decrease adhesion of *M.pneumoniae* to host cells *(Chu et al 2007, Gally et al 2011)*. Purified chinchilla BPIFA1 exhibited bactericidal activity against NT*Hi in vitro* (McGillivary & Bakaletz 2010).

Therefore, I hypothesized that *Bpifa1*$^{-/-}$ mMECs would show increased susceptibility to NT*Hi* infection in comparison to *Wt* cultures. BPIFA1 expressing cells appeared to be resistant to early infection at 24 hpi. However, there was no difference in the level of initial adhesion of NT*Hi* between *Wt* and *Bpifa1*$^{-/-}$ mMECs at 1 hpi. The quantification of infection was challenging because of the batch variation seen in the cultures. Although each batch of *Bpifa1*$^{-/-}$ mMECs appeared to be infected to a greater degree than the *Wts*, as seen by IFC and also indicated by increased nuclear fragmentation in *Bpifa1*$^{-/-}$ mMECs, this difference did not reach of statistical significance. I also did not see a difference in the amount of infection at 48 and 72hpi by using viable counts, a more reliable method of quantification.

A possible reason for this observation may be that the viable counts were performed without washing the apical surfaces of cells with a view to compare the total associated bacteria. On the contrary, IFC was performed using cells whose apical surfaces had been washed and hence most bacteria detected were internalised bacteria. Perhaps, washing the cells before performing viable counts would give us a better comparison to the IFC data. However due to time constraints viable counts for analysing internalised bacteria could not be repeated. A previous study had reported a decrease in biofilm biomass of *P.aeruginosa* on incubation with recombinant BPIFA1 using a crystal violet biofilm assay but the researchers could not detect a reduction in CFU/ml using traditional viable counts methodology (Liu et al 2013a). They attributed this effect to the surfactant properties of BPIFA1, which helps in dispersing these matrix-encased bacterial communities, rather than to its antimicrobial properties. There is conflicting evidence on the formation of biofilms by NT*Hi* and its relevance in OM. Several studies showed that culture negative effusions from patients showed presence of NT*Hi* components and transcripts by PCR based methods (Bakaletz 2007, Swords 2012). We did not study the effect of BPIFA1 loss on NT*Hi* biofilm formation in mMECs, however this avenue requires further investigation using the model system.

4.3.4.2 Evaluating the immunomodulatory role of BPIFA1 upon NTHi infection

In this chapter I have evaluated the expression levels of *Cxcl2* and *Tnfα* alpha, two pro-inflammatory mediators commonly upregulated during bacterial OM, during NT*Hi* infection of mMECs. The chemokine Cxcl2/MIP2α is the murine homologue of human IL-8 and is a key mediator of overproduction of mucins and of neutrophil chemotaxis (Juhn et al 2008). NT*Hi* infection is known to stimulate *Cxcl2* upregulation in several murine tissues including the middle ear, lungs and the inner ear (Gaschler et al 2009, Lim et al 2007, Woo et al

2012). Moreover, *Cxcl2* was identified as the most upregulated gene when mice were trans-tympanically injected with NT*Hi* and on infection of the immortalized mouse middle ear epithelial cell line (mMEEC) with NT*Hi* (Preciado et al 2013). *TNFα* is produced through a TLR-2 mediated response to NT*Hi*. It results in infiltration of inflammatory cells as well as release of other pro-inflammatory cytokines through activation of the NFκB signalling cascade. Thus, it is a key early response cytokine and also plays an important role in OM sequelae (Larrick et al 1998, Moon et al 2006). *TNFα* was upregulated on NT*Hi* infection of primary human middle ear cells (Moon et al 2008, Tong et al 2001). My data shows that *Cxcl2* was significantly upregulated on NT*Hi* infection of *Wt* as well as *Bpifa1*$^{-/-}$ mMECS after 24 and 48 hours post infection in comparison to the respective MOCK controls. *Tnfα*, was also upregulated in the infected cultures of both genotypes, although this did not reach statistical significance. Taken together, the data suggests that the mMEC model responds to bacterial infection in a manner similar to the native middle ear epithelium. This opens up a new avenue to use the model for the study of the response of middle ear cells to different insults, injuries and infections. This will enable the study of interaction of host middle ear epithelial cells with a variety of bacterial as well as viral otopathogens.

Based on the structural homology to BPI, which is an anti-inflammatory protein, several pulmonary infection studies have suggested a similar role for BPIFA1. Recombinant BPIFA1 has shown to reduce IL-8 production in HBE cells upon *M.pneumoniae* infection (Chu et al 2007). Moreover, BAL fluid from *Bpifa1*$^{-/-}$ mice showed higher levels of *Cxcl2* amongst other cytokines during acute infection with infected with *P.aeruginosa* (Liu et al 2013b) whereas transgenic overexpression of BPIFA1 leads to decreased production of *Tnfα* (Lukinskiene et al 2011). We hypothesized that the loss of the anti-inflammatory function of BPIFA1 would lead to an increased *Cxcl2* and *Tnfα* response in the *Bpifa1*$^{-/-}$ mMECS upon infection. However, expression of both markers was seen at similar levels in *Wt* and *Bpifa1*$^{-/-}$ mMECS and I did not observe an anti-inflammatory effect of *Bpifa1* upon infection. The effect of

deletion of *Bpifa1* on expression of a wider spectrum of cytokines in original mouse middle ear epithelial cells has been evaluated in Chapter 5.

Epithelial remodelling, one of the most common features of OM and often a consequence of infection, is characterised by mucous metaplasia. There are several reports on induction of mucin genes upon NT*Hi* infection as well as on TNFα treatment using the current *in vitro* middle ear models (Lim & Moon 2012, Nakamura et al 2013, Samuel et al 2008). (Liu et al 2013b) showed that the decline in *Muc5ac, Muc5b* and *FoxJ1* in *Bpifa1*$^{-/-}$ lungs persisted upon acute *P.aeruginosa* infection. Therefore, I evaluated expression of the mucin genes, *Muc5ac* and *Muc5b* and the ciliated cell marker, *Foxj1* following infection and compared it between the two genotypes. Unfortunately, this study was particularly compromised by batch variation. I did not observe any clear trends or difference in the expression of epithelial genes, following NT*Hi* infection or between the two genotypes. The lack of change in expression could also be because this study tested an acute response to NT*Hi* infection whereas chronic persistence of infection may be needed to observe an obvious effect in the epithelial cell types.

4.3.5 Regulation of BPIFA1 following NT*Hi* infection

BPIFA1 is expressed at high basal levels in the upper airways and the middle ear and it is tightly modulated during infection. The direction of modulation may vary with the type of pathogen. A number of studies such as pulmonary infections with *M.pneumoniae* and *K.pneumoniae* report increased levels of BPIFA1 in the BALF of mice upon infection (Chu et al 2007, Liu et al 2013a). Our own study saw an initial non-significant decline in the cytoplasmic levels of BPIFA1 staining with progression of NT*Hi* infection using IFC. My initial assumption was that the decrease in cytoplasmic BPIFA1 might be accompanied by increase in secreted BPIFA1 in the apical washes. On the contrary, a significant decrease in

secreted BPIFA1 was observed at 48hpi and 72hpi. I reasoned that this decrease might be due to proteolytic cleavage of BPIFA1 during infection. A previous report has shown that BPIFA1 secreted by HBE cells is degraded when treated with neutrophil elastase (Jiang et al 2013b). Another study showed that inhibiting proteinase activity during *P.aeruginosa* infection increased the levels of BPIFA1 in BAL fluids of mice (Jiang et al 2013a). However, the western blotting data did not show any obvious degradation bands in the infected samples compared to the MOCKs. Another explanation for this observation could be that secreted BPIFA1 binds to NT*Hi* present in the wash and is pelleted out during the centrifugation step of the protocol and hence the reduced levels in the supernatants. In future, bacterial pull down assays can be performed to detect BPIFA1 bound to NT*Hi.* In order to test the decrease in BPIFA1 levels further, I quantified mRNA levels of *Bpifa1* using RT-qPCR and found that there was indeed a decrease in every batch of infected sample compared to its corresponding MOCK control from the same batch. Although batch variation was observed, this decrease was statistically significant at 48 hpi. My observation is supported by the study by Britto et 2013, where the authors report a reduction in lung *Bpifa1* mRNA and BPIFA1 protein in BAL fluids following acute infection with *P. aeruginosa, S. pneumoniae, influenza A* as well as LPS stimulation. The authors also replicated this observation in mTECs treated with LPS where they saw a reduction in *Bpifa1* mRNA and protein at a similar time point used in this study. Thus, modulation in BPIFA1 levels functions as a biosensor of pathogenic insult, which may signal the host to mount an immune response against the pathogen. However, it is not clear if this decrease is a transcriptional downregulation of BPIFA1 promoter activity or a change in the phenotype of epithelial cells due to infection.

4.3.6 Potential for utilising mMECs as a model for studying OM pathogenesis

A number of mouse models are available for the study of OM. These include mice deficient in innate immunity genes such as *Evi1*, *Fbxo11, TLRs* and *Myd88,* ciliary development genes such as *Dnahc5* (Rye et al 2011a) and goblet cells (Roy et al 2014). It is known that primary cells cultured from CF and asthma patients maintain the disease phenotype in culture (Davies et al 2003, Matsui et al 1998). It will be interesting to investigate if the mMEC culture system can be utilised to reproduce the OM phenotype of these mouse mutants *in vitro* and enable comparative studies between unaffected and diseased cultures.

OM often encompasses complex responses involving the middle ear epithelium, sub-epithelial mesenchyme, inflammatory cells and middle ear effusion, making it challenging to identify epithelial cell-specific responses. The mMEC culture system provides us with the ability to isolate and assay responses of specific sub populations of epithelial cells. Our cell isolation method eliminates the influence of explants and excludes fibroblasts from culture, which were two of the most important confounding factors in previous models of primary middle ear epithelial cells. mMECs are a 3-dimentional model of the middle ear epithelium and hence mimics the *in vivo* physiology more closely compared to the available cell lines. Thus mMECs have several advantages over the currently available *in vitro* middle ear models.

The possibility of replicating the phenotype of the genetic models of OM, the capacity to easily manipulate differentiation of cells by modifying culture conditions and the ability to infect cells with various otopathogens, makes the model applicable to the wider OM community.

4.3.7 Batch variation

A major confounding factor throughout the studies outlined in this chapter was the variation among different batches of mMECs. Firstly, it is well known that primary cultures show substantial disparity between different batches, and the growth media used may influence this. Although the media used for mMEC cultures has been carefully optimised to promote growth of upper respiratory epithelial cells (You et al 2002), an influence of lot-to-lot variation in media components such as serum and growth factors cannot be overlooked. Secondly only a small portion of the cells seeded was found to adhere to the membrane at day 3, which then proliferated and differentiated to establish an epithelial culture. Depending on the proportion of cells attached and their fate, the composition of the epithelium established in cultures can be variable, leading to a different proportion of goblet cells, secretory cells and ciliated cells in each batch of mMECs and hence the difference in the levels of various epithelial markers expressed.

NT*Hi* showed a heterogeneous pattern of infection in mMECs. Although each batch of *Bpifa1*$^{-/-}$ mMECs appeared to be infected at a greater level than *Wt* mMECs by IFC, the difference in levels of infection among batches made descriptive statistical evaluation of the results challenging. Owing to time constraints, an evaluation of susceptibility of the different cell types, other than BPIFA1 expressing cells, to NT*Hi* infection was not possible. However, a variation in proportions of the different cell types being infected may partially be accountable for the discrepancy in levels of infection among different batches.

Lastly, contamination of isolated RNA by components of the TRI reagent added to the variation seen among biological replicates in the RT-qPCR data. This aspect has been discussed in detail in the general discussion. However, despite the batch variation, I have presented individual data points where relevant in an attempt to describe any trends in data.

In future, this problem can be addressed by increasing the number of batches used for study in addition to using multiple wells from each batch. However, this was not feasible during this study due to the time period required for proliferation and differentiation of each batch of mMECs and sacrifice of wells from each batch for model validation and for confirmation of differentiation of cells.

4.4 Key experimental conclusions

- I have developed a novel *in vitro* model of mouse middle ear epithelial cells (mMECs) at the ALI, which recapitulates the characteristics of the native murine ME epithelium.
- The various epithelial cell populations in differentiated mMECs were systematically characterised and compared to those seen within the native middle ear, using transcriptional and proteomic approaches.
- mMEC secretions included a multitude of innate defence proteins.
- mMECs supported the growth of the otopathogen, NT*Hi* and mounted a response to the infection by upregulation of *Cxcl2,* suggesting that the model can be successfully utilised to study host pathogen interactions in the middle ear.
- *Bpifa1*$^{-/-}$ mMECs were morphologically similar to *Wt* mMECs and did not show differences in expression of other epithelial markers.
- *Bpifa1*$^{-/-}$ mMECs demonstrated slightly enhanced susceptibility to NT*Hi* infection, albeit not statistically significant. However, *Bpifa1* did not exhibit an overt anti-inflammatory role during infection.
- BPIFA1 was expressed at high basal levels in naïve *Wt* mMEC cultures. BPIFA1 expressing cells appeared to be resistant to initial infection and the levels of *Bpifa1* reduced upon infection. These findings indicate a role for BPIFA1 in impeding early infection under steady state conditions and acting as a biosensor, signalling activation of a host immune response upon infection. However, whether the regulation is a result of an effect on BPIFA1 promoter activity or a phenotypic change in the epithelial cells needs to be investigated further.

CHAPTER 5: ASSESSMENT OF THE EFFECTS OF *BPIFA1* DELETION IN AN EXISTING MODEL OF OTITIS MEDIA

5.1.1 Introduction:

The *Evi1*$^{Jbo/+}$ mouse is a well-established model of chronic OM and conductive hearing loss. *Evi1*$^{Jbo/+}$ mice spontaneously develop OM, characterised by accumulation of inflammatory fluid in the middle ear cavity and increase in middle ear mucosal thickness. The causative mutation in these mice is a SNP in the transcription factor; *Evi1*, which consists of two ZnF domains and a proline rich linker domain (Parkinson et al 2006). Each domain interacts with several co-activators and co-repressors and is thus involved in regulating multiple signalling pathways as described in Section 1.12.1.2. Of these, the interactions with the TGF-β signalling pathway via its first ZnF domain and the intermediate repressor domain are most widely studied (Izutsu et al 2001, Kurokawa et al 1998a, Kurokawa et al 1998b). The mutation in *Evi1*$^{Jbo/+}$ mice is in the second ZnF domain, which has been recently shown to act as a negative feedback regulator of NF-κB signalling (Xu et al 2012). However, it is not known if this mutation also has an effect on the binding capacity of the first ZnF domain or the intermediate repressor domain.

Several studies have identified components of both TGFβ and NFκB signalling pathways as candidate genes in susceptibility to OM development (MacArthur et al 2014, Rye et al 2011a, Segade et al 2006). Fig 5.1 describes the potential involvement of the two signalling cascades in OM susceptibility in *Evi1*$^{Jbo/+}$ mice. The transcription factor NFκB is a hetero or homo dimer of multiple REL proteins, the most common one being a heterodimer of REL A/p65 and p50 (Chen & Greene 2004). Under normal physiological conditions the p65/p50 complex is maintained in an inactive state in the cytoplasm via the interaction with the inhibitor molecule IKK. However, an inflammatory stimulus leads to the degradation of IKK and translocation of the p65/p50 complex to the nucleus, where it binds to the target DNA sequences and activates several pro-inflammatory markers such as TNFα, IL1β, IL-10 as well as chemo attractants such as IL-8 (Cxcl2 in mice) which leads to infiltration of inflammatory

cells (Chen & Greene 2004). A recent study has shown that EVI1 which itself is induced by the inflammatory stimulus such as NTHi and TNFα and negatively regulates the NFκB signalling cascade by physically interacting with the p65 subunit of NFκB and preventing its acetylation (Xu et al 2012). Thus functional EVI1 acts as a negative feedback regulator of the NFκB signalling pathway and helps to prevent an excessive inflammatory response. Inflammatory stimuli also activate TGFβ signalling via induction of SMAD3, which in turn forms a complex with SMAD4. The SMAD3/SMAD4 complex translocates to the nucleus where it binds to and activates target genes involved in various regulatory processes such as cell proliferation, differentiation, wound repair and apoptosis (Kurokawa et al 1998a, Makinde et al 2007). EVI1 physically binds SMAD3 and thus alters DNA binding ability of the SMAD3/SMAD4. Thus by quenching SMAD3, it antagonizes TGFβ signalling (Rye et al 2011a). Moreover, there is significant cross talk between the TGFβ and NFκB signalling pathways since the SMAD3/SMAD4 complex promotes acetylation of p65 (Ishinaga et al 2007). Thus a mutation in *Evi1* may cause a loss of its function to negatively regulate the NFκB and TGFβ signalling pathways leading to chronic inflammation in the middle ear and failure of proper resolution of this inflammation in $Evi1^{Jbo/+}$ mice.

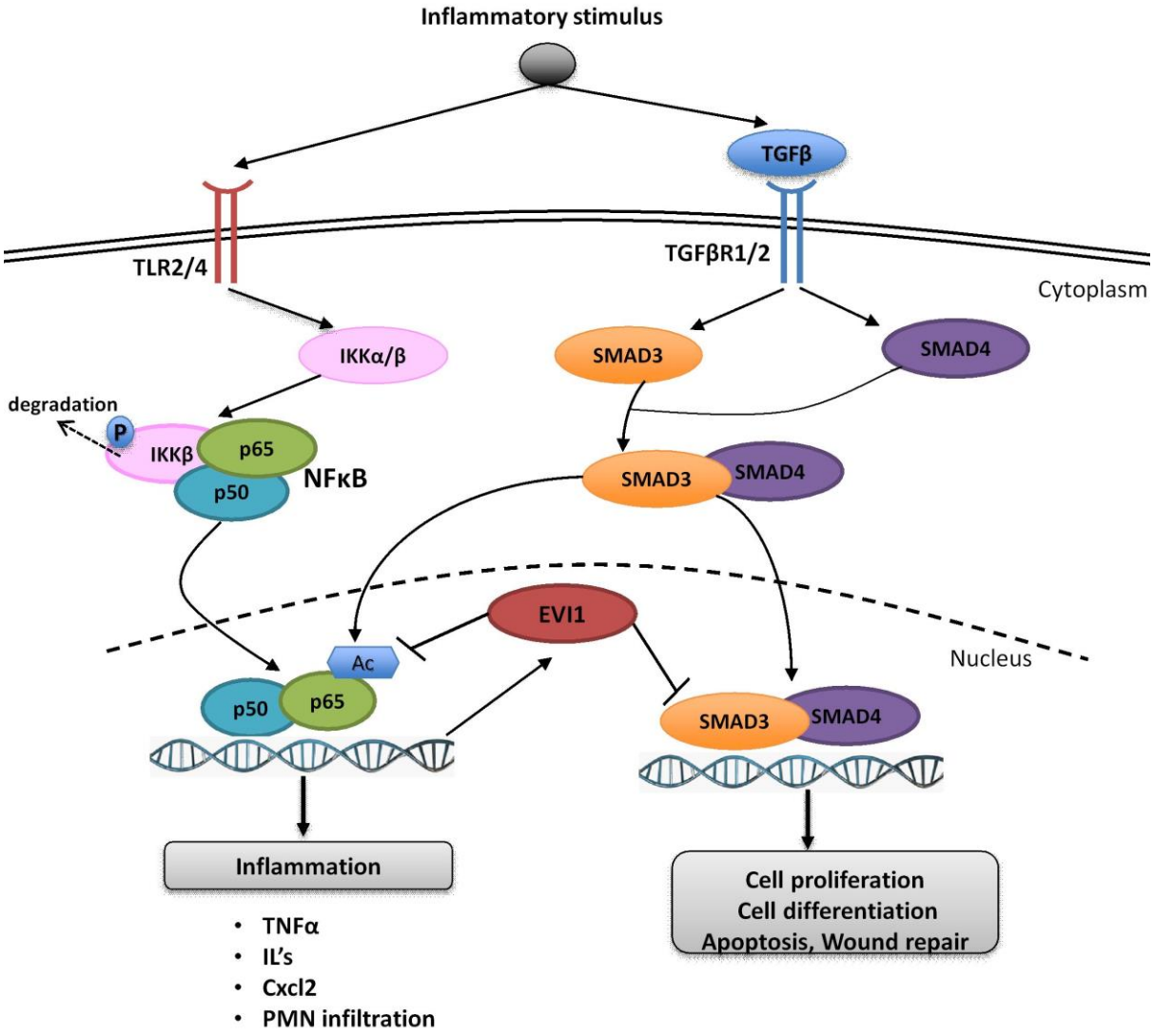

Figure 5.1 Potential role and interaction between NFκB and TGFβ signalling pathways in susceptibility to OM in *Evi1*$^{Jbo/+}$ mice.
EVI1 acts as a negative regulator of NFκB and TGFβ signalling pathways and thus a mutation in *Evi1*$^{Jbo/+}$ mice may result in excess inflammation and failure of proper resolution of infection in.

BPIFA1 is a major secretory product of the upper airway epithelium (Campos et al 2004) and is also abundantly expressed in the middle ear epithelium (Section 1.8.2). In Chapters 3 and 4, I have mainly focussed on investigating the antimicrobial role of BPIFA1 by assessing the susceptibility of *Bpifa1*$^{-/-}$ mice and *Bpifa1*$^{-/-}$ mMECs to the ototpathogen NT*Hi*. However, another important putative role for BPIFA1 in host defence is through an

immunomodulatory function, suggested on the basis of its structural similarity to the anti-inflammatory protein, BPI (LeClair 2003). Several studies have supported an anti-inflammatory role for BPIFA1 in the presence of an inflammatory stimulus. For example, *Bpifa1* ablation was associated with exaggerated levels of pro-inflammatory mediators CXCL2, TNFα, IL1β and IL6 in BAL fluids after infection with *K.pneumoniae* and *M.pneumoniae* compared to *Wt* mice (Liu et al 2013a, Liu et al 2013b). On the other hand, treatment of human primary airway epithelial cultures with recombinant BPIFA1 reduced the mRNA levels of *IL8* after infection with *M.pneumoniae* (Chu et al 2007) and transgenic mice overexpressing *Bpifa1* showed lower levels of IL1β and CXCL2 in BAL fluids after exposure to *P.aeruginosa* compared to *Wt* control mice (Lukinskiene et al 2011). Moreover *Bpifa1*$^{-/-}$ mice showed increased neutrophilic infiltration in pulmonary infection models of *M.pneumoniae, P.aeruginosa and K.pneumoniae* and showed increased bacterial clearance (Gally et al 2011, Liu et al 2013a, Liu et al 2013b).

Previous studies in our lab have suggested a decrease in staining intensity of BPIFA1 with OM progression in *Evi1*$^{Jbo/+}$ mice and indicated partial proteolytic degradation of BPIFA1 in *Evi1*$^{Jbo/+}$ ear exudates, suggesting an involvement or BPIFA1 in OM development in these mice (Section 1.13). Based on these data and the anti-inflammatory role of BPIFA1, I postulated that *Bpifa1* deletion in the existing inflammatory microenvironment of *Evi1*$^{Jbo/+}$ mice may lead to an exacerbation of the OM phenotype. This is the first study to report the use of compound *Bpifa1* mutants.

5.1.2 Aims of this study

The primary aim of this chapter was to ascertain if *Bpifa1* ablation led to an exacerbation of the OM phenotype in *Evi1*$^{Jbo/+}$ mice, an established model of chronic OM. Subsequently, the effect of *Bpifa1* deletion on a repertoire of inflammatory, epithelial and sub-epithelial markers in the middle ear mucosa was evaluated, in order to uncover its role in aggravation of OM. Lastly, this chapter aimed to recapitulate the OM phenotype *in vitro* using the mMEC culture system.

5.1.3 Study design

Fig 5.2 gives a brief layout of the study plan for this chapter. *Bpifa1*$^{-/-}$*Evi1*$^{Jbo/+}$ compound mutants and their control genotypes were generated on the C3H/HeH background as described in Section 2.1.3. Viability of this line was assessed by analysing genotype ratios of the progeny (Section 5.2.1). It is known that *Evi1*$^{Jbo/+}$ mice develop CSOM by P28 (Parkinson et al 2006). Morphometric analysis of middle ear mucosal thickness and presence of middle ear effusion was performed on *Bpifa1*$^{-/-}$*Evi1*$^{Jbo/+}$ mice at P21 and P28 in order to evaluate if loss of *Bpifa1* leads to accelerated and exaggerated OM development (Section 5.2.2). *Bpifa1*$^{-/-}$*Evi1*$^{Jbo/+}$ mice between 7-10 weeks of age were analysed for body weights and persistence of OM in adulthood (Section 5.2.3 and Section 5.2.4). RT-qPCR for expression of inflammatory and epithelial genes was performed on isolated middle ear mucosal cells, in order to further investigate the OM phenotype (Section 5.2.5.1 and Section 5.2.5.2). The mMEC culture system (developed in Chapter 4) was utilised to attempt recapitulation of the OM phenotype *in vitro*. Expression of inflammatory and epithelial genes was compared between mMECs cultures from *Bpifa1*$^{-/-}$*Evi1*$^{Jbo/+}$ mice and the control genotypes at a

transcriptional as well as proteomic level (Section 5.2.6). Furthermore, the effect of *Bpifa1* ablation on the proliferative potential of mMECs and fibroblasts was analysed (Section 5.2.7). Lastly, IHC was used in order to identify of the effect of *Bpifa1* ablation on other epithelial and sub-epithelial proteins *in vivo* (Section 5.2.6).

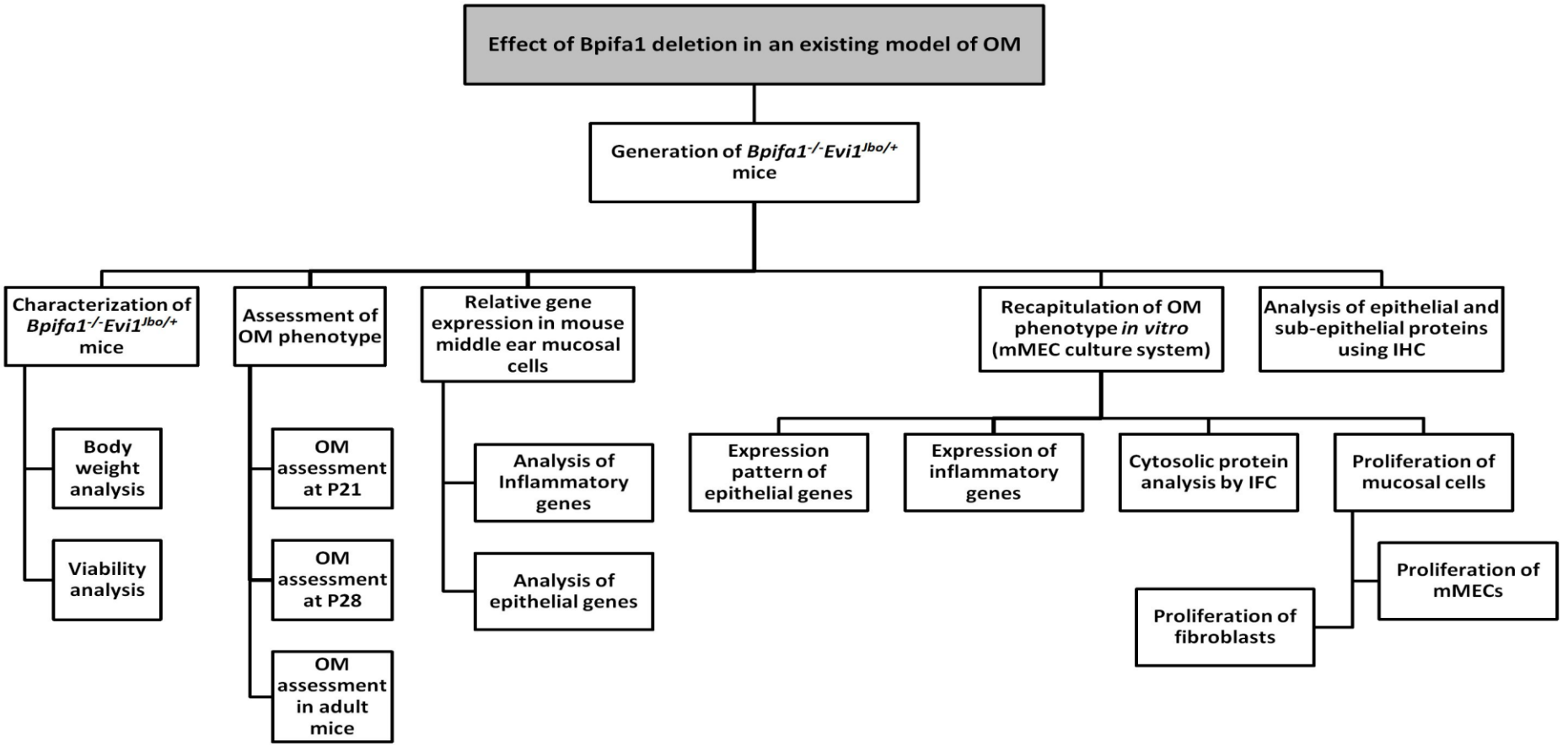

Figure 5.2 Study plan for this chapter

5.2 Results

5.2.1 Genotype ratio analysis of the *Bpifa1*$^{-/-}$*Evi1*$^{Jbo/+}$ line

The breeding strategy for generation of the compound mutants is described in detail in Section 2.1.3, Fig.2.2. Briefly, *Bpifa1*$^{+/-}$ mice on a C57BL/6 background, were made congenic on the C3H/HeH background by recurrent backcrossing and then outcrossed with *Evi1*$^{Jbo/+}$ mice (which are maintained on the C3H/HeH background), in order to produce *Bpifa1*$^{+/-}$ *Evi1*$^{Jbo/+}$ mice. To generate *Bpifa1*$^{-/-}$*Evi1*$^{Jbo/+}$ compound mutants and other control genotypes mentioned in Table 5.1, *Bpifa1*$^{+/-}$ mice were crossed with *Bpifa1*$^{+/-}$*Evi1*$^{Jbo/+}$ mice. The viability of the *Bpifa1*$^{-/-}$*Evi1*$^{Jbo/+}$ line, assessed by analysing genotype ratios of the progeny from this cross (Chi-square test) exhibited normal Mendelian ratios at weaning age, P21 (Table 5.1). All mice were inspected daily by ward technicians and no anomalies were observed in the general health and behaviour of *Bpifa1*$^{-/-}$*Evi1*$^{Jbo/+}$mice.

Table 5.1: Numbers of live mice for the *Bpifa1*$^{-/-}$*Evi1*$^{Jbo/+}$ line

Genotype	Observed numbers	% Observed	Expected numbers	% Expected	P-value
***Bpifa1*$^{+/-}$*Evi1*$^{Jbo/+}$**	91	22.09	104	25	0.5329
***Bpifa1*$^{+/-}$**	108	26.21	104	25	
***Bpifa1*$^{-/-}$*Evi1*$^{Jbo/+}$**	43	10.44	51	12.5	
***Bpifa1*$^{-/-}$**	48	11.65	51	12.5	
***Evi1*$^{Jbo/+}$**	56	13.59	51	12.5	
Wt	67	16.02	51	12.5	
Total	412	100	412	100	

5.2.2 Loss of *Bpifa1* exacerbates the OM phenotype of *Evi1*$^{Jbo/+}$ mice.

Morphometric analysis was performed on H&E stained middle ear sections from offspring of the *Bpifa1*$^{-/-}$*Evi1*$^{Jbo/+}$ line at P21 and P28. In order to determine if the loss of *Bpifa1* exacerbated the phenotype in an existing model of OM, *Bpifa1*$^{-/-}$*Evi1*$^{Jbo/+}$ mice were

compared with *Evi1*$^{Jbo/+}$ mice. In addition, *Bpifa1*$^{+/-}$*Evi1*$^{Jbo/+}$ mice were used to assess whether haploinsufficiency of *Bpifa1* resulted in a similar effect. In Chapter 3, I have shown that *Bpifa1*$^{+/-}$ and *Bpifa1*$^{-/-}$ mice do not develop spontaneous OM on a C57BL/6 background (Section 3.2.3). Here, the two genotypes were used as controls to test if the C3H/HeH background influenced OM development. Lastly, *Wt* mice were included in the study as the baseline comparison.

Here, the two criteria used for assessment of the OM phenotype were:

(i) The presence of middle ear exudate. (ii) The thickness of the middle ear mucosa.

5.2.2.1 OM development at P21

Histological assessment of middle ear sections identified an OM phenotype in a proportion of *Bpifa1*$^{-/-}$*Evi1*$^{Jbo/+}$ and *Evi1*$^{Jbo/+}$ at P21, characterised by the presence of middle ear fluids and thickening of the mucoperiosteum that was not present in the *Bpifa1*$^{-/-}$ and *Wt* mice. The middle ear fluids collected from both *Bpifa1*$^{-/-}$*Evi1*$^{Jbo/+}$ and *Evi1*$^{Jbo/+}$ *mice* were either cellular or serous. Fig 5.3 shows representative images of the middle ear cavities from mice of the 4 genotypes.

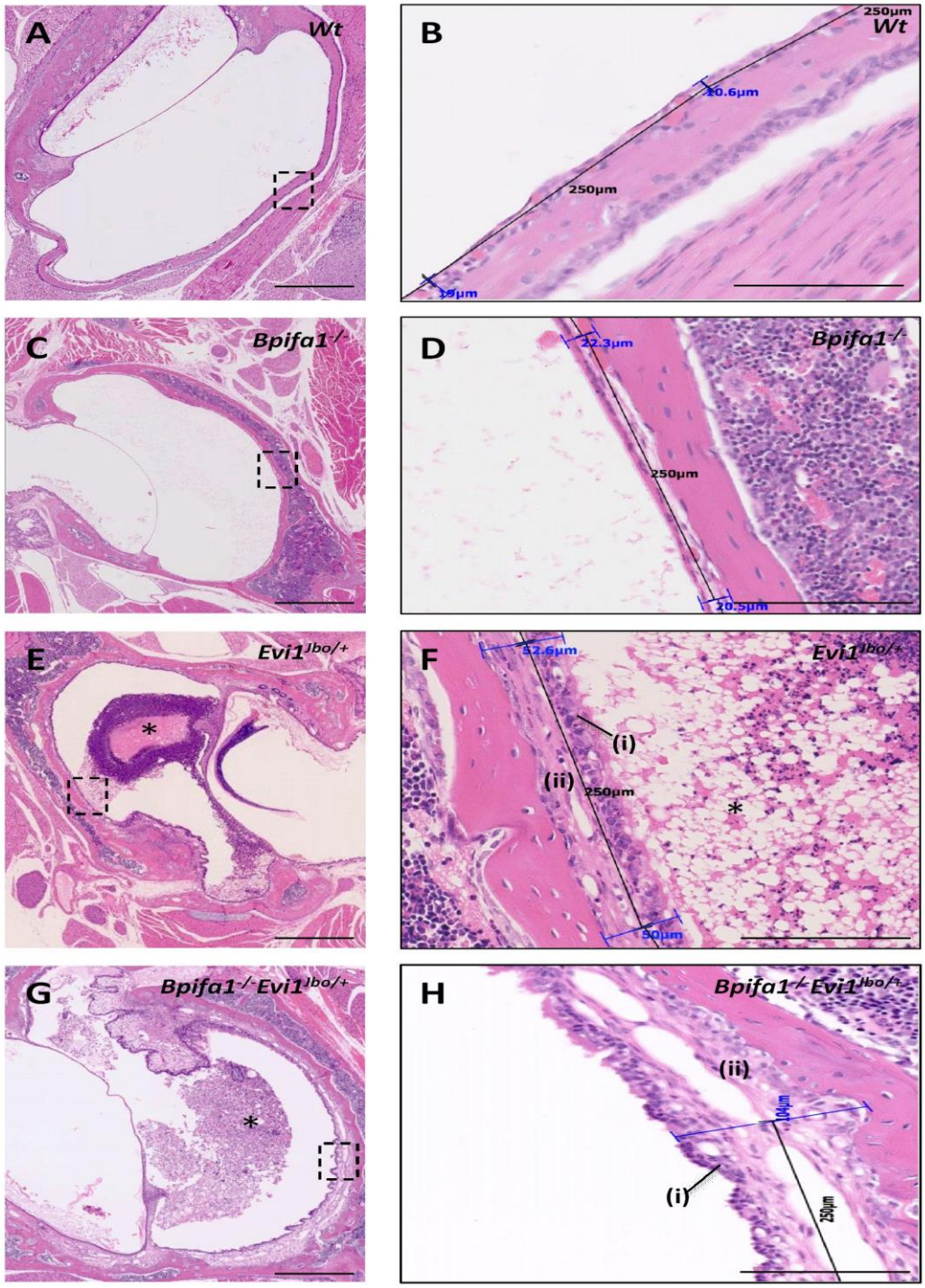

Figure 5.3 H&E stained middle ear sections at P21

Dorsal plane H&E sections from middle ears of *Wt* (A, B), and *Bpifa1*$^{-/-}$ (C, D) mice show no OM development. H&E sections from middle ears of *Evi1*$^{Jbo/+}$ (E, F) *and Bpifa1*$^{-/-}$*Evi1*$^{Jbo/+}$ (G, H) mice demonstrate presence of an OM phenotype marked by mucosal thickening and presence of inflammatory ear fluids (asterisk). Mucosal thickening is a combination of epithelial hyperproliferation (i) and sup-epithelial mesenchyme expansion (ii). Mucosa of *Bpifa1*$^{-/-}$*Evi1*$^{Jbo/+}$ (H) is more thickened than *Evi1*$^{Jbo/+}$ mice (F). Scale bar 500µm for low magnification images and 100µm for high magnification images. *Wt* ears (n=28), *Bpifa1*$^{-/-}$ ears (n=16), *Evi1*$^{Jbo/+}$ ears (n=32) and *Bpifa1*$^{-/-}$ *Evi1*$^{Jbo/+}$ ears (n= 31).

OM can develop unilaterally or bilaterally. Hence development of OM in each ear was considered as an independent event for analysis. At this time point, the number of fluid containing *Bpifa1*$^{-/-}$*Evi1*$^{Jbo/+}$ middle ears (21/30) was higher than that for both *Bpifa1*$^{+/-}$ *Evi1*$^{Jbo/+}$ (16/31) and *Evi1*$^{Jbo/+}$ (16/32) ears, however this difference was not statistically significant. 3/19 *Bpifa1*$^{+/-}$ and 4/28 *Wt* ears also showed middle ear fluid, however this was significantly lower compared to *Bpifa1*$^{-/-}$*Evi1*$^{Jbo/+}$ mice (p = 0.000006). None of the *Bpifa1*$^{-/-}$ mice (n=16 ears) displayed an OM phenotype (Fig 5.4).

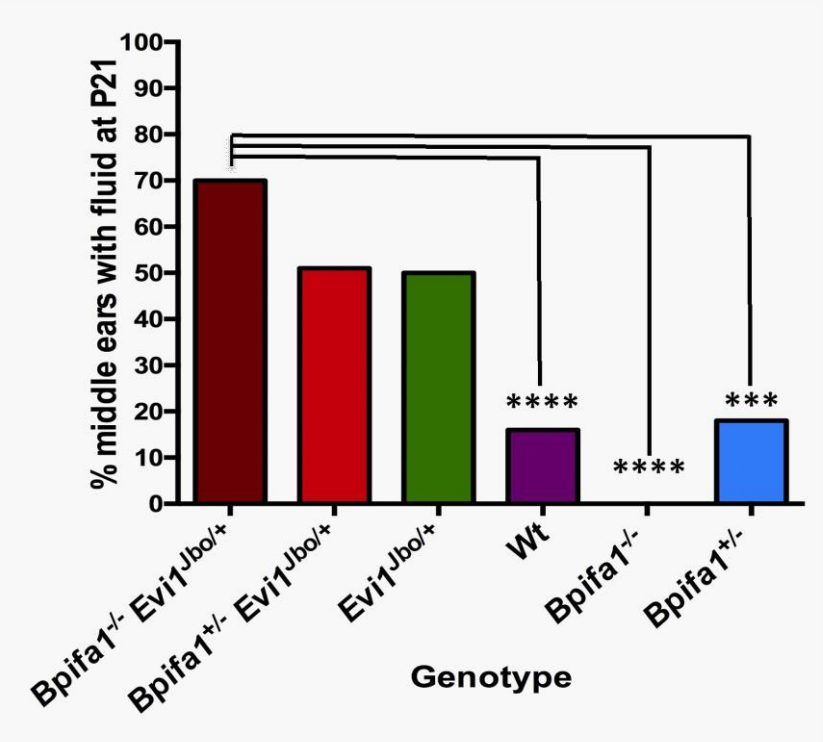

Figure 5.4 Percentage ears with middle ear fluids at P21
The percentage of *Bpifa1*$^{-/-}$*Evi1*$^{Jbo/+}$ (n=30), *Bpifa1*$^{+/-}$*Evi1*$^{Jbo/+}$ (n=31), *Evi1*$^{Jbo/+}$ (n=32), Wt (n=28), *Bpifa1*$^{-/-}$ (n=16) and *Bpifa1*$^{+/-}$ (n=19) middle ears with inflammatory effusion at P21. The difference between *Bpifa1*$^{-/-}$*Evi1*$^{Jbo/+}$ and *Evi1*$^{Jbo/+}$ mice was not significant at P21. Fishers exact test ****p<0.0001.

There were no sex related differences in the numbers of *Bpifa1*$^{-/-}$*Evi1*$^{Jbo/+}$ (n=13) *Bpifa1*$^{+/-}$ *Evi1*$^{Jbo/+}$ (n=10) and *Evi1*$^{Jbo/+}$ (n=9) mice that had middle ear fluids (Fig 5.5 A). There were also no significant differences in the percentage of mice developing middle ear fluids in one ear versus the percentage of mice developing middle ear fluids in both ears (Fig 5.5 B).

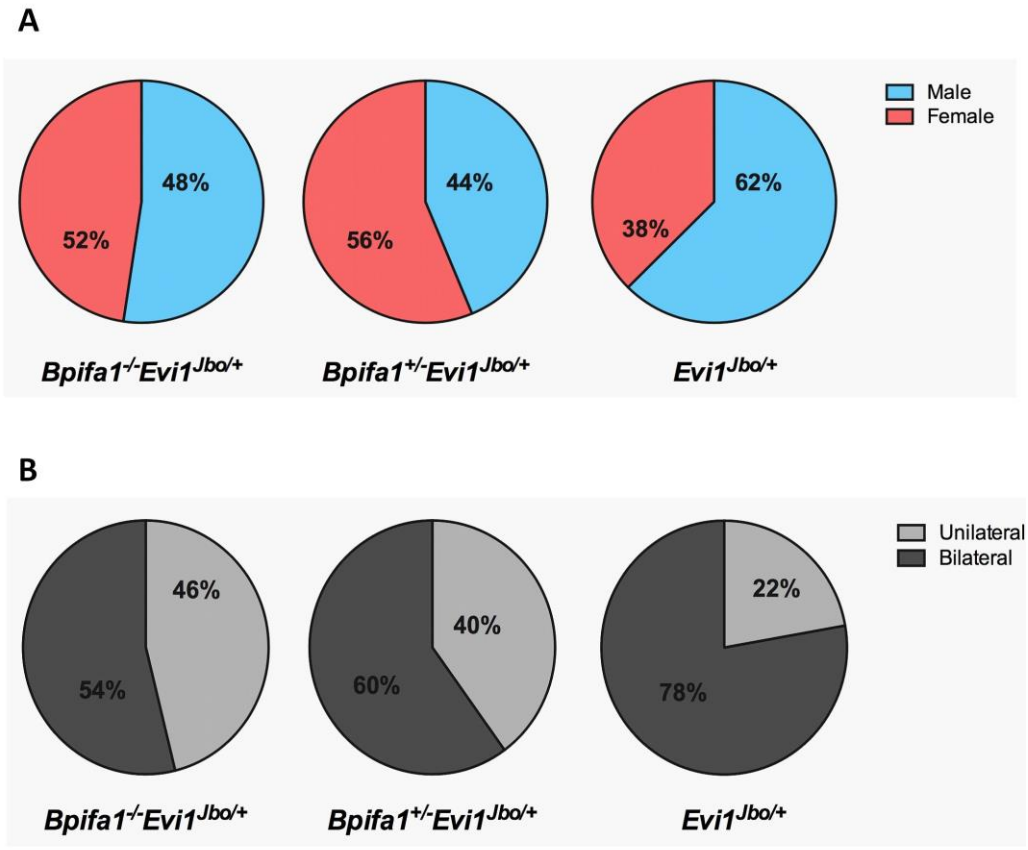

Figure 5.5 Analysis of mice with middle ear fluids at P21
No sex related differences were seen between percentages of mice with middle ear fluids (A). No difference was seen between percentage of mice with unilateral and bilateral OM (B). *Bpifa1*$^{-/-}$ *Evi1*$^{Jbo/+}$ (n=13) *Bpifa1*$^{+/-}$*Evi1*$^{Jbo/+}$ (n=10) and *Evi1*$^{Jbo/+}$ (n=9); Fishers exact test.

Bpifa1$^{-/-}$*Evi1*$^{Jbo/+}$ middle ears (n=30) showed significantly more thickened mucosa compared to *Evi1*$^{Jbo/+}$ ears (n= 32 p<0.01), *Bpifa1*$^{+/-}$*Evi1*$^{Jbo/+}$ ears (n=21, p<0.0001), *Wt* ears (n=28, p<0.0001), *Bpifa1*$^{+/-}$ ears (n=19, p<0.0001) and *Bpifa1*$^{-/-}$ ears (n=16, p<0.0001). However, at this point, there was no difference in the mucosal thickening in *Bpifa1*$^{+/-}$*Evi1*$^{Jbo/+}$ and *Evi1*$^{Jbo/+}$ mice (Fig. 5.6).

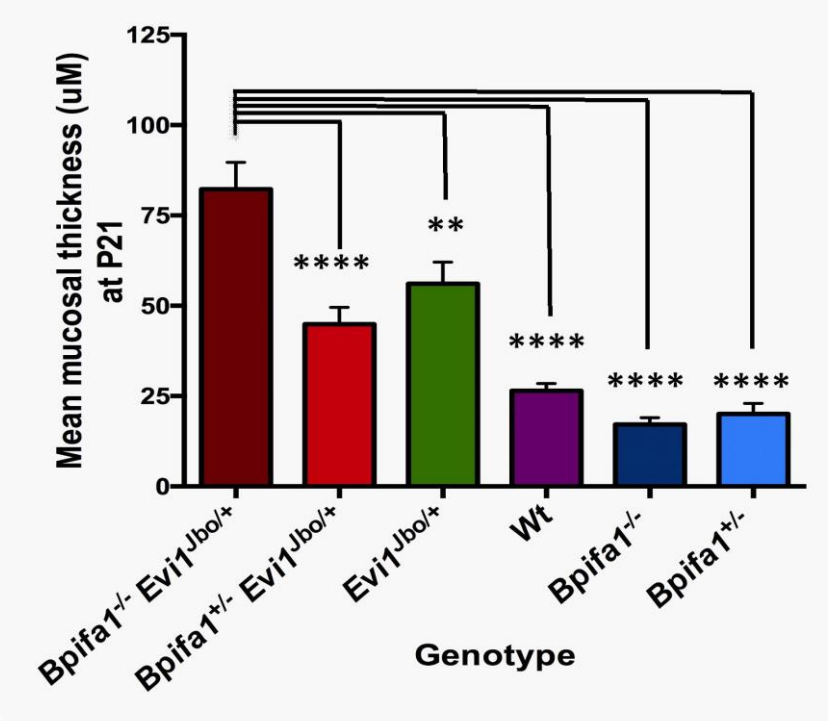

Figure 5.6 Mucosal thicknesses at P21
Mean mucosal thickness of *Bpifa1*$^{-/-}$*Evi1*$^{Jbo/+}$ (n=30) middle ears was significantly higher compared *Bpifa1*$^{+/-}$*Evi1*$^{Jbo/+}$ (n=31), *Evi1*$^{Jbo/+}$ (n=32), Wt (n=28), *Bpifa1*$^{-/-}$ (n=16) and *Bpifa1*$^{+/-}$ (n=19) middle ears at P28. One-way ANOVA with Tukey's posthoc test **p< 0.01; ****p< 0.0001.

Overall, the data shows that a higher proportion of *Bpifa1*$^{-/-}$*Evi1*$^{Jbo/+}$ display an OM phenotype at P21, suggesting that the loss of *Bpifa1* accelerates the development of OM in *Evi1*$^{Jbo/+}$ mice.

5.2.2.2 OM development at P28

Bpifa1$^{-/-}$*Evi1*$^{Jbo/+}$ and *Evi1*$^{Jbo/+}$ retained the OM phenotype at P28, evidenced by a thickened epithelial lining and fluid in the middle ear cavities. The middle ear fluids of both *Bpifa1*$^{-/-}$ *Evi1*$^{Jbo/+}$ and *Evi1*$^{Jbo/+}$ were mostly cellular, but sometimes serous fluids were seen. *Bpifa1*$^{-/-}$ mice and *Wt* mice did not exhibit an OM phenotype. Fig 5.7 shows representative images of the middle ear cavities from these 4 genotypes of mice.

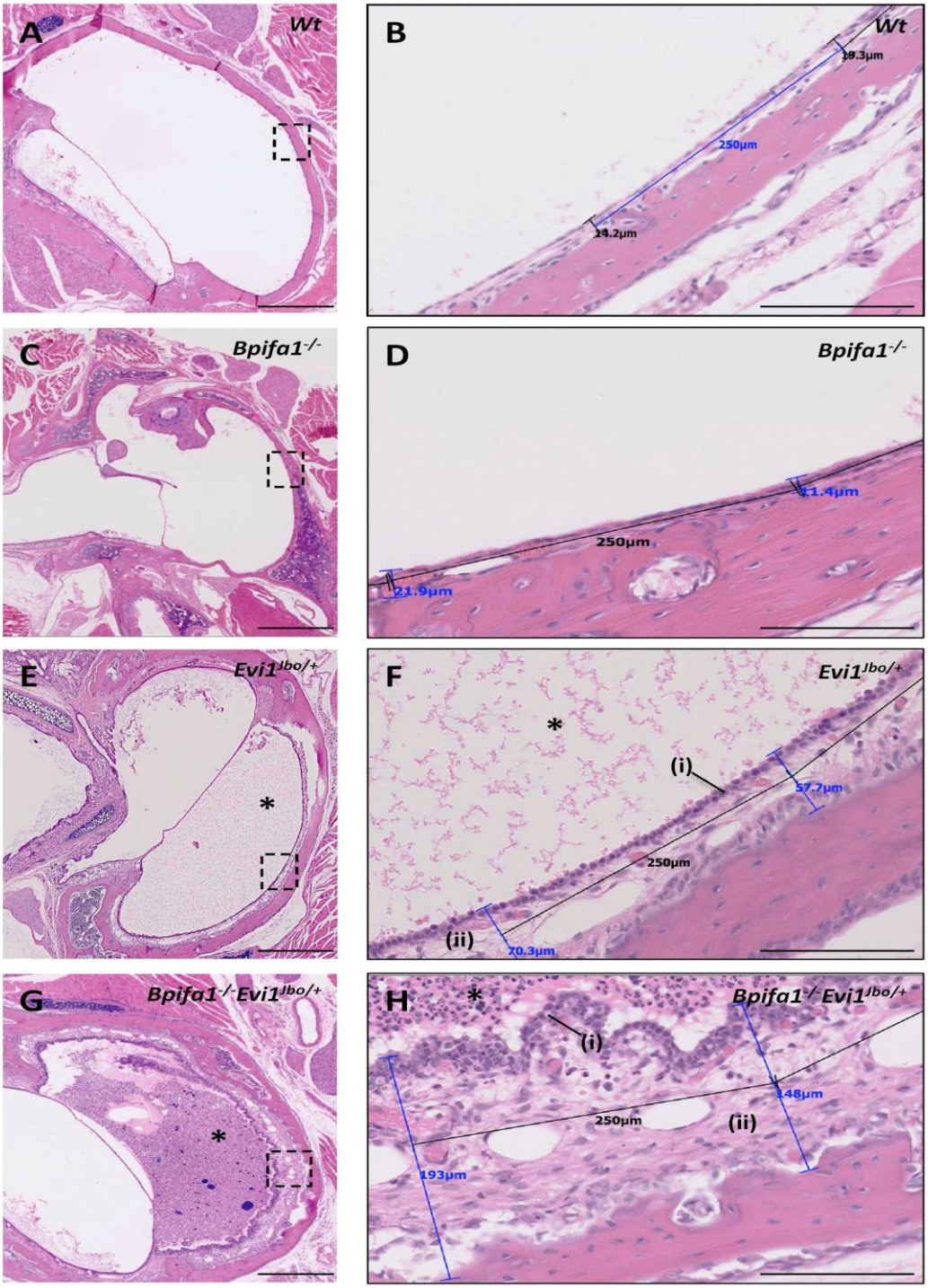

Figure 5.7 H&E stained middle ear sections at P28

Dorsal plane H&E sections from middle ears of *Wt* (A, B), and *Bpifa1*$^{-/-}$ (C, D) mice show no OM development. H&E sections from middle ears of *Evi1*$^{Jbo/+}$ (E, F) *and Bpifa1*$^{-/-}$*Evi1*$^{Jbo/+}$ (G, H) mice demonstrate presence of an OM phenotype marked by mucosal thickening and the presence of inflammatory ear fluids (asterisk). Mucosal thickening is a combination of epithelial hyperproliferation (i) and sup-epithelial mesenchyme expansion (ii). Mucosa of *Bpifa1*$^{-/-}$*Evi1*$^{Jbo/+}$ (H) is more thickened than *Evi1*$^{Jbo/+}$ mice (F). Scale bar 500µm for low magnification images and 100µm for high magnification images. *Wt* ears (n=28), *Bpifa1*$^{-/-}$ ears (n=12), *Evi1*$^{Jbo/+}$ ears (n=34) and *Bpifa1*$^{-/-}$ *Evi1*$^{Jbo/+}$ ears (n= 32).

As was mentioned previously, each ear was considered an independent sample for analysis for development of OM (Fig 5.8). At P28, the number of *Bpifa1*$^{-/-}$*Evi1*$^{Jbo/+}$ ears (30/32) that had middle ear exudate was significantly higher compared to *Evi1*$^{Jbo/+}$ ears (23/34; p=0.0117). The increase in the number of fluid containing ears from P28 was significant for *Bpifa1*$^{-/-}$*Evi1*$^{Jbo/+}$ mice (p= 0.02) but not for *Evi1*$^{Jbo/+}$ mice. The number of *Bpifa1*$^{+/-}$*Evi1*$^{Jbo/+}$ ears with fluids (26/34) was also higher than *Evi1*$^{Jbo/+}$ mice (23/34), however this difference was not statistically significant. Only 4/28 *Wt* ears showed presence of fluid (this was very limited in volume), however this was significantly less compared to *Bpifa1*$^{-/-}$*Evi1*$^{Jbo/+}$ mice (p<0.0001). None of the *Bpifa1*$^{+/-}$ (n=14) and *Bpifa1*$^{-/-}$ (n=12) ears showed any fluid (p<0.0001)

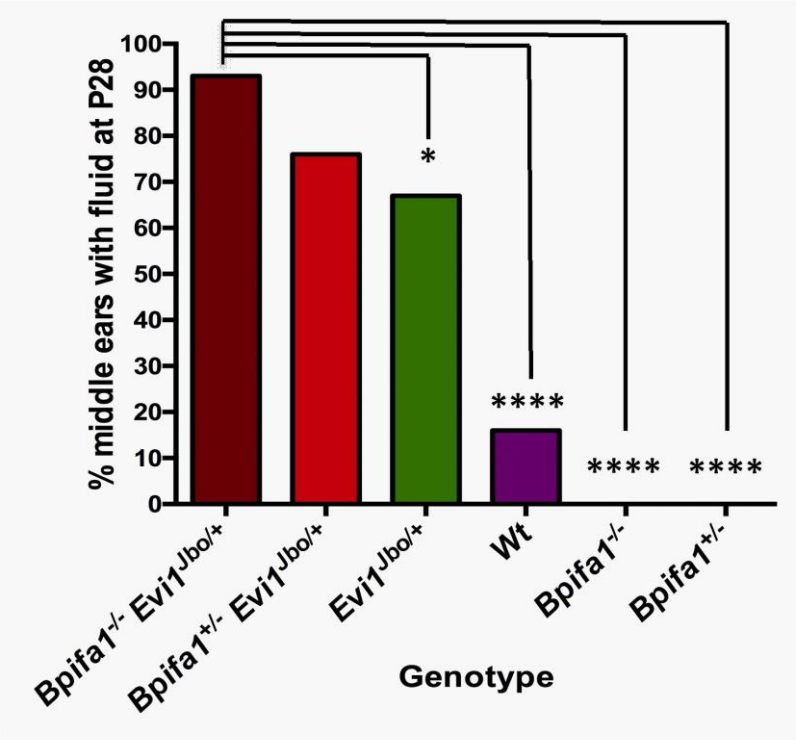

Figure 5.8 Percentage ears with middle ear fluids at P28
The percentage of *Bpifa1*$^{-/-}$*Evi1*$^{Jbo/+}$ (n=32) middle ears with fluid was significantly higher compared to *Evi1*$^{Jbo/+}$ (n=34), Wt (n=28), *Bpifa1*$^{-/-}$ (n=12) and *Bpifa1*$^{+/-}$ (n=14) middle ears but not compared to *Bpifa1*$^{+/-}$*Evi1*$^{Jbo/+}$ (n=31) middle ears at P28; Fishers exact test *p< 0.05; ****p< 0.0001.

All *Bpifa1*$^{-/-}$*Evi1*$^{Jbo/+}$ mice analysed (n=16) showed either unilateral or bilateral middle ear fluids. The percentage of *Bpifa1*$^{-/-}$*Evi1*$^{Jbo/+}$ developing bilateral OM (14/16) was significantly higher (p= 0.03) compared to both *Bpifa1*$^{+/-}$*Evi1*$^{Jbo/+}$ (10/16) and Evi1$^{Jbo/+}$ mice (7/16) (Fig 5.9A). No sex related differences were seen in the number of mice showing fluid development for either genotype (Fig 5.9B).

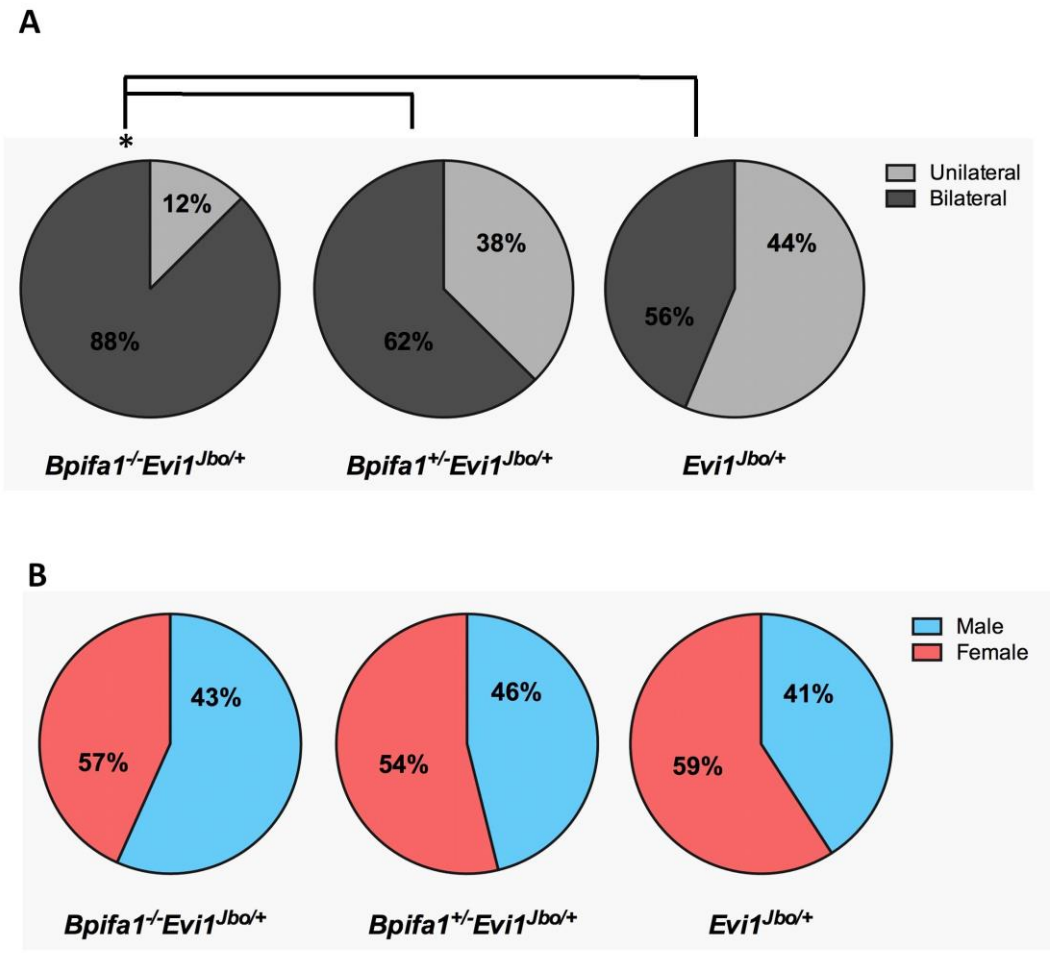

Figure 5.9 Analysis of mice with middle ear fluids at P28
The percentage of *Bpifa1*$^{-/-}$*Evi1*$^{Jbo/+}$ mice with bilateral OM was significantly higher than *Bpifa1*$^{+/-}$*Evi1*$^{Jbo/+}$ and *Evi1*$^{Jbo/+}$ mice (A). No sex related differences were seen between percentages of mice with middle ear fluids (B). n=16 mice of each genotype; Fishers exact test; *p< 0.05.

Quantification of the mucosal thickness (**Fig 5.10**) revealed that *Bpifa1*$^{-/-}$*Evi1*$^{Jbo/+}$ ears (n=32) showed significantly thickened mucosa compared to *Evi1*$^{Jbo/+}$ ears (n=34, p<0.0001) as well

as all the other control genotypes: Also, there was a significant difference in the mucosal thickening of *Bpifa1*$^{+/-}$*Evi1*$^{Jbo/+}$ ears (n=34) compared to *Evi1*$^{Jbo/+}$ ears (p=0.036).

The data confirms that the loss of *Bpifa1* alone does not lead to spontaneous OM development on the C3H/HeH background, reiterating my observations on the C57BL/6 (**Section 3.2.3**). However, the loss of *Bpifa1* significantly exacerbates the OM phenotype in *Evi1*$^{Jbo/+}$ mice.

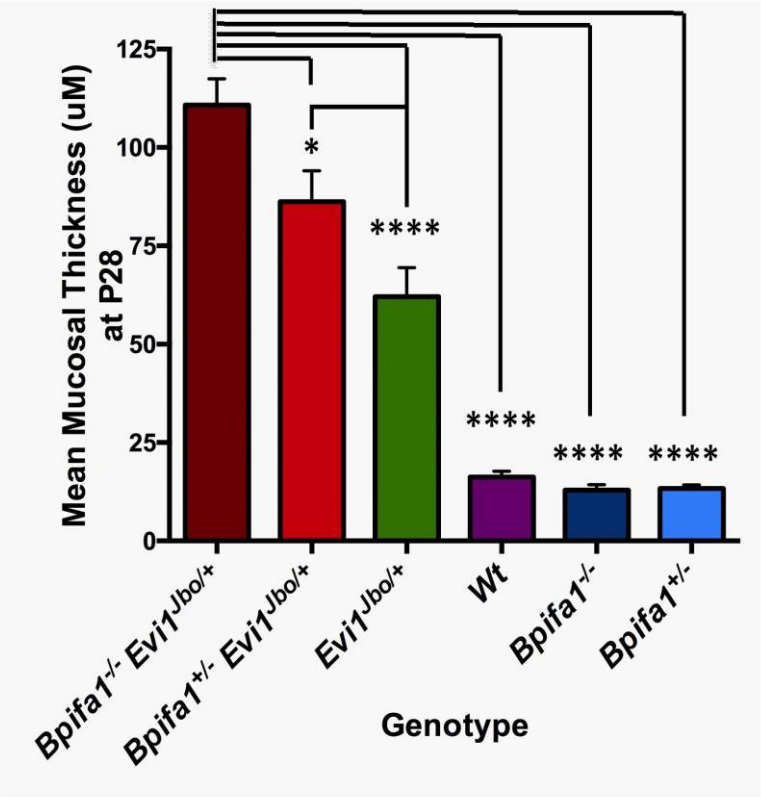

Figure 5.10 Mean middle ear mucosal thickness at P28
Mean mucosal thickness of *Bpifa1*$^{-/-}$*Evi1*$^{Jbo/+}$ (n=32) middle ears was significantly higher compared *Bpifa1*$^{+/-}$*Evi1*$^{Jbo/+}$ (n=34), *Evi1*$^{Jbo/+}$ (n=34), Wt (n=28), *Bpifa1*$^{-/-}$ (n=12) and *Bpifa1*$^{+/-}$ (n=14) middle ears middle ears at P28. Mean mucosal thickness of *Bpifa1*$^{+/-}$*Evi1*$^{Jbo/+}$ middle ears compared *Evi1*$^{Jbo/+}$ middle ears was also significantly higher; One-way ANOVA with Tukey's posthoc test **p< 0.01; ****p< 0.0001.

To investigate if the difference in the OM phenotype of *Bpifa1*$^{-/-}$*Evi1*$^{Jbo/+}$ and *Evi1*$^{Jbo/+}$ mice, was due to inherent differences between the middle ear epithelial cells between the two genotypes, I moved on to some *in vitro* studies. For this, cohorts of 7-10 week old *Bpifa1*$^{-/-}$ *Evi1*$^{Jbo/+}$, *Evi1*$^{Jbo/+}$, *Bpifa1*$^{-/-}$ and *Wt* mice were sent to University of Sheffield for cell isolations. The aim of the study was to investigate the potential differences in gene expression in freshly isolated middle ear mucosal cells of these mice as well as to use the mMEC model system developed in Chapter 4 in order to recapitulate the OM phenotype *in vitro*. Prior to performing these experiments, I analysed body weights and assessed OM status in these adult mice.

5.2.3. Analysis of body weights

Bpifa1$^{-/-}$*Evi1*$^{Jbo/+}$ mice appeared to be smaller in size compared to their *Wt* littermate controls. Therefore, I compared body weights of *Bpifa1*$^{-/-}$*Evi1*$^{Jbo/+}$, *Evi1*$^{Jbo/+}$, *Bpifa1*$^{-/-}$ and *Wt* mice between 7-9 weeks of age. Male *Bpifa1*$^{-/-}$*Evi1*$^{Jbo/+}$ mice weighed significantly less compared to male *Wt* (p=0.049) and *Bpifa1*$^{-/-}$ mice (p=0.035). *Evi1*$^{Jbo/+}$ mice also weighed less, but this difference was not statistically significant (Fig 5.11A). *Bpifa1*$^{-/-}$*Evi1*$^{Jbo/+}$ as well as *Evi1*$^{Jbo/+}$ females weighed significantly less compared to *Wt* (p= 0.016, 0.024 respectively) and *Bpifa1*$^{-/-}$ (p= 0.005, 0.01 respectively) females (Fig 5.11B).

However, for both sexes, body weights did not differ between *Bpifa1*$^{-/-}$*Evi1*$^{Jbo/+}$ and *Evi1*$^{Jbo/+}$ mice, indicating that the lowered body weight of the compound mutants was a result of the *Evi1* mutation (Fig 5.11 A, B). This result also suggests that the loss of *Bpifa1* alone does not cause a change in body weights on the C3H/HeH background, similar to that seen with the mutation on the C57BL/6 background (Section 3.2.2.2)

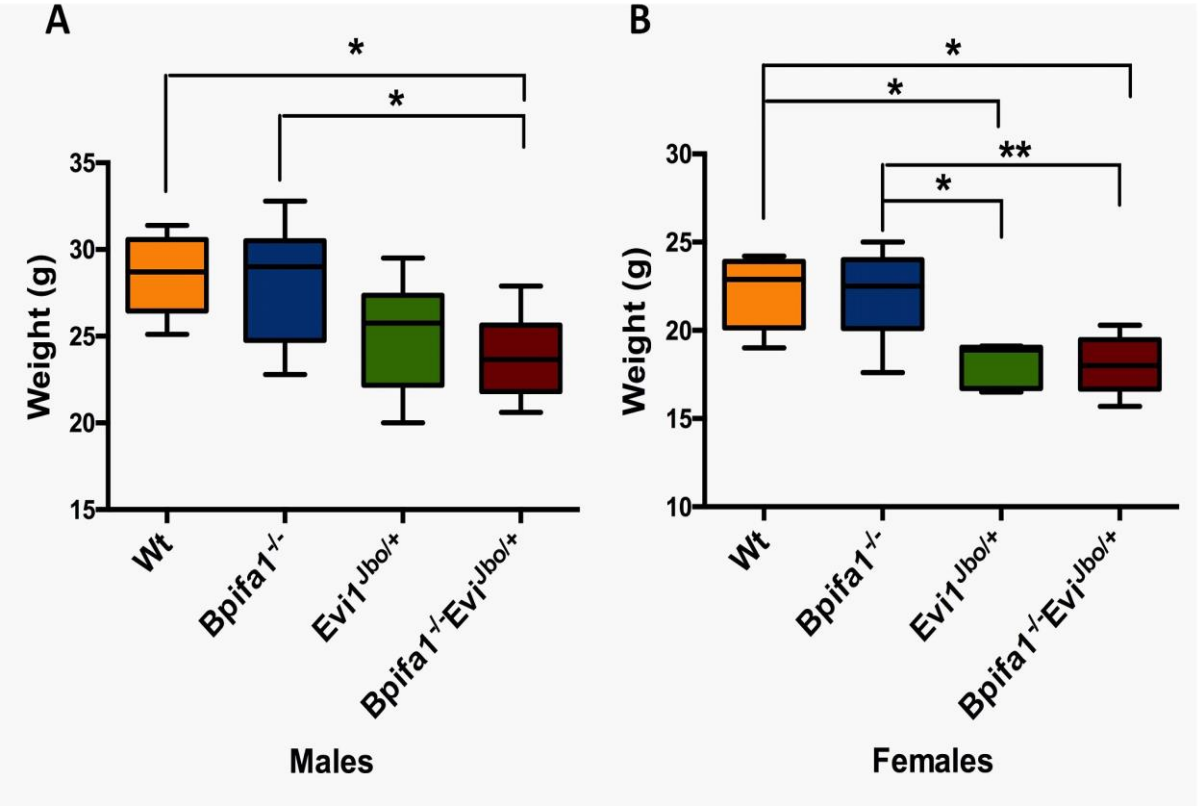

Figure 5.11 Body weight analyses of adult *Bpifa1$^{-/-}$Evi1$^{Jbo/+}$* mice
7-9 weeks old male *Bpifa1$^{-/-}$Evi1$^{Jbo/+}$* mice (n=6) weigh significantly less than their *Wt* (n=6), *Bpifa1$^{-/-}$* (n=10) and *Evi1$^{Jbo/+}$* (n=12) littermate controls (A) 7-9 weeks old female *Bpifa1$^{-/-}$Evi1$^{Jbo/+}$* mice (n=6) and *Evi1$^{Jbo/+}$* (n=5) weigh significantly less than their *Wt* (n=5) and *Bpifa1$^{-/-}$* (n=11) littermate controls (B). Data presented as box and whisker plots demonstrating minimum to maximum weights and horizontal line indicates median weight. Mean weights compared using One-way ANOVA with Tukey's posthoc test; **p< 0.01; *p< 0.05.

5.2.4. Persistence of OM in adult *Bpifa1$^{-/-}$Evi1$^{Jbo/+}$* mice

In order to assess the persistence of OM in adult mice (as the morphometric assessment described above was performed in 3-4 week old mice), I semi-quantitatively evaluated the Tm appearance in 7–10 week old *Bpifa1$^{+/-}$Evi1$^{Jbo/+}$* mice and their *Evi1$^{Jbo/+}$*, *Bpifa1$^{-/-}$* and *Wt* littermate controls. Using a dissecting microscope, the Tm was scored as 'cloudy' or 'clear' based on the visibility of the malleus ossicle. (Fig 5.12 A, B). Mice with OM have a cloudy Tm due to fluid accumulation in the middle ear cavity. The penetrance of OM was higher in *Bpifa1$^{+/-}$Evi1$^{Jbo/+}$* mice (88.6%, n=44 ears) compared to *Evi1$^{Jbo/+}$* (74%, n=54 ears). Statistically, the difference between the number of cloudy ears between these two

genotypes was borderline insignificant (p=0.058). Only 1/42 *Bpifa1*$^{-/-}$ ears and none of the *Wt* ears were cloudy (Fig 5.12 C).

The volume of middle ear fluids sampled from cloudy ears displayed a large range. The average volume of middle ear fluids recovered from *Bpifa1*$^{+/-}$*Evi1*$^{Jbo/+}$ mice (0.63 µl) and that from *Evi1*$^{Jbo/+}$ ears (0.56 µl) was not statistically significant (Fig 5.12 D). Due to the lack of time, a detailed analysis of the middle ear fluids could not be performed. However, a brief look at cytospun fluids from both *Bpifa1*$^{+/-}$*Evi1*$^{Jbo/+}$ and *Evi1*$^{Jbo/+}$ revealed abundant neutrophils and a smaller proportion of macrophages (Fig 5.12 E, F)

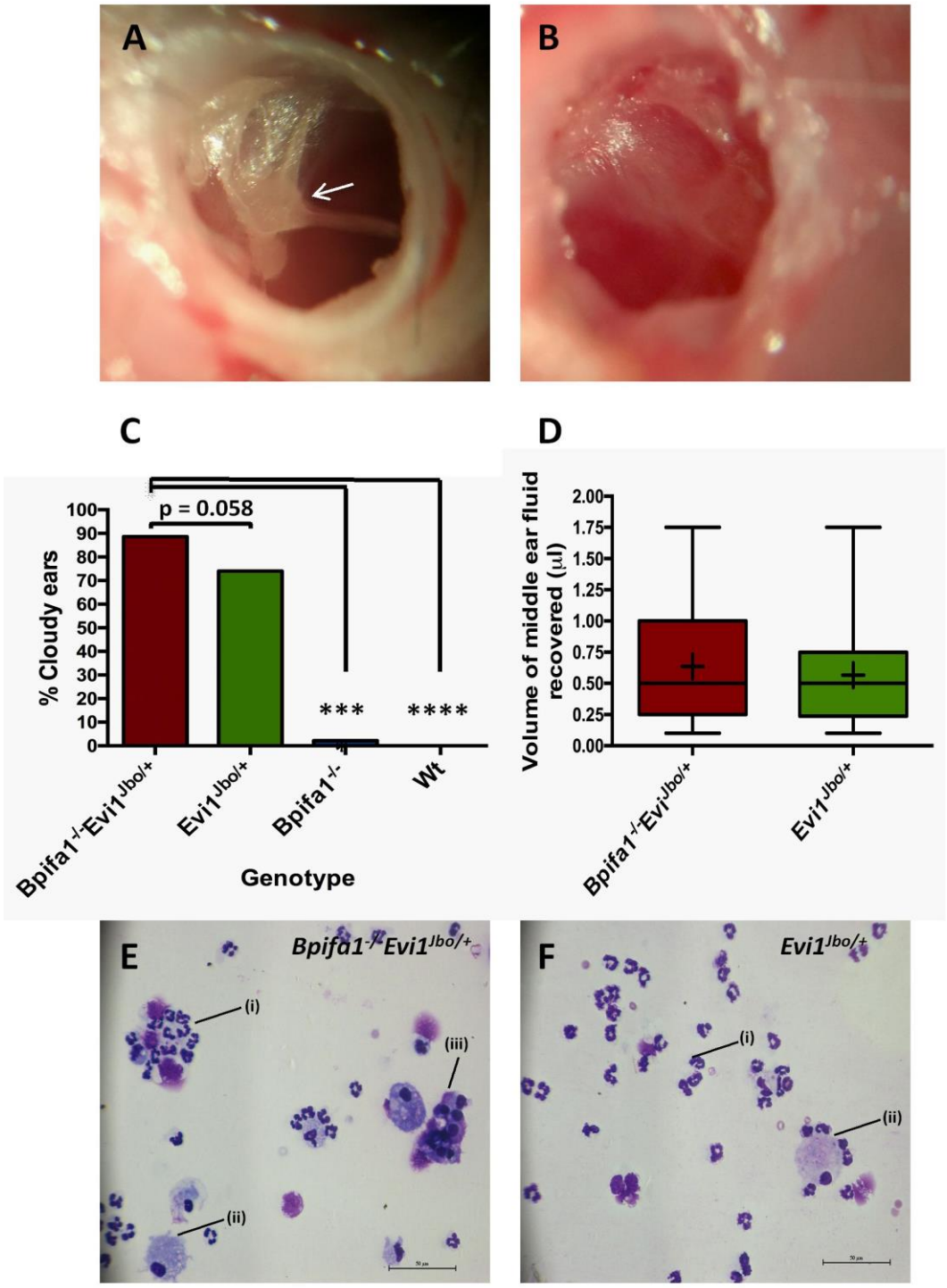

Figure 5.12 Persistence of OM in adult *Bpifa1*$^{-/-}$*Evi1*$^{Jbo/+}$ mice
Representative images showing a clear (A) and a cloudy (B) ear drum. Arrowhead shows the visibility of the malleus ossicle. The percentage of *Bpifa1*$^{-/-}$*Evi1*$^{Jbo/+}$ cloudy ears is higher than *Evi1*$^{Jbo/+}$, *Bpifa1*$^{-/-}$ and *Wt* littermate controls, as calculated using One-way ANOVA with Tukey's post hoc test; ****p< 0.0001 (C) Volumes of ear fluids recovered do not differ between *Bpifa1*$^{-/-}$*Evi1*$^{Jbo/+}$ and *Evi1*$^{Jbo/+}$ middle ears; two tailed t-test (D). Middle ear fluids from *Bpifa1*$^{-/-}$*Evi1*$^{Jbo/+}$ (E) and *Evi1*$^{Jbo/+}$ mice (F) show the presence of neutrophils (i), macrophages (ii) and sloughed epithelial cells (iii). *Bpifa1*$^{-/-}$ *Evi1*$^{Jbo/+}$ (n=44), *Evi1*$^{Jbo/+}$ (n=54), *Bpifa1*$^{-/-}$ (n=42), *Wt* (n=66).

5.2.5 Relative gene regulation in *Bpifa1*$^{-/-}$*Evi1*$^{Jbo/+}$ middle ear mucosal cells

Both *Bpifa1*$^{-/-}$*Evi1*$^{Jbo/+}$ and *Evi1*$^{Jbo/+}$ mice demonstrated a thickened middle ear mucosa. I speculated that the mucosal thickening is a combined effect of remodelling of the middle ear epithelial cells as well as the underlying sub-epithelial layer, which includes fibroblasts. Therefore, I decided to evaluate the expression of inflammatory and epithelial genes in the middle ear mucosal lining, encompassing the epithelial cells as well as fibroblasts. To do this, middle ear cavities were dissected from 3 individual batches (each batch was 5-6 mice) of 7-10 week old *Bpifa1*$^{-/-}$*Evi1*$^{Jbo/+}$, *Evi1*$^{Jbo/+}$, *Bpifa1*$^{-/-}$ and *Wt* mice and treated with Pronase overnight to strip off the mucosal layer, in accordance to the mMEC cell isolation protocol (Section 2.8.1.3). For RT-qPCR analysis of inflammatory and epithelial genes, a proportion of these freshly isolated cells were directly lysed in TRI reagent, without undergoing the differential fibroblast separation step. These cells will be referred to as mouse middle-ear mucosal cells (mMMCs) throughout this thesis.

The remainder of the isolated cells underwent routine fibroblast separation using differential adherence to plastic and were then seeded on transwell membranes for culture and ALI differentiation according to the standard mMEC culture protocol. In doing this the aim was to model the OM phenotype *in vitro*. Experiments with cultured mMECs from the 4 genotypes are described in Section 5.2.6 and Section 5.2.7.

5.2.5.1 Expression of inflammatory genes in Bpifa1$^{-/-}$*Evi1*$^{Jbo/+}$ *middle ear mucosa*

I was interested in evaluating if the exacerbation of the OM phenotype in *Bpifa1*$^{-/-}$*Evi1*$^{Jbo/+}$ mice was due to an enhanced inflammatory response, arising from the mucosal cells as a result of *Bpifa1* ablation. In order to test this, gene expression analysis for a selected panel

of inflammatory markers was performed on mMMCs isolated from *Bpifa1*$^{-/-}$*Evi1*$^{Jbo/+}$, *Evi1*$^{Jbo/+}$, *Bpifa1*$^{-/-}$ and *Wt* mice using RT-qPCR.

The pro-inflammatory cytokines *Cxcl2* (Fig 5.13A), *Il1β* (Fig 5.13B), *Tnfα* (Fig 5.13C) and the anti-inflammatory cytokine, *Tgfβ* (Fig 5.13D) were significantly upregulated in *Evi1*$^{Jbo/+}$ and *Bpifa1*$^{-/-}$*Evi1*$^{Jbo/+}$ mMMCs compared to *Wt* and *Bpifa1*$^{-/-}$ mMMCs. *Il6* was significantly upregulated in *Bpifa1*$^{-/-}$*Evi1*$^{Jbo/+}$ mMMCs compared to *Wt* mMMCs (Fig 5.13E). The statistically significant fold changes for all inflammatory genes analyzed in this study are detailed in Table 5.2. Thus, the middle ear mucosa of *Evi1*$^{Jbo/+}$ and *Bpifa1*$^{-/-}$*Evi1*$^{Jbo/+}$ mice was severely inflamed. However, there was no significant difference in the expression levels for any of the markers between *Wt* and *Bpifa1*$^{-/-}$ mMMCs and *Evi1*$^{Jbo/+}$ and *Bpifa1*$^{-/-}$*Evi1*$^{Jbo/+}$ mMMCs, suggesting that the loss of *Bpifa1* did not aggravate the cytokine response.

Table 5.2 Statistically significant fold changes in expression of inflammatory genes in *Evi1*$^{Jbo/+}$ and *Bpifa1*$^{-/-}$*Evi1*$^{Jbo/+}$ mMMCs compared to *Wt* and *Bpifa1*$^{-/-}$ mMMCs

Gene	Genotype	FC compared to Wt	p-value	FC compared to Bpifa1$^{-/-}$	p-value
Cxcl2	***Evi1***$^{Jbo/+}$	52.18	0.0002	20.45	0.0023
	Bpifa1$^{-/-}$***Evi1***$^{Jbo/+}$	47.30	0.0005	18.54	0.0046
Il1β	***Evi1***$^{Jbo/+}$	32.71	0.0001	17.26	0.0008
	Bpifa1$^{-/-}$***Evi1***$^{Jbo/+}$	24.27	0.0003	12.81	0.0023
Tnfα	***Evi1***$^{Jbo/+}$	12.40	0.0002	4.88	0.0078
	Bpifa1$^{-/-}$***Evi1***$^{Jbo/+}$	15.53	0.0001	6.11	0.0035
Tgfβ	***Evi1***$^{Jbo/+}$	2.33	0.0002	2.11	0.0008
	Bpifa1$^{-/-}$***Evi1***$^{Jbo/+}$	2.18	0.0008	1.98	0.0033
Il6	***Bpifa1***$^{-/-}$***Evi1***$^{Jbo/+}$	5.02	0.0287		

I also analysed the expression of *Vegf*, a marker of hypoxia, in mMMCs isolated from the 4 genotypes of mice. *Vegf* expression was upregulated 2.7 fold in *Bpifa1*$^{-/-}$*Evi1*$^{Jbo/+}$ mice (p=0.016) and 2.3 fold in *Evi1*$^{Jbo/+}$ mice (p=0.024) compared to Wt mice, suggesting the presence of a hypoxic environment in the inflamed mucosa of the *Bpifa1*$^{-/-}$*Evi1*$^{Jbo/+}$ and

Evi1$^{Jbo/+}$ mice (Fig 5.13F). The upregulation compared to *Bpifa1*$^{-/-}$ mMMCs was not significant. Also, there there was no significant difference in *Vegf* expression levels between *Wt* and *Bpifa1*$^{-/-}$ mMMCs and between *Evi1*$^{Jbo/+}$ and *Bpifa1*$^{-/-}$*Evi1*$^{Jbo/+}$ mMMCs.

Expression of all target genes was normalized against three endogenous controls; *Atp5b, Canx* and *Cyc1,* identified using the geNORM assay (Section 2.19.4). Data is presented as individual RQ values for 3 biological replicates of each genotype ± SEM (Fig 5.13).

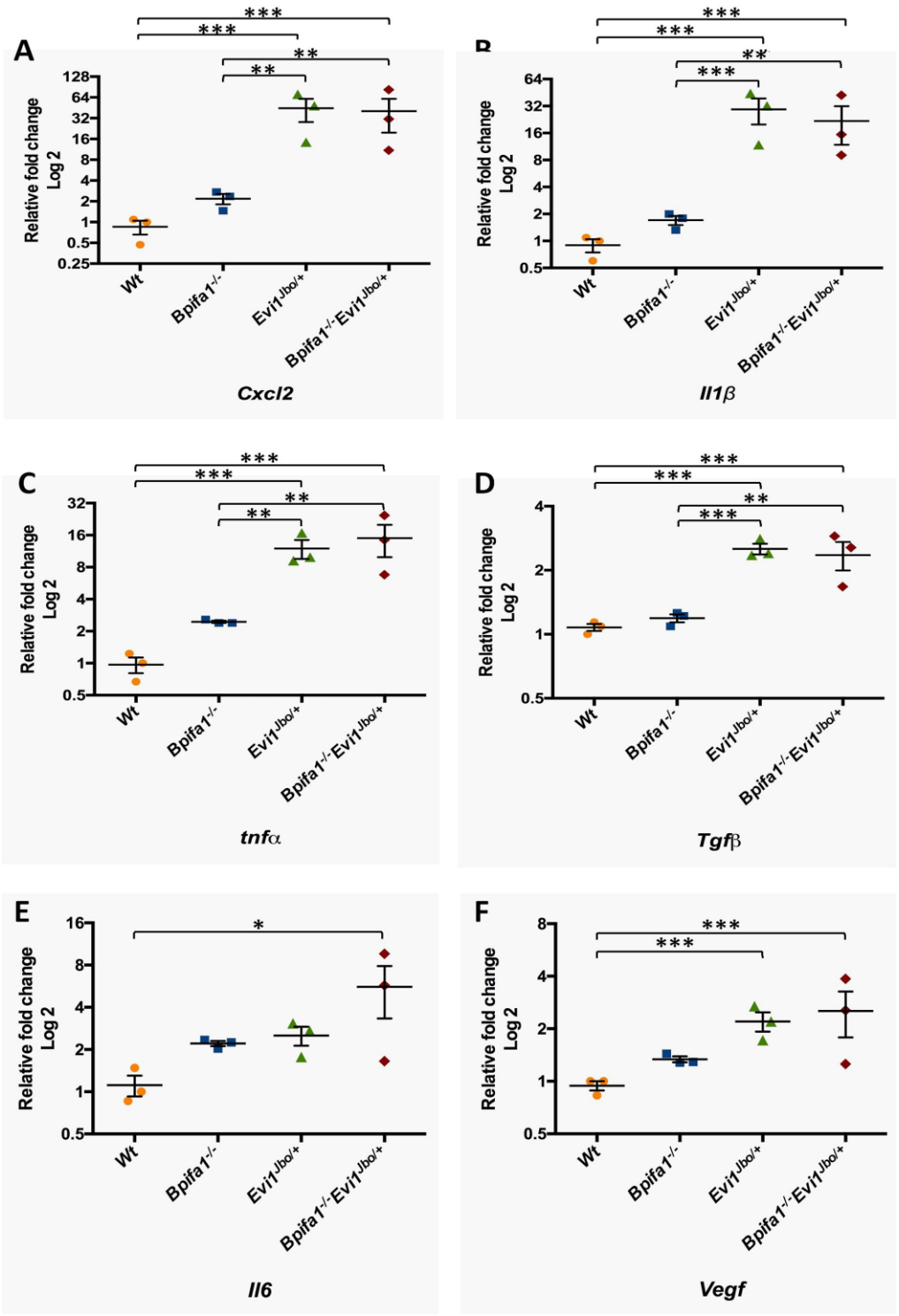

Figure 5.13 Gene expression of inflammatory markers in *Bpifa1*$^{-/-}$*Evi1*$^{Jbo/+}$ mMMCs

Significant up regulation of *Cxcl2* (A), *Il1β* (B), *Tnfα* (C) *Tgfβ* (D) in *Bpifa1*$^{-/-}$*Evi1*$^{Jbo/+}$ and *Evi1*$^{Jbo/+}$ mMMCs compared to *Wt* and *Bpifa1*$^{-/-}$ mMMCs. Significant upregulation of *Il6* (E) in *Bpifa1*$^{-/-}$*Evi1*$^{Jbo/+}$ compared to *Wt* mMMCs and of *Vegf (F) in Bpifa1*$^{-/-}$*Evi1*$^{Jbo/+}$ and *Evi1*$^{Jbo/+}$ mMMCs compared to *Wt* mMMCs. Overall, no effect of *Bpifa1* deletion was seen on gene expression. Data were analysed using One-way ANOVA plus Tukey's posthoc test and represented as individual RQ values ± SEM for three independent batches of freshly isolated mMMCs. ****p<0.0001, ***p<0.001, **p<0.01, *p<0.05

5.2.5.2 Expression of epithelial genes in Bpifa1$^{-/-}$Evi1$^{Jbo/+}$ middle ear mucosa

Our preliminary studies had shown a decrease in BPIFA1 staining in the *Evi1$^{Jbo/+}$* middle ear compared to *Wt* mice using IHC (Section 1.13). In order to confirm if this was due to an inherent difference in gene expression, I compared expression of *Bpifa1* in mMMCs isolated from *Wt* and *Evi1$^{Jbo/+}$* mice using RT-qPCR. This analysis showed that there was a significant down-regulation (3.18 fold, p= 0.0017) of *Bpifa1* mRNA in *Evi1$^{Jbo/+}$* mMMCs (Fig 5.14 A).

I also evaluated levels of *Evi1* expression between the 4 genotypes. There was a small but significant down-regulation in *Evi1* in *Evi1$^{Jbo/+}$* and *Bpifa1$^{-/-}$Evi1$^{Jbo/+}$* mMMCs compared to both *Wt* (1.56 fold, p=0.02 and 1.75-fold p=0.04 respectively) and *Bpifa1$^{-/-}$* mMMCs (1.62 fold, p=0.02 and 1.82-fold p=0.03 respectively) (Fig 5.14 B).

Next, I compared expression of other epithelial markers, *Foxj1*, *Muc5ac* and *Muc5b* using RT-qPCR. The rationale behind this experiment was to evaluate if *Bpifa1* ablation leads to an alteration of epithelial sub-populations in presence and absence of an inflammatory environment in the middle ear mucosa. The fold changes and significance levels for all epithelial genes analyzed are detailed in Table 5.3. The ciliated cell marker, *Foxj1* was significantly downregulated in *Evi1$^{Jbo/+}$* and *Bpifa1$^{-/-}$Evi1$^{Jbo/+}$* mMMCs compared to both *Wt* and *Bpifa1$^{-/-}$* mMMCs (Fig 5.14 C). The goblet cell marker, *Muc5ac* was also down regulated significantly in *Bpifa1$^{-/-}$Evi1$^{Jbo/+}$* mice compared to *Wt* mice and in both *Bpifa1$^{-/-}$Evi1$^{Jbo/+}$* and *Evi1$^{Jbo/+}$* mice compared to *Bpifa1$^{-/-}$*. *Muc5ac* was also down regulated 2.6 fold in *Evi1$^{Jbo/+}$* compared to *Wt* mice, although this difference did not reach statistical significance (Fig 5.14 D). *Muc5b* expression was highly variable between individual batches and did not reach statistical significance (Fig 5.14 E). Expression of *Foxj1*, the mucin genes and *Evi1* appeared to be higher in *Bpifa1$^{-/-}$* mice compared to *Wt* mice, but this did not reach statistically significance. Also, there was no difference in the level of expression of any of the markers between *Evi1$^{Jbo/+}$* and *Bpifa1$^{-/-}$Evi1$^{Jbo/+}$* mice.

Table 5.3 Fold changes for expression of epithelial genes in *Evi1*$^{Jbo/+}$ and *Bpifa1*$^{-/-}$*Evi1*$^{Jbo/+}$ mMMCs compared to *Wt* and *Bpifa1*$^{-/-}$ mMMCs

Gene	Genotype	FC compared to Wt	p-value	FC compared to Bpifa1$^{-/-}$	p-value
Bpifa1	**Evi1$^{Jbo/+}$**	-3.18	0.0017	-	-
Foxj1	**Evi1$^{Jbo/+}$**	-2.95	0.0019	-3.65	0.0006
	Bpifa1$^{-/-}$Evi1$^{Jbo/+}$	-4.42	0.0003	-5.5	0.0001
Muc5ac	**Evi1$^{Jbo/+}$**	-2.59	> 0.05 (ns)	-6.94	0.007
	Bpifa1$^{-/-}$Evi1$^{Jbo/+}$	-4.73	0.022	-12.67	0.001
Muc5b	**Evi1$^{Jbo/+}$**	2.35	> 0.05 (ns)	-1.38	> 0.05 (ns)
	Bpifa1$^{-/-}$Evi1$^{Jbo/+}$	1.81	> 0.05 (ns)	-1.79	> 0.05 (ns)
Evi1	**Evi1$^{Jbo/+}$**	-1.56	0.02	1.62	0.02
	Bpifa1$^{-/-}$Evi1$^{Jbo/+}$	-1.75	0.04	1.82	0.03

NB: p>0.05 (ns) = non significant

Overall, the data indicate that *Evi1*$^{Jbo/+}$ mice show epithelial cellular alterations marked by down regulation of *Bpifa1, Foxj1* and *Muc5ac.* However, there is no added effect of *Bpifa1* deletion on alteration of epithelial genes.

Expression of all target genes was normalized against three endogenous controls; *Atp5b, Canx* and *Cyc1* identified using the geNORM assay (Section 2.19.4). Data is presented as individual RQ values for 3 biological replicates of each genotype ± SEM (Fig 5.14).

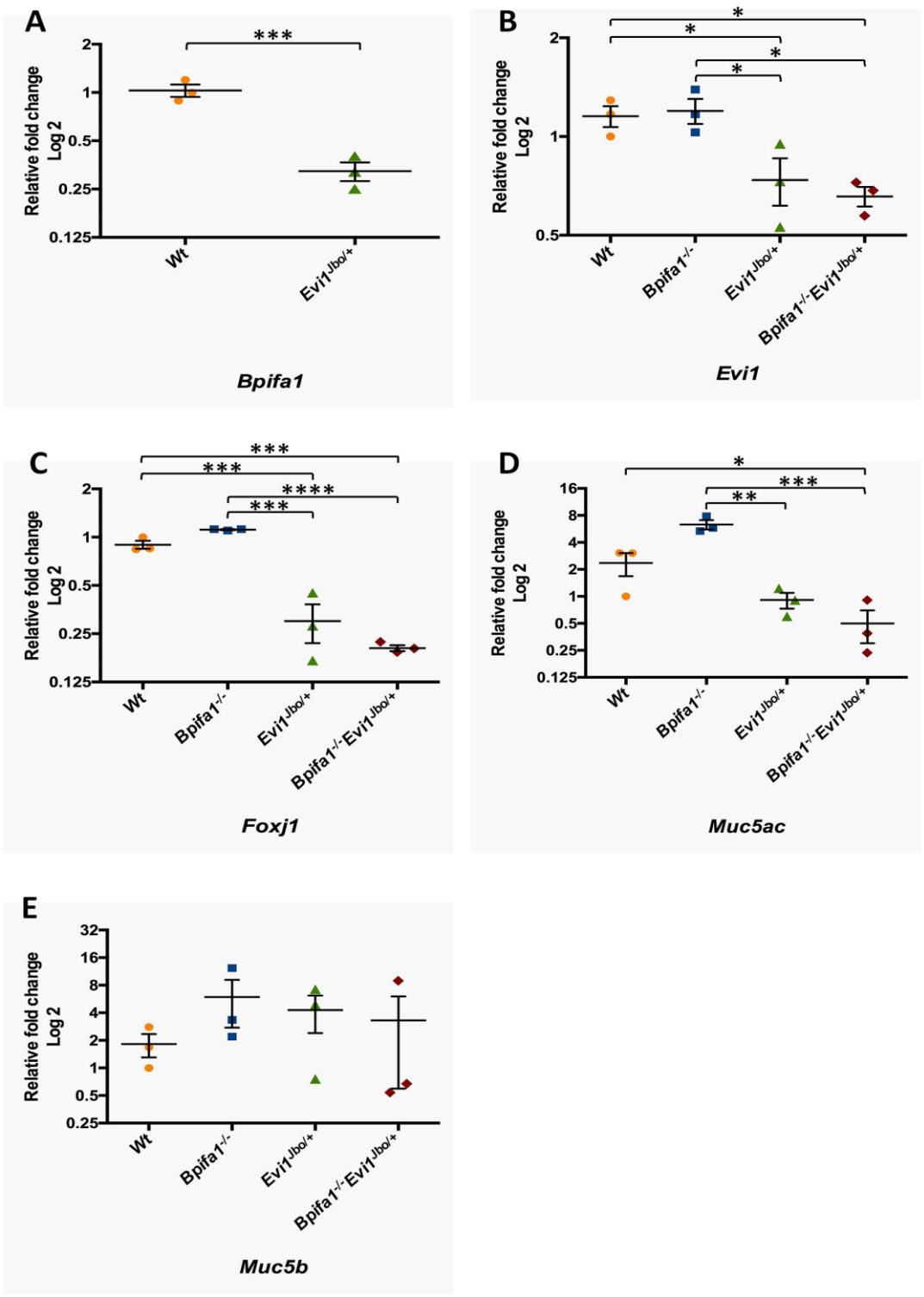

Figure 5.14 Expression of epithelial markers in *Bpifa1*$^{-/-}$*Evi1*$^{Jbo/+}$ mMMCs
Significant downregulation of *Bpifa1 in Evi1*$^{Jbo/+}$ mMMCs compared to *Wt* mMMCs (A) and of *Evi1 (B) and Foxj1 (C) in Bpifa1*$^{-/-}$*Evi1*$^{Jbo/+}$ and *Evi1*$^{Jbo/+}$ mMMCs compared to *Wt* and *Bpifa1*$^{-/-}$ mMMCs. Significant downregulation of *Muc5ac* (D) in *Bpifa1*$^{-/-}$*Evi1*$^{Jbo/+}$ and *Evi1*$^{Jbo/+}$ mMMCs (D). *Muc5b* expression was variable. Overall, no effect of *Bpifa1* deletion was seen on expression of other epithelial genes. Data were analysed using One-way ANOVA plus Tukey's posthoc test and represented as individual RQ values ± SEM for three independent batches of freshly isolated mMMCs. ****p<0.0001, ***p<0.001, **p<0.01, *p<0.05.

5.2.6 Modelling the OM phenotype of *Bpifa1*$^{-/-}$*Evi1*$^{Jbo/+}$ and *Evi1*$^{Jbo/+}$ mice *in vitro* using the mMEC culture system

In Chapter 4, I described the development of a novel model for the culture of mouse middle ear epithelial cells at ALI, which recapitulates the native murine middle ear epithelium *in vitro*. In order to evaluate whether I could utilise the mMEC culture system to model the OM phenotype *in vitro*, I isolated middle ear cells from 7-10 week old *Bpifa1*$^{-/-}$ *Evi1*$^{Jbo/+}$, *Evi1*$^{Jbo/+}$, *Bpifa1*$^{-/-}$ and *Wt* mice using pronase treatment of dissected middle ear cavities. Fibroblasts were separated using differential adherence method and the epithelial cells (mMECs) were seeded on transwell membranes at an initial seeding density of 10,000 cells/ well in the presence of ROCKi. The cells were then cultured using the routine mMEC culture protocol (Section 2.8.1.5) in submerged culture till confluence and differentiated at ALI for 14 days.

5.2.6.1 Culture characteristics

The culture characteristics of mMECs from the 4 genotypes of mice were largely similar to those described for *Wt* and *Bpifa1*$^{-/-}$ cells on the C57BL/6 background in Chapter 4 (Section 4.2.2.1, Table 4.1). Cells reached confluence within 8- 10 days submerged culture in presence of ROCKi and differentiated by Day 14 at ALI (Fig 5.15). This was evidenced by elevated clusters of cells with actively beating cilia. There were no gross differences between the mMECs cultured from the 4 genotypes except that *Bpifa1*$^{-/-}$*Evi1*$^{Jbo/+}$ and *Evi1*$^{Jbo/+}$ cultures appeared to be more abundant in elevated clusters of cells compared to *Wt* and *Bpifa1*$^{-/-}$ cultures, when observed under the light microscope (personal observation).

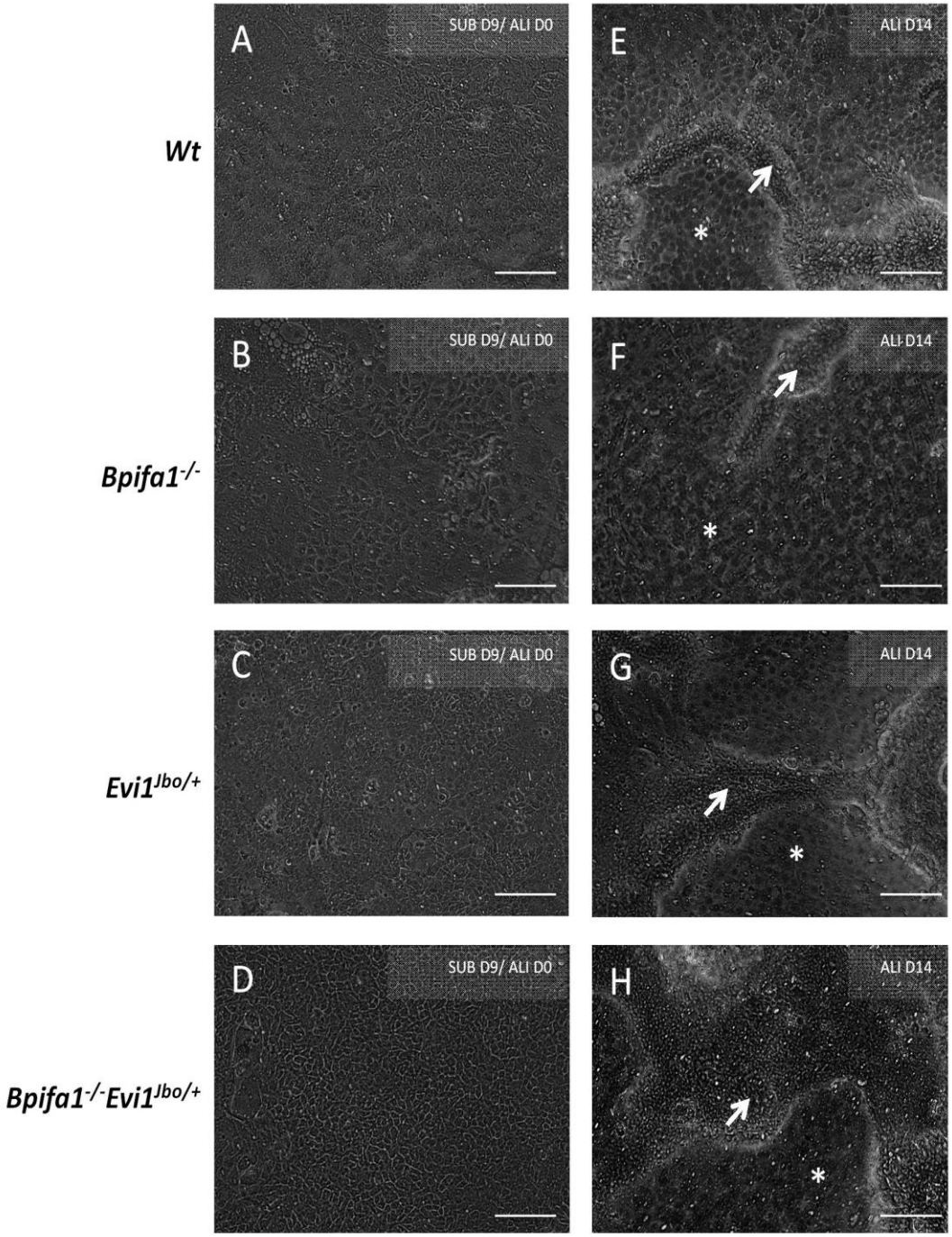

Figure 5.15 Morphological characteristics of *Bpifa1*$^{-/-}$*Evi1*$^{Jbo/+}$ mMECs
Phase contrast images showing *Wt (A, E), Bpifa1*$^{-/-}$ (B, F), *Evi1*$^{Jbo/+}$ (C, G) and *Bpifa1*$^{-/-}$*Evi1*$^{Jbo/+}$ (D, H) mMECs in culture under 10x magnification. No difference is seen in the growth characteristics between the genotypes. Cells became confluent between 8-9 days in submerged culture (A, B, C, D) and differentiated by ALI Day 14 (E, F, G, H). White arrowheads mark elevated cells with cilia and asterisk mark flatter polygonal cells. Scale bar = 200 µm.

5.2.6.2 Expression of epithelial and inflammatory genes in Bpifa1$^{-/-}$Evi1$^{Jbo/+}$ mMECs

ALI day 14 mMECs from *Bpifa1$^{-/-}$Evi1$^{Jbo/+}$*, *Evi1$^{Jbo/+}$ Bpifa1$^{-/-}$* and *Wt* mice were analysed using RT-qPCR to evaluate differential expression of epithelial and inflammatory genes. The objective of this study was to investigate if the pattern of genetic alterations seen in the mucosal cells, mMMCs from OM affected mice (Section 5.2.5) was retained after culturing the cells *in vitro.* Expression of target genes was normalized against three endogenous controls; *Atp5b, Ppia* and *Cyc1,* identified using the geNORM assay (Section 2.19.4). Data is presented as individual RQ values for 3 biological replicates of each genotype ± SEM.

The expression of *Bpifa1* was 3.41 fold lower ($p<0.0001$; 2 tailed t-test) *in Evi1$^{Jbo/+}$* mMECs compared to *Wt* mMECs (Fig 5.16A). This finding was in line with our observation in mMMCs (Section 5.2.5.2) as well as in IHC data from our lab (Section 1.13,), confirming that the levels of *Bpifa1* reduce with development of OM in *Evi1$^{Jbo/+}$* mice.

I showed above that *Foxj1* and *Muc5ac* expression was down regulated in the inflamed mucosa of *Bpifa1$^{-/-}$Evi1$^{Jbo/+}$*, *Evi1$^{Jbo/+}$* mice and expression of the ciliated and mucin gene markers did not vary with *Bpifa1* ablation (Fig 5.14, Table 5.3). However, this expression pattern changed considerably when cells were cultured *in vitro*. Compared to *Wt* ALI Day 14 mMECs, *Foxj1* expression showed a small reduction of 1.4 fold in *Bpifa1$^{-/-}$Evi1$^{Jbo/+}$* mMECs. This change was statistically significance($p=0.0076$), probably due to the smaller variation seen between the batches for this particular marker. *Foxj1* expression did not change in *Evi1$^{Jbo/+}$* mMECs (Fig 5.16B). Expression of *Muc5ac* and *Muc5b* did not differ between *Wt*, *Evi1$^{Jbo/+}$* and *Bpifa1$^{-/-}$Evi1$^{Jbo/+}$* mMECs (Fig 5.16C, D). However, the expression of all the three genes was significantly lower in *Bpifa1$^{-/-}$* mMECs compared to the other genotypes. *FoxJ1* expression was reduced 1.8 fold ($p<0.0001$), *Muc5ac* was reduced 5.2 fold ($p=0.0103$) and *Muc5b* was reduced 7.5 fold (0.0002) in *Bpifa1$^{-/-}$* mMECs compared to *Wt*

mMECs (Fig 5.16B-D). Expression of the basal cell marker, *p63* did not differ between the 4 genotypes (Fig 5.16E).

Overall, the data indicates that although mMECs differentiate to express the different epithelial subtypes, they do not retain the expression pattern of majority of the genes seen in the native middle ear mucosa from *Bpifa1*$^{-/-}$*Evi1*$^{Jbo/+}$, *Evi1*$^{Jbo/+}$ *Bpifa1*$^{-/-}$ and *Wt* mice.

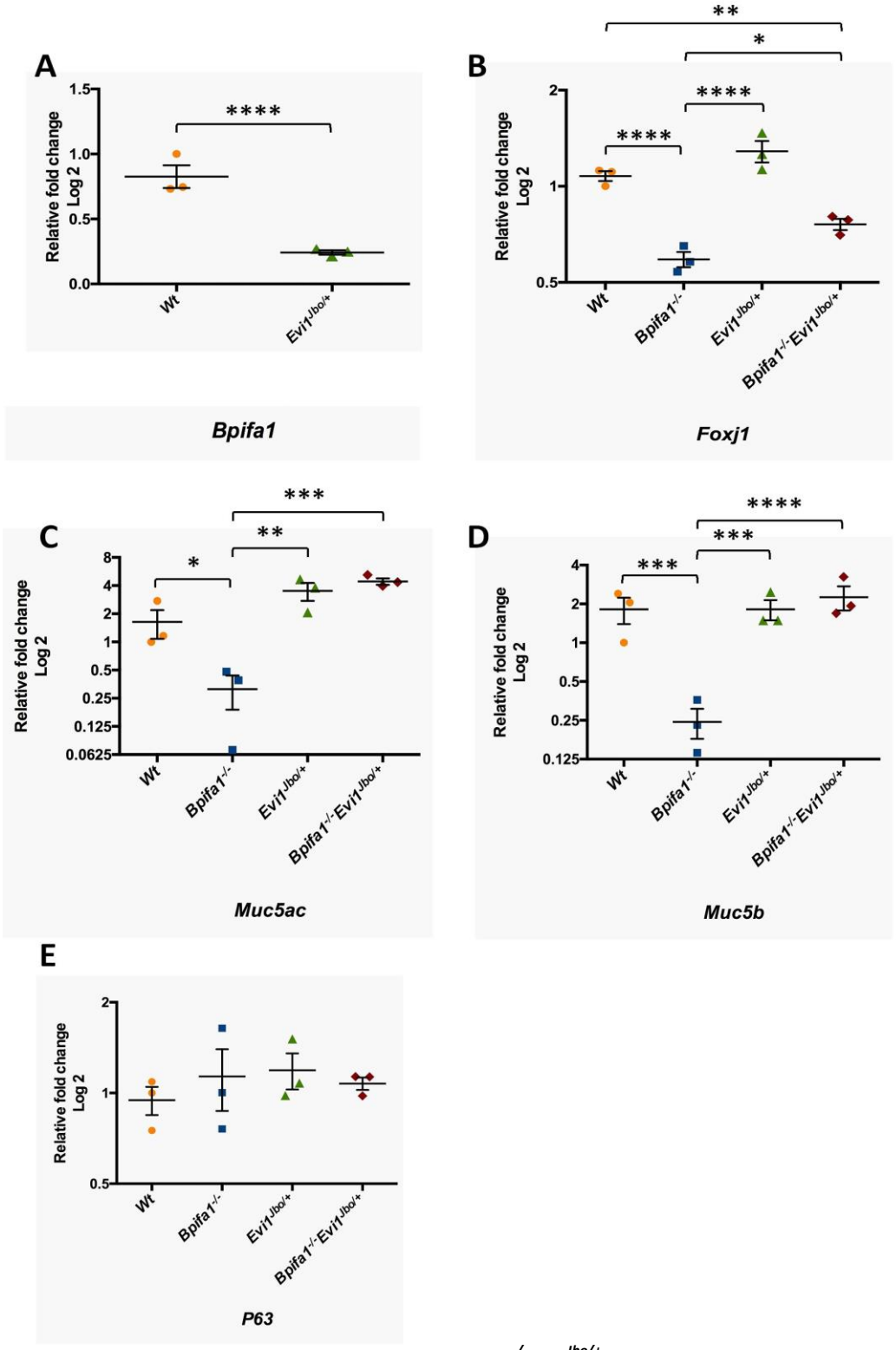

Figure 5.16 Expression of epithelial markers in *Bpifa1*$^{-/-}$*Evi1*$^{Jbo/+}$ mMECs

Significant downregulation of *Bpifa1 in Evi1*$^{Jbo/+}$ mMECs compared to *Wt* mMECs. 2 tailed Student's t-test (A). Expression pattern of *Foxj1 (B) Muc5ac* (C) and *Muc5b* (D) was altered in mMECs compared to that seen in mMMCs (Fig 5.13). *p63* expression did not differ between the genotypes. Data were analysed using One-way ANOVA plus Tukey's posthoc test and represented as mean individual RQ values ± SEM for three independent batches of cultured mMECs. ****p<0.0001, ***p<0.001, **p<0.01, *p<0.05.

The expression of inflammatory genes was upregulated in the mucosal cells of *Bpifa1*$^{-/-}$ *Evi1*$^{Jbo/+}$ and *Evi1*$^{Jbo/+}$ mice but their expression did not change additionally due to *Bpifa1* ablation (Section 5.2.5.1). I was interested in investigating whether cultured cells retained the elevated expression of these inflammatory genes. *Cxcl2 was* upregulated 6 fold (p=0.0012, Fig 5.17A), *Tgfβ* showed a small increase of 1.25 fold (p=0.02, Fig 5.17B) and *Il6* was upregulated 8.5 fold (p=0.002, Fig 5.17C) in *Bpifa1*$^{-/-}$*Evi1*$^{Jbo/+}$ mMECs compared to *Wt* mMECs, in line with our previous observation in freshly isolated mMMCs (Fig 5.13, Table 5.2). However, the upregulation in *Evi1*$^{Jbo/+}$ mMECs was not significant (Fig 5.17A-C). There was also a significant difference in the levels of *Cxcl2* in *Bpifa1*$^{-/-}$ mMECs compared to *Wt* mMECs (p=0.0089, Fig 5.17A) and *Il6* in *Bpifa1*$^{-/-}$*Evi1*$^{Jbo/+}$mMECs compared to *Evi1*$^{Jbo/+}$mMECs (p=0.047, Fig 5.17C). Thus, my data indicates that although mMECs maintained expression of inflammatory genes, the pattern of expression differed widely to that seen in the native middle ear mucosa from *Bpifa1*$^{-/-}$*Evi1*$^{Jbo/+}$, *Evi1*$^{Jbo/+}$, *Bpifa1*$^{-/-}$ and *Wt* mice.

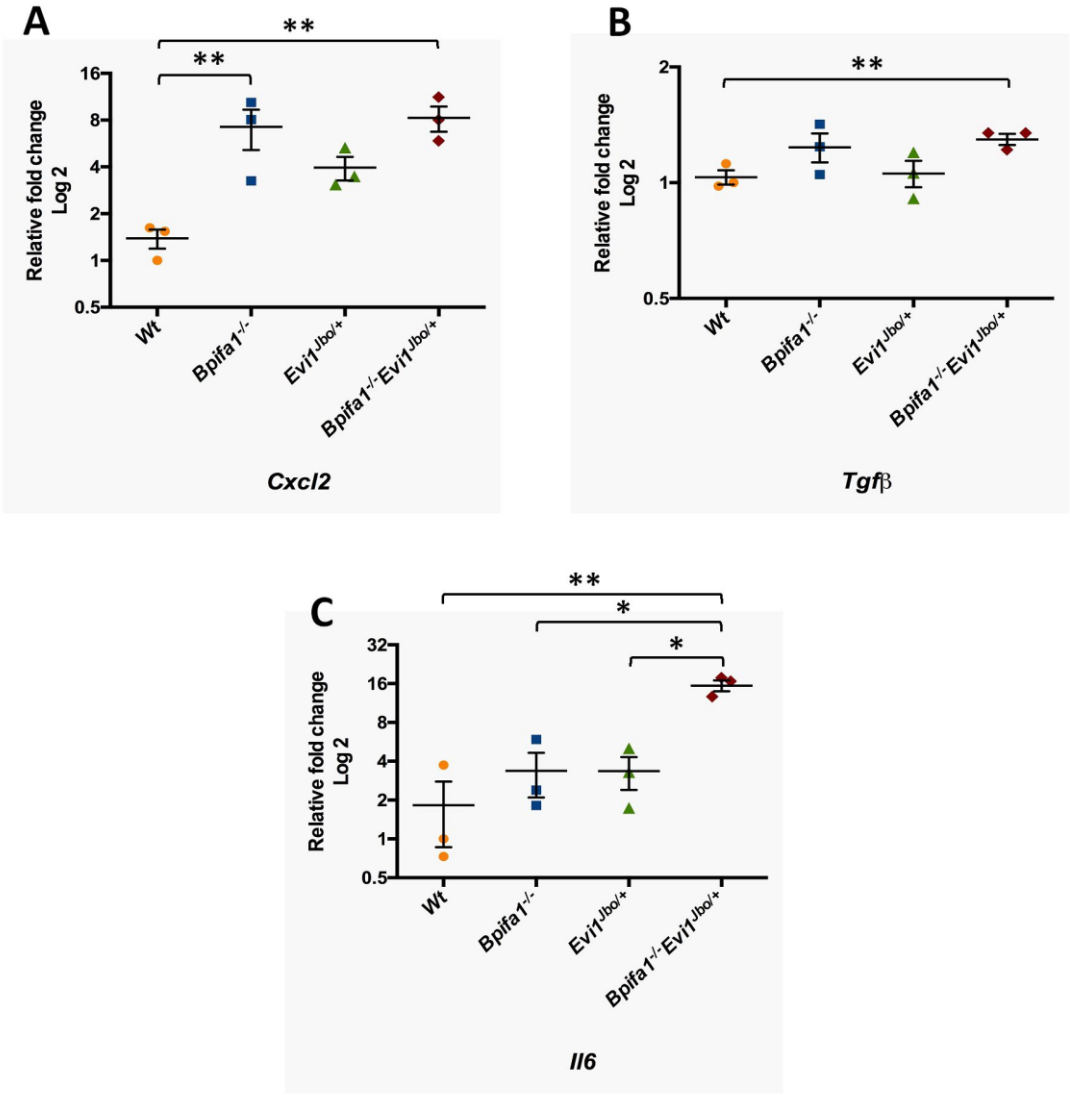

Figure 5.17 Expression of epithelial markers in *Bpifa1*$^{-/-}$*Evi1*$^{Jbo/+}$ mMECs
Significant upregulation of *Cxcl2 (A), Tgfβ (B) and Il6 in Bpifa1*$^{-/-}$*Evi1*^{Jbo}mMECs compared to *Wt* mMECs. The expression pattern of all three genes is altered in mMECs compared to that seen in mMMCs (Fig 5.12). Data were analysed using One-way ANOVA plus Tukey's posthoc test and represented as individual RQ values ± SEM for three independent batches of cultured mMECs. **p<0.01, *p<0.05.

5.2.6.3 Localisation of epithelial proteins in mMEC cultures using IFC microscopy

IFC microscopy of ALI day 14 *Bpifa1*$^{-/-}$*Evi1*$^{Jbo/+}$, *Evi1*$^{Jbo/+}$ *Bpifa1*$^{-/-}$ and *Wt* mMECs confirmed successful differentiation of cells at the proteomic level. BPIFA1 staining was localised to the non-ciliated cells and the intensity of staining appeared to be reduced in *Evi1*$^{Jbo/+}$

cultures compared to *Wt* cultures (Fig 5.18A, B). As expected BPIFA1 staining was absent in ALI day 14 *Bpifa1*$^{-/-}$ and *Bpifa1*$^{-/-}$*Evi1*$^{Jbo/+}$ mMECs (Fig 5.18C, D). Ciliated cells, marked by FOXJ1 and goblet cells marked by MUC5B were observed in clusters and localised to the elevated layers of cells (Fig 5.18E- H). This is consistent with the observations in C57BL/6 *Wt* and *Bpifa1*$^{-/-}$ mMECs (Sections 4.2.6 and 4.2.8).

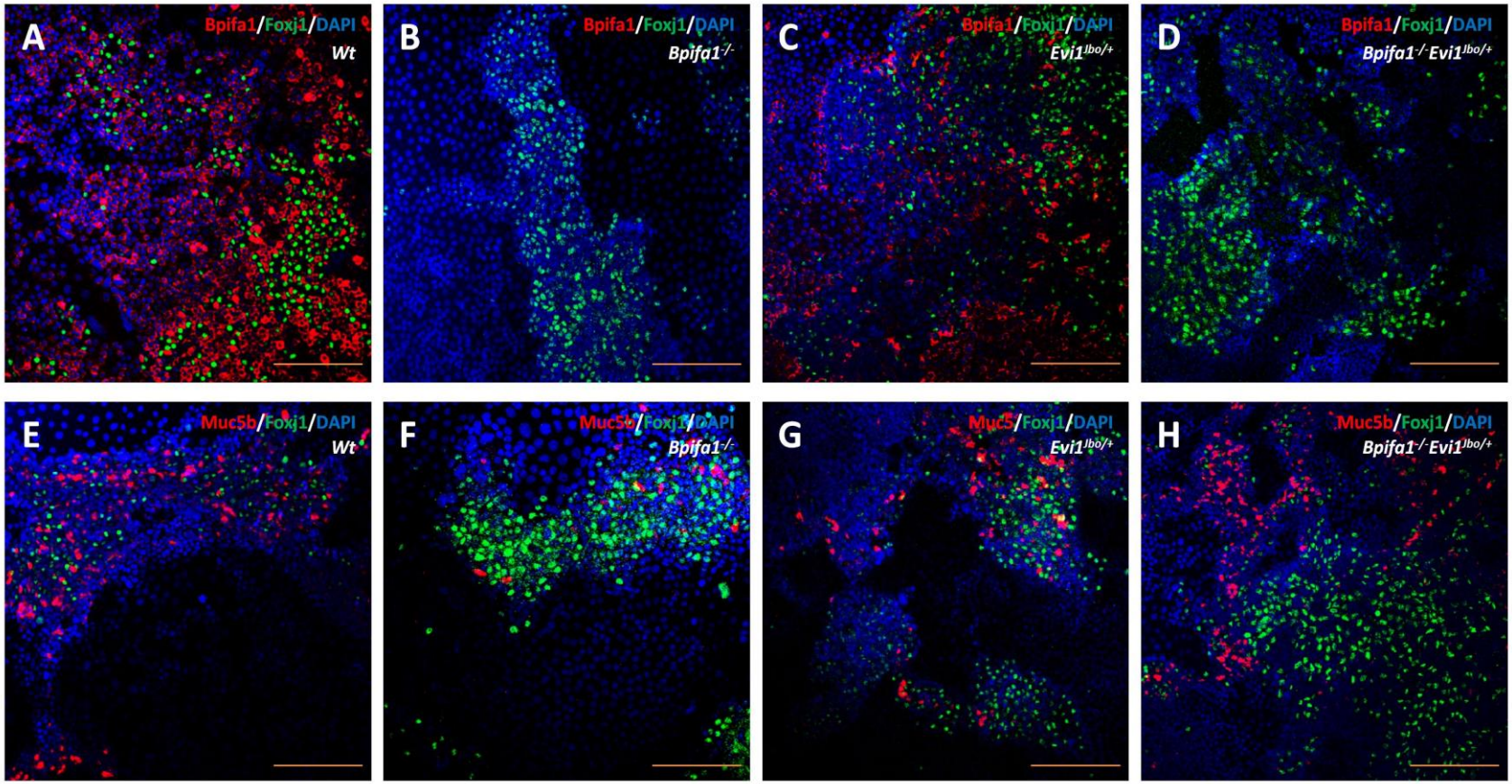

Figure 5.18 Localisation of epithelial markers in *Bpifa1*$^{-/-}$*Evi1*$^{Jbo/+}$ mMECs
Immunofluorescence confocal images (representative of three independent batches) showing BPIFA1 localisation in non-ciliated cells of ALI Day 14 *Wt* and *Evi1*$^{Jbo/+}$ mMECs (A, C). BPIFA1 staining is absent in *Bpifa1*$^{-/-}$ and *Bpifa1*$^{-/-}$*Evi1*$^{Jbo/+}$mMECs (B, D). MUC5B and FOXJ1 localise to the elevated clusters of cells in ALI Day 14 *Wt, Bpifa1*$^{-/-}$, *Evi1*$^{Jbo/+}$ and *Bpifa1*$^{-/-}$*Evi1*$^{Jbo/+}$mMECs (E, F, G, H). Scale bar =100µm

In order to quantify the difference in the levels of these proteins between the 4 groups of mice, 8-10 20x fields, spanning one half of the transwell membrane were analysed from 3 individual batches of ALI day 14 mMECs. The level of cytosolic BPIFA1 protein was significantly lower in *Evi1*$^{Jbo/+}$ mMECs compared to *Wt* mMECs, as demonstrated by both the mean integrated fluorescence intensity for BPIFA1 staining (Fig 5.19A p=0.0105) as well as the percentage of BPIFA1 positive cells (Fig 5.19B p=0.0074). This supports our observation of reduced mRNA levels of *Bpifa1* in *Evi1*$^{Jbo/+}$ mMMCs (Section 5.2.5.2) and mMECs (Section 5.2.6.2).

In contrast to a downregulation of *Foxj1* seen by RT-qPCR analysis of mMMCs, the percentage of ciliated cells was higher in *Evi1*$^{Jbo/+}$ and *Bpifa1*$^{-/-}$*Evi1*$^{Jbo/+}$ mMECs, although this did not reach statistical significance (Fig 5.19C). The percentage of MUC5B positive cells was highly variable in the *Wt* mMECs and did not differ between the 4 genotypes (Fig 5.19D).

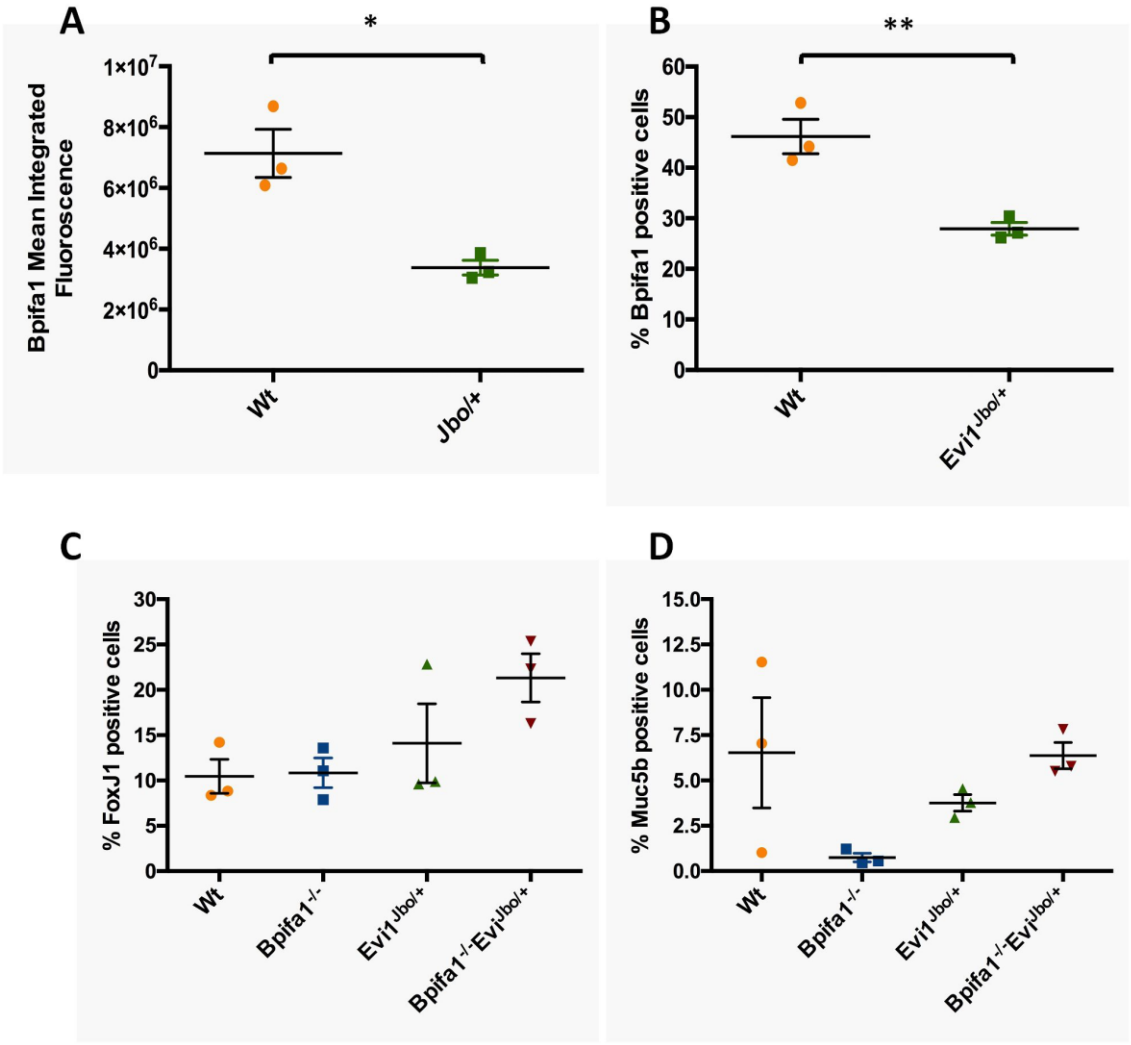

Figure 5.19 Quantification of epithelial sub-populations in mMMECs
Mean integrated fluorescence intensity for BPIFA1 (A) and percentage of BPIFA1 positive cells (B) is significantly lower in ALI Day 14 *Evi1*$^{Jbo/+}$ mMECs compared to ALI Day 14 Wt mMECs; 2 tailed t-test **p< 0.01, *p<0.05. There is no difference between percentage of Foxj1 and Muc5b positive cells between ALI Day 14 *Wt, Bpifa1*$^{-/-}$, *Evi1*$^{Jbo/+}$ *and Bpifa1*$^{-/-}$*Evi1*$^{Jbo/+}$ mMECs; One-way ANOVA with Tukey's posthoc test. Data representative of three independent batches of mMECs.

5.2.7 Proliferation rates of *Bpifa1*$^{-/-}$*Evi1*$^{Jbo/+}$ mMECs and fibroblasts

I postulated that the thickening of the middle ear mucosa of *Bpifa1*$^{-/-}$*Evi1*$^{Jbo/+}$ and *Evi1*$^{Jbo/+}$ mice, was a consequence of hyperproliferation of cells in the epithelial and sub-epithelial lining of the middle ear cavity. Since the average mucosal thickness in *Bpifa1*$^{-/-}$*Evi1*$^{Jbo/+}$ middle ears was significantly higher than that of *Evi1*$^{Jbo/+}$ middle ears, I sought to investigate whether loss of *Bpifa1* contributed to the enhanced proliferative capacity of the middle ear

mucosal cells. I seeded mMECs isolated from the middle ear cavities of *Bpifa1*$^{-/-}$*Evi1*$^{Jbo/+}$, *Evi1*$^{Jbo/+}$ *Bpifa1*$^{-/-}$ and *Wt* mice at an initial density of 50,000 cells/transwell in absence of ROCKi to compare their population doubling times. Similarly, population doubling time for fibroblasts separated by differential adherence was also compared between the 4 genotypes. No differences were seen between the doubling times of either mMECs (Fig 5.20A) or fibroblasts (Fig 5.20B) cultured from the 4 genotypes, indicating that the cells proliferated at similar rates.

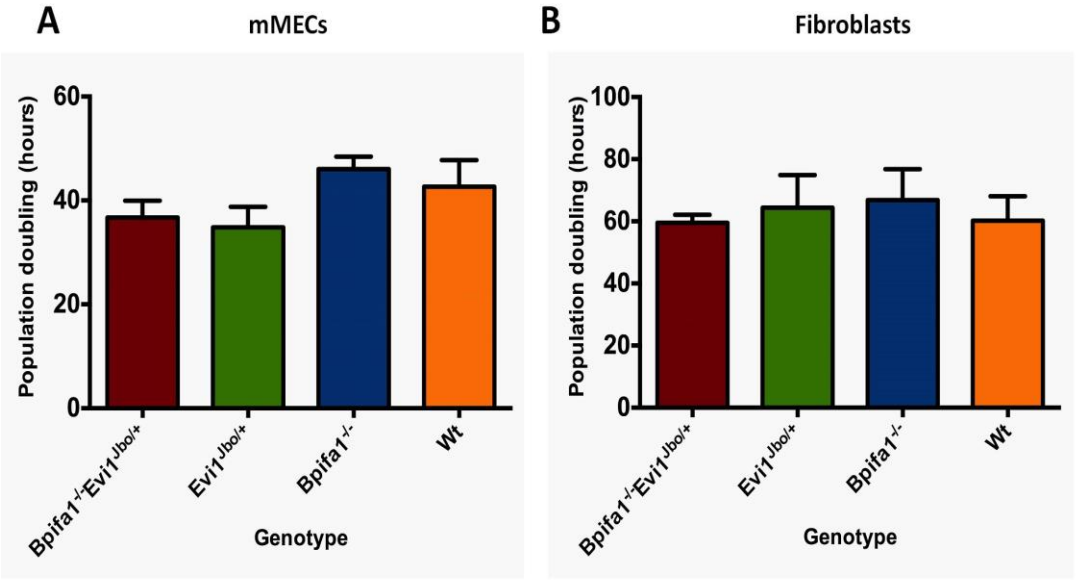

Figure 5.20 Proliferation rates of mMECs and fibroblasts
There was no significant difference between the population doubling times of *Wt, Bpifa1*$^{-/-}$, *Evi1*$^{Jbo/+}$ *and Bpifa1*$^{-/-}$*Evi1*$^{Jbo/+}$ mMECs (A) and fibroblasts (B) in culture. One-way ANOVA with Tukey's posthoc test.

5.2.8 IHC for epithelial and sub-epithelial markers

Since the exacerbated OM phenotype of *Bpifa1*$^{-/-}$*Evi1*$^{Jbo/+}$ mice is not a result of an increased strength in cytokine response and the OM phenotype could not be successfully replicated *in vitro*, I sought to investigate the changes in the native middle ear mucosa using IHC. The aim of this study was to identify the effects of *Bpifa1* deletion on proteins of the middle ear epithelium and the sub-epithelial connective tissue, which may contribute to the increased mucosal thickening. Under my direction, a placement student in the lab, Catherine Russell, performed IHC on dorsal middle ear sections from P28 *Bpifa1*$^{-/-}$*Evi1*$^{Jbo/+}$, *Evi1*$^{Jbo/+}$ *Bpifa1*$^{-/-}$ and *Wt* mice for this analysis.

5.2.8.1 Intensity of BPIFA1 staining is reduced in Evi1$^{Jbo/+}$ *mice*

BPIFA1 was expressed strongly throughout the *Wt* middle ear epithelium (Fig 5.21A, E). The expression pattern was the same as described previously (Sections 1.8.2 and 3.2.2). BPIFA1 staining was also seen in the surface epithelium of *Evi1*$^{Jbo/+}$ middle ears; however, the intensity of staining was reduced compared to *Wt* mice. The middle ear exudates stained positive for the BPIFA1. No staining was seen in the underlying sub-epithelial mesenchyme, except occasional staining in submucosal glands. (Fig 5.21C, G). This was consistent with my preliminary observations in *Evi1*$^{Jbo/+}$ mice (Mulay MSc thesis 2011). This was also in line with my RT-qPCR data from isolated mMMCs and cultured mMECs. As expected, *Bpifa1*$^{-/-}$ (Fig 5.21B, F) and *Bpifa1*$^{-/-}$*Evi1*$^{Jbo/+}$ (Fig 5.21D, H) middle ears completely lacked positivity for BPIFA1. Also staining was absent in *Wt* negative control sections stained for the protein (Fig 5.21I, J).

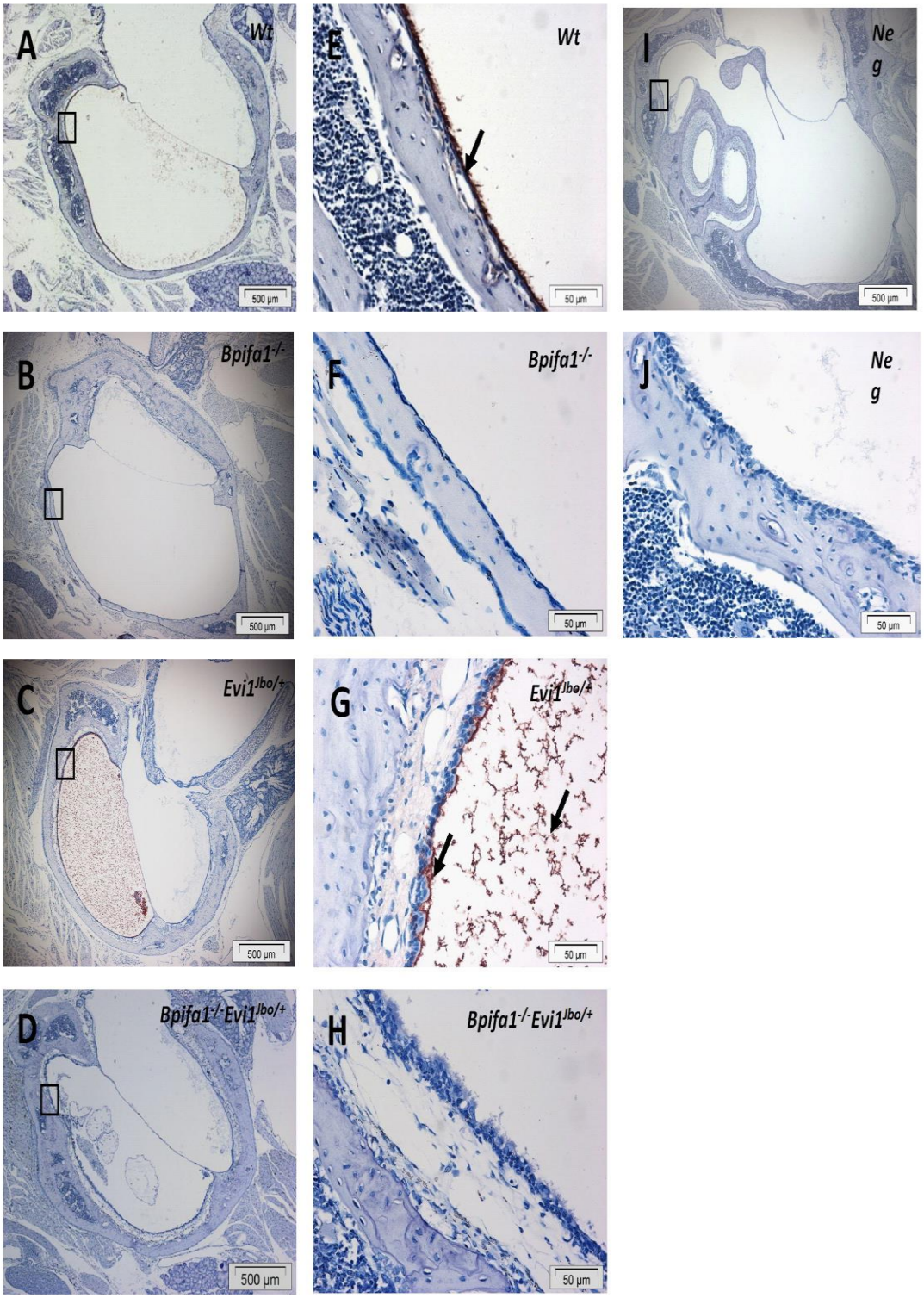

Figure 5.21 Localisation of BPIFA1 in P28 middle ears of *Wt*, *Bpifa1*$^{-/-}$, *Evi1*$^{Jbo/+}$ and *Bpifa1*$^{-/-}$ *Evi1*$^{Jbo/+}$ mice.

IHC analysis of middle ear sections showing abundant staining of BPIFA1 along the *Wt* middle ear epithelium (A, E) and reduction in staining intensity along *Evi1*$^{Jbo/+}$ middle ear epithelium. BPIFA1 staining is also seen in the middle ear effusion of *Evi1*$^{Jbo/+}$ (C, G). BPIFA1 staining is completely absent in *Bpifa1*$^{-/-}$ (B, F) *and Bpifa1*$^{-/-}$*Evi1*$^{Jbo/+}$ (D, H) middle ears and in the *Wt* negative control (I , J). Data is representative of n=3 mice for all genotypes. Scale bar: 500µm for 4x images and 50µm for 60x images. Arrowheads indicate positive staining

5.2.8.2 Intensity of Lactotransferrin staining increased with OM development

Lacotransferrin intensely stained the thin middle ear epithelium of *Wt* and *Bpifa1*$^{-/-}$ mice. The staining was continuous throughout the middle ear cavity (Fig 5.22A-D). The mucosal lining of in *Evi1*$^{Jbo/+}$ and *Bpifa1*$^{-/-}$*Evi1*$^{Jbo/+}$ middle ears was considerably thickened, and this thickening was seen both in the epithelial layer and the underlying mesenchyme. Unlike BPIFA1, Lactotransferrin staining was observed in both the surface epithelial cells as well as the underlying sub-epithelial layer. The amount of staining increased in the thickened middle ear mucosa (Fig 5.22E-H). Negative antibody controls from both *Wt* and *Bpifa1*$^{-/-}$ *Evi1*$^{Jbo/+}$ were completely devoid of Lactotransferrin staining (Fig 5.22I-L)

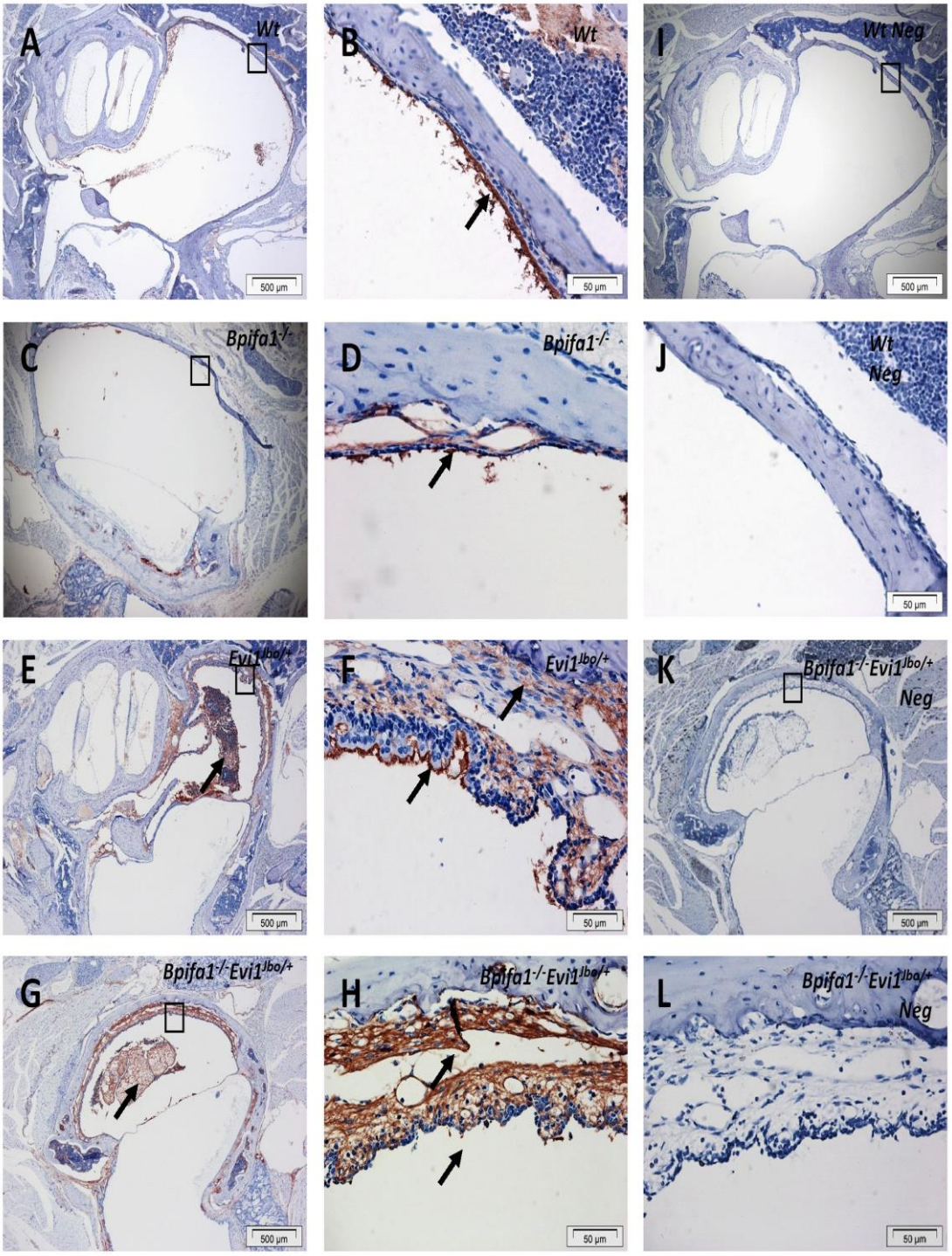

Figure 5.22 Localisation of Lactotransferrin in P28 middle ears of *Wt*, *Bpifa1*$^{-/-}$, *Evi1*$^{Jbo/+}$ and *Bpifa1*$^{-/-}$ *Evi1*$^{Jbo/+}$ mice.

IHC analysis of middle ear sections showing intense Lactotransferrin staining along the thin *Wt* (A, B) and *Bpifa1*$^{-/-}$ (C, D) middle ear epithelium. Staining intensity increased further in the inflamed and thickened mucosa of *Evi1*$^{Jbo/+}$ (E, F) and *Bpifa1*$^{-/-}$*Evi1*$^{Jbo/+}$ (G, H) middle ear. Arrowheads indicate staining in middle ear epithelial cells and sub-epithelial mesenchyme. Lactotransferrin staining is completely absent in negative controls from Wt (I, J) *and Bpifa1*$^{-/-}$*Evi1*$^{Jbo/+}$ (K, L) middle ears. Data is representative of n=3 mice for all genotypes. Scale bar 500µm for 4x images and 50µm for 60x images.

5.2.8.3 Intensity of collagen staining increased with OM development

Collagen fibres are an integral part of the extracellular matrix (ECM) of the sub-epithelial stroma. A thin layer of collagen staining (as shown by picro-sirus red staining) was observed underlying the epithelial cells in *Wt* and *Bpifa1*$^{-/-}$ middle ears (Fig 5.23A-D). Expansion of the sub-epithelial mesenchyme in *Evi1*$^{Jbo/+}$ and *Bpifa1*$^{-/-}$*Evi1*$^{Jbo/+}$ middle ears was accompanied by an expansion of the collagen fibres throughout the mesenchyme as well as an increase in the intensity of staining (Fig 5.23E-H).

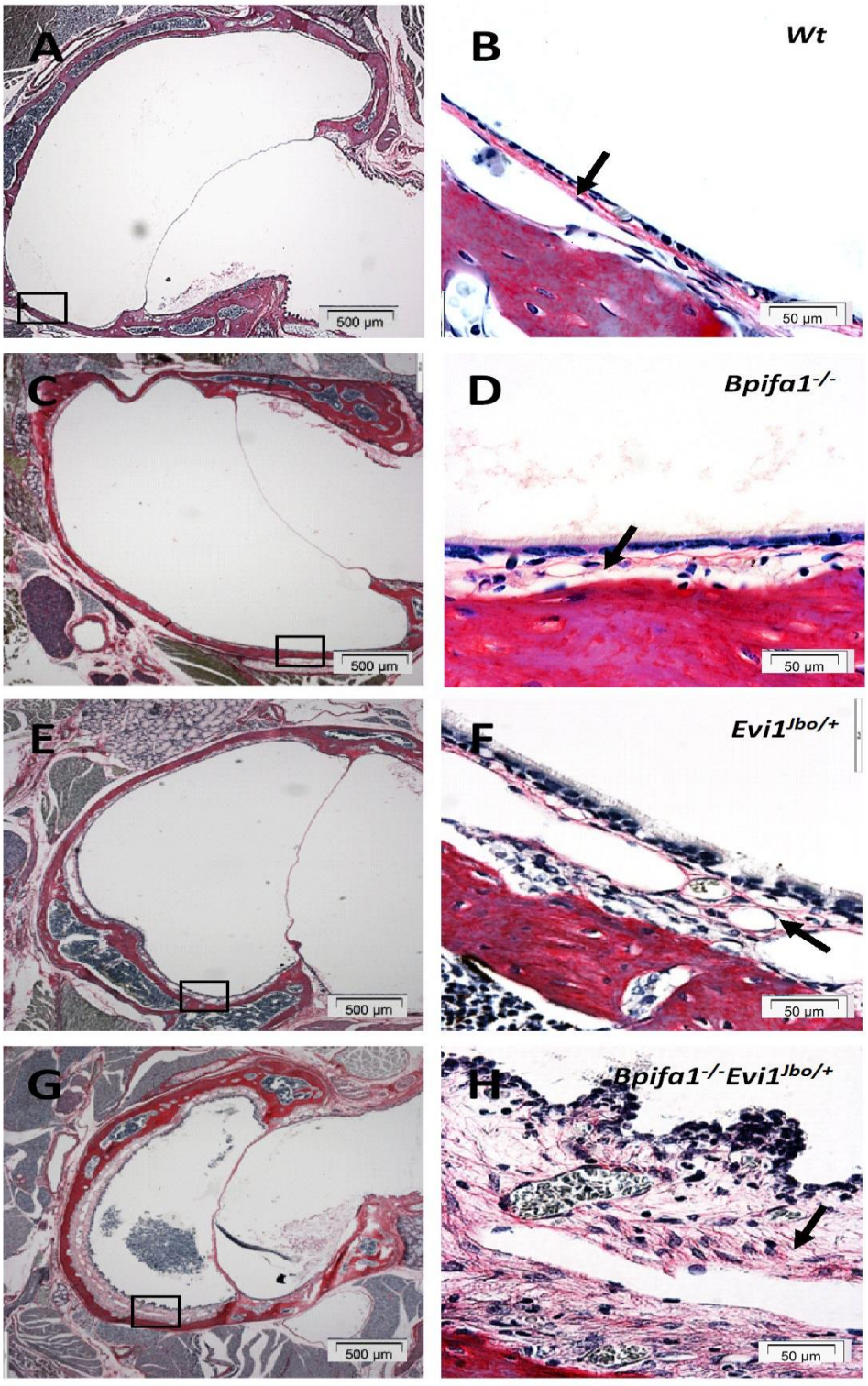

Figure 5.23 Collagen deposition in P28 middle ears of *Wt*, *Bpifa1*$^{-/-}$, *Evi1*$^{Jbo/+}$ and *Bpifa1*$^{-/-}$ *Evi1*$^{Jbo/+}$ mice.

Picrosirius red chemical staining showing collagen fibres in the sub-epithelial mesenchyme of *Wt* (A, B) and *Bpifa1*$^{-/-}$ (C, D) middle ear epithelium. Staining intensity increased in the inflamed and expanded mesenchyme of *Evi1*$^{Jbo/+}$ (E, F) and *Bpifa1*$^{-/-}$*Evi1*$^{Jbo/+}$ (G, H) middle ear indicating increased deposition of collagen fibres. Arrowheads indicate positive staining. Scale bar 500µm for 4x images and 50µm for 60x images.

5.2.8.4 Intensity of α smooth muscle actin (α-SMA) staining increased with OM development

α-SMA is a marker of terminally differentiated fibroblasts. Very little or no staining for α-SMA was seen across all the *Wt* and *Bpifa1*$^{-/-}$ middle ears (Fig 5.24A-D). α-SMA strongly stained the thickened mesenchyme of *Evi1*$^{Jbo/+}$ and *Bpifa1*$^{-/-}$*Evi1*$^{Jbo/+}$ middle ears, in a unique pattern. Unlike collagen which localised throughout the mesenchyme, α-SMA staining was only seen in the bottom half of the mesenchymal layer towards the bony cartilage of the bulla (Fig 5.24E-H). As expected, no staining was seen in the negative controls (Fig 5.24E-H)

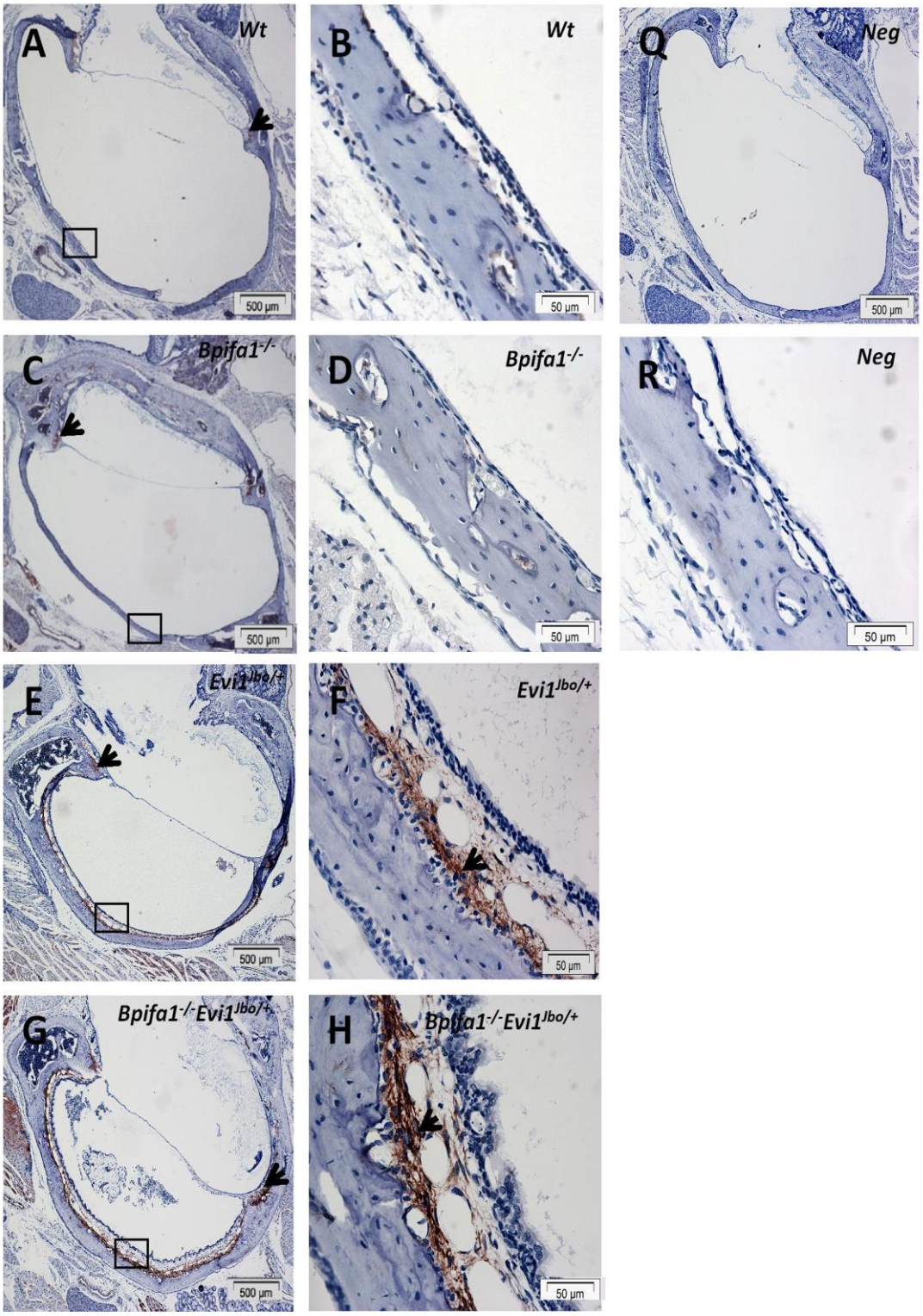

Figure 5.24 Localisation of α-SMA in P28 middle ears of *Wt*, *Bpifa1*$^{-/-}$, *Evi1*$^{Jbo/+}$ and *Bpifa1*$^{-/-}$ *Evi1*$^{Jbo/+}$ mice.

IHC analysis of middle ear sections showing no α-SMA staining in the thin sub-epithelial mesenchyme of *Wt* (A, B) and *Bpifa1*$^{-/-}$ (C, D) middle ear epithelium. Intense α-SMA staining in the lower half of the expanded mesenchyme of *Evi1*$^{Jbo/+}$ (E, F) and *Bpifa1*$^{-/-}$*Evi1*$^{Jbo/+}$ (G, H) middle ear. Arrowheads indicate positive staining. Data is representative of n=3 mice for all genotypes. Scale bar 500µm for 4x images and 50µm for 60x images.

5.3 Discussion

This is the first study to describe the effect of *Bpifa1* deletion in a compound mutant model. *Bpifa1*$^{-/-}$*Evi1*$^{Jbo/+}$ compound mutants were generated for the experiments performed in this chapter in order to investigate the effect of the loss of *Bpifa1* in an established model of genetic OM. *Evi1*$^{Jbo/+}$ mice are routinely studied on the C3H/HeH background since previous studies in our lab have shown that OM susceptibility varies with the mouse strain (Bhutta 2012, Tyrer PhD thesis 2013). Generation of compound mutants therefore required the transfer of *Bpifa1*$^{+/-}$ mice from the original C57BL/6 background to the C3H/HeH background through repeated backcrossing with *Wt* C3H/HeH mice.

5.3.1 Characterisation of *Bpifa1*$^{-/-}$*Evi1*$^{Jbo/+}$ mutants

Bpifa1$^{-/-}$*Evi1*$^{Jbo/+}$ compound mutant mice did not exhibit any anomalies in viability and overt behaviour up to 3 months of age (the maximum time for which compound mutants were maintained for this study). However, adult *Bpifa1*$^{-/-}$*Evi1*$^{Jbo/+}$ and *Evi1*$^{Jbo/+}$ mice had lower body weights compared to Wt mice. I did not observe a significant difference between the weights of *Bpifa1*$^{-/-}$*Evi1*$^{Jbo/+}$ and *Evi1*$^{Jbo/+}$ or between *Wt* and *Bpifa1*$^{-/-}$ mice, suggesting that the smaller size was an effect of the *Evi1* mutation. Through previous work in our lab, it is known that *Evi1*$^{Jbo/+}$ mice are smaller in size compared to *Wt* mice (Parkinson et al 2006). Although *Evi1*$^{Jbo/+}$ mice exhibit no respiratory distress or craniofacial abnormalities (Parkinson et al 2006), data from a previous PhD student's work indicated that *Evi1*$^{Jbo/+}$ lungs have reduced number of airways (Tyrer PhD thesis 2013). *Evi1* has been suggested to be involved in the development of the airways and also in airway remodelling through its role in repression of the TGF-β signalling pathway (Duvernelle et al 2003, Perkins et al 1991). Also a GWAS study identified *Evi1* as a candidate gene for maintenance of pulmonary function (Soler Artigas et al 2011). Analysis of histological sections from *Bpifa1*$^{-/-}$

Evi1$^{Jbo/+}$ and *Evi1*$^{Jbo/+}$ lungs was out of the scope of this study. However, given the putative roles of both *BPIFA1* and *EVIi1* in the pulmonary innate immunity, this aspect warrants further evaluation.

5.3.2 Loss of *Bpifa1* leads to an exacerbation of the OM phenotype in Evi1$^{Jbo/+}$ mice

The *Evi1*$^{Jbo/+}$ mouse is a powerful model of human OM, since disease development in these mice is non-syndromic i.e. the development of OM is not associated with any significant phenotype outside the middle ear, apart from formation of an extra digit(Parkinson et al 2006). In SPF conditions, *Evi1*$^{Jbo/+}$ mice develop mild spontaneous OM at P13. As shown in Chapter 3, the middle ear cavitates between P10-P15 (Section 3.2.1). Hence the development of OM in *Evi1*$^{Jbo/+}$ mice is immediately following the formation of the middle ear cavity and the percentage of affected mice increases through P21 until the phenotype becomes chronic at P28 (Parkinson et al 2006).

In this study, *Bpifa1*$^{-/-}$*Evi1*$^{Jbo/+}$ demonstrated greater penetrance of OM compared to *Evi1*$^{Jbo/+}$ mice. This was evidenced by a significantly increased thickening of the middle ear mucosa at both P21 and P28 in *Bpifa1*$^{-/-}$*Evi1*$^{Jbo/+}$ mice and a higher incidence of middle ear fluids. The frequency of middle ear fluids in *Evi1*$^{Jbo/+}$ bullae at P28 (67% ears) was consistent with the previously published literature (Parkinson et al 2006), whereas all *Bpifa1*$^{-/-}$*Evi1*$^{Jbo/+}$ mice showed fluid development at this time point, with a significantly higher tendency for development of bilateral OM.

Mucosal thickening in affected mice was characterised by remodelling of the otherwise thin middle ear epithelium into a disorganised, multi-layered epithelium as well as expansion of the sub-epithelial mesenchyme. It is known that along with the inflammatory exudate within the middle ear cavity, OM is also associated with infiltration of the

mesenchymal tissue with inflammatory cells (Juhn et al 2008). Due to time constraints, I did not analyse the inflammatory cell populations in the middle ears of diseased mice. However, H&E sections of middle ears indicated that the exudate in *Evi1*$^{Jbo/+}$ and *Bpifa1*$^{-/-}$ *Evi1*$^{Jbo/+}$ mice was largely purulent, albeit sometimes a serous exudate was also observed. Cytospun fluids from adult mice appeared to showed a larger proportion of neutrophils compared to macrophages. This is supported by previous studies in *Evi1*$^{Jbo/+}$ mice which report the presence of a neutrophilic exudate, containing a smaller percentage of foamy macrophages and sloughed off epithelial cells (Cheeseman et al 2011, Parkinson et al 2006). In future, IHC analysis for neutrophilic and macrophage markers such as Gr-1 and F4/80 as well as fluorescence associated cell sorting (FACS) analysis would provide a comparison of inflammatory sub-populations in the middle ears of *Evi1*$^{Jbo/+}$ and *Bpifa1*$^{-/-}$ *Evi1*$^{Jbo/+}$ mice. The type of middle ear effusion has been suggested to be an indication of the stage of OM development and mucous effusions often point to a more severe disease in patients (Kubba et al 2000). Use of markers such as matrix mettaloproteinase-2 (MMP-2), which are specific to mucous effusions (Moon et al 2008) may provide further insight into the exacerbation of OM phenotype of *Bpifa1*$^{-/-}$*Evi1*$^{Jbo/+}$ mice.

In order to maximise the potential for analysis, penetrance of OM was also assessed in adult *Bpifa1*$^{-/-}$*Evi1*$^{Jbo/+}$ mice that were transported to University if Sheffield for isolation of middle ear cells. The incidence of middle ear fluids was higher in *Bpifa1*$^{-/-}$*Evi1*$^{Jbo/+}$ mice compared to *Evi1*$^{Jbo/+}$ as assessed by the appearance of the Tm. This result was borderline insignificant. However, it is important to note that such assessment of OM is only semi-quantitative and is less powerful than histological analysis and it does not allow for analysis of the mucosal thickness. Also, these mice were analysed within an age range 7-9 weeks rather than at a single time point, which may add to phenotypic variation. Therefore, it is likely that *Bpifa1*$^{-/-}$*Evi1*$^{Jbo/+}$ retain the aggravated OM phenotype in adulthood and this aspect needs further exploration.

In line with my observations in C57BL/6 from Chapter 3, *Bpifa1*$^{-/-}$ mice on the C3H/HeH background did not demonstrate OM at any of the time points tested. Therefore, the data clearly indicated that loss of *Bpifa1* alone does not lead to spontaneous development of OM irrespective of the genetic background. However, loss of *Bpifa1* in a pre-existing inflammatory environment in *Evi1*$^{Jbo/+}$ middle ears accelerates and worsens the OM phenotype.

5.3.3 Loss of *Bpifa1* does not lead to an exacerbated inflammatory cytokine response

Several studies have suggested an anti-inflammatory role for BPIFA1. *Bpifa1* ablation in mouse models showed higher levels of inflammatory compared to *Wt* mice upon bacterial infection and overexpression of the protein was accompanied by reduced in the levels of pro-inflammatory mediators (Liu et al 2013a, Liu et al 2013b, Lukinskiene et al 2011). In an allergic setting, *Bpifa1* deficient mice stimulated with ovalbumin showed increased airway inflammation which was reversed by overexpression of *Bpifa1* (Wright et al 2010). In addition, preliminary IHC data from our lab suggested that that intensity of BPIFA1 staining in the *Evi1*$^{Jbo/+}$ middle ear epithelium reduced with OM progression. BPIFA1 was detectable in *Evi1*$^{Jbo/+}$ in middle ear exudates, however there was evidence of proteolytic degradation of the protein, suggesting that a reduction in levels or loss of the anti-inflammatory function of *Bpifa1* may contribute to OM pathogenies (Mulay MSc thesis 2011). In Chapter 4, I have shown that the loss of *Bpifa1* alone did not lead to an enhanced pro-inflammatory response in mMECs following NT*Hi* infection (Section 4.2.15). However, I speculated that *Bpifa1* ablation in the pre-existing inflammatory environment of the *Evi1*$^{Jbo/+}$ bullae might cause an exaggeration of the inflammatory response *in vivo* and this, in turn, may contribute to the exacerbated OM phenotype seen in *Bpifa1*$^{-/-}$*Evi1*$^{Jbo/+}$ mice.

Preliminary, semi-quantitative analysis of *Evi1*$^{Jbo/+}$ ear exudates using mouse cytokine arrays in our lab indicated intense expression of IL1β and CXCL2 (Mulay MSc thesis 2011). Moreover gene expression analysis of *Evi1*$^{Jbo/+}$ middle ear fluids compared with venous blood showed significant upregulation of a variety of inflammatory markers, including *Il1β, Cxcl2, Tnfα, Il6* and *Tgfβ* (Cheeseman et al 2011). A major limitation of analysing middle ear fluids is that *Wt* mice do not have effusions (or a middle ear lining fluid that can be sampled), thus impeding a direct comparison in the gene expression of *Wt* and *Evi1*$^{Jbo/+}$middle ear contents. Analysis of middle ear fluids is also sub-optimal because they contain a mixture of inflammatory cells, bacterial remains and debris from sloughed off epithelial cells. Therefore, in order to provide a direct comparison between the mucosa of OM affected mice and normal mice, I isolated mMMCs from the *Bpifa1*$^{-/-}$*Evi1*$^{Jbo/+}$, *Evi1*$^{Jbo/+}$, *Bpifa1*$^{-/-}$ and *Wt* mice. This provided the opportunity to study potential changes in the inflammatory gene repertoire of middle ear epithelial cells as well as the sub-epithelial stromal cells.

My data show that all inflammatory genes studied were upregulated in mMMCs from *Bpifa1*$^{-/-}$*Evi1*$^{Jbo/+}$ mice. The neutrophil chemoattractant, *Cxcl2*, was the most differentially expressed gene in our study followed by *Il1β, Tnfα, and Tgfβ and Il6.* This elevation in expression was consistent with that seen in *Evi1*$^{Jbo/+}$ exudates (when compared to venous blood) (Cheeseman et al 2011). However, expression of none of the inflammatory genes differed between *Wt* and *Bpifa1*$^{-/-}$ mMMCs and between *Evi1*$^{Jbo/+}$ and *Bpifa1*$^{-/-}$*Evi1*$^{Jbo/+}$ mMMCs. Thus, it appears that *Bpifa1* does not play an anti-inflammatory role in OM development**.**

5.3.4 The inflamed mucosa of *Evi1*$^{Jbo/+}$ and *Bpifa1*$^{-/-}$*Evi1*$^{Jbo/+}$ mice is hypoxic

Previous studies in our lab have shown that the microenvironment of the inflamed *Evi1*$^{Jbo/+}$ middle ear cavities is chronically hypoxic (Cheeseman et al 2011). Inflammatory cells in the middle ear fluids, the inflamed middle ear epithelium, as well as the sub-epithelial connective tissue of *Evi1*$^{Jbo/+}$ mice, stained positive for markers of hypoxia and levels of *Hif1α, Vegf* and other *Vegf* signalling pathway genes are elevated in the ear fluids of *Evi1*$^{Jbo/+}$ mice. Similarly, middle ear fluids from *Tgif*$^{-/-}$ and *Fbxo11*$^{Jf/+}$ mice also showed high VEGF levels (Cheeseman et al 2011, Tateossian et al 2013). *Vegf* is a downstream signalling protein of the *Hif1α* signalling pathway and is involved in induction of angiogenesis, recruitment of inflammatory cells and vascular permeabilissation, thus contributing to fluid development within the middle ear (Cheeseman et al 2011). VEGF protein is also detectable in effusions from OM patients (Sekiyama et al 2011) .

The *Evi1*$^{Jbo/+}$ mutation is suggested to impact on TGFβ signalling (Kurokawa et al 1998b) and there is substantial crosstalk between the hypoxia and TGFβ signalling pathways. It has been shown that SMAD3 co-operates with HIF1α in presence of hypoxia to co-activate the transcription of *VEGF* (Sanchez-Elsner et al 2001). In this study, *Vegf* was significant upregulated in *Evi1*$^{Jbo/+}$ *and Bpifa1*$^{-/-}$*Evi1*$^{Jbo/+}$ mMMCs compared to *Wt* and *Bpifa1*$^{-/-}$ mMMCs. Moreover, *Il1β, Tnfα,* which are known to regulate *Hif1α* (Frede et al 2007), were also upregulated. Thus the data confirms the presence of a hypoxic milieu in the inflamed middle ear mucosa and provides further support to the view that disruption in TGFβ signalling increases overall susceptibility to OM. In future, the presence of hypoxia can be further tested in *Bpifa1*$^{-/-}$*Evi1*$^{Jbo/+}$ mice via in intraperitoneal injection of pimonidazole, which is a marker of hypoxia and IHC on middle ear sections from these mice using anti-pimonidazole antibodies (Cheeseman et al 2011). As seen with the other inflammatory genes such as *Cxcl2, Il1β, Tnfα* etc, loss of *Bpifa1* did not influence the levels of *Vegf*.

It was interesting that elevation of *Vegf* was maintained in the inflamed mMMCs despite incubation in normoxic conditions during the overnight pronase cell isolation process. However, there is a possibility that this may have altered the true *Vegf* levels and a more careful analysis is required to identify differences in *Evi1*$^{Jbo/+}$ *and* *Bpifa1*$^{-/-}$*Evi1*$^{Jbo/+}$ mMMCs. Perhaps this type of analysis could be done by *in situ* gene analysis or through the use of gene expression in samples of mucosa isolated by laser capture microdissection.

5.3.5 Cellular alterations in the inflamed mMMCs

Along with the upregulation of inflammatory markers, I observed a downregulation of the ciliated cell marker, *Foxj1* and goblet cell marker, *Muc5ac* in *Evi1*$^{Jbo/+}$ *and* *Bpifa1*$^{-/-}$*Evi1*$^{Jbo/+}$ mMMCs compared to *Wt* mMMCs. My assumption is that this is the consequence of an altered cellular phenotype in the during inflammation. As shown in Fig 5.1, EVI1 is a transcriptional repressor of TGFβ/SMAD signalling via direct inhibition of SMAD3 (Kurokawa et al 1998b). PAMPs such as those derived from NT*Hi* and pro-inflammatory mediators such as TNFα, can signal through TLR2 or TLR4, which can lead to activation of the MAP kinase protein, p38 via MyD88 signalling. p38 regulates MUC5AC production and over activation of p38 is often implicated in diseases such as COPD (Fig 5.25). Activation of TGFβ signalling down regulates p38 activity via SMAD3 and thus prevents excessive MUC5AC production in the event of TLR2 mediated inflammation (Jono et al 2003). A mutation in the *Evi1* locus may lead to over activation of TGFβ signalling leading to over-suppression of MUC5AC, and thus impair mucocilliary clearance. This hypothesis is supported by the observation of reduced levels of *Muc5ac* in *Evi1*$^{Jbo/+}$ *and* *Bpifa1*$^{-/-}$*Evi1*$^{Jbo/+}$ mMMCs. There is no published report on changes in genetic levels of ciliated cell markers in *Evi1*$^{Jbo/+}$ mice, however reduction in the number of ciliated cells is often implicated in OM pathogenesis (Straetemans et al 2001).

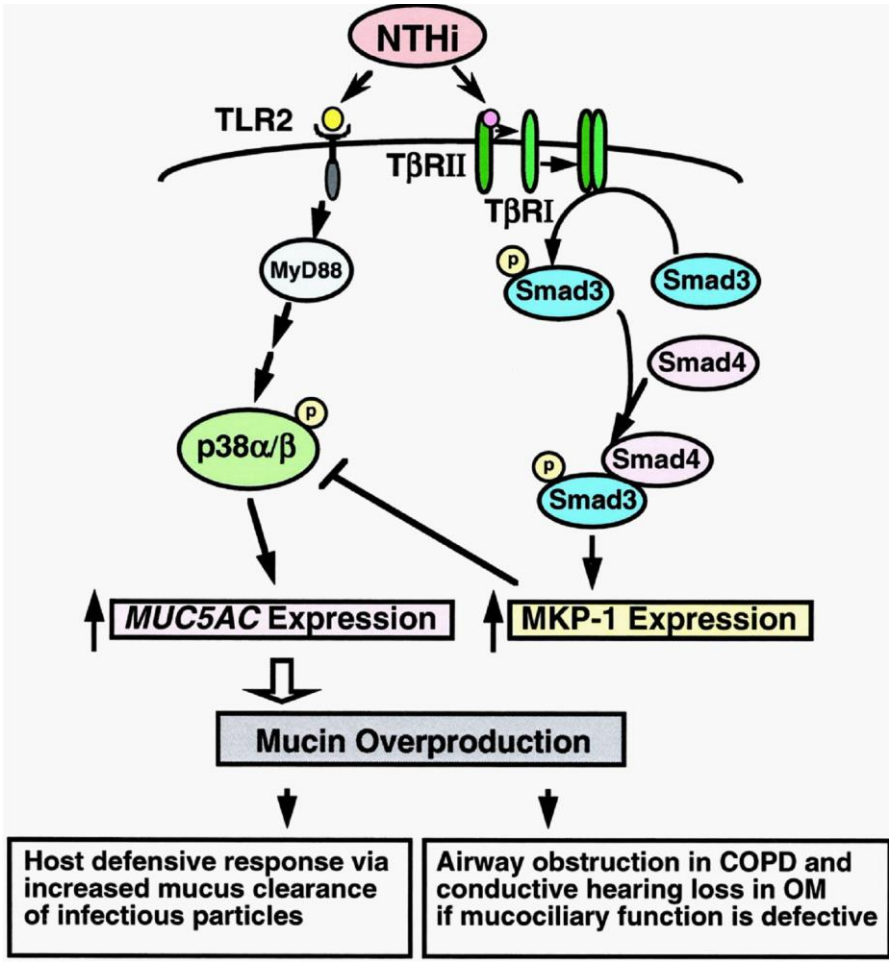

Figure 5.25 TGFβ signalling downregulated MUC5AC production
Activation of TGFβ signalling prevents over production of MUC5AC via inhibition of p38. Image reproduced from (Jono et al 2003), copyright American society for Biochemistry and Molecular biology. In *Evi1*$^{Jbo/+}$ mice, over activation of TGFβ signalling can lead to increased suppression of Muc5ac production leading to mucociliary impairment.

Expression of *EVI1* is upregulated due to chromosomal rearrangements in myeloid leukaemia (Goyama & Kurokawa 2010, Hirai 1999, Kurokawa et al 2000). However, there is limited literature on the expression of *Evi1* itself during OM in *Evi1*$^{Jbo/+}$ mice. *Evi1* mRNA was upregulated in middle ear fluids of *Evi1*$^{Jbo/+}$ mice compared to venous blood (Cheeseman et al 2011). However, as mentioned before, analysis of ear exudates is sub-optimal due to the lack of an appropriate control in *Wt* mice. IHC for EVI1 showed that the protein localised to neutrophils in the exudates, basal epithelial cells and sub-epithelial fibroblasts of *Evi1*$^{Jbo/+}$ middle ear at P13 and P21, before the onset of chronic OM, and was not seen in the

healthy, *Wt* middle ear (Parkinson et al 2006). It has also been shown that NT*Hi* and TNFα lead to an up regulation of EVI1 *in vitro* and *in vivo* (Xu et al 2012). Therefore, I compared *Evi1* expression specifically in the mucosal cells of adult mice and observed a small (<2 fold), yet significant (probably due to less variation within batches compared), reduction its expression in the inflamed mMMCs from Evi*1*$^{Jbo/+}$ *and Bpifa1*$^{-/-}$*Evi1*$^{Jbo/+}$ mice compared to *Wt* mice. IHC analysis for EVI1 was not performed in this study. However, it is unclear if levels of EVI1 protein should be altered in *Evi1*$^{Jbo/+}$ middle ear epithelium, since the causative mutation in these mice is a SNP. Perhaps the mutation causes a loss capacity of EVI1 to bind to its target co-repressors and a subsequent alteration in its function as a repressor of the Tgfβ and NfκB signalling pathways, thus setting in a feedback loop for activating these inflammatory pathways and leading to cellular alterations.

It is important to note that there was no added effect of deletion of *Bpifa1* on the expression any of the epithelial genes analysed. This is contrast to a previously published study that suggested a downregulation of *Foxj1* and *Muc5ac* in whole lung tissue of naïve *Bpifa1*$^{-/-}$ mice compared to *Wt* mice (Liu et al 2013a). Analysis of cellular composition of the airways of mutant mice may help to resolve this discrepancy.

I also observed a significant down regulation of *Bpifa1* in *Evi1*$^{Jbo/+}$ mMMCs compared to Wt mMMCs and this is discussed in detail in **Section 5.3.8**. Overall, my data suggests that the *Evi1*$^{Jbo/+}$ mutation results in significant remodelling of middle ear epithelium, marked by downregulation of ciliated, goblet and *Bpifa1* expressing cells, leading to dysregulation of the mucocilliary system and retention of fluid in the middle ear cavity.

5.3.6 Lack of recapitulation of the OM phenotype *in vitro*

I have shown that the loss of *Bpifa1* did not increase the expression of cytokines in the original mucosal cells. I therefore postulated that *Bpifa1* is involved in maintaining the stability of the middle ear epithelium, rather than serving an anti-inflammatory function

per se. In order to examine this in detail I cultured middle ear epithelial cells *in vitro* using the mMEC model established in Chapter 4. As with *Wt* cells, mMECs form the mutant mice differentiated into a variety of epithelial sub-types, both on a transcriptional and a protein level within 14 days of culture at the ALI. However, the majority of the epithelial and inflammatory markers did not retain the trends seen in the original mucosal cells (mMMCs). In addition, the pattern of expression of epithelial genes was also not consistent with that observed previously in C57BL/6 mMECs (Chapter4, Fig 4.12). There are two possible explanations for this failure to recapitulate the OM phenotype *in vitro.*

The first reason might be the lack of the specific microenvironment of the inflamed middle ears of $Evi1^{Jbo/+}$ and $Bpifa1^{-/-}Evi1^{Jbo/+}$ mice in mMECs. OM development is a collective outcome of the response to an insult to the middle ear epithelium and the isolated environment of the middle ear cavity. Development of hypoxia due to reduced ventilation in the middle ear space is an important contributing factor to the development of inflammation during OM pathogenesis (Corbeel 2007). Recent studies from our lab have highlighted the role of hypoxia and Vegf mediated signalling in development of OM in $Evi1^{Jbo/+}$ mice (Cheeseman et al 2011). Elevation of *Vegf* in $Evi1^{Jbo/+}$ and $Bpifa1^{-/-}Evi1^{Jbo/+}$ mMMCs in this study emphasizes the involvement of hypoxia in development of the OM phenotype. The absence of a hypoxia in mMEC cultures may be one of the reasons for the failure to recreate the microenvironment required for OM development. Use of hypoxia incubator chambers for the culture of $Evi1^{Jbo/+}$ and $Bpifa1^{-/-}Evi1^{Jbo/+}$ mMECs may provide a more suitable environment for recapitulation of the native phenotype. As mentioned previously, EVI1 is predominantly localised to neutrophil leukocytes and fibroblasts in the $Evi1^{Jbo/+}$ middle ear (Parkinson et al 2006). The absence of these cell types in our culture system may be another reason for the lack of the OM phenotype *in vitro.* The mucosal thickening observed in OM is due to combined expansion of both epithelial cells and the underlying mesenchymal tissue, indicating cross-talk between the two cell types. The

mMEC system models a pure population of epithelial cells. Lack of mesenchymal cells such as fibroblasts in culture may be another aspect contributing to the lack of the microenvironment required for OM development. Establishment of direct contact cultures by growing mMECs on one side of the transwell membrane and fibroblasts on the other may better mimic the organ morphology of the middle ear mucosa.

The second reason for the lack of recapitulation of the OM phenotype *in vitro* may be a variation in the population of basal cells that initiate mMEC cultures. In Chapter 4, I have shown that only a small proportion of the seeded mMECs was found attached to the transwell membrane at submerged day 3 (Section 4.2.2.1). It is widely accepted that due abundant expression of junctional, cytosketal and adhesive proteins, basal cells easily anchor to the underlying matrix and act as initiators of *in vitro* cultures of airway epithelial cells (Rock et al 2010). Basal cells of the respiratory epithelium are adult stem cells that produce multipotent progenitor cells, which in turn give rise to ciliated cells, secretory cells and goblet cells of the respiratory epithelium (Rock et al 2009, Rock et al 2010). Therefore, depending on the fate of the initiator basal and progenitor cells attached to the membrane, the percentage of differentiated cell types can vary between the different batches of mMEC cultures and even between different transwells of the same batch of mMECs. Perhaps, a strategy to fractionate tagged basal cells using FACS prior to establishment of mMEC cultures may yield more uniform cultures. Moreover, depending on the microenvironment and type of stress, differentiated epithelial cells can transdifferentiate to then give rise to a new cell type, which is often the case in various pathological diseases in the airways. Lineage tracing experiments have led to seminal findings in the field of airway epithelial biology (Patel et al 2011, Rock et al 2009, Turner et al 2011). Extrapolating this reasoning to the middle ear epithelium, it is plausible that mMECs get reprogrammed once put into *in vitro* culture and establish a fresh epithelium irrespective of the genotype. In vivo lineage tracing of mouse middle ear epithelial sub-types may help to better

understand the origin and fate of the different epithelial sub-populations in mMEC cultures. Additionally, culture conditions can be modified to replicate specific disease phenotypes. For example, addition of IL13 to culture media has shown to promote differentiation into goblet cells (Kondo et al 2002, Turner et al 2011).

5.3.7 Changes in the *Evi1*$^{Jbo/+}$ and *Bpifa1*$^{-/-}$*Evi1*$^{Jbo/+}$ middle ear mucosa during chronic inflammation

5.3.7.1 Changes in epithelial proteins

IHC for BPIFA1 indicated a reduction in staining intensity for the protein in the epithelial cells of *Evi1*$^{Jbo/+}$ middle ears, supporting the gene expression analysis of mMMCs. Regulation of *Bpifa1* during OM in *Evi1*$^{Jbo/+}$ mice has been discussed in further detail in Section 5.3.8. In Chapter 4, Lactotransferrin was identified as the most abundant protein in apical washes from ALI Day 14 mMEC cultures (Sections 4.2.5 and 4.2.10) and the intense staining for Lactotransferrin in the middle ear supports this finding. In order to monitor changes in the production of this protein during OM, IHC analysis on middle ear sections from the 4 genotypes of mice was performed. Lactotransferrin was strongly expressed in the thin mucoperiosteum of *Wt* and *Bpifa1*$^{-/-}$ mice, in line with our observation in mMECs. The staining intensity for Lactotransterrin increased further with inflammation in *Evi1*$^{Jbo/+}$ and *Bpifa1*$^{-/-}$*Evi1*$^{Jbo/+}$ mice and the protein localised to epithelial cells, underlying mesenchyme and the inflammatory exudate in the middle ear cavity. Lactotransferrin, is an iron chelating protein produced by secretory cells of mucosal epithelia and is well-known for its anti-microbial host defence role in the middle ear (Lim et al 2000). It is also produced by PMN granules and therefore concentration of Lactotransferrin increases during inflammatory processes (Legrand et al 2005). Thus, localisation of Lactotransferrin to the sub-epithelial layer in the inflamed *Evi1*$^{Jbo/+}$ and *Bpifa1*$^{-/-}$*Evi1*$^{Jbo/+}$ middle ears and an

increase in its staining intensity may be a result of its production by the inflammatory cells infiltrating this space.

IHC was also performed for a range of other epithelial markers such as Reg3Ɣ, MUC5B and p63 (basal cell marker) to investigate the effect of the loss of *Bpifa1* on changes to the middle ear sub epithelial cell populations. However, it was challenging to interpret results from these experiments, due to lack of consistency of staining between individual mice. These issues could not be resolved in the time frame available.

5.3.7.2 Fibrosis of Evi1$^{Jbo/+}$ and Bpifa1$^{-/-}$Evi1$^{Jbo/+}$ middle ear mucosa

Histological assessment demonstrated a thickened mucosa in *Evi1$^{Jbo/+}$* and *Bpifa1$^{-/-}$Evi1$^{Jbo/+}$* middle ears, characterised by a multi-layered epithelium and expansion of the sub-epithelial mesenchyme accompanied by infiltration of inflammatory cells. It would be expected that that very rapid expansion of the mucosal layer in the middle ears of the mutant mice would be accompanied by a significant cellular proliferation. The second ZnF domain of EVI1 has been shown to be involved in regulation of activator protein (AP)-1 through transactivation of *c-Fos.* AP-1 is involved in control of cell proliferation, differentiation and apoptosis (Shaulian & Karin 2002, Tanaka et al 1994). The mucosal thickening was significantly greater in *Bpifa1$^{-/-}$Evi1$^{Jbo/+}$* ears compared to *Evi1$^{Jbo/+}$* ears, which led me to speculate if the loss of *Bpifa1* further enhances the proliferative capacity of the cells. However, proliferation rates of mMECs as well as fibroblasts cultured from *Wt*, *Bpifa1$^{-/-}$*, *Evi1$^{Jbo/+}$* and *Bpifa1$^{-/-}$Evi1$^{Jbo/+}$* mice did not differ significantly, perhaps due to the inability of mMECs to retain the OM phenotype *in vitro.*

An interesting observation in this study was that mucosal thickening in the middle ears of *Evi1$^{Jbo/+}$* and *Bpifa1$^{-/-}$Evi1$^{Jbo/+}$* mice was accompanied by increased deposition the ECM component, collagen and accumulation of myofibroblast marker, αSMA. This type of

epithelial remodelling in airways is a hallmark of fibrotic airways diseases such as IPF, and asthma (Makinde et al 2007, Selman & Pardo 2002). Although the presence of fibrosis in the middle ear epithelium during OM has been described before (Ishii et al 1980, Juhn et al 2008), to my knowledge, there is no specific evidence on the role of myofibroblasts during OM disease development. Myofibroblasts originate from differentiation of mesenchymal fibroblasts at the site of injury and have an intermediate morphology between fibroblasts and smooth muscle cells (James et al 2006). They are involved in the production of ECM components such as collagen and fibronectin, under the influence of growth factors such as TGFβ, and help in wound contraction and airway remodelling which often follows inflammation as an epithelial repair response. Myofibroblasts are key contributors to sub-epithelial fibrosis, which is characterised by elevated levels of TGFβ, enhanced accumulation of the repair proteins, collagen and fibronectin, increased proliferation of fibroblasts and reduced levels of apoptosis (Desmouliere et al 1993, Makinde et al 2007) Fibrosis is a a consequence of excessive remodelling and is associated with dysregulation of TGFβ signalling (Selman & Pardo 2002). Indeed the SMAD3/SMAD4 complex directly binds to and activates transcription of the gene, *plasminogen activator inhibitor (PAI)* gene (Kurokawa et al 1998b) which is elevated in fibrosis in various organs such as the lung, heart skin and kidneys (Ghosh & Vaughan 2012).

The number of myofibroblasts correlates to the degree of sub epithelial thickening (Baum & Duffy 2011). In this study, mMECs from *Evi1*$^{Jbo/+}$ and *Bpifa1*$^{-/-}$*Evi1*$^{Jbo/+}$ mice showed elevated levels of *Tgfβ*. TGFβ is secreted by inflammatory cells such as macrophages, mast cells, lymphocytes as well as structural cells of the mucosa such as epithelial cells and fibroblasts and diffuses across the different cell types to elicit specific functions and facilitate airway remodelling. This is suggestive of significant epithelial-mesenchymal cross talk (Makinde et al 2007). *Bpifa1*$^{-/-}$*Evi1*$^{Jbo/+}$ mucosa was significantly more thickened compared to *Evi1*$^{Jbo/+}$ mice, suggesting that loss of *Bpifa1* is responsible for exacerbation of

fibrosis in an existing inflammatory microenvironment. Perhaps the absence of *Bpifa1* further disrupts epithelial-mesenchymal cross talk and acts as a signal for an enhanced fibrotic response, preventing resolution of inflammation. There is one other report which showed that transgenic mice over expressing *Bpifa1* demonstrated reduced levels of pulmonary fibrosis compared to *Wt* mice when challenged with sterile carbon nanotubules (Di et al 2013). However, the mechanism underlying such a function remains to be clarified

5.3.8 Regulation of *Bpifa1* during OM in *Evi1*$^{Jbo/+}$ mice.

BPIFA1 is abundantly produced by the non-ciliated cells of the *Wt* middle ear epithelium. There was significant down regulation *Bpifa1* mRNA in mMMCs and a decrease in intensity of BPIFA1 staining in *Evi1*$^{Jbo/+}$ middle ears compared to *Wt* middle ears. This reduction in BPIFA1 was also replicated in mMECs, where ALI Day 14 mMECs from *Evi1*$^{Jbo/+}$ mice showed significantly lower levels of BPIFA1 on a transcriptional and proteomic level. BPIFA1 is a secreted protein and has been identified in ear effusions of OME patients (Val et al 2016). Previous studies in our lab detected this protein in *Evi1*$^{Jbo/+}$ exudates using western blots (Section 1.13). A recently performed proteomic analysis of *Evi1*$^{Jbo/+}$ exudates at MRC, Harwell has identified abundant levels of BPIFA1 in the ear effusions (unpublished data).

The severity and age of onset of OM in *Evi1*$^{Jbo/+}$ mice is dependent on the air quality and microbiological status of their environment. In SPF conditions, which were used for housing the mice used in this study, *Wt* mice resolve middle ear fluids by weaning age whereas, *Evi1*$^{Jbo/+}$ mice retain fluids, leading to the development of chronic non-syndromic OM by P28 (Parkinson et al 2006). It is interesting that *Evi1*$^{Jbo/+}$ mice develop OM in gnotobiotic conditions as well, where the incidence of OM is unaltered but age of onset is shifted to P54 (Hood et al 2016, Rye et al 2011a). Thus, the *Evi1*$^{Jbo/+}$ mouse is a genetic model of chronic OM, and the presence of endogenous bacteria is not a requisite for development of

OM. The inflammatory response in *Evi1*$^{Jbo/+}$ mice may be triggered as a reaction to sterile irritants such as bedding particles. Several studies have shown that BPIFA1 levels decrease during irritant induced inflammation of the airways. For example, BPIFA1 secretion is reduced upon exposure to cigarette smoke (Britto & Cohn 2015). More importantly, BPIFA1 protein levels were reduced in the nasal lavage fluids of perennial allergic rhinitis sufferers compared to sporadic allergic rhinitis suffers and healthy controls (Irander et al 2014) and in subjects with extended periods of exposure to occupational allergens (Fornander et al 2013, Lindahl et al 2001). These studies indicate that presence of chronic inflammation induced by irritants can down-regulate levels of BPIFA1. This reasoning can be extrapolated to the reduction of BPIFA1 in *Evi1*$^{Jbo/+}$ mice where a pre-existing existing chronic inflammatory condition leads to decreased levels of BPIFA1. It is plausible that the pre-existing inflammation in *Evi1*$^{Jbo/+}$ mice causes remodelling of the epithelium, leading to a reduction of BPIFA1secreting cells, perhaps through phenotypic changes in the epithelial cells such as mechanisms like epithelial-mesenchymal transition. The decrease in BPIFA1 may thus act as a biosensor to signal the middle ear mucosa to enhance the defence response in the form of fibrosis. In case of the *Bpifa1*$^{-/-}$*Evi1*$^{Jbo/+}$ mutants, the complete absence of BPIFA1, coupled with the presence of a hypoxic, inflammatory microenvironment, may cause excessive fibrosis, thus adding to the viscous cycle of OM.

5.4 Key experimental conclusions

- *Bpifa1*$^{-/-}$*Evi1*$^{Jbo/+}$ mice exhibit no differences in viability and overt behaviour compared to Wt mice. *Bpifa1* deletion does not further lower body weights of *Evi1*$^{Jbo/+}$ mice.
- *Bpifa1* ablation leads to an exacerbation of OM phenotype in *Evi1*$^{Jbo/+}$ mice, characterised by increase in percentage of middle ears with fluid development and increase in thickness of the middle ear mucosa.
- There is an up regulation of pro-inflammatory genes, *Cxcl2, Tnfα, Il1β and Il6* and the anti-inflammatory gene, *Tgfβ* in the inflamed middle ear mucosa of *Evi1*$^{Jbo/+}$ and *Bpifa1*$^{-/-}$*Evi1*$^{Jbo/+}$ mice
- Exacerbation of OM in *Bpifa1*$^{-/-}$*Evi1*$^{Jbo/+}$ mice is not due to increase in the magnitude of this cytokine response.
- Cellular alterations in *Evi1*$^{Jbo/+}$ and *Bpifa1*$^{-/-}$*Evi1*$^{Jbo/+}$ middle ear mucosa are marked by decrease in levels of the ciliated cells marker, *Foxj1* and the goblet cell marker, *Muc5ac*. However, there is no additive effect of *Bpifa1* deletion.
- The inflamed mucosa of *Evi1*$^{Jbo/+}$ and *Bpifa1*$^{-/-}$*Evi1*$^{Jbo/+}$ mice is hypoxic.
- There was a lack of recapitulation of the OM phenotype *in vitro* using the mMEC model system.
- OM in *Evi1*$^{Jbo/+}$ and *Bpifa1*$^{-/-}$*Evi1*$^{Jbo/+}$ mice is accompanied by mucosal fibrosis, characterised by hyper-proliferation of the epithelium, expansion of the sub-epithelial mesenchyme, increased deposition of collagen and accumulation of myofibroblasts. Loss of *Bpifa1* leads to an increase in the fibrotic phenotype of *Evi1*$^{Jbo/+}$ mice.
- *Bpifa1* is expressed at high basal levels in *Wt* middle ear epithelial cells and an existing inflammatory environment in *Evi1*$^{Jbo/+}$ mice is accompanied by reduction in

levels of BPIFA1. Fall in BPIFA1 may be due to phenotypic changes in the epithelial layer, and may act as a signal for exaggeration of the host fibrotic response. However, further studies are warranted to test this postulation.

- This study underlines the necessity for investigation of mutations in *Bpifa1* in combination with other inflammatory and allergic phenotypes in order to better understand aetiology of OM as well as other respiratory diseases.

CHAPTER 6: GENERAL DISCUSSION

The overall aim of this thesis was to explore the role of the putative URT innate immunity molecule, BPIFA1 in the context of antimicrobial host defence of the middle ear epithelium and the effect of its loss on the development of OM.

OM is the most prevalent paediatric disease and leading cause of childhood deafness. Due to the multifarious aetiology of OM, the main aim of the common treatment options is to eliminate infection and inflammation rather than targeting the pathological mechanisms underlying OM, thus making it the largest cause of antibiotic prescription (Daniel 2012). However, over recent years several candidate gene association studies as have been performed in order better understand the complex pathophysiology of the disease (Allen et al 2013, Casselbrant et al 2009, MacArthur et al 2014, Segade et al 2006). These studies, along with mouse models of OM have highlighted the role for innate immunity genes in OM susceptibility (Hardisty-Hughes et al 2006, Parkinson et al 2006, Rye et al 2011a, Tateossian et al 2013). A GWAS performed utilising the Western Australian Pregnancy Cohort demonstrated that polymorphisms in *BPIFA1* are significantly associated with the OM phenotype (Rye et al 2012b). The cases recruited in this study were children between an average age of 1-3 years with OM characterised by bulging and scarred Tm, presence of tympanostomy tubes or rAOM. However, associations with BPIFA1 have not been replicated in other populations, primarily due to the lack of power and difference in phenotypes of patients recruited (Rye et al 2012b, Rye et al 2011b).

Previous studies during my Masters project had shown that the middle ear epithelium of *Wt* mice demonstrates abundant levels of BPIFA1 and staining intensity for the protein was reduced in during OM development in the $Evi1^{Jbo/+}$ model of chronic OM. The protein was also detected in ear exudates from these mice although it was partially degraded, most likely due to the action of proteases released by the inflammatory cells (Mulay MSc thesis 2011). More recently, a study was published demonstrating that aged $Bpifa1^{-/-}$ mice show

enhanced susceptibility to OM (Bartlett et al 2015). Taken together, there was strong evidence to support my hypothesis that BPIFA1 is involved in protection of the middle ear and a loss of this protein may be associated with the development of OM. In order to test this hypothesis, I utilised *Bpifa1*$^{-/-}$ and *Bpifa1*$^{-/-}$*Evi1*$^{Jbo/+}$ mice as well as a novel *in vitro* model of the middle ear epithelium.

Major findings and contributions to the field

6.1 Expression of BPIFA1 in the murine middle ear

BPIFA1 is one of the most highly expressed proteins in the epithelia of nasal passages, oropharynx, trachea and bronchi of humans and mice (Bingle & Bingle 2000, Bingle & Bingle 2011). It forms a major component of secretions from these sites such as in the nasal lavage, saliva, sputum and BAL fluids (Bingle & Bingle 2011, Campos et al 2004). In this thesis, a longitudinal study tracking the development of the middle ear cavity from P0 to P30, showed that BPIFA1 is present in the middle ear from the day of birth. It localises to the epithelial cells and submucosal glands and occasionally stains the mesenchymal material occupying the middle ear space till P15. After cavitation of the middle ear, BPIFA1 localises to the non-ciliated cells and coats the middle ear epithelial surfaces and cilia. *Bpifa1* gene expression had been reported in the chinchilla middle ear in 2010 (McGillivary & Bakaletz 2010) but the first report of the expression of BPIFA1 in the murine middle ear cavity was published by (Bartlett et al 2015). This report showed staining for the protein by IHC between 10-18months of age. As mentioned before the protein has also been detected in effusions of OM patients (Preciado et al 2010) and *Evi1*$^{Jbo/+}$ mice (Mulay MSc thesis 2011). High basal levels of BPIFA1 in the healthy murine middle ear throughout the life span suggest a role in initial protection of the middle ear epithelium. Taken together the data shows that the middle ear is a significant site of BPIFA1 expression and studies

focussing on the involvement of this protein in development of OM can provide further insight into the overall function of BPIFA1 in host defence of respiratory epithelia.

6.2 Loss of *Bpifa1* alone does not lead spontaneous development or induction of OM

Using ABR assessments and histological analysis I have shown that the loss of *Bpifa1* alone does not lead to the spontaneous development of OM in mice, irrespective of their genetic background. My data contradicts a recent report suggesting that aged *Bpifa1*$^{-/-}$ mice show increased susceptibility to OM (Bartlett et al 2015), albeit I did not study OM development in *Bpifa1*$^{-/-}$ mice beyond 6 months of age due to time limitations. It is important to note however that the penetrance of OM in *Bpifa1*$^{-/-}$ mice in the study by Bartlett and co-workers was only 30% and did not differ significantly from that in *Wt* mice. Characterisation of OM was rather based on scoring criteria such as difference in mucosal thickness and amount of inflammatory cells and debris seen in the middle ear cavity. Also the mice were aged between 10-18 months of age, which is rather late in the timeline of what is almost exclusively a paediatric disease. It has been previously shown that mice over expressing BPIFA1 showed reduced levels lung fibrosis when exposed to the sterile irritant, single walled carbon nanotubules (Di et al 2013, Ghafouri et al 2003). Studies from our lab have shown that gnotobiotic *Evi1*$^{Jbo/+}$ mice develop OM and their middle ear fluids sometimes contain foreign bodies suggesting that irritants such as bedding material can enter the middle ear space intranasally and trigger an inflammatory response (Hood et al 2016). Therefore, it is likely that the limited OM phenotype described by Bartlett *et al* in *Bpifa1*$^{-/-}$ mice may be a combined effect of the loss of *Bpifa1*, and an allergic response to inhaled irritants due to compromised immunity caused by their advanced age, rather than a specific effect of *Bpifa1* deletion alone. However, in future our *Bpifa1*$^{-/-}$ mice within this age range must be studied to make a conclusive assessment.

This study is the first to attempt to induce OM in *Bpifa1*$^{-/-}$ mice. I found that IN challenge of *Bpifa1*$^{-/-}$ mice does not significantly increase the nasopharyngeal carriage of the otopathogen, NT*Hi* into the middle ear. The importance of NT*Hi* is as the causative pathogen in OM is growing since the advent of the PCV7 vaccine, with the bacterium being isolated from majority of the AOM and COME patients (Giebink 1991, Ngo et al 2016). The IN route of infection replicates the retrograde ascension of bacteria from the NP into the middle ear during OM pathogenesis. I believe that the major reason for low infection rates observed in the NT*Hi* challenge experiments was the lack of a pre-existing fluid in the middle ear cavity of *Bpifa1*$^{-/-}$ mice. This is based on the observation from our lab that *Wt* middle ears very rarely show development of fluids or culture positivity on IN challenge with NT*Hi*, whereas different mouse models of spontaneous OM such as *Evi1*$^{Jbo/+}$, *Fbxo11*$^{Jf/+}$ and *Tgif*$^{-/-}$, all of which have pre-existing middle ear inflammation facilitate access of NT*Hi* into the middle ears (Hood et al 2016). This suggests that in the absence of a craniofacial abnormality, an inflamed hypoxic microenvironment may promote bacterial entrance and survival in the middle ear cavity (Cheeseman et al 2011, Hood et al 2016). It is also plausible that the presence of fluid creates a pressure difference between the middle ear and the NP, promoting ascension of bacteria, although such pressure measurements have not been performed in *Evi1*$^{Jbo/+}$.

Although trans-bullar injection of bacteria has shown to guarantee middle ear colonisation in both mice and chinchillas (Sabirov & Metzger 2008), it is an artificial route that bypasses NP colonisation, a major site of BPIFA1 production. In humans, OM is often initiated by a viral URT infection that compromises the local mucosal immunity, leading to an ascension of bacteria into the middle ear (Bakaletz 2010). Indeed, studies in animal models have also shown that IN inoculation with a single dose of bacteria are often unsuccessful whereas co-incident infection with respiratory viruses or repeated doses of bacterial infection (Bakaletz 2009, Giebink 1981, Sabirov & Metzger 2008, Short et al 2013), promote middle ear

colonisation. Perhaps, as I have shown that *Bpifa1*$^{-/-}$ mice that do not spontaneously develop OM, this would be a better experimental strategy to more closely mimic the biological processes leading to infectious OM.

A potentially important variable confounding the bacterial challenge studies I undertook in this thesis was the discrepancy between the genetic backgrounds of mice used for the experiments. Not only does genetic background influence development of spontaneous OM (Bhutta 2012), but it has also shown to affect the susceptibility of mice to nasopharyngeal carriage after IN inoculation with bacteria (McCool & Weiser 2004). Since transferring the *Bpifa1*$^{-/-}$ line from the original C57BL/6 to C3H/HeH background was a time consuming process, these experiments were performed within the initial phase of the transfer with mice that were readily available, potentially preventing a direct comparison between the results from the NT*Hi* challenge experiments at the different time points used.

The other variable confounding the bacterial challenge studies was the higher susceptibility of *Bpifa1* mutants to the NT*Hi*^{375SR} strain compared to the NT*Hi*^{162SR} strain. The two NT*Hi* strains were obtained from a Finish pneumococcal vaccine study and contain structural modifications in their LPS side-chains (Cody et al 2003, Hood et al 1999). A previous study from our lab screened infection rates in *Evi1*$^{Jbo/+}$ mice with 7 different NT*Hi* strains in order to identify the most efficient strains for IN challenge (Hood et al 2016). As described before, there is inconsistent evidence on the binding activity of BPIFA1 to LPS (Britto & Cohn 2015, Campos et al 2004). However, two recent studies from the same group, have identified the α4 helix of BPIFA1 as being important in LPS binding and bacteriostatic activity against the Gram-negative bacteria, *P.aeruginosa* and *B.cepacia* (Ahmad et al 2016, Walton et al 2016). Due to the low infection rates seen in *Bpifa1*$^{-/-}$ mice, an *in vivo* screen with different NT*Hi* strains such as that performed in *Evi1*$^{Jbo/+}$ mice would not be ethically justifiable. However, an *in vitro* study to compare LPS-binding activity of BPIFA1 to different

NT*Hi* strains may provide a better foundation for testing the antimicrobial effect of BPIFA1 *in vivo*.

6.3 Exacerbation of the OM phenotype in *Bpifa1*$^{-/-}$ *Evi1*$^{Jbo/+}$ mice

The *Evi1*$^{Jbo/+}$ mouse is a model of chronic OM, characterised by a thickening of the mucoperiosteum, presence of inflammatory exudate and chronic hypoxia in the middle ear (Cheeseman et al 2011, Parkinson et al 2006). These mice bear a SNP in the *Evi1* gene, which functions a repressor of NFκB and TGFβ signalling pathways (Kurokawa et al 1998b, Xu et al 2012). *Evi1*$^{Jbo/+}$ mice develop CSOM around P28. In order to study the effect of loss of *Bpifa1* in an existing model of chronic OM, *Bpifa1*$^{-/-}$*Evi1*$^{Jbo/+}$ mice were generated. This is the first study to report the effect of *Bpifa1* deletion in a compound mutant model. *Bpifa1*$^{-/-}$ *Evi1*$^{Jbo/+}$ middle ears demonstrated acceleration and exacerbation of the OM phenotype, characterised by significantly more thickened mucosa and very high incidence of middle ear fluids. All *Bpifa1*$^{-/-}$*Evi1*$^{Jbo/+}$ mice showed fluid development by P28.

Gene expression in the middle ear epithelial cells of *Evi1*$^{Jbo/+}$ has not been studied before, however previous studies of *Evi1*$^{Jbo/+}$ exudates demonstrated elevation of inflammatory gene networks and hypoxia signalling genes compared to venous blood (Cheeseman et al 2011). *Wt* mice do not have middle ear fluids making a direct comparison between OM affected and healthy middle ears challenging. In this study, I have demonstrated an up-regulation of the pro-inflammatory mediators *Cxcl2, Tnfα, Il1β and Il6; the* anti-inflammatory mediator, *Tgfβ* and the hypoxia marker, *Vegf* in the middle ear mucosa of *Evi1*$^{Jbo/+}$ and *Bpifa1*$^{-/-}$*Evi1*$^{Jbo/+}$ mice. I have also shown that *Evi1*$^{Jbo/+}$ and *Bpifa1*$^{-/-}$*Evi1*$^{Jbo/+}$ middle ears demonstrate epithelial cellular alterations characterised by significant down regulation of the ciliated cell marker, *Foxj1* and the goblet cell marker, *Muc5ac.* Moreover, *Evi1*$^{Jbo/+}$ mice also demonstrate reduced levels of *Bpifa1*. Despite the exacerbated OM phenotype in *Bpifa1*$^{-/-}$*Evi1*$^{Jbo/+}$ mice, there was no additive effect of the loss of *Bpifa1* on the

expression of any the inflammatory and epithelial markers. I also did not observe any differences between basal levels of cytokines and epithelial markers between *Wt* and *Bpifa1*$^{-/-}$ mice. These observations differ from previous reports suggesting that BPIFA1 has an anti-inflammatory function and serves to reduce levels of pro-inflammatory cytokines during bacterial infections and allergic inflammation (Britto & Cohn 2015, Liu et al 2013a, Liu et al 2013b, Lukinskiene et al 2011, Wright et al 2010). My findings also contradict the report suggesting that loss of *Bpifa1* down regulates ciliated and goblet cell markers (albeit that this was in the airways not in the middle ear), at steady state and during infection, thus impairing mucociliary clearance (Liu et al 2013a).

The middle ear mucosa of *Evi1*$^{Jbo/+}$ and *Bpifa1*$^{-/-}$*Evi1*$^{Jbo/+}$ mice was highly thickened and this thickening was a result of an apparent hyper-proliferation of epithelial cells into multiple layers as well as expansion of the mesenchyme. As described previously in *Evi1*$^{Jbo/+}$ mice, other factors including connective tissue oedema, dilation of lymphatics, blood vessels and infiltration of the sub-epithelial mesenchyme may contribute to this thickening (Parkinson et al 2006). Such vasodilation is also supported by high levels of *Vegf* in *Evi1*$^{Jbo/+}$ and *Bpifa1*$^{-/-}$*Evi1*$^{Jbo/+}$observed in this study, which may be contribute to the inflammatory cell infiltration and fluid build up in the middle ear cavity (Cheeseman et al 2011, Husseman et al 2012).

An interesting feature observed in the the inflamed *Evi1*$^{Jbo/+}$ and *Bpifa1*$^{-/-}$ middle ears was fibrosis of the sub-epithelial mesenchyme indicated by the increased staining for the myofibroblast marker, αSMA and by collagen deposition, a characteristic feature of fibrotic pulmonary diseases such as asthma, IPF (Akram et al 2013). Accumulation of myofibroblasts and collagen is indicative epithelial remodelling due to an over-active wound repair response following inflammation, suggesting over-activation of the TGFβ signalling pathway (a target for EVI1) (Makinde et al 2007). The increased thickness of

Bpifa1$^{-/-}$*Evi1*$^{Jbo/+}$ mucoperiosteum compared to that of *Evi1*$^{Jbo/+}$ mice suggests that the increased fibrosis due to loss of BPIFA1. This is an interesting suggestion since loss of BPIFA1 has been associated with an allergen-induced asthma-like phenotype in mice (Thaikoottathil et al 2012) and overexpression of BPIFA1 has been shown to protect against pulmonary fibrosis (Di et al 2013). However, the mechanism of such a role for BPIFA1 remains to be elucidated. The development of OM in *Evi1*$^{Jbo/+}$ mice in germ free conditions suggests that bacterial infection is not a pre-requisite for OM development in these mice, although infection does accelerate disease onset. Perhaps physical irritants such as bedding particles may initiate the development of AOM in *Evi1*$^{Jbo/+}$ (Hood et al 2016). Patients with bronchial asthma mainly develop an allergic form of OM called Eosinophilic Otitis media (EOM) (Kanazawa et al 2015). However *Evi1*$^{Jbo/+}$ middle ears do not have the phenotype of human EOM as they lack eosinophils and IgG levels are not different between Wt and *Evi1*$^{Jbo/+}$ mice (Parkinson et al 2006). Nevertheless, given the suggested involvement of BPIFA1 in allergen induced asthma and the apparent increased in the fibrotic phenotype of *Bpifa1*$^{-/-}$*Evi1*$^{Jbo/+}$ ears, it may be useful the analyse of the inflammatory cell types in the *Bpifa1*$^{-/-}$*Evi1*$^{Jbo/+}$ exudates in detail and also to evaluate levels of T_H2 cytokines such as IL-13, IL-4 and IL-5 in *Bpifa1*$^{-/-}$*Evi1*$^{Jbo/+}$ mice (Kanazawa et al 2015).

6.4 The mMEC culture system

The middle ear and its secretions play a key role in role in host defence and epithelial abnormalities are commonly implicated in OM development. Human middle ear tissue can be acquired only during surgical procedures and sampling of the mucosa is a terminal procedure in most animals. *In vitro* studies can enable maximum utilisation of the available sample, allow the effect of modifying culture conditions and also enable studies of host pathogenen interactions. Prior to my thesis there was a lack of a well-characterised *in vitro*

model of the middle ear epithelium that replicates the complex cellular composition of the middle ear. Primary cultures of middle ear epithelial cells are often contaminated and overgrown by fibroblasts (Nakamura et al 1991, Vanblitterswijk et al 1986). Currently the two most widely models used for *in vitro* study of OM are the normal human middle ear epithelial cell line (NHMEEC) and the mouse middle ear cell line (MMEEC), both immortalised cells lines from the middle ear (Chun et al 2002, Lim & Moon 2012, Tsuchiya et al 2005). However, there is a lack of complete differentiation into the various epithelial cell populations using these cell lines, especially at the proteomic level. Moreover, cell lines do not fully mimic the 3-dimentional physiology of middle ear cells and the different intracellular interactions. This has considerably limited our understanding of the different cell types in the middle ear epithelium and their involvement in OM pathophysiology.

In this thesis, I have developed a novel *in vitro* model of mouse middle ear epithelial cells at ALI that recapitulates the characteristics of the native murine ME epithelium. The protocol used for the culture of mMECs was adopted from that used for the culture of mouse tracheal epithelial cells, mTECs (You et al 2002). (Lechner et al 1982, Wu et al 1997, You & Brody 2013, You et al 2002). Addition of ROCKi to the culture medium enhances the proliferation of basal cells (Butler et al 2016, Horani et al 2013) and thus increases number of transwells that can be generated for culture. I have demonstrated that mMECs undergo differentiation into the varied cell populations seen within the native middle ear. Proteomic analysis confirmed that the cultures secrete a multitude of innate defence proteins from their apical surface. *Wt* mMECs produced abundant amounts of BPIFA1 and secreted BPIFA1 was detected in the apical washes from the cells. I have shown that the mMECs supported the growth of the otopathogen, NT*Hi* and also mounted an inflammatory response upon infection, suggesting that the model can be successfully utilised to study host pathogen interactions. *Bpifa1*$^{-/-}$ mMECs were morphologically similar to *Wt* mMECs and also did not differ in expression pattern of epithelial markers, contrary to the report

suggesting that loss of BPIFA1 results in down regulation of ciliated and goblet cells (Liu et al 2013a). *Bpifa1*$^{-/-}$ mMECs demonstrated slightly enhanced susceptibility to NT*Hi* infection, however this did not reach statistical significance due batch variation. I was unable to perform biofilm dispersal assays (Ahmad et al 2016, Liu et al 2013a, Liu et al 2013b) to test the surfactant activity of BPIFA1. However, this is an avenue that should be explored in future. However, the mRNA and protein levels of BPIFA1 significantly decreased upon NT*Hi* infection.

I believe that the mMEC culture system has the potential to serve as a platform for validation of treatments designed to reverse aspects of epithelial remodelling underpinning OM development. I believe that these cells can be targets for genetic modulation studies. Previous studies have demonstrated successful gene silencing in primary HBE cells and mTECs using lentiviral transduction systems (Horani et al 2012, Vladar & Stearns 2007). More recently, the CRISPR/CAS9 genome editing system has been utilised in HBE cells and mouse tracheal organoid cultures (Gao et al 2015). The physiological similarities of mMEC cells with airway epithelial cells and the use of similar culture conditions for their growth means that the mMEC model might be amenable to gene editing studies in future.

6.4.1 Limitations of the mMEC culture system

6.4.1.1 Batch variation

A confounding factor in the use of the mMEC culture system appears to be the variation among different batches of culture in terms of expression of markers as well as susceptibility to NT*Hi* infection. Primary cultures are known to show considerable variability between different batches depending on the media components. However, I believe the major reason for the variation seen in mMEC cultures was the difference in the basal cell populations attaching to the membrane. Depending on the fate of the initiator basal cells

attached to the membrane, the percentage of differentiated cell types can vary between the different batches of mMEC cultures and even between different transwells from the same batch of mMECs, establishing a new epithelium each time. In order to reduce this issue tagged basal cells could be fractionated using FACS prior to the establishment of mMEC cultures in order to potentially yield more uniform cultures.

Along with the difference in cell populations mentioned above, contamination of isolated RNA by components of the TRI reagent may have added to the variation seen among biological replicates in the RT-qPCR data. Cells were lysed in TRI reagent, which contains phenol and guanidinium thiocyanate prior to RNA extraction. The RNA was found to contaminated to variable degrees with phenol and guanidine salts leading incorrect absorbance ratios during RNA quantification. This problem was identified late in the project, because I performed all RT-qPCR experiments at MRC, Harwell towards the end of this study and appears to be more of a problem when RNA yields are low. In order to mitigate the problem, all RNA was cleaned of contaminants prior to the RT-qPCR experiments and a screen of 12 endogenous controls was performed to identify the 3 most stable controls for normalisation of target genes for each cell type analysed (details in the materials and methods section). Thus the variability between samples was reduced to the minimum possible level. However, it still meant that while larger differences in gene expression between samples could easily be detected, subtle differences sometimes did not reach statistical significance. In future a TRI-reagent free system should be utilised for RNA extraction of mMECs.

6.4.1.2 Lack of recapitulation of the OM phenotype of in mMECs

Although mMEC cultures from *Evi1*$^{Jbo/+}$ and *Bpifa1*$^{-/-}$*Evi1*$^{Jbo/+}$ differentiated into epithelial sub-populations, they failed to retain the elevated expression of inflammatory cytokines

and epithelial cellular markers seen in the freshly isolated mMMCs. As mentioned above differences in adherence of specific populations of basal cells initiating the cultures and their cell fate may be one of the major reasons for limitation. Also depending on the environmental stress differentiated cells can transdifferentiate to give rise to a new cell types a process which is associated with various pathological diseases in the airways (Turner et al 2011). In order to overcome this issue, lineage tagging specific basal cell populations or other cells of interest could be used to identify the origin of the cells in culture (Patel et al 2011). Moreover, culture conditions can be modified to favour differentiation of a specific cell type in order to recapitulate a particular phenotype. For example, addition of IL-13 to TBE cultures has been shown to promote differentiation of goblet cells (Kondo et al 2002).

The second reason for the lack of recapitulation of the OM phenotype may be the absence of the specific microenvironment found in *Evi1*$^{Jbo/+}$ and ears. The absence of a hypoxia in mMEC cultures may be one of the reasons for the failure to recreate the microenvironment required for OM development. OM development is due to a combination of the response to an insult to the middle ear epithelium and the isolated environment of the middle ear cavity. Also the absence of other cell types such as fibroblasts and neutrophils, from the cultures, which are the main sites of EVI1 expression in *Evi1*$^{Jbo/+}$ mice (Parkinson et al 2006) may further prevent the recapitulation of the OM phenotype.

In this work I have developed a novel system for the culture of murine middle ear cells that recapitulates the cell types in the native middle ear. Additional optimisation will be needed in order to replicate the OM phenotype in culture. However, the availability of this new model of the middle ear epithelium makes the mMEC model valuable to the wider OM community.

6.5 Regulation of BPIFA1 during infection and inflammation

A consistent observation in this study was the down regulation of *Bpifa1* in the middle ear epithelial cells upon infection with NT*Hi* as well in the inflamed microenvironment of the *Evi1*$^{Jbo/+}$ ears. NT*Hi* infection of *Wt* mMECs led to a decrease in mRNA and cytosolic and secreted protein levels of BPIFA1 at 48hpi. mMMCs isolated from *Evi1*$^{Jbo/+}$ mice showed reduced expression of *Bpifa1,* mirroring the decrease in the staining intensity for BPIFA1 observed in the *Evi1*$^{Jbo/+}$ middle ear epithelium by IHC. Reduced expression *Bpifa1* was also seen in mMECs cultured from *Evi1*$^{Jbo/+}$ mice.

As discussed in the individual chapter discussions, several studies have shown that infection by bacterial pathogens as well as inflammatory cytokines regulate the levels of BPIFA1 and the direction of regulation is dependent on the type of stimulus and the type of tissue under study (Britto & Cohn 2015). However, there is no mechanistic data on the true transcriptional regulation of BPIFA1. Therefore, whether the fluctuations in levels of BPIFA1 reflect a regulation of its promoter activity is highly debatable. I would like to draw the attention to two particular studies in this context. A study in ovalbumin-stimulated mice that develop allergic asthma–like phenotype demonstrated reduced levels of the epithelial reticulon 4B (NogoB). NogoB is expressed by airway epithelial and smooth muscle cells and is involved in controlling vascular injury and promoting wound healing during stress response (Wright et al 2010). The researchers showed that *NogoB*$^{-/-}$ mice displayed an exaggerated asthma phenotype and using genome-wide microarray analysis found that *Bpifa1* was the most differentially expressed gene in these mice. While *NogoB*$^{-/-}$ mice demonstrated a marked reduction of expression of *Bpifa1*, mice overexpressing *NogoB* showed elevated levels of BPIFA1 and transgenic expression of *Bpifa1* under the Clara-cell secretory promoter rescued the phenotype in *NogoB*$^{-/-}$ mice. The mechanism for such a proposed regulation of *Bpifa1* by NogoB has not been elucidated. Another study showed

that LPS stimulation of human nasal epithelial cells increased the levels of BPIFA1, along with an increase in levels of phosphorylated JNK and cJun, and further treatment of cells with IL-13 attenuated the levels of BPIFA1 (Tsou et al 2015). The study thus suggests that BPIFA1 expression is regulated through the JNK pathway.

Based on the observations in this thesis, I believe it is unlikely that such fluctuations in BPIFA1 levels are an indication of its true transcriptional regulation, but are rather a consequence of phenotypic changes in the cell types. For example, the up regulation of JNK and cJun in the above study (Tsou et al 2015) may be a consequence of activation of the JNK pathway due to infection, whereas the elevation in BPIFA1 may be a result of epithelial remodelling in the presence of this inflammation. Moreover, IL-13 is known to promote differentiation of goblet cells in cultures through MAP kinase regulation (Atherton et al 2003). Since BPIFA1 is expressed by non-goblet cells (Bingle et al 2005), there may be reduction in the proportion of BPIFA1 expressing cells in culture.

In my thesis, the down regulation of *Bpifa1* observed in *Wt* mMECs upon NT*Hi* infection and in *Evi1*$^{Jbo/+}$ mice in the presence of the OM phenotype, may also be a result of an insult to the epithelium due to the presence of infection or inflammation, thus leading to phenotypic alterations in the cells. I believe that it is unlikely to be the primary cause for generation of an inflammatory response. It is possible that the changes seen in the middle ear epithelium of the *Evi1*$^{Jbo/+}$ mice involve a loss of other cell types such as ciliated cells. This is indicated through a down-regulation of FoxJ1 mRNA in *Evi1*$^{Jbo/+}$ mMMCs compared to Wt mMMCs. In future, this change can be confirmed at a protein level by staining Wt and *Evi1*$^{Jbo/+}$ for FOXJ1 protein using IHC. Also, it will be of interest to test whether the downregulation of the epithelial markers is a result of denudation or loss of integrity of the epithelium itself, as a result of the extensive expansion of the sub-epithelial mesenchyme. This issue can be addressed by co-staining for secretory (BPIFA1), ciliated (FOXJ1) and goblet (MUC5B) cells with a more universal epithelial marker such as pan-cytokeratin.

6.5.1 Presence of an inflammatory stimulus is a pre-requisite for BPIFA1 function

As discussed above the down regulation of *Bpifa1* in this study may be a consequence of phenotypic changes in the epithelial cell populations in the presence of infection or inflammation rather than being a causal factor for initiation of an inflammatory response. This also explains why loss of *Bpifa1* alone does not lead to the development of OM in *Bpifa1*$^{-/-}$ mice. Previous work has largely focused on evaluation of a role for BPIFA1 only the presence of an inflammatory or infectious stimulus. For example, in the presence of infection by bacterial and viral pathogens (Britto et al 2013, Gally et al 2011, Liu et al 2013a, Liu et al 2013b, Lukinskiene et al 2011, Zhou et al 2008); in case of chronic allergies such as rhino sinusitis (Irander et al 2014, Tsou et al 2015) and induction by allergic stimuli such as cigarette smoke or occupational irritants (Fornander et al 2013, Ghafouri et al 2003); in pre-existing pulmonary diseases such as CF and COPD (Bingle et al 2007, Di et al 2003) or other URT malignancies such as non-small cell carcinomas and nasopharyngeal carcinomas (Bingle & Bingle 2011). Indeed, existing studies with *Bpifa1*$^{-/-}$ mice did not report any phenotype or immunological abnormalities in the naïve *Bpifa1*$^{-/-}$ mice (Gally et al 2011, Liu et al 2013a). In this study, in addition to the absence of OM in *Bpifa1*$^{-/-}$ mice, no anomalies were detected in 42 different tissues encompassing all the major organs of *Bpifa1*$^{-/-}$ mice. Thus, the presence of an infectious or inflammatory stimulus seems to be required to uncover functional roles of BPIFA1, suggesting that the high levels of BPIFA1 at steady state may be critical for initial protection against epithelial insults and pathogens and an alteration in its levels may exacerbate an existing inflammatory response.

6.6 Proposed role of BPIFA1 in the middle ear and development of Otitis media

I have shown that BPIFA1 is secreted by the non-ciliated cells of the middle ear epithelium and it coats the surface of the middle ear epithelium. Similar to other sites in the URT, BPIFA1 is produced at high basal levels in the middle ear and these high levels of protein are involved in preventing initial infection in the middle ear. The exact role BPIFA1 plays in host defence remains incompletely understood. However, BPIFA1 decreases susceptibility against a wide range of bacteria and viruses. Recent studies in our lab have shown that *Bpifa1*$^{-/-}$ mice have increased susceptibility to pulmonary infection by *Influenza A* virus (Akram et al, unpublished data). In this study I have shown that loss of *Bpifa1* increases susceptibility to a pre-existing inflammatory stimulus. The regulation of ENaC seems an unlikely role for BPIFA1 in the middle ear. The current hypothesis behind BPIFA1 regulation of ENaC is that BPIFA1 inhibits the activity of ENaC via the physical interaction through its N-terminus S18 peptide and blocks ENaC cleavage (Garcia-Caballero et al 2009). In CF lungs, loss of BPIFA1 activity due to low PH leads to hyperactivity of the ENaC channel and increased transport of sodium and water through the channel leading to dehydration of the airways and formation of mucous plugs (Garland et al 2013). ENaC is expressed by the middle ear epithelium (Choi et al 2006) and the presence of periciliary fluid has been described in the middle ear (Kubba et al 2000). Although fluid build-up in the ear is a result of vasodilation (inflammation and exudation), previously published literature shows that increased ENaC helps middle ear fluid clearance (Li et al 2005, Song et al 2012, Xu et al 2015). According to the BPIFA1- mediated inhibition of ENaC hypothesis, the absence of BPIFA1 in this study might be expected to lead to dehydration of middle ear cavity, which is the opposite of the OM phenotype, characterised by fluid build-up within the middle ear cavity. Indeed, a condition called Pseudohypoaldosteronism, in which ENaC activity is severely diminished, leads to chronic rhinorrhea and increased bronchus secretions (Kerem et al 1999). However, disruption of the periciliary layer due to increased activity of ENaC

could still impact mucociliary clearance. It is unclear whether ENaC regulation by BPIFA1 is specific to the airways. Also, the N-terminus region of BPIFA1, (including the S18 region) is the most variable among primates and lower mammals, which may suggest that this function is restricted to primates (Bingle & Craven 2002).

Taking account of all of the available data, I hypothesize that BPIFA1 is secreted into the surface lining fluid of the middle ear acts as a non-specific physical barrier to help maintain the homeostasis of the middle ear epithelium. It is known that the epithelium along with its secretions orchestrates various aspects of the inflammatory as well as wound repair response through cross-talk with ligands on the epithelial surface as well as with components of the sub-epithelial mesenchyme. The exact mechanism by which BPIFA1 regulates these interactions and maintains homeostasis is unresolved. However, in the absence of an infection or insult to the epithelium, lack of BPIFA1 does not result in an inflammatory response and thus *Bpifa1*$^{-/-}$ mice do not show a phenotype under steady state conditions. However, absence of BPIFA1 superimposed on an insult to the epithelium in the form of infection or as a consequence of inflammation, may make the epithelium more susceptible to the initial injury and thus lead to an exacerbated host defence response and epithelial remodelling, as seen in the *Bpifa1*$^{-/-}$*Evi1*$^{Jbo/+}$ middle ears. This may be due to an alteration of the physical interaction of BPIFA1 with other components of the epithelium or due to a change in the composition of the secretions within the middle ear lining fluid, thus altering its biophysical properties such as surface tension. Further investigation is needed to explore the mechanistic role BPIFA1 in protection of the middle ear and its involvement in OM pathogenesis.

6.7 Future studies

6.7.1 Studies with *Bpifa1*$^{-/-}$ mice

In this thesis I have shown that *Bpifa1*$^{-/-}$ mice maintained in SPF conditions do not spontaneously develop OM, at least up to 6 months of age. The study by Bartlett and co-workers suggests that *Bpifa1*$^{-/-}$ mice between 10-18 months of age develop low penetrance OM (Bartlett et al 2015). I believe the reason for this phenotype is the combined effect of loss of BPIFA1, the air quality in which the mice were housed and the compromised immunity due to advanced age. Therefore, in future the *Bpifa1*$^{-/-}$ line should be aged till 18 months in SPF conditions and evaluated for spontaneous OM development.

I have also shown that loss of *Bpifa1* did not lead to increased ascension of NT*Hi* from the NP into the middle ear. Due to the variability observed between NT*Hi*^{375SR} and NT*Hi*^{162SR} strains, a screen could be carried out to identify strains of NT*Hi* which may infect *Bpifa1*$^{-/-}$ mice more effectively.

6.7.2 Studies with *Bpifa1*$^{-/-}$*Evi1*$^{Jbo/+}$ mice

In the preliminary experiment performed in this thesis, cytospun exudates from *Evi1*$^{Jbo/+}$ and *Bpifa1*$^{-/-}$*Evi1*$^{Jbo/+}$ showed a high proportion of neutrophils and lower proportion of macrophages in the exudates. Previous studies have shown that *Evi1*$^{Jbo/+}$ exudates are neutrophil rich (Cheeseman et al 2011, Parkinson et al 2006). However, FACs analysis of inflammatory cells should be carried out to identify the differences in proportions and types of inflammatory cells between *Evi1*$^{Jbo/+}$ and *Bpifa1*$^{-/-}$*Evi1*$^{Jbo/+}$ mice. My studies have not confirmed if there is an increase in the fibrotic phenotype of *Bpifa1*$^{-/-}$*Evi1*$^{Jbo/+}$ mice compared to *Evi1*$^{Jbo/+}$ mice. Analysis of T_H2 cytokines such as IL-4, IL-5 and IL13 and quantification of myofibroblasts and cell proliferation will provide further insight into the phenotype of *Bpifa1*$^{-/-}$*Evi1*$^{Jbo/+}$ mice.

6.7.3 Lineage tracing experiments

In order to establish more homogenous mMEC cultures and avoid variation between individual batches, basal cells could be tagged and FACs sorted prior to seeding them on transwell membranes. Also lineage tags for specific epithelial sub-types of interest, ciliated cells, BPIFA1 expressing cells, goblet cells, could be used to trace the origin and fate of trans differentiated cells. Also, a combination of epithelial and mesenchymal tags would allow for the study of changes in epithelial phenotype during remodelling of the middle ear epithelia.

6.7.4 Recapitulation of the OM phenotype in mMECs

In order to recapitulate the OM phenotype in vitro, mMECs from *Evi1*$^{Jbo/+}$ *and Bpifa1*$^{-/-}$ *Evi1*$^{Jbo/+}$ could be established as direct contact cultures by growing mMECs on one side of the transwell membrane and fibroblasts on the other. This may better mimic the organ morphology of the middle ear mucosa. Also the cells may be cultured in hypoxic incubators in order to better recreate the microenvironment of *Evi1*$^{Jbo/+}$ *ears.* Furthermore, a mucous phenotype could be induced by treating the cells with IL-13, a known inducer of goblet cells.

6.7.5 *BPIFA1* deletion in other mouse models of OM

This is the first report of deletion of *BPIFA1* in combination with another genetic mutation. The generation of compound mutations enables the study of interaction between two genes in order to develop a better understanding of the pathophysiology of OM. Based on the data from my thesis, it will be interesting to know if deletion of *Bpifa1* leads to an exacerbation of the phenotype in other models of OM. *Fbxo11*$^{Jf/+}$ and *Tgif*$^{-/-}$ are two models of spontaneous OM at MRC Harwell and both have mutations which are implicated in the

TGFβ signalling pathway. Of these the *Fbxo11*$^{Jf/+}$ mouse is particularly interesting because preliminary studies during my Masters project have identified expression of BPIFA1 in *Fbxo11*$^{Jf/+}$ middle ear epithelium and exudates. The mutation in *Fbxo11*$^{Jf/+}$ is implicated in regulation of phosphoSmad2 in epithelial cells of the airways, palatal shelves and eyelids (Rye et al 2011a, Tateossian et al 2015) and two studies have identified the association of this gene with OM susceptibility (Rye et al 2011b, Segade et al 2006).

6.8 Conclusion

Otitis media is the most prevalent paediatric disease, cause of paediatric surgery, antibiotic prescription and childhood conductive deafness. Identification of genes involved in OM susceptibility is key to understanding the complex pathophysiology of the disease and for development of better therapeutics. Through this thesis I have explored a role for the putative URT innate immunity protein, BPIFA1, in the protection of the middle ear and in the development of OM. BPIFA1 is expressed at high basal levels in the murine middle ear. Deletion of *Bpifa1* alone does not lead to spontaneous development of OM and does not result in increased nasopharyngeal carriage of the human ototpathogen NT*Hi*. However, deletion of *Bpifa1* in *Evi1*$^{Jbo/+}$ mice, a model of OM significantly exacerbates the OM phenotype. Through this study, I have also developed a novel in vitro model the murine middle ear epithelial cells that closely mimics the *in situ* middle ear epithelium and expresses markers for ciliated cells, goblet cells and secretory cells. The mMEC culture system can be applied as an effective tool to study the interaction between the ME epithelium and various otopathogens. Overall, the data from this thesis suggests that BPIFA1 may function as a non-specific mucosal defense protein that helps to maintain the homeostasis of the middle ear epithelium at high basal levels. Loss of BPIFA1 superimposed on an insult to the epithelium, in the form of infection or inflammation, increases the

susceptibility epithelium to injury leading to an exacerbated host defense response and excessive epithelial remodeling. This may be due to the uncoupling of its interaction with other components of the epithelium or the within the secretions of the middle ear lining fluid. Further investigation is required to explore the mechanistic role BPIFA1 in maintenance of the homeostasis of the middle ear.

BIBLIOGRAPHY

Action On Hearing Loss. 2015. About deafness and hearing loss statistics.

Admyre C, Grunewald J, Thyberg J, Gripenback S, Tornling G, et al. 2003. Exosomes with major histocompatibility complex class II and co-stimulatory molecules are present in human BAL fluid. *European Respiratory Journal* 22: 578-83

Ahmad S, Tyrell J, Walton W, Tripathy A, Rednibo M, Tarran R. 2016. SPLUNC1 has antimicrobial and antibiofilm activity against Burkholderia cepacia complex. *Antimicrobial Agents and Chemotheraphy* Accepted Manuscript published online

Akashi-Takamura S, Miyake K. 2008. TLR accessory molecules. *Curr Opin Immunol* 20: 420-5

Akram KM, Samad S, Spiteri M, Forsyth NR. 2013. Mesenchymal Stem Cell Therapy and Lung Diseases. *Mesenchymal Stem Cells: Basics and Clinical Application Ii* 130: 105-29

Allen EK, Chen W-M, Weeks DE, Chen F, Hou X, et al. 2013. A Genome-Wide Association Study of Chronic Otitis Media with Effusion and Recurrent Otitis Media Identifies a Novel Susceptibility Locus on Chromosome 2. *Jaro-Journal of the Association for Research in Otolaryngology* 14: 791-800

Amesara R, Kim Y, Sano S, Harada T, Juhn SK. 1992. PRIMARY CULTURES OF MIDDLE-EAR EPITHELIAL-CELLS FROM CHINCHILLAS. *European Archives of Oto-Rhino-Laryngology* 249: 164-67

Atherton HC, Jones G, Danahay H. 2003. IL-13-induced changes in the goblet cell density of human bronchial epithelial cell cultures: MAP kinase and phosphatidylinositol 3-kinase regulation. *American Journal of Physiology-Lung Cellular and Molecular Physiology* 285: L730-L39

Auger F, Gendron MC, Chamot C, Marano F, Dazy AC. 2006. Responses of well-differentiated nasal epithelial cells exposed to particles: Role of the epithelium in airway inflammation. *Toxicology and Applied Pharmacology* 215: 285-94

Bakaletz LO. 2007. Bacterial biofilms in otitis media - Evidence and relevance. *Pediatric Infectious Disease Journal* 26: S17-S19

Bakaletz LO. 2009. Chinchilla as a robust, reproducible and polymicrobial model of otitis media and its prevention. *Expert Review of Vaccines* 8: 1063-82

Bakaletz LO. 2010. Immunopathogenesis of polymicrobial otitis media. *J Leukoc Biol* 87: 213-22

Barnes FA, Bingle L, Bingle CD. 2008. Pulmonary Genomics, Proteomics, and PLUNCs. *Am J Respir Cell Mol Biol* 38: 377-9

Bartlett JA, Gakhar L, Penterman J, Singh PK, Mallampalli RK, et al. 2011. PLUNC: a multifunctional surfactant of the airways (vol 39, pg 1012, 2011). *Biochemical Society Transactions* 39: 1549-49

Bartlett JA, Meyerholz DK, Wohlford-Lenane CL, Naumann PW, Salzman NH, McCray PB. 2015. Increased susceptibility to otitis media in a Splunc1-deficient mouse model. *Disease Models & Mechanisms* 8: 501-08

Baum J, Duffy HS. 2011. Fibroblasts and Myofibroblasts: What Are We Talking About? *Journal of Cardiovascular Pharmacology* 57: 376-79

Bernstei.Jm, Tomasi TB, Ogra P. 1974. IMMUNOCHEMISTRY OF MIDDLE-EAR EFFUSIONS. *Archives of Otolaryngology-Head & Neck Surgery* 99: 320-26

Bhutta MF. 2012. Mouse models of otitis media: strengths and limitations. *Otolaryngology--head and neck surgery : official journal of American Academy of Otolaryngology-Head and Neck Surgery* 147

Bingle CD, Bingle L. 2000. Characterisation of the human plunc gene, a gene product with an upper airways and nasopharyngeal restricted expression pattern. *Biochim Biophys Acta* 1493: 363-7

Bingle CD, Bingle L, Craven CJ. 2011a. Distant cousins: genomic and sequence diversity within the BPI fold-containing (BPIF)/PLUNC protein family. *Biochemical Society Transactions* 39: 961-65

Bingle CD, Craven CJ. 2002. PLUNC: a novel family of candidate host defence proteins expressed in the upper airways and nasopharynx. *Hum Mol Genet* 11: 937-43

Bingle CD, Craven CJ. 2003. Comparative analysis of the PLUNC (palate, lung and nasal epithelium clone) protein families. *Biochem Soc Trans* 31: 806-9

Bingle CD, Craven CJ. 2004. Meet the relatives: a family of BPI- and LBP-related proteins. *Trends Immunol* 25: 53-5

Bingle CD, Leclair EE, Havard S, Bingle L, Gillingham P, Craven CJ. 2004. Phylogenetic and evolutionary analysis of the PLUNC gene family. *Protein Science* 13: 422-30

Bingle CD, Seal RL, Craven CJ. 2011b. Systematic nomenclature for the PLUNC/PSP/BSP30/SMGB proteins as a subfamily of the BPI fold-containing superfamily. *Biochemical Society Transactions* 39: 977-83

Bingle L, Barnes FA, Cross SS, Rassl D, Wallace WA, et al. 2007. Differential epithelial expression of the putative innate immune molecule SPLUNC1 in cystic fibrosis. *Respir Res* 8: 79

Bingle L, Bingle CD. 2011. Distribution of human PLUNC/BPI fold-containing (BPIF) proteins. *Biochemical Society Transactions* 39: 1023-27

Bingle L, Cross SS, High AS, Wallace WA, Devine DA, et al. 2005. SPLUNC1 (PLUNC) is expressed in glandular tissues of the respiratory tract and in lung tumours with a glandular phenotype. *J Pathol* 205: 491-7

Bluestone CD. 1998. Epidemiology and pathogenesis of chronic suppurative otitis media: implications for prevention and treatment. *Int J Pediatr Otorhinolaryngol* 42: 207-23

Britto CJ, Cohn L. 2015. Bactericidal/Permeability-Increasing Protein Fold-Containing Family Member A1 in Airway Host Protection and Respiratory Disease. *American Journal of Respiratory Cell and Molecular Biology* 52: 525-34

Britto CJ, Liu Q, Curran DR, Patham B, Dela Cruz CS, Cohn L. 2013. Short Palate, Lung, and Nasal Epithelial Clone-1 Is a Tightly Regulated Airway Sensor in Innate and Adaptive Immunity. *American Journal of Respiratory Cell and Molecular Biology* 48: 717-24

Brockson ME, Novotny LA, Jurcisek JA, McGillivary G, Bowers MR, Bakaletz LO. 2012. Respiratory Syncytial Virus Promotes Moraxella catarrhalis-Induced Ascending Experimental Otitis Media. *Plos One* 7

Brown SDM, Hardisty-Hughes RE, Mburu P. 2008. Quiet as a mouse: dissecting the molecular and genetic basis of hearing. *Nature Reviews Genetics* 9: 277-90

Butler CR, Hynds RE, Gowers KHC, Lee DDH, Brown JM, et al. 2016. Rapid Expansion of Human Epithelial Stem Cells Suitable for Airway Tissue Engineering. *American journal of respiratory and critical care medicine* 194: 156-68

Campbell RG, Birman CS, Morgan L. 2009. Management of otitis media with effusion in children with primary ciliary dyskinesia: A literature review. *International Journal of Pediatric Otorhinolaryngology* 73: 1630-38

Campos MA, Abreu AR, Nlend MC, Cobas MA, Conner GE, Whitney PL. 2004. Purification and characterization of PLUNC from human - Tracheobronchial secretions. *American Journal of Respiratory Cell and Molecular Biology* 30

Carola R, Harley J, Noback C. 1992. *Human Anatomy and Physiology*. New York: McGraw-Hill.

Casey JR, Pichichero ME. 2004. Changes in frequency and pathogens causing acute otitis media in 1995-2003. *Pediatric Infectious Disease Journal* 23: 824-28

Cash HL, Whitham CV, Behrendt CL, Hooper LV. 2006. Symbiotic bacteria direct expression of an intestinal bactericidal lectin. *Science* 313: 1126-30

Casselbrant ML, Mandel EM. 2001. The genetics of otitis media. *Curr Allergy Asthma Rep* 1: 353-7

Casselbrant ML, Mandel EM, Jung J, Ferrell RE, Tekely K, et al. 2009. Otitis media: a genome-wide linkage scan with evidence of susceptibility loci within the 17q12 and 10q22.3 regions. *BMC Med Genet* 10: 85

Casselbrant ML, Mandel EM, Rockette HE, Kurs-Lasky M, Fall PA, et al. 2004. The genetic component of middle ear disease in the first 5 years of life. *Arch Otolaryngol Head Neck Surg* 130: 273-8

Cheeseman MT, Tyrer HE, Williams D, Hough TA, Pathak P, et al. 2011. HIF-VEGF pathways are critical for chronic otitis media in Junbo and Jeff mouse mutants. *PLoS genetics* 7

Chen LF, Greene WC. 2004. Shaping the nuclear action of NF-kappa B. *Nature Reviews Molecular Cell Biology* 5: 392-401

Chiang SC, Veldhuizen EJA, Barnes FA, Craven CJ, Haagsman HP, Bingle CD. 2011. Identification and characterisation of the BPI/LBP/PLUNC-like gene repertoire in chickens reveals the absence of a LBP gene. *Developmental and Comparative Immunology* 35: 285-95

Choi JY, Kim CH, Lee WS, Kim HN, Song KS, Yoon JH. 2002. Ciliary and secretory differentiation of normal human middle ear epithelial cells. *Acta Oto-Laryngologica* 122: 270-75

Choi JY, Son EJ, Kim JL, Lee JH, Park HY, et al. 2006. ENaC- and CFTR-dependent ion and fluid transport in human middle ear epithelial cells. *Hearing Research* 211: 26-32

Choi SM, McAleer JP, Zheng MQ, Pociask DA, Kaplan MH, et al. 2013. Innate Stat3-mediated induction of the antimicrobial protein Reg3 gamma is required for host defense against MRSA pneumonia. *Journal of Experimental Medicine* 210: 551-61

Chu HW, Gally F, Thaikoottathil J, Janssen-Heininger YM, Wu Q, et al. 2010. SPLUNC1 regulation in airway epithelial cells: role of toll-like receptor 2 signaling. *Respiratory Research* 11

Chu HW, Thaikoottathil J, Rino JG, Zhang G, Wu Q, et al. 2007. Function and regulation of SPLUNC1 protein in Mycoplasma infection and allergic inflammation. *J Immunol* 179: 3995-4002

Chun YM, Moon SK, Lee HY, Webster P, Brackmann DE, et al. 2002. Immortalization of normal adult human middle ear epithelial cells using a retrovirus containing the E6/E7 genes of human papillomavirus type 16. *Annals of Otology Rhinology and Laryngology* 111: 507-17

Clarke LL, Burns KA, Bayle JY, Boucher RC, Vanscott MR. 1992. SODIUM-CONDUCTIVE AND CHLORIDE-CONDUCTIVE PATHWAYS IN CULTURED MOUSE TRACHEAL EPITHELIUM. *American Journal of Physiology* 263: L519-L25

Cody AJ, Field D, Feil EJ, Stringer S, Deadman ME, et al. 2003. High rates of recombination in otitis media isolates of non-typeable Haemophilus influenzae. *Infection Genetics and Evolution* 3: 57-66

Corbeel L. 2007. What is new in otitis media? *Eur J Pediatr* 166: 511-9

Daly KA, Brown WM, Segade F, Bowden DW, Keats BJ, et al. 2004. Chronic and recurrent otitis media: a genome scan for susceptibility loci. *Am J Hum Genet* 75: 988-97

Davidson DJ, Kilanowski FM, Randell SH, Sheppard DN, Dorin JR. 2000. A primary culture model of differentiated murine tracheal epithelium. *American Journal of Physiology-Lung Cellular and Molecular Physiology* 279: L766-L78

Davies DE, Wicks J, Powell RM, Puddicombe SM, Holgate ST. 2003. Airway remodeling in asthma: New insights. *Journal of Allergy and Clinical Immunology* 111: 215-25

Desmouliere A, Geinoz A, Gabbiani F, Gabbiani G. 1993. TRANSFORMING GROWTH-FACTOR-BETA-1 INDUCES ALPHA-SMOOTH MUSCLE ACTIN EXPRESSION IN GRANULATION-TISSUE MYOFIBROBLASTS AND IN QUIESCENT AND GROWING CULTURED FIBROBLASTS. *Journal of Cell Biology* 122: 103-11

Di YP. 2011. Functional roles of SPLUNC1 in the innate immune response against Gram-negative bacteria. *Biochemical Society Transactions* 39: 1051-55

Di YP, Harper R, Zhao YH, Pahlavan N, Finkbeiner W, Wu R. 2003. Molecular cloning and characterization of spurt, a human novel gene that is retinoic acid-inducible and encodes a secretory protein specific in upper respiratory tracts. *Journal of Biological Chemistry* 278: 1165-73

Di YP, Tkach AV, Yanamala N, Stanley S, Gao S, et al. 2013. Dual Acute Proinflammatory and Antifibrotic Pulmonary Effects of Short Palate, Lung, and Nasal Epithelium Clone-1 after Exposure to Carbon Nanotubes. *American Journal of Respiratory Cell and Molecular Biology* 49: 759-67

Dimova S, Brewster ME, Noppe M, Jorissen A, Augustijns P. 2005. The use of human nasal in vitro cell systems during drug discovery and development. *Toxicology in Vitro* 19: 107-22

Duvernelle C, Freund V, Frossard N. 2003. Transforming growth factor-beta and its role in asthma. *Pulmonary Pharmacology & Therapeutics* 16: 181-96

Emanuel D, Sumalai M, Letowski T. 2009. Auditory Function: Physiology and Function of the Hearing System.

Emes RD, Goodstadt L, Winter EE, Ponting CP. 2003. Comparison of the genomes of human and mouse lays the foundation of genome zoology. *Human Molecular Genetics* 12: 701-09

Eriksson P, Kallin B, Vanthooft FM, Bavenholm P, Hamsten A. 1995. ALLELE-SPECIFIC INCREASE IN BASAL TRANSCRIPTION OF THE PLASMINOGEN-ACTIVATOR INHIBITOR-1 GENE IS ASSOCIATED WITH MYOCARDIAL-INFARCTION. *Proceedings of the National Academy of Sciences of the United States of America* 92: 1851-55

Faden H. 2001. The microbiologic and immunologic basis for recurrent otitis media in children. *European Journal of Pediatrics* 160: 407-13

Faden H, Duffy L, Williams A, Krystofik DA, Wolf J. 1996. Epidemiology of nasopharyngeal colonization with nontypeable Haemophilus influenzae in the first two years of life. *Acta Oto-Laryngologica*: 128-29

Fireman P. 1997. Otitis media and eustachian tube dysfunction: connection to allergic rhinitis. *J Allergy Clin Immunol* 99: S787-97

Fornander L, Graff P, Wahlen K, Ydreborg K, Flodin U, et al. 2013. Airway Symptoms and Biological Markers in Nasal Lavage Fluid in Subjects Exposed to Metalworking Fluids. *Plos One* 8

Fray MD, Pickard AR, Harrison M, Cheeseman MT. 2008. Upgrading mouse health and welfare: direct benefits of a large-scale rederivation programme. *Laboratory Animals* 42: 127-39

Frede S, Berchner-Pfannschmidt U, Fandrey J. 2007. Regulation of hypoxia-inducible factors during inflammation. *Oxygen Biology and Hypoxia* 435: 405-19

Gakhar L, Bartlett JA, Penterman J, Mizrachi D, Singh PK, et al. 2010. PLUNC is a novel airway surfactant protein with anti-biofilm activity. *PLoS One* 5: e9098

Gally F, Di YP, Smith SK, Minor MN, Liu Y, et al. 2011. SPLUNC1 Promotes Lung Innate Defense Against Mycoplasma pneumoniae Infection in Mice. *American Journal of Pathology* 178: 2159-67

Gao X, Bali AS, Randell SH, Hogan BLM. 2015. GRHL2 coordinates regeneration of a polarized mucociliary epithelium from basal stem cells. *Journal of Cell Biology* 211: 669-82

Garcia-Caballero A, Rasmussen JE, Gaillard E, Watson MJ, Olsen JC, et al. 2009. SPLUNC1 regulates airway surface liquid volume by protecting ENaC from proteolytic cleavage. *Proceedings of the National Academy of Sciences of the United States of America* 106: 11412-17

Garland AL, Walton WG, Coakley RD, Tan CD, Gilmore RC, et al. 2013. Molecular basis for pH-dependent mucosal dehydration in cystic fibrosis airways. *Proceedings of the National Academy of Sciences of the United States of America* 110: 15973-78

Gaschler GJ, Skrtic M, Zavitz CCJ, Linclahl M, Onnervik PO, et al. 2009. Bacteria Challenge in Smoke-exposed Mice Exacerbates Inflammation and Skews the Inflammatory Profile. *American Journal of Respiratory and Critical Care Medicine* 179: 666-75

Geyik MF, Kokoglu OF, Hosoglu S, Ayaz C. 2002. Acute bacterial meningitis as a complication of otitis media and related mortality factors. *Yonsei Medical Journal* 43: 573-78

Ghafouri B, Kihlstrom E, Stahlbom B, Tagesson C, Lindahl M. 2003. PLUNC (palate, lung and nasal epithelial clone) proteins in human nasal lavage fluid. *Biochemical Society Transactions* 31: 810-14

Ghosh AK, Vaughan DE. 2012. PAI-1 in tissue fibrosis. *Journal of Cellular Physiology* 227: 493-507

Giebink GS. 1981. THE PATHOGENESIS OF PNEUMOCOCCAL OTITIS-MEDIA IN CHINCHILLAS AND THE EFFICACY OF VACCINATION IN PROPHYLAXIS. *Reviews of Infectious Diseases* 3: 342-53

Giebink GS. 1991. IMMUNOPROPHYLAXIS OF OTITIS-MEDIA. *Immunobiology of Proteins and Peptides Vi: Human Immunodeficiency Virus, Antibody Immunoconjugates, Bacterial Vaccines, and Immunomodulators* 303: 149-58

Giebink GS, Berzins IK, Schiffman G, Quie PG. 1979. EXPERIMENTAL OTITIS-MEDIA IN CHINCHILLAS FOLLOWING NASAL COLONIZATION WITH TYPE-7F STREPTOCOCCUS-PNEUMONIAE - PREVENTION AFTER VACCINATION WITH PNEUMOCOCCAL CAPSULAR POLYSACCHARIDE. *Journal of Infectious Diseases* 140: 716-23

Goyama S, Kurokawa M. 2009. Pathogenetic significance of ecotropic viral integration site-1 in hematological malignancies. *Cancer Science* 100: 990-95

Goyama S, Kurokawa M. 2010. Evi-1 as a critical regulator of leukemic cells. *International Journal of Hematology* 91: 753-57

Hardisty RE, Erven A, Logan K, Morse S, Guionaud S, et al. 2003. The deaf mouse mutant Jeff (Jf) is a single gene model of otitis media. *J Assoc Res Otolaryngol* 4: 130-8

Hardisty-Hughes RE, Tateossian H, Morse SA, Romero MR, Middleton A, et al. 2006. A mutation in the F-box gene, Fbxo11, causes otitis media in the Jeff mouse. *Hum Mol Genet* 15: 3273-9

Harkema JR, Carey SA, Wagner JG. 2006. The nose revisited: A brief review of the comparative structure, function, and toxicologic pathology of the nasal epithelium. *Toxicologic Pathology* 34: 252-69

He ZW, Xie L, Xu LG, Lan K, Liu WD, et al. 2000. Cloning of a novel gene associated with human nasopharyngeal carcinoma. *Chinese Science Bulletin* 45: 2267-72

Hendrixson DR, Qiu J, Shewry SC, Fink DL, Petty S, et al. 2003. Human milk lactoferrin is a serine protease that cleaves Haemophilus surface proteins at arginine-rich sites. *Molecular Microbiology* 47: 607-17

Herman P, Friedlander G, Huy PTB, Amiel C. 1992. ION-TRANSPORT BY PRIMARY CULTURES OF MONGOLIAN GERBIL MIDDLE-EAR EPITHELIUM. *American Journal of Physiology* 262: F373-F80

Hernandez M, Leichtle A, Pak K, Ebmeyer J, Euteneuer S, et al. 2008. Myeloid Differentiation Primary Response Gene 88 Is Required for the Resolution of Otitis Media. *Journal of Infectious Diseases* 198: 1862-69

Hirai H. 1999. The transcription factor Evi-1. *International Journal of Biochemistry & Cell Biology* 31: 1367-71

Hirano T, Kodama S, Fujita K, Maeda K, Suzuki M. 2007. Role of Toll-like receptor 4 in innate immune responses in a mouse model of acute otitis media. *Fems Immunology and Medical Microbiology* 49: 75-83

Hirst RA, Jackson CL, Coles JL, Williams G, Rutman A, et al. 2014. Culture of Primary Ciliary Dyskinesia Epithelial Cells at Air-Liquid Interface Can Alter Ciliary Phenotype but Remains a Robust and Informative Diagnostic Aid. *Plos One* 9

Hobbs CA, Blanchard MG, Alijevic O, Da Tan C, Kellenberger S, et al. 2013. Identification of the SPLUNC1 ENaC- inhibitory domain yields novel strategies to treat sodium hyperabsorption in cystic fibrosis airway epithelial cultures. *American Journal of Physiology-Lung Cellular and Molecular Physiology* 305: L990-L1001

Hood D, Moxon R, Purnell T, Richter C, Williams D, et al. 2016. A new model for non-typeable Haemophilus influenzae middle ear infection in the Junbo mutant mouse. *Disease Models & Mechanisms* 9: 69-79

Hood DW, Makepeace K, Deadman ME, Rest RF, Thibault P, et al. 1999. Sialic acid in the lipopolysaccharide of Haemophilus influenzae: strain distribution, influence on serum resistance and structural characterization. *Molecular Microbiology* 33: 679-92

Horani A, Druley TE, Zariwala MA, Pate AC, Levinson BT, et al. 2012. Whole-Exome Capture and Sequencing Identifies HEATR2 Mutation as a Cause of Primary Ciliary Dyskinesia. *American Journal of Human Genetics* 91: 685-93

Horani A, Nath A, Wasserman MG, Huang T, Brody SL. 2013. Rho-Associated Protein Kinase Inhibition Enhances Airway Epithelial Basal-Cell Proliferation and Lentivirus Transduction. *American Journal of Respiratory Cell and Molecular Biology* 49: 341-47

Hou J, Yashiro K, Okazaki Y, Saijoh Y, Hayashizaki Y, Hamada H. 2004. Identification of a novel left-right asymmetrically expressed gene in the mouse belonging to the BPI/PLUNC superfamily. *Developmental Dynamics* 229: 373-79

Huangfu M, Saunders JC. 1983. AUDITORY DEVELOPMENT IN THE MOUSE - STRUCTURAL MATURATION OF THE MIDDLE-EAR. *Journal of Morphology* 176: 249-59

Hunter SE, Singla AK, Prazma J, Jewett BS, Randell SH, Pillsbury HC. 1999. Mucin production in the middle ear in response to lipopolysaccharides. *Otolaryngology-Head and Neck Surgery* 120: 884-88

Husseman J, Palacios SD, Rivkin AZ, Oehl H, Ryan AF. 2012. The Role of Vascular Endothelial Growth Factors and Fibroblast Growth Factors in Angiogenesis during Otitis Media. *Audiology and Neuro-Otology* 17: 148-54

Ibanez-Tallon I, Gorokhova S, Heintz N. 2002. Loss of function of axonemal dynein Mdnah5 causes primary ciliary dyskinesia and hydrocephalus. *Human Molecular Genetics* 11: 715-21

Irander K, Borres MP, Ghafouri B. 2014. The effects of physical exercise and smoking habits on the expression of SPLUNC1 in nasal lavage fluids from allergic rhinitis subjects. *International Journal of Pediatric Otorhinolaryngology* 78: 618-22

Ishii T, Toriyama M, Suzuki JI. 1980. Histopathological study of otitis media with effusion. *Ann Otol Rhinol Laryngol Suppl* 89: 83-6

Ishinaga H, Jono H, Lim JH, Kweon S-M, Xu H, et al. 2007. TGF-beta induces p65 acetylation to enhance bacteria-induced NF-kappa B activation. *Embo Journal* 26: 1150-62

Iwasaki A, Medzhitov R. 2010. Regulation of adaptive immunity by the innate immune system. *Science* 327: 291-5

Izutsu K, Kurokawa M, Imai Y, Maki K, Mitani K, Hirai H. 2001. The corepressor CtBP interacts with Evi-1 to repress transforming growth factor beta signaling. *Blood* 97: 2815-22

James AJ, Penrose JF, Cazaly AM, Holgate ST, Sampson AP. 2006. Human bronchial fibroblasts express the 5-lipoxygenase pathway. *Respiratory Research* 7

Jeep S. 1990. [Correlation of immunoglobulins, the complement system and inflammatory mediators with reference to the pathogenesis of serous otitis media]. *Laryngorhinootologie* 69: 201-7

Jiang D, Persinger R, Wu Q, Gross A, Chu HW. 2013a. alpha 1-antitrypsin promotes SPLUNC1-mediated lung defense against Pseudomonas aeruginosa infection in mice. *Respiratory Research* 14

Jiang D, Wenzel SE, Wu Q, Bowler RP, Schnell C, Chu HW. 2013b. Human Neutrophil Elastase Degrades SPLUNC1 and Impairs Airway Epithelial Defense against Bacteria. *Plos One* 8

Johnson VJ, Yucesoy B, Reynolds JS, Fluharty K, Wang W, et al. 2007. Inhalation of toluene diisocyanate vapor induces allergic rhinitis in mice. *Journal of Immunology* 179: 1864-71

Jono H, Shuto T, Xu HD, Kai H, Lim DJ, et al. 2002. Transforming growth factor-beta-Smad signaling pathway cooperates with NF-kappa B to mediate nontypeable Haemophilus influenzae-induced MUC2 mucin transcription. *Journal of Biological Chemistry* 277: 45547-57

Jono H, Xu H, Kai H, Lim DJ, Kim YS, et al. 2003. Transforming growth factor-beta-Smad signaling pathway negatively regulates nontypeable Haemophilus influenzae-induced MUC5AC mucin transcription via mitogen-activated protein kinase (MAPK) phosphatase-1-dependent inhibition of p38 MAPK. *Journal of Biological Chemistry* 278: 27811-19

Juhn SK, Jung MK, Hoffman MD, Drew BR, Preciado DA, et al. 2008. The Role of Inflammatory Mediators in the Pathogenesis of Otitis Media and Sequelae. *Clinical and Experimental Otorhinolaryngology* 1: 117-38

Kanazawa H, Yoshida N, Iino Y. 2015. New Insights into Eosinophilic Otitis Media. *Current Allergy and Asthma Reports* 15

Kapsogeorgou EK, Abu-Helu RF, Moutsopoulos HM, Manoussakis MN. 2005. Salivary gland epithelial cell exosomes - A source of autoantigenic ribonucleoproteins. *Arthritis and Rheumatism* 52: 1517-21

Keller S, Sanderson MP, Stoeck A, Altevogt P. 2006. Exosomes: From biogenesis and secretion to biological function. *Immunology Letters* 107: 102-08

Kerschner JE, Li JZ, Tsushiya K, Khampang P. 2010a. Mucin gene expression and mouse middle ear epithelium. *International Journal of Pediatric Otorhinolaryngology* 74: 864-68

Kerschner JE, Tripathi S, Khampang P, Papsin BC. 2010b. MUC5AC expression in human middle ear epithelium of patients with otitis media. *Arch Otolaryngol Head Neck Surg* 136: 819-24

Kesimer M, Scull M, Brighton B, DeMaria G, Burns K, et al. 2009. Characterization of exosome-like vesicles released from human tracheobronchial ciliated epithelium: a possible role in innate defense. *Faseb Journal* 23: 1858-68

Kim CH, Kim K, Jik Kim H, Kook Kim J, Lee JG, Yoon JH. 2006. Expression and regulation of PLUNC in human nasal epithelium. *Acta Otolaryngol* 126: 1073-8

Kondo M, Tamaoki J, Takeyama K, Nakata J, Nagai A. 2002. Interleukin-13 induces goblet cell differentiation in primary cell culture from guinea pig tracheal epithelium. *American Journal of Respiratory Cell and Molecular Biology* 27: 536-41

Krunkosky TM, Martin LD, Fischer BM, Voynow JA, Adler KB. 2003. Effects of TNF alpha on expression of ICAM-1 in human airway epithelial cells in vitro: Oxidant-mediated pathways and transcription factors. *Free Radical Biology and Medicine* 35: 1158-67

Kubba H, Pearson JP, Birchall JP. 2000. The aetiology of otitis media with effusion: a review. *Clin Otolaryngol Allied Sci* 25: 181-94

Kurokawa M, Mitani K, Imai Y, Ogawa S, Yazaki Y, Hirai H. 1998a. The t(3;21) fusion product, AML1/Evi-1, interacts with Smad3 and blocks transforming growth factor-beta-mediated growth inhibition of myeloid cells. *Blood* 92: 4003-12

Kurokawa M, Mitani K, Irie K, Matsuyama T, Takahashi T, et al. 1998b. The oncoprotein Evi-1 represses TGF-beta signalling by inhibiting Smad3. *Nature* 394: 92-96

Kurokawa M, Mitani K, Yamagata T, Takahashi T, Izutsu K, et al. 2000. The Evi-1 oncoprotein inhibits c-Jun N-terminal kinase and prevents stress-induced cell death. *Embo Journal* 19: 2958-68

Lechner JF, Haugen A, McClendon IA, Pettis EW. 1982. CLONAL GROWTH OF NORMAL ADULT HUMAN BRONCHIAL EPITHELIAL-CELLS IN A SERUM-FREE MEDIUM. *In Vitro-Journal of the Tissue Culture Association* 18: 633-42

LeClair EE. 2003. Four reasons to consider a novel class of innate immune molecules in the oral epithelium. *J Dent Res* 82: 944-50

LeClair EE, Nguyen L, Bingle L, MacGowan A, Singleton V, et al. 2001. Genomic organization of the mouse plunc gene and expression in the developing airways and thymus. *Biochemical and Biophysical Research Communications* 284: 792-97

LeClair EE, Nomellini V, Bahena M, Singleton V, Bingle L, et al. 2004. Cloning and expression of a mouse member of the PLUNC protein family exclusively expressed in tongue epithelium. *Genomics* 83: 658-66

Lee MK, Yoo JW, Lin HX, Kim DD, Choi YM, et al. 2005. Air-liquid interface culture of serially passaged human nasal epithelial cell monolayer for in vitro drug transport studies. *Drug Delivery* 12: 305-11

Legrand D, Elass E, Carpentier M, Mazurier J. 2005. Lactoferrin: a modulator of immune and inflammatory responses. *Cellular and Molecular Life Sciences* 62: 2549-59

Leichtle A, Hernandez M, Pak K, Yamasaki K, Cheng C-F, et al. 2009. TLR4-mediated induction of TLR2 signaling is critical in the pathogenesis and resolution of otitis media. *Innate Immunity* 15: 205-15

Leichtle A, Lai Y, Wollenberg B, Wasserman SI, Ryan AF. 2011. Innate signaling in otitis media: pathogenesis and recovery. *Curr Allergy Asthma Rep* 11: 78-84

Li JP, Kania R, Lecain E, Ar A, Sauvaget E, et al. 2005. In vivo demonstration of the absorptive function of the middle ear epithelium. *Hearing Research* 210: 1-8

Lim DJ. 1979. NORMAL AND PATHOLOGICAL MUCOSA OF THE MIDDLE-EAR AND EUSTACHIAN-TUBE. *Clinical Otolaryngology* 4: 213-32

Lim DJ, Chun YM, Lee HY, Moon SK, Chang KH, et al. 2000. Cell biology of tubotympanum in relation to pathogenesis of otitis media - a review. *Vaccine* 19: S17-S25

Lim DJ, Moon SK. 2012. Establishment of Cell Lines from the Human Middle and Inner Ear Epithelial Cells. *Human Cell Transformation: Role of Stem Cells and the Microenvironment* 720: 15-25

Lim DJ, Shimada T, Yoder M. 1973. DISTRIBUTION OF MUCUS-SECRETING CELLS IN NORMAL MIDDLE-EAR MUCOSA. *Archives of Otolaryngology-Head & Neck Surgery* 98: 2-9

Lim JH, Jono H, Koga T, Woo CH, Ishinaga H, et al. 2007. Tumor Suppressor CYLD Acts as a Negative Regulator for Non-Typeable Haemophilus influenza-Induced Inflammation in the Middle Ear and Lung of Mice. *Plos One* 2: 10

Lin J, Tsuprun V, Kawano H, Paparella MM, Zhang Z, et al. 2001. Characterization of mucins in human middle ear and Eustachian tube. *Am J Physiol Lung Cell Mol Physiol* 280: L1157-67

Lindahl M, Stahlbom B, Tagesson C. 2001. Identification of a new potential airway irritation marker, palate lung nasal epithelial clone protein, in human nasal lavage fluid with two-dimensional electrophoresis and matrix-assisted laser desorption/ionization-time of flight. *Electrophoresis* 22: 1795-800

Liu X, Sheng HB, Ma R, Yang JM, Luo WW, et al. 2016. Notch signaling is active in normal mouse middle ear epithelial cells. *Experimental and Therapeutic Medicine* 11: 1661-67

Liu Y, Bartlett JA, Di ME, Bomberger JM, Chan YR, et al. 2013a. SPLUNC1/BPIFA1 Contributes to Pulmonary Host Defense against Klebsiella pneumoniae Respiratory Infection. *American Journal of Pathology* 182: 1519-31

Liu YY, Di ME, Chu HW, Liu XY, Wang L, et al. 2013b. Increased Susceptibility to Pulmonary Pseudomonas Infection in Splunc1 Knockout Mice. *Journal of Immunology* 191: 4259-68

Loonen LMP, Stolte EH, Jaklofsky MTJ, Meijerink M, Dekker J, et al. 2014. REG3 gamma-deficient mice have altered mucus distribution and increased mucosal inflammatory responses to the microbiota and enteric pathogens in the ileum. *Mucosal Immunology* 7: 939-47

Lopez-Souza N, Favoreto S, Wong H, Ward T, Yagi S, et al. 2009. In vitro susceptibility to rhinovirus infection is greater for bronchial than for nasal airway epithelial cells in human subjects. *Journal of Allergy and Clinical Immunology* 123: 1384-90

Lukinskiene L, Liu Y, Reynolds SD, Steele C, Stripp BR, et al. 2011. Antimicrobial Activity of PLUNC Protects against Pseudomonas aeruginosa Infection. *Journal of Immunology* 187: 382-90

MacArthur CJ, Wilmot B, Wang L, Schuller M, Lighthall J, Trune D. 2014. Genetic susceptibility to chronic otitis media with effusion: Candidate gene single nucleotide polymorphisms. *Laryngoscope* 124: 1229-35

Makinde T, Murphy RF, Agrawal DK. 2007. The regulatory role of TGF-beta in airway remodeling in asthma. *Immunology and Cell Biology* 85: 348-56

Matsui H, Grubb BR, Tarran R, Randell SH, Gatzy JT, et al. 1998. Evidence for periciliary liquid layer depletion, not abnormal ion composition, in the pathogenesis of cystic fibrosis airways disease. *Cell* 95: 1005-15

McCool TL, Weiser JN. 2004. Limited role of antibody in clearance of Streptococcus pneumoniae in a murine model of colonization. *Infection and Immunity* 72: 5807-13

McGillivary G, Bakaletz LO. 2010. The multifunctional host defense peptide SPLUNC1 is critical for homeostasis of the mammalian upper airway. *PLoS One* 5: e13224

McGuire JF. 2002. Surfactant in the middle ear and eustachian tube: a review. *Int J Pediatr Otorhinolaryngol* 66: 1-15

Melhuish TA, Wotton D. 2000. The interaction of the carboxyl terminus-binding protein with the Smad corepressor TGIF is disrupted by a holoprosencephaly mutation in TGIF. *Journal of Biological Chemistry* 275: 39762-66

Melhus A, Ryan AF. 2003. A mouse model for acute otitis media. *Apmis* 111: 989-94

Miles AA, Misra SS, Irwin JO. 1938. The estimation of the bactericidal power of the blood. *Journal of Hygiene* 38: 732-49

Mittal R, Kodiyan J, Gerring R, Mathee K, Li J-D, et al. 2014. Role of innate immunity in the pathogenesis of otitis media. *International Journal of Infectious Diseases* 29: 259-67

Monasta L, Ronfani L, Marchetti F, Montico M, Brumatti LV, et al. 2012. Burden of Disease Caused by Otitis Media: Systematic Review and Global Estimates. *Plos One* 7: 12

Moon SK, Lee HY, Li JD, Nagura M, Kang SH, et al. 2002. Activation of a Src-dependent Raf-MEK1/2-ERK signaling pathway is required for IL-1 alpha-induced upregulation of beta-defensin 2 in human middle ear epithelial cells. *Biochimica Et Biophysica Acta-Molecular Cell Research* 1590: 41-51

Moon SK, Lim DJ, Lee HK, Kim HN, Yoon JH. 2000. Mucin gene expression in cultured human middle ear epithelial cells. *Acta Oto-Laryngologica* 120: 933-39

Moon SK, Linthicum FH, Jr., Yang HD, Lee SJ, Park K. 2008. Activities of matrix metalloproteinases and tissue inhibitor of metalloproteinase-2 in idiopathic hemotympanum and otitis media with effusion. *Acta Oto-Laryngologica* 128: 144-50

Mulay A. MSc thesis 2011. *Characteisation of Plunc expression in a mouse model of Otitis media*

Musa M, Wilson K, Sun L, Mulay A, Bingle L, et al. 2012. Differential localisation of BPIFA1 (SPLUNC1) and BPIFB1 (LPLUNC1) in the nasal and oral cavities of mice. *Cell and Tissue Research* 350

Nakamura A, Demaria TF, Arya G, Lim DJ, Vanblitterswijk C. 1991. SERIAL CULTURE AND CHARACTERIZATION OF THE CHINCHILLA MIDDLE-EAR EPITHELIUM. *Annals of Otology Rhinology and Laryngology* 100: 1024-31

Nakamura Y, Komori M, Yamakawa K, Hamajima Y, Suzuki M, et al. 2013. Math 1, retinoic acid, and TNF-alpha synergistically promote the differentiation of mucous cells in mouse middle ear epithelial cells in vitro. *Pediatric Research* 74: 259-65

Ngo CC, Massa HM, Thornton RB, Cripps AW. 2016. Predominant Bacteria Detected from the Middle Ear Fluid of Children Experiencing Otitis Media: A Systematic Review. *Plos One* 11

Ning F, Wang C, Berry KZ, Kandasamy P, Liu H, et al. 2014. Structural characterization of the pulmonary innate immune protein SPLUNC1 and identification of lipid ligands. *Faseb Journal* 28: 5349-60

Noveroske JK, Weber JS, Justice MJ. 2000. The mutagenic action of N-ethyl-N-nitrosourea in the mouse. *Mammalian Genome* 11: 478-83

Parkinson N, Hardisty-Hughes RE, Tateossian H, Tsai HT, Brooker D, et al. 2006. Mutation at the Evi1 locus in Junbo mice causes susceptibility to otitis media. *PLoS Genet* 2: e149

Patel AC, Brody SL, Stappenbeck TS, Holtzman MJ. 2011. Tracking Cell Lineage to Rediscover (again) the Switch from Ciliated to Mucous Cells. *American Journal of Respiratory Cell and Molecular Biology* 44: 261-63

Patel JA, Nair S, Revai K, Grady J, Saeed K, et al. 2006. Association of proinflammatory cytokine gene polymorphisms with susceptibility to otitis media. *Pediatrics* 118: 2273-79

Perkins AS, Mercer JA, Jenkins NA, Copeland NG. 1991. PATTERNS OF EVI-1 EXPRESSION IN EMBRYONIC AND ADULT TISSUES SUGGEST THAT EVI-1 PLAYS AN IMPORTANT REGULATORY ROLE IN MOUSE DEVELOPMENT. *Development* 111: 479-87

Pillai DK, Sankoorikal BJV, Johnson E, Seneviratne AN, Zurko J, et al. 2014. Directional Secretomes Reflect Polarity-Specific Functions in an In Vitro Model of Human Bronchial Epithelium. *American Journal of Respiratory Cell and Molecular Biology* 50: 292-300

Portier F, Kania R, Planes C, Hsu WC, Couette S, et al. 2005. Enhanced sodium absorption in middle ear epithelial cells cultured at air-liquid interface. *Acta Oto-Laryngologica* 125: 16-22

Preciado D, Burgett K, Ghimbovschi S, Rose M. 2013. NTHi Induction of Cxcl2 and Middle Ear Mucosal Metaplasia in Mice. *Laryngoscope* 123: E66-E71

Preciado D, Goyal S, Rahimi M, Watson AM, Brown KJ, et al. 2010. MUC5B Is the predominant mucin glycoprotein in chronic otitis media fluid. *Pediatr Res* 68: 231-6

Rasmussen F. 1993. PROTRACTED SECRETORY OTITIS-MEDIA - THE IMPACT OF FAMILIAL FACTORS AND DAY-CARE-CENTER ATTENDANCE. *International Journal of Pediatric Otorhinolaryngology* 26: 29-37

Rivkin AZ, Palacios SD, Pak K, Bennett T, Ryan AF. 2005. The role of Fas-mediated apoptosis in otitis media: Observations in the lpr/lpr mouse. *Hearing Research* 207: 110-16

Robinson PJ, Lodge S, Jones BM, Walker CC, Grant HR. 1992. The effect of palate repair on otitis media with effusion. *Plast Reconstr Surg* 89: 640-5

Rock JR, Onaitis MW, Rawlins EL, Lu Y, Clark CP, et al. 2009. Basal cells as stem cells of the mouse trachea and human airway epithelium. *Proceedings of the National Academy of Sciences of the United States of America* 106: 12771-75

Rock JR, Randell SH, Hogan BLM. 2010. Airway basal stem cells: a perspective on their roles in epithelial homeostasis and remodeling. *Disease Models & Mechanisms* 3: 545-56

Rollins BM, Garcia-Caballero A, Stutts MJ, Tarran R. 2010. SPLUNC1 expression reduces surface levels of the epithelial sodium channel (ENaC) in Xenopus laevis oocytes. *Channels* 4: 255-59

Roy MG, Livraghi-Butrico A, Fletcher AA, McElwee MM, Evans SE, et al. 2014. Muc5b is required for airway defence. *Nature* 505: 412-+

Ryan AF, Ebmeyer J, Furukawa M, Pak K, Melhus A, et al. 2006. Mouse models of induced otitis media. *Brain Research* 1091: 3-8

Rye MS, Bhutta MF, Cheeseman MT, Burgner D, Blackwell JM, et al. 2011a. Unraveling the genetics of otitis media: from mouse to human and back again. *Mamm Genome* 22: 66-82

Rye MS, Blackwell JM, Jamieson SE. 2012a. Genetic susceptibility to otitis media in childhood. *Laryngoscope* 122: 665-75

Rye MS, Warrington NM, Scaman ESH, Vijayasekaran S, Coates HL, et al. 2012b. Genome-Wide Association Study to Identify the Genetic Determinants of Otitis Media Susceptibility in Childhood. *Plos One* 7

Rye MS, Wiertsema SP, Scaman ESH, Oommen J, Sun W, et al. 2011b. FBXO11, a regulator of the TGF beta pathway, is associated with severe otitis media in Western Australian children. *Genes and Immunity* 12: 352-59

Sabirov A, Metzger DW. 2008. Mouse models for the study of mucosal vaccination against otitis media. *Vaccine* 26: 1501-24

Sade J. 1967. Ciliary activity and middle ear clearance. *Archives of otolaryngology (Chicago, Ill. : 1960)* 86: 128-35

Samuel EA, Burrows A, Kerschner JE. 2008. Cytokine regulation of mucin secretion in a human middle ear epithelial model. *Cytokine* 41: 38-43

Sanchez-Elsner T, Botella LM, Velasco B, Corbi A, Attisano L, Bernabeu C. 2001. Synergistic cooperation between hypoxia and transforming growth factor-beta pathways on human vascular endothelial growth factor gene expression. *Journal of Biological Chemistry* 276: 38527-35

Sayeed S, Nistico L, St Croix C, Di YP. 2013. Multifunctional Role of Human SPLUNC1 in Pseudomonas aeruginosa Infection. *Infection and Immunity* 81: 285-91

Schachern PA, Tsuprun V, Cureoglu S, Ferrieri PA, Briles DE, et al. 2010. Effect of Apolactoferrin on Experimental Pneumococcal Otitis Media. *Archives of Otolaryngology-Head & Neck Surgery* 136: 1127-31

Schilder AG, Chonmaitree T, Cripps AW, Rosenfeld RM, Casselbrant ML, et al. 2016. Otitis media. *Nat Rev Dis Primers* 2: 16063

Schousboe LP, Ovesen T, Ottosen PD, Ledet T, Elbrond O. 1995. CULTURE OF RABBIT MIDDLE-EAR EPITHELIAL-CELLS - A METHOD FOR PRIMARY CULTURE AND SUBCULTURE WITH IDENTIFICATION, CHARACTERIZATION AND GROWTH SPECIFICATION. *Acta Oto-Laryngologica* 115: 787-95

Segade F, Daly KA, Allred D, Hicks PJ, Cox M, et al. 2006. Association of the FBX011 gene with chronic otitis media with effusion and recurrent otitis media - The Minnesota COME/ROM Family Study. *Archives of Otolaryngology-Head & Neck Surgery* 132: 729-33

Sekiyama K, Ohori J-i, Matsune S, Kurono Y. 2011. The role of vascular endothelial growth factor in pediatric otitis media with effusion. *Auris Nasus Larynx* 38: 319-24

Selman M, Pardo A. 2002. Idiopathic pulmonary fibrosis: an epithelial/fibroblastic cross-talk disorder. *Respiratory research* 3: 3-3

Sentani K, Oue N, Sakamoto N, Arihiro K, Aoyagi K, et al. 2008. Gene expression profiling with microarray and SAGE identifies PLUNC as a marker for hepatoid adenocarcinoma of the stomach. *Modern Pathology* 21: 464-75

Seo SR, Lallemand F, Ferrand N, Pessah M, L'Hoste S, et al. 2004. The novel E3 ubiquitin ligase Tiul1 associates with TGIF to target Smad2 for degradation. *Embo Journal* 23: 3780-92

Seshadri S, Lin DC, Rosati M, Carter RG, Norton JE, et al. 2012. Reduced expression of antimicrobial PLUNC proteins in nasal polyp tissues of patients with chronic rhinosinusitis. *Allergy* 67

Shaulian E, Karin M. 2002. AP-1 as a regulator of cell life and death. *Nature Cell Biology* 4: E131-E36

Shinefield H, Black S, Ray P, Fireman B, Schwalbe J, Lewis E. 2002. Efficacy, immunogenicity and safety of heptavalent pneumococcal conjugate vaccine in low birth weight and preterm infants. *Pediatric Infectious Disease Journal* 21: 182-86

Short KR, Reading PC, Brown LE, Pedersen J, Gilbertson B, et al. 2013. Influenza-Induced Inflammation Drives Pneumococcal Otitis Media. *Infection and Immunity* 81: 645-52

Sipila M, Karma P, Pukander J, Timonen M, Kataja M. 1988. THE BAYESIAN-APPROACH TO THE EVALUATION OF RISK-FACTORS IN ACUTE AND RECURRENT ACUTE OTITIS-MEDIA. *Acta Oto-Laryngologica* 106: 94-101

Soler Artigas M, Loth DW, Wain LV, Gharib SA, Obeidat Me, et al. 2011. Genome-wide association and large-scale follow up identifies 16 new loci influencing lung function. *Nature Genetics* 43: 1082-90

Song J-J, Kwon SK, Cho CG, Park S-W, Chae S-W. 2012. Expression of ENaC in LPS-induced inflammation of middle ear mucosa. *Acta Oto-Laryngologica* 132

Sood R, Talwar-Trikha A, Chakrabarti SR, Nucifora G. 1999. MDS1/EVI1 enhances TGF-beta 1 signaling and strengthens its growth-inhibitory effect, but the leukemia-associated fusion protein AML1/MDS1/EVI1, product of the t(3;21), abrogates growth-inhibition in response to TCF-beta 1. *Leukemia* 13: 348-57

Stol K, van Selm S, van den Berg S, Bootsma HJ, Blokx WA, et al. 2009. Development of a non-invasive murine infection model for acute otitis media. *Microbiology* 155: 4135-44

Straetemans M, van Heerbeek N, Tonnaer E, Ingels KJ, Rijkers GT, Zielhuis GA. 2001. A comprehensive model for the aetiology of otitis media with effusion. *Med Hypotheses* 57: 784-91

Streubel S-O, Ross H. 2013. Otitis media Updates and Current Approaches In *Otolaryngology for the Pediatrician*, pp. 41-63

Su AI, Wiltshire T, Batalov S, Lapp H, Ching KA, et al. 2004. A gene atlas of the mouse and human protein-encoding transcriptomes. *Proceedings of the National Academy of Sciences of the United States of America* 101: 6062-67

Swords WE. 2012. Nontypeable Haemophilus influenza biofilms: role in chronic airway infections. *Frontiers in Cellular and Infection Microbiology* 2

Takeno S. 1990. Tissue culture of middle ear epithelium of the guinea pig--differences of the cellular growth activity in the middle ear cavity using collagen gel culture method. *Nihon Jibiinkoka Gakkai kaiho* 93: 2038-46

Tanaka T, Nishida J, Mitani K, Ogawa S, Yazaki Y, Hirai H. 1994. EVI-1 RAISES AP-1 ACTIVITY AND STIMULATES C-FOS PROMOTER TRANSACTIVATION WITH DEPENDENCE ON THE 2ND ZINC-FINGER DOMAIN. *Journal of Biological Chemistry* 269: 24020-26

Tarran R. 2004. Regulation of airway surface liquid volume and mucus transport by active ion transport. *Proceedings of the American Thoracic Society* 1: 42-6

Tarran R, Redinbo MR. 2014. Mammalian short palate lung and nasal epithelial clone 1 (SPLUNC1) in pH-dependent airway hydration. *International Journal of Biochemistry & Cell Biology* 52: 130-35

Tateossian H, Morse S, Parker A, Mburu P, Warr N, et al. 2013. Otitis media in the Tgif knockout mouse implicates TGF signalling in chronic middle ear inflammatory disease. *Human Molecular Genetics* 22: 2553-65

Tateossian H, Morse S, Simon MM, Dean CH, Brown SDM. 2015. Interactions between the otitis media gene, Fbxo11, and p53 in the mouse embryonic lung. *Disease Models & Mechanisms* 8: 1531-42

Teele DW, Klein JO, Rosner B. 1989. EPIDEMIOLOGY OF OTITIS-MEDIA DURING THE 1ST 7 YEARS OF LIFE IN CHILDREN IN GREATER BOSTON - A PROSPECTIVE, COHORT STUDY. *Journal of Infectious Diseases* 160: 83-94

Thaikoottathil JV, Martin RJ, Di PY, Minor M, Case S, et al. 2012. SPLUNC1 Deficiency Enhances Airway Eosinophilic Inflammation in Mice. *American Journal of Respiratory Cell and Molecular Biology* 47: 253-60

Thompson H, Tucker AS. 2013. Dual Origin of the Epithelium of the Mammalian Middle Ear. *Science* 339: 1453-56

Tonnaer EL, Sanders EA, Curfs JH. 2003. Bacterial otitis media: a new non-invasive rat model. *Vaccine* 21: 4539-44

Toyama K, Kim Y, Paparella MM, Lin JZ. 2004. Temperature-sensitive SV40-immortalized rat middle ear epithelial cells. *Annals of Otology Rhinology and Laryngology* 113: 967-+

Tsou Y-A, Lin C-D, Chen H-C, Hsu H-Y, Wu L-T, et al. 2015. Interleukin-13 Inhibits Lipopolysaccharide-Induced BPIFA1 Expression in Nasal Epithelial Cells. *Plos One* 10

Tsuchiya K, Kim Y, Ondrey FG, Lin JZ. 2005. Characterization of a temperature-sensitive mouse middle ear epithelial cell line. *Acta Oto-Laryngologica* 125: 823-29

Turner J, Roger J, Fitau J, Combe D, Giddings J, et al. 2011. Goblet Cells Are Derived from a FOXJ1-Expressing Progenitor in a Human Airway Epithelium. *American Journal of Respiratory Cell and Molecular Biology* 44: 276-84

Tyrer H. PhD thesis 2013. MRC Harwell

Ueyama S, Jin SJ, Rhim JS, Ueyama T, Lim DJ. 2001. Immortalization of rat middle ear epithelial cells by adeno 12-SV40 hybrid virus. *Annals of Otology Rhinology and Laryngology* 110: 132-41

Underwood M, Bakaletz L. 2011. Innate Immunity and the Role of Defensins in Otitis Media. *Current Allergy and Asthma Reports* 11

Vaishnava S, Yamamoto M, Severson KM, Ruhn KA, Yu XF, et al. 2011. The Antibacterial Lectin RegIII gamma Promotes the Spatial Segregation of Microbiota and Host in the Intestine. *Science* 334: 255-58

Val S, Poley M, Brown K, Choi R, Jeong S, et al. 2016. Proteomic Characterization of Middle Ear Fluid Confirms Neutrophil Extracellular Traps as a Predominant Innate Immune Response in Chronic Otitis Media. *Plos One* 11

Valadi H, Ekstrom K, Bossios A, Sjostrand M, Lee JJ, Lotvall JO. 2007. Exosome-mediated transfer of mRNAs and microRNAs is a novel mechanism of genetic exchange between cells. *Nature Cell Biology* 9: 654-U72

van Niel G, Raposo G, Candalh C, Boussac M, Hershberg R, et al. 2001. Intestinal epithelial cells secrete exosome-like vesicles. *Gastroenterology* 121: 337-49

van Rozendaal BAWM, van Golde LMG, Haagsman HP. 2001. Localization and functions of SP-A and SP-D at mucosal surfaces. *Pediatric Pathology and Molecular Medicine* 20: 319-39

Vanblitterswijk CA, Ponec M, Vanmuijen GNP, Wijsman MC, Koerten HK, Grote JJ. 1986. CULTURE AND CHARACTERIZATION OF RAT MIDDLE-EAR EPITHELIUM. *Acta Oto-Laryngologica* 101: 453-66

Vargas PA, Speight PM, Bingle CD, Barrett AW, Bingle L. 2008. Expression of PLUNC family members in benign and malignant salivary gland tumours. *Oral Dis* 14: 613-9

Vladar EK, Stearns T. 2007. Molecular characterization of centriole assembly in ciliated epithelial cells. *Journal of Cell Biology* 178: 31-42

Voronina VA, Takemaru K-I, Treuting P, Love D, Grubb BR, et al. 2009. Inactivation of Chibby affects function of motile airway cilia. *Journal of Cell Biology* 185: 225-33

Walton WG, Ahmad S, Little MS, Kim CSK, Tyrrell J, et al. 2016. Structural Features Essential to the Antimicrobial Functions of Human SPLUNC1. *Biochemistry* 55: 2979-91

Waterston RH, Lindblad-Toh K, Birney E, Rogers J, Abril JF, et al. 2002. Initial sequencing and comparative analysis of the mouse genome. *Nature* 420: 520-62

Weiss J. 2003. Bactericidal/permeability-increasing protein (BPI) and lipopolysaccharide-binding protein (LBP): structure, function and regulation in host defence against Gram-negative bacteria. *Biochemical Society Transactions* 31: 785-90

Weston WM, LeClair EE, Trzyna W, McHugh KM, Nugent P, et al. 1999. Differential display identification of plunc, a novel gene expressed in embryonic palate, nasal epithelium, and adult lung. *Journal of Biological Chemistry* 274: 13698-703

Wheeler TT, Haigh BJ, Broadhurst MK, Hood KA, Maqbool NJ. 2011. The BPI-like/PLUNC family proteins in cattle. *Biochemical Society Transactions* 39: 1006-11

WHO. 2015. Deafness and Hearing Loss fact sheet. pp. 05/09/16

Woo JI, Oh S, Lim D, Moon S. 2012. ERK2-dependent activation of c-Jun is required for nontypeable H. influenzae-induced Cxcl2 up-regulation in the inner ear fibrocytes. *Faseb Journal* 26: 1

Woodfield G, Dugdale A. 2008. Evidence behind the WHO guidelines: Hospital care for children: What is the most effective antibiotic regime for chronic suppurative otitis media in children. *Journal of Tropical Pediatrics* 54: 151-56

Woodworth BA, Antunes MB, Bhargave G, Palmer JN, Cohen NA. 2007. Murine tracheal and nasal septal epithelium for air-liquid interface cultures: A comparative study. *American Journal of Rhinology* 21: 533-37

Wright JR. 1997. Immunomodulatory functions of surfactant. *Physiological Reviews* 77: 931-62

Wright PL, Yu J, Di YPP, Homer RJ, Chupp G, et al. 2010. Epithelial reticulon 4B (Nogo-B) is an endogenous regulator of Th2-driven lung inflammation. *Journal of Experimental Medicine* 207: 2595-607

Wu Q, Lu Z, Verghese MW, Randell SH. 2005. Airway epithelial cell tolerance to Pseudomonas aeruginosa. *Respiratory Research* 6

Wu R, Zhao YH, Chang MMJ. 1997. Growth and differentiation of conducting airway epithelial cells in culture. *European Respiratory Journal* 10: 2398-403

Xu J, Zong Y, Li X, Zhang Y, Li J. 2015. Divergent expression of alpha-ENaC in middle ear mucosa in the course of otitis media with effusion induced by barotrauma. *Acta Oto-Laryngologica* 135: 651-54

Xu XB, Woo CH, Steere RR, Lee BC, Huang YX, et al. 2012. EVI1 Acts as an Inducible Negative-Feedback Regulator of NF-kappa B by Inhibiting p65 Acetylation. *Journal of Immunology* 188: 6371-80

Yamaya M, Finkbeiner WE, Chun SY, Widdicombe JH. 1992. DIFFERENTIATED STRUCTURE AND FUNCTION OF CULTURES FROM HUMAN TRACHEAL EPITHELIUM. *American Journal of Physiology* 262: L713-L24

Yeh TH, Tsai CH, Chen YS, Hsu WC, Cheng CH, et al. 2007. Increased communication among nasal epithelial cells in air-liquid interface culture. *Laryngoscope* 117: 1439-44

Yin H, Xue W, Chen S, Bogorad RL, Benedetti E, et al. 2014. Genome editing with Cas9 in adult mice corrects a disease mutation and phenotype. *Nature Biotechnology* 32: 551-53

You Y, Brody SL. 2013. Culture and differentiation of mouse tracheal epithelial cells. *Methods in molecular biology (Clifton, N.J.)* 945: 123-43

You YJ, Richer EJ, Huang T, Brody SL. 2002. Growth and differentiation of mouse tracheal epithelial cells: selection of a proliferative population. *American Journal of Physiology-Lung Cellular and Molecular Physiology* 283: L1315-L21

Yuasa H, Oike Y, Iwama A, Nishikata I, Sugiyama D, et al. 2005. Oncogenic transcription factor Evi1 regulates hematopoietic stem cell proliferation through GATA-2 expression. *Embo Journal* 24: 1976-87

Zhou H-D, Li X-L, Li G-Y, Zhou M, Liu H-Y, et al. 2008. Effect of SPLUNC1 protein on the Pseudomonas aeruginosa and Epstein-Barr virus. *Molecular and Cellular Biochemistry* 309: 191-97

APPENDIX I

Table S3: Solutions used for IHC

Solution	Constituents	Amount
Phosphate Buffered Saline (PBS) pH 7.5	NaCl (Sigma-Aldrich)	42.4 g
	Sodium phosphate (dibasic) (Fischer Scientific)	7.12 g
	Potassium phosphate (monobasic) (Sigma , UK)	1.25 g
0.01 M Sodium Citrate	Sodium Citrate (Sigma)	1.18 g
	Distilled water	400 ml
Biotinylated Secondary antibody	PBS	10 ml
	100% normal goat serum	150 µl
	Concentrated biotinylated secondary antibody	50 µl
VECTASTAIN Elite ABC reagent	PBS	5 ml
	Reagent A	100 µl
	Reagent B	100 µl
VECTOR Nova Red Coloring reagent	Distilled water	5 ml
	Solution A	150 µl
	Solution B	100 µl
	Solution C	100 µl
	Solution D	100 µl

Table S4: Solutions used for Western blotting

Solution	Constituents	Amount
10 X Running Buffer	Tris Base (Fischer Scientific)	30.3 g
	Glycine (Fischer Scientific)	190 g
	20 % SDS (Sigma-Aldrich)	50 mls
	Distilled water	Make up vol 1000 ml
1 X Running Buffer	10 X Running Buffer	100 ml
	Distilled water	900 ml
1 X Transfer Buffer	Tris Base (Fischer Scientific)	2.9 g
	Glycine (Fischer Scientific)	1.45 g
	20 % SDS (Sigma-Aldrich)	925 µl
1 X TBS- TWEEN	Tris HCl pH 8 (BioRad)	100 ml
	NaCl (Sigma-Aldrich Co)	97.3 g
	Tween – 20 (Fischer Scientific, UK)	5 ml
	Distilled water	Make up vol 1000ml
EZ- ECL chemiluminescence reagent	Solution A	1 ml
	Solution B	1ml
2 X Lysis buffer	1M DTT	1 ml
	20 % SDS (Sigma-Aldrich)	1ml
	Glycerol	2 ml
	Tris HCl 0.5M pH 6.8 (BioRad)	1.25 ml
	0.2 % Bromophenol blue	200 µl
	Protease inhibitor	1 tablet
	Distilled water	4.55 ml

Table S3: Solutions for Weigert's Haematoxylin

Solution	Constituents	Amount
Weigert's Solution A	Haematoxylin (VWR)	1 g
	IDA (Genta)	100 ml
Weigert's Solution B	30% aqueous ferric chloride(BDH)	4 ml
	Distilled water	100 ml
	Concentrated HCL (VWR)	1 ml

APPENDIX II

Table S4 A: Detailed histology screen for 6 month old *Bpifa1*$^{-/-}$ mice Part 1 (n=6)

Mouse i.d	SPLUNC-C3-IC/3.3D	3.3G	4.3C	4.3D	4.3F	6.2b
Salivary gl	lymphoid agg	LA	nad	LA	LA	nad
trachea thyroid para	absent	nad	peri trach muscle sol focus myofiber regen	trach thyroid nad parat absent	trach thyroid nad parat absent	
LN	nad	absent	absent	absent	nad	nad
skin	nad	absent	absent		absent	absent
lung	1 sub pleural lymphoid agg.	1 peri bronch LA	nad	1 peribronch LA	3 peribronch LA	1 peribronch LA
heart	nad	nad	nad	nad	nad	nad
tongue	scatt mast cells	scatt mast cells	scatt mc	scatt mc	scatt mc	scatt mc
kidney	nad	nad	nad	nad	nad	sol focus mineraliz
adrenal	x zone vac, sub cap hyperpl	x zone vac	tang cut x zone vac, sub cap hyperpl	cortex only sub cap hyperpl	x zone vac, sub cap hyperpl	x zone vac, sub cap hyperpl
liver	glycogen accumuation	gly accum. gall bladder nad	gly accum. gall bladder nad	glycogen accumuation	glycogen accumuation	glyc and scatt fat accumuation
LN	nad	nad	absent	pancreatic LN nad	absent	absent
spleen	consp. megakaryocytes	consp. megakary.	artef. Sub cap rarefaction	red pulp congestion	artef. Sub cap rarefaction	artef. Sub cap rare and pigment macroph
exoc pancreas	scatt fat cells	scatt fat cells	scatt fat cells	scatt fat cells	focal autolysis	nad

Mouse i.d	SPLUNC-C3-IC/3.3D	3.3G	4.3C	4.3D	4.3F	6.2b
islet	nad	1 islet cavitated	nad	nad	nad	nad
thymus	absent	absent	absent	nad	absent	nad
stomach	nad	nad	nad	nad	nad	nad
SI	nad	nad	nad	nad	nad	nad
LI	nad	apopt cells over Peyers patch	nad	nad	nad	nad
islet	nad	nad	nad	nad	nad	nad
exoc pancreas	nad	scatt fat cells	artef degen + fat cells	nad	nad	nad
esophagus	nad	nad	nad	nad	nad	nad
perineal skin	nad	nad	nad	nad	nad	nad
vagina	nad	nad	normal NLs	nad	normal NLs	focal intraepith normal NLs
uterus	nad	nad	nad	nad	nad	tangential sectins
urinary bladder	nad	nad	absent	absent	nad	nad
skin	nad	nad	nad	nad	nad	nad
muscle	nad	nad	nad	nad	nad	nad
eyes	retinal degeneration	RD	nad	nad	nad	RD
optic nerve	nad	nad	nad	nad	absent	nad
cerebell brain stem	nad	nad	small sect. nad	dark na	dark na	dark na
thalamus cortex x2	dark neuron artefact	1 focus perivasc mast cells	dark na	dark na	dark na	dark na
rostral cortex	nad	dark na	dark na	dark na	dark na	dark na

Mouse i.d	SPLUNC-C3-IC/3.3D	3.3G	4.3C	4.3D	4.3F	6.2b
cord x3	dark neuron artefact	dark na	dark na	dark na	dark na	dark na
pituitary	absent	pars distalis only nad	nad	pars distalis and nervosa nad	pd pi pn nad	pd pi only nad
nerve sciatic	nad	nad	small sect. nad	small sect. nad	nad	nad
knee	closed growth plate	closed growth plate	closed growth plate	closed growth plate	closed growth plate	closed growth plate foc degen
veterbra	degen inter vert cartilage	degen inter vert cartilage	degen inter vert cartilage	degen inter vert cartilage	degen inter vert cartilage	degen inter vert cartilage
rostral snout	nad	nad ?orientation	nad	nad	nad	nad
mid snout	vm organ conspic blood vasculature	nad	fluid nasolacrymal tube	nad	nad	nad
caudal nasal passages	nad includes harderian gland	nad	nad	nad includes harderian gland	nad	nad
ovary	nad	nad	nad	one absent other nad	nad	nad
tube	nad	nad	nad	nad	nad	nad
ME	unilat eosinophilic secretion few detach cells	nad	unilat eosinophilic secretion few detach cells	unilat eosinophilic secretion few detach cells	one bulla superfical cut nad	nad
oropharynx	nad	nad	nad	nad	nad	nad
teeth	nad	nad	nad	nad	nad	nad

Table S4 B: Detailed histology screen for 6 month old *Bpifa1*$^{-/-}$ mice Part 1 (n=7)

Mouse i.d	6.2F	1.7A	1.7B	4.3H	6.2J	6.2N	6.2K
Salivary gl	nad	nad	nad	nad	nad	nad	nad
trachea thyroid para	widely patent tracheal glands with ciliated epith, thyroid nad para absent	conspicuous tracheal gland, thryroid nad	nad para absent	trachea thyroid para nad	trachea thyroid para nad	trachea thyroid nad	trachea thyroid nad
LN	absent	nad	nad	nad	nad	nad	nad
skin	absent	absent	nad	absent	absent	absent	absent
lung	1 sub pleural LA	airway consp epithcell cytoplasm	nad	nad	nad	focal subcap lymphoid cells otherwise NAD	
heart	nad	nad	nad	nad	nad	nad	nad
tongue	scatt mc	scatt mc	scatt mc	scatt mc	scatt mc	scatt mc	scatt mc
kidney	sol focus mineraliz	nad	nad	nad tub vac	nad tub vac	nad tub vac	nad tub vac
adrenal	x zone vac, sub cap hyperpl	both tangential x zone vac, sub cap hyperpl	both tangential x zone vac	nad	intra medul ?BV widely patent	nad, tangential	tangential, tangential
liver	glyc accum	absent	glyc accum	nad	nad	glyc accumulation gall bladder nad	glyc accumulation gall bladder nad
LN	nad	nad	absent	nad	absent	nad	nad
spleen	nad	absent	nad	nad	nad	nad	nad
exoc pancreas	nad	nad	scatt fat cells	nad	nad	nad	nad

Mouse i.d	6.2F	1.7A	1.7B	4.3H	6.2J	6.2N	6.2K
islet	scatt fat cells	nad	nad	nad	nad	some have conspicuous capillaries	some have conspicuous capillaries
thymus	nad	nad	nad	nad	nad	absent	nad
stomach	nad	nad	nad	nad	nad	nad	nad
SI	nad	nad	nad	nad	nad	nad	nad
LI	nad	nad	nad	nad	nad	nad	nad
islet	nad	absent	absent	nad	absnt	absent	absent
exoc pancreas	nad	absent	nad	nad	nad	absent	absent
esophagus	nad	nad	nad	nad	nad	nad	nad
perineal skin	nad	nad	absent	MALE	MALE	MALE	MALE
vagina	absent	nad	nad	prostate, coag gl seminal ves nad	vas defr, prostate, coag gl seminal ves nad	vas defr, prostate focal dilation effete cells in lumen, coag gl seminal ves nad	vas defr, prostate, coag gl seminal ves nad
uterus	nad	nad	nad	edpidymis testis nad	edpidymis testis nad	edpidymis testis nad	edpidymis nad testis occasional tubule degen cells multinucleates
urinary bladder	nad	nad	basophlic atrefact	nad	nad	nad	nad
skin	nad	nad	nad	nad	nad	nad	nad
muscle	nad	altered focus	nad	nad	nad	nad	nad
eyes	nad (1 only)	nad	rd	nad	rd	nad	rd

Mouse i.d	6.2F	1.7A	1.7B	4.3H	6.2J	6.2N	6.2K
optic nerve	absent	nad	rd	nad	rd	tangential retina nad	rd
cerebell brain stem	dark na	dark na	dark na	dark na	dark na	dark na	dark na
thalamus cortex x2	dark na	dark na	dark na	mineralization	dark na	dark na	dark na
rostral cortex	focal cort cells	focal cort cells	dark na	dark na	dark na	dark na	dark na
cord x3	dark na	dark na	dark na	dark na	dark na	dark na	dark na
pituitary	pd pi pn nad	pd pi nad pn edge	pd pi pn nad	pd pi pn nad	pd pi pn nad	pd pi pn nad	pd pi pn nad
nerve sciatic	artef frag nad	nad	nad	nad	nad	nad	nad
knee	closed growth plate	closed growth plate	closed growth plate	closed growth plate	closed growth plate	closed growth plate focal degen cart	closed growth plate focal cart. Degen
veterbra	degen inter vert cartilage	degen inter vert cartilage	nad	nad	degen inter vert cartilage	degen inter vert cartilage	degen inter vert cartilage
rostral snout	few squames + NL	nad	nad	nad	nad	nad	nad
mid snout	nad	nad	nad	nad	nad	nad	nad
caudal nasal passages	nad	nad	eosinophilic material	nad	nad	nad	nad
ovary	nad	nad	nad	MALE	MALE	MALE	
tube	absent	nad	nad				
ME	nad nasopharynx nad	nad nasopharynx nad	nad	nad	missing	nad	nad

Mouse i.d	6.2F	1.7A	1.7B	4.3H	6.2J	6.2N	6.2K
oropharynx	absent	nad	nad	absent	slide	absent	absent
teeth	absent	nad	nad	nad		nad	nad

Abbreviations for histology analysis	
nad	no abnormality detected
dark na	dark neurone artefact
focal cortical cells	
tang cut	tangential cut
x zone vac	x zone vacuolatiion = female specific change
sub cap hyp	sub capsular hyperplasia
degen inter vert cartilage	degeneration of intervertebral cartilage
pi	pars intermedia
pn	pars nervosa
pd	pars distalis

****Most of the abbreviations record that the concerned tissue was examined and nothing or only incidental non-pathological changes were noted.**

APPENDIX III

Table S5 Top 500 proteins detected by MS analysis of Wt ALI Day mMEC washes

Accession Number	Protein Name (Wt ALI Day 14 mMECs)	Gene name	Peptide count	emPAI
P08071	Lactotransferrin	TRFL_MOUSE	47	202.53
Q921I1	Serotransferrin	TRFE_MOUSE	40	29.58
O09131	Glutathione S-transferase omega-1	GSTO1_MOUSE	17	28.64
P60710	Actin, cytoplasmic 1	ACTB_MOUSE	23	24.63
P50446	Keratin, type II cytoskeletal 6A	K2C6A_MOUSE	35	19.14
P08074	Carbonyl reductase [NADPH] 2	CBR2_MOUSE	16	19.04
Q9Z331	Keratin, type II cytoskeletal 6B	K2C6B_MOUSE	36	18.18
P62806	Histone H4	H4_MOUSE	6	17.1
P10107	Annexin A1	ANXA1_MOUSE	24	14.87
P11679	Keratin, type II cytoskeletal 8	K2C8_MOUSE	33	14.67
P19001	Keratin, type I cytoskeletal 19	K1C19_MOUSE	35	14.07
Q61781	Keratin, type I cytoskeletal 14	K1C14_MOUSE	35	13
O09049	Regenerating islet-derived protein 3-gamma	REG3G_MOUSE	8	11.38
P35700	Peroxiredoxin-1	PRDX1_MOUSE	14	11.13
Q06890	Clusterin	CLUS_MOUSE	22	10.47
P11672	Neutrophil gelatinase-associated lipocalin	NGAL_MOUSE	9	10.45
Q61147	Ceruloplasmin	CERU_MOUSE	55	10.1
Q61414	Keratin, type I cytoskeletal 15	K1C15_MOUSE	32	9.92
P17742	Peptidyl-prolyl cis-trans isomerase A	PPIA_MOUSE	14	9.81
Q922U2	Keratin, type II cytoskeletal 5	K2C5_MOUSE	34	8.7
Q9QWL7	Keratin, type I cytoskeletal 17	K1C17_MOUSE	33	7.76
O08709	Peroxiredoxin-6	PRDX6_MOUSE	15	7.38
P10649	Glutathione S-transferase Mu 1	GSTM1_MOUSE	18	6.68
P07356	Annexin A2	ANXA2_MOUSE	23	6.63
P52480	Pyruvate kinase PKM	KPYM_MOUSE	36	6.57
P68372	Tubulin beta-4B chain	TBB4B_MOUSE	21	6.13
Q6ZWY9	Histone H2B type 1-C/E/G	H2B1C_MOUSE	11	6.12
Q8BND5	Sulfhydryl oxidase 1	QSOX1_MOUSE	43	6.1
Q9DCV7	Keratin, type II cytoskeletal 7	K2C7_MOUSE	35	6.01
P16858	Glyceraldehyde-3-phosphate dehydrogenase	G3P_MOUSE	21	5.87
Q61398	Procollagen C-endopeptidase enhancer 1	PCOC1_MOUSE	23	5.56
P07744	Keratin, type II cytoskeletal 4	K2C4_MOUSE	31	5.43
O35639	Annexin A3	ANXA3_MOUSE	24	5.16
P68033	Actin, alpha cardiac muscle 1	ACTC_MOUSE	23	5.06
P26040	Ezrin	EZRI_MOUSE	39	5.04
P99024	Tubulin beta-5 chain	TBB5_MOUSE	21	4.94
Q05816	Fatty acid-binding protein, epidermal	FABP5_MOUSE	9	4.92

Accession Number	Protein Name (Wt ALI Day 14 mMECs)	Gene name	Peptide count	emPAI
P08249	Malate dehydrogenase, mitochondrial	MDHM_MOUSE	24	4.77
P97361	BPI fold-containing family A member 1	BPIA1_MOUSE	9	4.74
P01027	Complement C3	CO3_MOUSE	111	4.68
Q8BGZ7	Keratin, type II cytoskeletal 75	K2C75_MOUSE	36	4.22
P56480	ATP synthase subunit beta, mitochondrial	ATPB_MOUSE	30	4.18
P62830	60S ribosomal protein L23	RL23_MOUSE	10	4.08
P05784	Keratin, type I cytoskeletal 18	K1C18_MOUSE	32	3.99
P50543	Protein S100-A11	S10AB_MOUSE	5	3.92
P28654	Decorin	PGS2_MOUSE	23	3.86
P40142	Transketolase	TKT_MOUSE	34	3.7
Q9QUI0	Transforming protein RhoA	RHOA_MOUSE	13	3.7
Q8VCT4	Carboxylesterase 1D	CES1D_MOUSE	27	3.69
Q9Z2K1	Keratin, type I cytoskeletal 16	K1C16_MOUSE	35	3.64
P57780	Alpha-actinin-4	ACTN4_MOUSE	61	3.61
P17563	Selenium-binding protein 1	SBP1_MOUSE	31	3.49
P17182	Alpha-enolase	ENOA_MOUSE	28	3.36
P11499	Heat shock protein HSP 90-beta	HS90B_MOUSE	40	3.31
P08730	Keratin, type I cytoskeletal 13	K1C13_MOUSE	31	3.29
P14211	Calreticulin	CALR_MOUSE	27	3.28
Q9D379	Epoxide hydrolase 1	HYEP_MOUSE	29	3.27
P63017	Heat shock cognate 71 kDa protein	HSP7C_MOUSE	37	3.24
Q00493	Carboxypeptidase E	CBPE_MOUSE	28	3.17
P06797	Cathepsin L1	CATL1_MOUSE	12	3.11
P62962	Profilin-1	PROF1_MOUSE	9	3.1
P27773	Protein disulfide-isomerase A3	PDIA3_MOUSE	35	3.05
P62908	40S ribosomal protein S3	RS3_MOUSE	19	3.05
Q7TMM9	Tubulin beta-2A chain	TBB2A_MOUSE	21	3.03
Q8VDD5	Myosin-9	MYH9_MOUSE	127	3.03
P09103	Protein disulfide-isomerase	PDIA1_MOUSE	39	3.02
P68368	Tubulin alpha-4A chain	TBA4A_MOUSE	22	2.99
P68373	Tubulin alpha-1C chain	TBA1C_MOUSE	22	2.99
Q8VED5	Keratin, type II cytoskeletal 79	K2C79_MOUSE	32	2.98
Q61805	Lipopolysaccharide-binding protein	LBP_MOUSE	19	2.96
Q9Z1Q5	Chloride intracellular channel protein 1	CLIC1_MOUSE	17	2.96
Q07797	Galectin-3-binding protein	LG3BP_MOUSE	26	2.94
Q61646	Haptoglobin	HPT_MOUSE	20	2.94
Q7TPR4	Alpha-actinin-1	ACTN1_MOUSE	60	2.92
P62821	Ras-related protein Rab-1A	RAB1A_MOUSE	18	2.9
O88844	Isocitrate dehydrogenase [NADP] cytoplasmic	IDHC_MOUSE	30	2.87
P08228	Superoxide dismutase [Cu-Zn]	SODC_MOUSE	11	2.78
P18760	Cofilin-1	COF1_MOUSE	12	2.72
P19157	Glutathione S-transferase P 1	GSTP1_MOUSE	10	2.71
Q9R0P5	Destrin	DEST_MOUSE	13	2.7

Accession Number	Protein Name (Wt ALI Day 14 mMECs)	Gene name	Peptide count	emPAI
P06151	L-lactate dehydrogenase A chain	LDHA_MOUSE	23	2.62
P20029	78 kDa glucose-regulated protein	GRP78_MOUSE	39	2.61
P10126	Elongation factor 1-alpha 1	EF1A1_MOUSE	23	2.54
Q60605	Myosin light polypeptide 6	MYL6_MOUSE	11	2.51
Q62159	Rho-related GTP-binding protein RhoC	RHOC_MOUSE	11	2.5
Q9D1G1	Ras-related protein Rab-1B	RAB1B_MOUSE	17	2.5
P07901	Heat shock protein HSP 90-alpha	HS90A_MOUSE	39	2.47
P10605	Cathepsin B	CATB_MOUSE	15	2.47
P68040	Guanine nucleotide-binding protein subunit beta-2-like 1	GBLP_MOUSE	22	2.47
P97429	Annexin A4	ANXA4_MOUSE	22	2.4
Q64669	NAD(P)H dehydrogenase [quinone] 1	NQO1_MOUSE	15	2.38
O54974	Galectin-7	LEG7_MOUSE	10	2.33
P33267	Cytochrome P450 2F2	CP2F2_MOUSE	29	2.3
P47739	Aldehyde dehydrogenase, dimeric NADP-preferring	AL3A1_MOUSE	25	2.29
Q61508	Extracellular matrix protein 1	ECM1_MOUSE	37	2.29
Q9R0P3	S-formylglutathione hydrolase	ESTD_MOUSE	16	2.28
P47738	Aldehyde dehydrogenase, mitochondrial	ALDH2_MOUSE	26	2.24
P17751	Triosephosphate isomerase	TPIS_MOUSE	18	2.19
P63038	60 kDa heat shock protein, mitochondrial	CH60_MOUSE	36	2.16
Q61362	Chitinase-3-like protein 1	CH3L1_MOUSE	22	2.16
P25785	Metalloproteinase inhibitor 2	TIMP2_MOUSE	14	2.08
Q8BFZ3	Beta-actin-like protein 2	ACTBL_MOUSE	24	2.08
Q9DCW4	Electron transfer flavoprotein subunit beta	ETFB_MOUSE	14	2.08
P63101	14-3-3 protein zeta/delta	1433Z_MOUSE	19	2.07
Q03265	ATP synthase subunit alpha, mitochondrial	ATPA_MOUSE	36	2.07
Q62266	Cornifin-A	SPR1A_MOUSE	13	2.01
P21956	Lactadherin	MFGM_MOUSE	23	1.99
P15626	Glutathione S-transferase Mu 2	GSTM2_MOUSE	18	1.97
Q9CQV3	Serpin B11	SPB11_MOUSE	24	1.97
P63242	Eukaryotic translation initiation factor 5A-1	IF5A1_MOUSE	8	1.93
P11276	Fibronectin	FINC_MOUSE	108	1.84
P51881	ADP/ATP translocase 2	ADT2_MOUSE	21	1.84
P05064	Fructose-bisphosphate aldolase A	ALDOA_MOUSE	23	1.82
Q01853	Transitional endoplasmic reticulum ATPase	TERA_MOUSE	45	1.82
P70296	Phosphatidylethanolamine-binding protein 1	PEBP1_MOUSE	9	1.81
P21981	Protein-glutamine gamma-glutamyltransferase 2	TGM2_MOUSE	36	1.79
P26043	Radixin	RADI_MOUSE	39	1.79
P62245	40S ribosomal protein S15a	RS15A_MOUSE	11	1.76

Accession Number	Protein Name (Wt ALI Day 14 mMECs)	Gene name	Peptide count	emPAI
Q6IFX2	Keratin, type I cytoskeletal 42	K1C42_MOUSE	33	1.75
Q9DCD0	6-phosphogluconate dehydrogenase, decarboxylating	6PGD_MOUSE	29	1.74
P54116	Erythrocyte band 7 integral membrane protein	STOM_MOUSE	17	1.71
P26041	Moesin	MOES_MOUSE	40	1.7
P18242	Cathepsin D	CATD_MOUSE	20	1.67
Q923D2	Flavin reductase (NADPH)	BLVRB_MOUSE	13	1.65
Q9R0Q7	Prostaglandin E synthase 3	TEBP_MOUSE	9	1.65
P23492	Purine nucleoside phosphorylase	PNPH_MOUSE	19	1.64
Q60932	Voltage-dependent anion-selective channel protein 1	VDAC1_MOUSE	18	1.64
Q9D051	Pyruvate dehydrogenase E1 component subunit beta, mitochondrial	ODPB_MOUSE	18	1.63
Q9WVA4	Transgelin-2	TAGL2_MOUSE	14	1.63
P37040	NADPH--cytochrome P450 reductase	NCPR_MOUSE	35	1.6
P61027	Ras-related protein Rab-10	RAB10_MOUSE	17	1.6
P67778	Prohibitin	PHB_MOUSE	18	1.58
P56382	ATP synthase subunit epsilon, mitochondrial	ATP5E_MOUSE	4	1.56
O88312	Anterior gradient protein 2 homolog	AGR2_MOUSE	10	1.53
P24369	Peptidyl-prolyl cis-trans isomerase B	PPIB_MOUSE	15	1.51
P50404	Pulmonary surfactant-associated protein D	SFTPD_MOUSE	23	1.5
P48678	Prelamin-A/C	LMNA_MOUSE	46	1.47
P61750	ADP-ribosylation factor 4	ARF4_MOUSE	12	1.47
Q61176	Arginase-1	ARGI1_MOUSE	18	1.47
Q8BSL7	ADP-ribosylation factor 2	ARF2_MOUSE	12	1.45
P62827	GTP-binding nuclear protein Ran	RAN_MOUSE	11	1.44
P10810	Monocyte differentiation antigen CD14	CD14_MOUSE	16	1.41
Q9CRB3	5-hydroxyisourate hydrolase	HIUH_MOUSE	7	1.41
Q61598	Rab GDP dissociation inhibitor beta	GDIB_MOUSE	28	1.4
P24549	Retinal dehydrogenase 1	AL1A1_MOUSE	23	1.39
P38647	Stress-70 protein, mitochondrial	GRP75_MOUSE	43	1.39
Q61468	Mesothelin	MSLN_MOUSE	29	1.38
Q9QYB1	Chloride intracellular channel protein 4	CLIC4_MOUSE	17	1.38
P24472	Glutathione S-transferase A4	GSTA4_MOUSE	12	1.36
Q8BFU2	Histone H2A type 3	H2A3_MOUSE	7	1.36
O35129	Prohibitin-2	PHB2_MOUSE	26	1.35
O88569	Heterogeneous nuclear ribonucleoproteins A2/B1	ROA2_MOUSE	19	1.33
P47911	60S ribosomal protein L6	RL6_MOUSE	19	1.33
Q9CPV4	Glyoxalase domain-containing protein 4	GLOD4_MOUSE	22	1.33
Q9WV54	Acid ceramidase	ASAH1_MOUSE	21	1.33
Q8BPB5	EGF-containing fibulin-like extracellular matrix protein 1	FBLN3_MOUSE	27	1.31

Accession Number	Protein Name (Wt ALI Day 14 mMECs)	Gene name	Peptide count	emPAI
Q8VDN2	Sodium/potassium-transporting ATPase subunit alpha-1	AT1A1_MOUSE	53	1.27
P97461	40S ribosomal protein S5	RS5_MOUSE	10	1.25
Q60931	Voltage-dependent anion-selective channel protein 3	VDAC3_MOUSE	17	1.25
Q64433	10 kDa heat shock protein, mitochondrial	CH10_MOUSE	10	1.25
Q62426	Cystatin-B	CYTB_MOUSE	6	1.24
Q99LC5	Electron transfer flavoprotein subunit alpha, mitochondrial	ETFA_MOUSE	23	1.24
P47757	F-actin-capping protein subunit beta	CAPZB_MOUSE	20	1.22
P51174	Long-chain specific acyl-CoA dehydrogenase, mitochondrial	ACADL_MOUSE	24	1.21
P08207	Protein S100-A10	S10AA_MOUSE	5	1.2
P84228	Histone H3.2	H32_MOUSE	6	1.2
Q9CR57	60S ribosomal protein L14	RL14_MOUSE	12	1.2
P09411	Phosphoglycerate kinase 1	PGK1_MOUSE	29	1.18
Q6IFZ6	Keratin, type II cytoskeletal 1b	K2C1B_MOUSE	39	1.18
P62267	40S ribosomal protein S23	RS23_MOUSE	8	1.15
Q91VR2	ATP synthase subunit gamma, mitochondrial	ATPG_MOUSE	17	1.15
Q9CQI6	Coactosin-like protein	COTL1_MOUSE	10	1.14
Q9D8N0	Elongation factor 1-gamma	EF1G_MOUSE	27	1.14
P10639	Thioredoxin	THIO_MOUSE	7	1.12
P84084	ADP-ribosylation factor 5	ARF5_MOUSE	13	1.12
P62264	40S ribosomal protein S14	RS14_MOUSE	6	1.11
Q9ER10	Brain-specific serine protease 4	BSSP4_MOUSE	15	1.11
Q91VI7	Ribonuclease inhibitor	RINI_MOUSE	27	1.1
P62702	40S ribosomal protein S4, X isoform	RS4X_MOUSE	20	1.09
P62717	60S ribosomal protein L18a	RL18A_MOUSE	14	1.09
P97351	40S ribosomal protein S3a	RS3A_MOUSE	19	1.08
Q99JY9	Actin-related protein 3	ARP3_MOUSE	21	1.08
P17879	Heat shock 70 kDa protein 1B	HS71B_MOUSE	37	1.07
P60766	Cell division control protein 42 homolog	CDC42_MOUSE	9	1.06
O88342	WD repeat-containing protein 1	WDR1_MOUSE	37	1.05
P08905	Lysozyme C-2	LYZ2_MOUSE	10	1.05
P29758	Ornithine aminotransferase, mitochondrial	OAT_MOUSE	23	1.05
P15532	Nucleoside diphosphate kinase A	NDKA_MOUSE	12	1.03
P48036	Annexin A5	ANXA5_MOUSE	25	1.03
P51410	60S ribosomal protein L9	RL9_MOUSE	11	1.03
Q61171	Peroxiredoxin-2	PRDX2_MOUSE	10	1.03
Q01768	Nucleoside diphosphate kinase B	NDKB_MOUSE	12	1.02
Q8K354	Carbonyl reductase [NADPH] 3	CBR3_MOUSE	20	1.02
Q91XV3	Brain acid soluble protein 1	BASP1_MOUSE	10	1.02
P62889	60S ribosomal protein L30	RL30_MOUSE	8	1.01
P99029	Peroxiredoxin-5, mitochondrial	PRDX5_MOUSE	15	1.01

Accession Number	Protein Name (Wt ALI Day 14 mMECs)	Gene name	Peptide count	emPAI
Q00612	Glucose-6-phosphate 1-dehydrogenase X	G6PD1_MOUSE	35	1.01
P14152	Malate dehydrogenase, cytoplasmic	MDHC_MOUSE	21	1
Q68FD5	Clathrin heavy chain 1	CLH1_MOUSE	95	0.99
Q6ZWN5	40S ribosomal protein S9	RS9_MOUSE	14	0.99
P60843	Eukaryotic initiation factor 4A-I	IF4A1_MOUSE	23	0.98
Q60930	Voltage-dependent anion-selective channel protein 2	VDAC2_MOUSE	16	0.98
Q9WV32	Actin-related protein 2/3 complex subunit 1B	ARC1B_MOUSE	19	0.98
P16110	Galectin-3	LEG3_MOUSE	10	0.97
P35441	Thrombospondin-1	TSP1_MOUSE	70	0.97
P05202	Aspartate aminotransferase, mitochondrial	AATM_MOUSE	29	0.95
P48962	ADP/ATP translocase 1	ADT1_MOUSE	22	0.95
P58252	Elongation factor 2	EF2_MOUSE	52	0.95
P62281	40S ribosomal protein S11	RS11_MOUSE	10	0.94
P62874	Guanine nucleotide-binding protein G(I)/G(S)/G(T) subunit beta-1	GBB1_MOUSE	13	0.94
Q9WTY4	Aquaporin-5	AQP5_MOUSE	8	0.94
Q9Z0K8	Pantetheinase	VNN1_MOUSE	23	0.94
O70435	Proteasome subunit alpha type-3	PSA3_MOUSE	14	0.93
P53994	Ras-related protein Rab-2A	RAB2A_MOUSE	15	0.93
Q3UV17	Keratin, type II cytoskeletal 2 oral	K22O_MOUSE	39	0.93
P35486	Pyruvate dehydrogenase E1 component subunit alpha, somatic form, mitochondrial	ODPA_MOUSE	25	0.92
P47791	Glutathione reductase, mitochondrial	GSHR_MOUSE	25	0.91
Q9DAU7	WAP four-disulfide core domain protein 2	WFDC2_MOUSE	6	0.91
P24452	Macrophage-capping protein	CAPG_MOUSE	14	0.9
P62259	14-3-3 protein epsilon	1433E_MOUSE	18	0.9
Q9CZM2	60S ribosomal protein L15	RL15_MOUSE	14	0.9
P11214	Tissue-type plasminogen activator	TPA_MOUSE	31	0.89
P62242	40S ribosomal protein S8	RS8_MOUSE	10	0.89
Q8BG05	Heterogeneous nuclear ribonucleoprotein A3	ROA3_MOUSE	20	0.89
Q9WUU7	Cathepsin Z	CATZ_MOUSE	14	0.89
P04104	Keratin, type II cytoskeletal 1	K2C1_MOUSE	35	0.88
Q61581	Insulin-like growth factor-binding protein 7	IBP7_MOUSE	18	0.88
P08113	Endoplasmin	ENPL_MOUSE	47	0.87
Q3THE2	Myosin regulatory light chain 12B	ML12B_MOUSE	11	0.86
Q6ZWV3	60S ribosomal protein L10	RL10_MOUSE	13	0.86
P27659	60S ribosomal protein L3	RL3_MOUSE	22	0.85
P62331	ADP-ribosylation factor 6	ARF6_MOUSE	9	0.85
P63323	40S ribosomal protein S12	RS12_MOUSE	7	0.85
P67984	60S ribosomal protein L22	RL22_MOUSE	6	0.85

Accession Number	Protein Name (Wt ALI Day 14 mMECs)	Gene name	Peptide count	emPAI
Q80X90	Filamin-B	FLNB_MOUSE	146	0.85
Q99LX0	Protein DJ-1	PARK7_MOUSE	13	0.85
P06745	Glucose-6-phosphate isomerase	G6PI_MOUSE	32	0.84
P16460	Argininosuccinate synthase	ASSY_MOUSE	25	0.84
P48758	Carbonyl reductase [NADPH] 1	CBR1_MOUSE	19	0.84
Q6ZWU9	40S ribosomal protein S27	RS27_MOUSE	5	0.83
Q91YQ5	Dolichyl-diphosphooligosaccharide--protein glycosyltransferase subunit 1	RPN1_MOUSE	40	0.83
Q9CXW4	60S ribosomal protein L11	RL11_MOUSE	9	0.83
O35640	Annexin A8	ANXA8_MOUSE	23	0.82
P56395	Cytochrome b5	CYB5_MOUSE	8	0.82
Q9CZ13	Cytochrome b-c1 complex subunit 1, mitochondrial	QCR1_MOUSE	22	0.82
O88593	Peptidoglycan recognition protein 1	PGRP1_MOUSE	10	0.81
Q60854	Serpin B6	SPB6_MOUSE	23	0.81
P14069	Protein S100-A6	S10A6_MOUSE	5	0.79
P61358	60S ribosomal protein L27	RL27_MOUSE	6	0.79
P62835	Ras-related protein Rap-1A	RAP1A_MOUSE	10	0.79
P62880	Guanine nucleotide-binding protein G(I)/G(S)/G(T) subunit beta-2	GBB2_MOUSE	13	0.79
Q9QXC1	Fetuin-B	FETUB_MOUSE	17	0.79
P11983	T-complex protein 1 subunit alpha	TCPA_MOUSE	35	0.78
P14206	40S ribosomal protein SA	RSSA_MOUSE	15	0.78
P62137	Serine/threonine-protein phosphatase PP1-alpha catalytic subunit	PP1A_MOUSE	19	0.78
P62911	60S ribosomal protein L32	RL32_MOUSE	8	0.77
P70441	Na(+)/H(+) exchange regulatory cofactor NHE-RF1	NHRF1_MOUSE	27	0.77
P61514	60S ribosomal protein L37a	RL37A_MOUSE	6	0.75
P61979	Heterogeneous nuclear ribonucleoprotein K	HNRPK_MOUSE	27	0.75
P63168	Dynein light chain 1, cytoplasmic	DYL1_MOUSE	5	0.75
P68254	14-3-3 protein theta	1433T_MOUSE	18	0.75
P0CG49	Polyubiquitin-B	UBB_MOUSE	28	0.74
P40124	Adenylyl cyclase-associated protein 1	CAP1_MOUSE	30	0.74
P62196	26S protease regulatory subunit 8	PRS8_MOUSE	28	0.74
Q9CQV8	14-3-3 protein beta/alpha	1433B_MOUSE	17	0.74
Q9Z2X1	Heterogeneous nuclear ribonucleoprotein F	HNRPF_MOUSE	22	0.74
O55234	Proteasome subunit beta type-5	PSB5_MOUSE	16	0.73
P10630	Eukaryotic initiation factor 4A-II	IF4A2_MOUSE	23	0.73
P47962	60S ribosomal protein L5	RL5_MOUSE	17	0.73
P08752	Guanine nucleotide-binding protein G(i) subunit alpha-2	GNAI2_MOUSE	20	0.72
Q9CQQ7	ATP synthase F(0) complex subunit B1, mitochondrial	AT5F1_MOUSE	18	0.72
Q9DBH5	Vesicular integral-membrane protein	LMAN2_MOUSE	21	0.72

Accession Number	Protein Name (Wt ALI Day 14 mMECs)	Gene name	Peptide count	emPAI
	VIP36			
P14602	Heat shock protein beta-1	HSPB1_MOUSE	12	0.71
P99026	Proteasome subunit beta type-4	PSB4_MOUSE	11	0.71
P80316	T-complex protein 1 subunit epsilon	TCPE_MOUSE	36	0.7
P12970	60S ribosomal protein L7a	RL7A_MOUSE	16	0.69
P51150	Ras-related protein Rab-7a	RAB7A_MOUSE	17	0.69
P63330	Serine/threonine-protein phosphatase 2A catalytic subunit alpha isoform	PP2AA_MOUSE	18	0.69
P97494	Glutamate--cysteine ligase catalytic subunit	GSH1_MOUSE	34	0.69
Q8BTM8	Filamin-A	FLNA_MOUSE	143	0.69
Q99KI0	Aconitate hydratase, mitochondrial	ACON_MOUSE	41	0.69
O54734	Dolichyl-diphosphooligosaccharide--protein glycosyltransferase 48 kDa subunit	OST48_MOUSE	22	0.68
O70570	Polymeric immunoglobulin receptor	PIGR_MOUSE	38	0.68
P47955	60S acidic ribosomal protein P1	RLA1_MOUSE	4	0.68
Q8BP67	60S ribosomal protein L24	RL24_MOUSE	10	0.68
Q91V41	Ras-related protein Rab-14	RAB14_MOUSE	15	0.68
Q9D154	Leukocyte elastase inhibitor A	ILEUA_MOUSE	23	0.68
Q9JII6	Alcohol dehydrogenase [NADP(+)]	AK1A1_MOUSE	23	0.68
P60122	RuvB-like 1	RUVB1_MOUSE	22	0.66
Q93092	Transaldolase	TALDO_MOUSE	23	0.66
Q99020	Heterogeneous nuclear ribonucleoprotein A/B	ROAA_MOUSE	14	0.66
Q9D2Q8	Protein S100-A14	S10AE_MOUSE	8	0.66
P09405	Nucleolin	NUCL_MOUSE	48	0.65
P25444	40S ribosomal protein S2	RS2_MOUSE	22	0.65
Q61503	5~-nucleotidase	5NTD_MOUSE	32	0.65
Q6IME9	Keratin, type II cytoskeletal 72	K2C72_MOUSE	34	0.65
Q9D1D4	Transmembrane emp24 domain-containing protein 10	TMEDA_MOUSE	10	0.65
P30115	Glutathione S-transferase A3	GSTA3_MOUSE	14	0.64
P54071	Isocitrate dehydrogenase [NADP], mitochondrial	IDHP_MOUSE	31	0.64
P80317	T-complex protein 1 subunit zeta	TCPZ_MOUSE	29	0.64
Q64727	Vinculin	VINC_MOUSE	84	0.64
Q9WTM5	RuvB-like 2	RUVB2_MOUSE	28	0.64
Q9CZU6	Citrate synthase, mitochondrial	CISY_MOUSE	21	0.63
P00405	Cytochrome c oxidase subunit 2	COX2_MOUSE	6	0.62
Q61937	Nucleophosmin	NPM_MOUSE	16	0.62
Q62186	Translocon-associated protein subunit delta	SSRD_MOUSE	8	0.62
Q69ZN7	Myoferlin	MYOF_MOUSE	131	0.62
O55142	60S ribosomal protein L35a	RL35A_MOUSE	9	0.61
P21107	Tropomyosin alpha-3 chain	TPM3_MOUSE	24	0.61
P34884	Macrophage migration inhibitory factor	MIF_MOUSE	5	0.61

Accession Number	Protein Name (Wt ALI Day 14 mMECs)	Gene name	Peptide count	emPAI
Q8VEM8	Phosphate carrier protein, mitochondrial	MPCP_MOUSE	21	0.61
Q9Z2U1	Proteasome subunit alpha type-5	PSA5_MOUSE	11	0.6
Q8BMS1	Trifunctional enzyme subunit alpha, mitochondrial	ECHA_MOUSE	40	0.59
O08756	3-hydroxyacyl-CoA dehydrogenase type-2	HCD2_MOUSE	16	0.58
P35550	rRNA 2~-O-methyltransferase fibrillarin	FBRL_MOUSE	24	0.58
P49312	Heterogeneous nuclear ribonucleoprotein A1	ROA1_MOUSE	19	0.58
O35737	Heterogeneous nuclear ribonucleoprotein H	HNRH1_MOUSE	25	0.57
O70456	14-3-3 protein sigma	1433S_MOUSE	19	0.57
P60867	40S ribosomal protein S20	RS20_MOUSE	6	0.57
P62315	Small nuclear ribonucleoprotein Sm D1	SMD1_MOUSE	5	0.57
P62855	40S ribosomal protein S26	RS26_MOUSE	6	0.57
Q9QUM9	Proteasome subunit alpha type-6	PSA6_MOUSE	13	0.57
P08003	Protein disulfide-isomerase A4	PDIA4_MOUSE	43	0.56
P0C0S6	Histone H2A.Z	H2AZ_MOUSE	6	0.56
P61982	14-3-3 protein gamma	1433G_MOUSE	18	0.56
P68510	14-3-3 protein eta	1433F_MOUSE	18	0.56
Q8BP47	Asparagine--tRNA ligase, cytoplasmic	SYNC_MOUSE	30	0.56
Q9JM76	Actin-related protein 2/3 complex subunit 3	ARPC3_MOUSE	12	0.56
P45376	Aldose reductase	ALDR_MOUSE	20	0.55
P50396	Rab GDP dissociation inhibitor alpha	GDIA_MOUSE	26	0.55
P62754	40S ribosomal protein S6	RS6_MOUSE	13	0.55
P62852	40S ribosomal protein S25	RS25_MOUSE	6	0.55
Q78IK2	Up-regulated during skeletal muscle growth protein 5	USMG5_MOUSE	3	0.55
P12265	Beta-glucuronidase	BGLR_MOUSE	33	0.54
P35980	60S ribosomal protein L18	RL18_MOUSE	9	0.54
P50580	Proliferation-associated protein 2G4	PA2G4_MOUSE	24	0.54
Q9R118	Serine protease HTRA1	HTRA1_MOUSE	21	0.54
O54990	Prominin-1	PROM1_MOUSE	41	0.53
P09803	Cadherin-1	CADH1_MOUSE	33	0.53
P63001	Ras-related C3 botulinum toxin substrate 1	RAC1_MOUSE	9	0.53
Q921F2	TAR DNA-binding protein 43	TADBP_MOUSE	17	0.53
P14685	26S proteasome non-ATPase regulatory subunit 3	PSMD3_MOUSE	39	0.52
P62082	40S ribosomal protein S7	RS7_MOUSE	11	0.52
Q8BFZ9	Erlin-2	ERLN2_MOUSE	24	0.52
Q8BHN3	Neutral alpha-glucosidase AB	GANAB_MOUSE	51	0.52
Q9D8W5	26S proteasome non-ATPase regulatory subunit 12	PSD12_MOUSE	34	0.52
O55143	Sarcoplasmic/endoplasmic reticulum calcium ATPase 2	AT2A2_MOUSE	54	0.51
Q60668	Heterogeneous nuclear ribonucleoprotein	HNRPD_MOUSE	15	0.51

Accession Number	Protein Name (Wt ALI Day 14 mMECs)	Gene name	Peptide count	emPAI
	D0			
Q9R0Q3	Transmembrane emp24 domain-containing protein 2	TMED2_MOUSE	11	0.51
O08807	Peroxiredoxin-4	PRDX4_MOUSE	16	0.5
P29341	Polyadenylate-binding protein 1	PABP1_MOUSE	38	0.5
P30412	Peptidyl-prolyl cis-trans isomerase C	PPIC_MOUSE	11	0.5
Q99K51	Plastin-3	PLST_MOUSE	40	0.5
Q9CYN9	Renin receptor	RENR_MOUSE	17	0.5
P12032	Metalloproteinase inhibitor 1	TIMP1_MOUSE	12	0.49
P14148	60S ribosomal protein L7	RL7_MOUSE	18	0.49
P57776	Elongation factor 1-delta	EF1D_MOUSE	20	0.49
P97430	Antileukoproteinase	SLPI_MOUSE	11	0.49
Q99PT1	Rho GDP-dissociation inhibitor 1	GDIR1_MOUSE	14	0.49
Q9DB20	ATP synthase subunit O, mitochondrial	ATPO_MOUSE	14	0.49
Q9WU78	Programmed cell death 6-interacting protein	PDC6I_MOUSE	52	0.49
P10493	Nidogen-1	NID1_MOUSE	46	0.48
P17225	Polypyrimidine tract-binding protein 1	PTBP1_MOUSE	22	0.48
P28474	Alcohol dehydrogenase class-3	ADHX_MOUSE	20	0.48
P62814	V-type proton ATPase subunit B, brain isoform	VATB2_MOUSE	29	0.48
P62849	40S ribosomal protein S24	RS24_MOUSE	7	0.48
P14733	Lamin-B1	LMNB1_MOUSE	39	0.47
P41105	60S ribosomal protein L28	RL28_MOUSE	11	0.47
P47963	60S ribosomal protein L13	RL13_MOUSE	14	0.47
P80315	T-complex protein 1 subunit delta	TCPD_MOUSE	37	0.47
Q8BFR5	Elongation factor Tu, mitochondrial	EFTU_MOUSE	31	0.47
Q9DC16	Endoplasmic reticulum-Golgi intermediate compartment protein 1	ERGI1_MOUSE	13	0.47
O70251	Elongation factor 1-beta	EF1B_MOUSE	14	0.46
P14824	Annexin A6	ANXA6_MOUSE	49	0.46
P14131	40S ribosomal protein S16	RS16_MOUSE	12	0.45
P24270	Catalase	CATA_MOUSE	35	0.45
P24527	Leukotriene A-4 hydrolase	LKHA4_MOUSE	39	0.45
P42932	T-complex protein 1 subunit theta	TCPQ_MOUSE	39	0.45
P53026	60S ribosomal protein L10a	RL10A_MOUSE	15	0.45
Q791V5	Mitochondrial carrier homolog 2	MTCH2_MOUSE	14	0.45
Q9CQX2	Cytochrome b5 type B	CYB5B_MOUSE	8	0.45
Q9DBG6	Dolichyl-diphosphooligosaccharide--protein glycosyltransferase subunit 2	RPN2_MOUSE	26	0.45
Q9WTP7	GTP:AMP phosphotransferase AK3, mitochondrial	KAD3_MOUSE	19	0.45
P13745	Glutathione S-transferase A1	GSTA1_MOUSE	14	0.44
P14869	60S acidic ribosomal protein P0	RLA0_MOUSE	18	0.44
P49722	Proteasome subunit alpha type-2	PSA2_MOUSE	13	0.44
P61079	Ubiquitin-conjugating enzyme E2 D3	UB2D3_MOUSE	5	0.44

Accession Number	Protein Name (Wt ALI Day 14 mMECs)	Gene name	Peptide count	emPAI
Q61206	Platelet-activating factor acetylhydrolase IB subunit beta	PA1B2_MOUSE	10	0.44
Q9CVB6	Actin-related protein 2/3 complex subunit 2	ARPC2_MOUSE	22	0.44
P14094	Sodium/potassium-transporting ATPase subunit beta-1	AT1B1_MOUSE	16	0.43
P61089	Ubiquitin-conjugating enzyme E2 N	UBE2N_MOUSE	11	0.43
P61255	60S ribosomal protein L26	RL26_MOUSE	9	0.43
P62334	26S protease regulatory subunit 10B	PRS10_MOUSE	27	0.43
Q8K183	Pyridoxal kinase	PDXK_MOUSE	16	0.43
Q921H8	3-ketoacyl-CoA thiolase A, peroxisomal	THIKA_MOUSE	22	0.43
Q9D0S9	Histidine triad nucleotide-binding protein 2, mitochondrial	HINT2_MOUSE	11	0.43
P06801	NADP-dependent malic enzyme	MAOX_MOUSE	32	0.42
P16675	Lysosomal protective protein	PPGB_MOUSE	22	0.42
Q62267	Cornifin-B	SPR1B_MOUSE	15	0.42
Q8K2B3	Succinate dehydrogenase [ubiquinone] flavoprotein subunit, mitochondrial	SDHA_MOUSE	36	0.42
Q9JJI8	60S ribosomal protein L38	RL38_MOUSE	3	0.42
P35979	60S ribosomal protein L12	RL12_MOUSE	11	0.41
P62270	40S ribosomal protein S18	RS18_MOUSE	12	0.41
Q8R081	Heterogeneous nuclear ribonucleoprotein L	HNRPL_MOUSE	24	0.41
Q9JJ00	Phospholipid scramblase 1	PLS1_MOUSE	13	0.41
P45952	Medium-chain specific acyl-CoA dehydrogenase, mitochondrial	ACADM_MOUSE	22	0.4
P60335	Poly(rC)-binding protein 1	PCBP1_MOUSE	20	0.4
P61939	Thyroxine-binding globulin	THBG_MOUSE	22	0.4
Q08761	Vitamin K-dependent protein S	PROS_MOUSE	37	0.4
Q61753	D-3-phosphoglycerate dehydrogenase	SERA_MOUSE	22	0.4
Q9D8E6	60S ribosomal protein L4	RL4_MOUSE	27	0.4
Q9WV55	Vesicle-associated membrane protein-associated protein A	VAPA_MOUSE	15	0.4
Q9Z2U0	Proteasome subunit alpha type-7	PSA7_MOUSE	16	0.4
O09167	60S ribosomal protein L21	RL21_MOUSE	9	0.39
P63325	40S ribosomal protein S10	RS10_MOUSE	13	0.39
Q8VEK3	Heterogeneous nuclear ribonucleoprotein U	HNRPU_MOUSE	43	0.39
Q922R8	Protein disulfide-isomerase A6	PDIA6_MOUSE	25	0.39
Q9DB77	Cytochrome b-c1 complex subunit 2, mitochondrial	QCR2_MOUSE	22	0.39
P13597	Intercellular adhesion molecule 1	ICAM1_MOUSE	26	0.38
P17710	Hexokinase-1	HXK1_MOUSE	57	0.38
P70333	Heterogeneous nuclear ribonucleoprotein H2	HNRH2_MOUSE	25	0.38
Q02053	Ubiquitin-like modifier-activating enzyme 1	UBA1_MOUSE	55	0.38
Q6URW6	Myosin-14	MYH14_MOUSE	126	0.38

Accession Number	Protein Name (Wt ALI Day 14 mMECs)	Gene name	Peptide count	emPAI
Q9DBJ1	Phosphoglycerate mutase 1	PGAM1_MOUSE	15	0.38
P26443	Glutamate dehydrogenase 1, mitochondrial	DHE3_MOUSE	35	0.37
P48771	Cytochrome c oxidase subunit 7A2, mitochondrial	CX7A2_MOUSE	5	0.37
P59999	Actin-related protein 2/3 complex subunit 4	ARPC4_MOUSE	13	0.37
P70195	Proteasome subunit beta type-7	PSB7_MOUSE	12	0.37
Q62425	Cytochrome c oxidase subunit NDUFA4	NDUA4_MOUSE	6	0.37
Q9D6R2	Isocitrate dehydrogenase [NAD] subunit alpha, mitochondrial	IDH3A_MOUSE	21	0.37
Q9R1P0	Proteasome subunit alpha type-4	PSA4_MOUSE	14	0.37
O55023	Inositol monophosphatase 1	IMPA1_MOUSE	17	0.36
P42208	Septin-2	SEPT2_MOUSE	21	0.36
Q8CAQ8	MICOS complex subunit Mic60	MIC60_MOUSE	55	0.36
Q99JY0	Trifunctional enzyme subunit beta, mitochondrial	ECHB_MOUSE	28	0.36
P04186	Complement factor B	CFAB_MOUSE	42	0.35
P13020	Gelsolin	GELS_MOUSE	34	0.35
P25085	Interleukin-1 receptor antagonist protein	IL1RA_MOUSE	7	0.35
P61211	ADP-ribosylation factor-like protein 1	ARL1_MOUSE	10	0.35
P70124	Serpin B5	SPB5_MOUSE	22	0.35
Q9QZ88	Vacuolar protein sorting-associated protein 29	VPS29_MOUSE	11	0.35
O08749	Dihydrolipoyl dehydrogenase, mitochondrial	DLDH_MOUSE	26	0.34
P47740	Fatty aldehyde dehydrogenase	AL3A2_MOUSE	21	0.34
P97384	Annexin A11	ANX11_MOUSE	22	0.34
P97449	Aminopeptidase N	AMPN_MOUSE	51	0.34
P97807	Fumarate hydratase, mitochondrial	FUMH_MOUSE	32	0.34
Q62465	Synaptic vesicle membrane protein VAT-1 homolog	VAT1_MOUSE	18	0.34
Q99K48	Non-POU domain-containing octamer-binding protein	NONO_MOUSE	23	0.34
Q9CQS8	Protein transport protein Sec61 subunit beta	SC61B_MOUSE	6	0.34
Q9DC53	Copine-8	CPNE8_MOUSE	33	0.34
Q9JKR6	Hypoxia up-regulated protein 1	HYOU1_MOUSE	58	0.34
O55022	Membrane-associated progesterone receptor component 1	PGRC1_MOUSE	10	0.33
Q07813	Apoptosis regulator BAX	BAX_MOUSE	10	0.33
Q9CQW2	ADP-ribosylation factor-like protein 8B	ARL8B_MOUSE	12	0.33
Q9DBS1	Transmembrane protein 43	TMM43_MOUSE	21	0.33
P36536	GTP-binding protein SAR1a	SAR1A_MOUSE	11	0.32
P46978	Dolichyl-diphosphooligosaccharide--protein glycosyltransferase subunit STT3A	STT3A_MOUSE	36	0.32
P80314	T-complex protein 1 subunit beta	TCPB_MOUSE	36	0.32
Q7TMK9	Heterogeneous nuclear ribonucleoprotein	HNRPQ_MOUSE	39	0.32

Accession Number	Protein Name (Wt ALI Day 14 mMECs)	Gene name	Peptide count	emPAI
	Q			
Q8BMF4	Dihydrolipoyllysine-residue acetyltransferase component of pyruvate dehydrogenase complex, mitochondrial	ODP2_MOUSE	33	0.32
Q8JZU2	Tricarboxylate transport protein, mitochondrial	TXTP_MOUSE	17	0.32
Q922B2	Aspartate--tRNA ligase, cytoplasmic	SYDC_MOUSE	38	0.32
Q9CQN1	Heat shock protein 75 kDa, mitochondrial	TRAP1_MOUSE	50	0.32
Q9DCN2	NADH-cytochrome b5 reductase 3	NB5R3_MOUSE	17	0.32
O70503	Estradiol 17-beta-dehydrogenase 12	DHB12_MOUSE	18	0.31
O88310	Intelectin-1a	ITL1A_MOUSE	17	0.31
P05201	Aspartate aminotransferase, cytoplasmic	AATC_MOUSE	27	0.31
P42669	Transcriptional activator protein Pur-alpha	PURA_MOUSE	15	0.31
P62305	Small nuclear ribonucleoprotein E	RUXE_MOUSE	4	0.31
Q02257	Junction plakoglobin	PLAK_MOUSE	44	0.31
Q9D1Q6	Endoplasmic reticulum resident protein 44	ERP44_MOUSE	24	0.31
Q9JKF1	Ras GTPase-activating-like protein IQGAP1	IQGA1_MOUSE	93	0.31
Q9QWR8	Alpha-N-acetylgalactosaminidase	NAGAB_MOUSE	27	0.31
Q9R1P1	Proteasome subunit beta type-3	PSB3_MOUSE	9	0.31
P19253	60S ribosomal protein L13a	RL13A_MOUSE	17	0.3
P27048	Small nuclear ribonucleoprotein-associated protein B	RSMB_MOUSE	14	0.3
P35279	Ras-related protein Rab-6A	RAB6A_MOUSE	17	0.3
P80313	T-complex protein 1 subunit eta	TCPH_MOUSE	33	0.3
P80318	T-complex protein 1 subunit gamma	TCPG_MOUSE	38	0.3
P97467	Peptidyl-glycine alpha-amidating monooxygenase	AMD_MOUSE	51	0.3
Q62167	ATP-dependent RNA helicase DDX3X	DDX3X_MOUSE	40	0.3
Q8K3J9	G-protein coupled receptor family C group 5 member C	GPC5C_MOUSE	11	0.3
Q9CQD1	Ras-related protein Rab-5A	RAB5A_MOUSE	14	0.3
Q9ESW8	Pyroglutamyl-peptidase 1	PGPI_MOUSE	10	0.3
Q9JIW9	Ras-related protein Ral-B	RALB_MOUSE	10	0.3
Q9WUM5	Succinyl-CoA ligase [ADP/GDP-forming] subunit alpha, mitochondrial	SUCA_MOUSE	15	0.3
Q9Z0L8	Gamma-glutamyl hydrolase	GGH_MOUSE	17	0.3
O08547	Vesicle-trafficking protein SEC22b	SC22B_MOUSE	13	0.29
O70554	Small proline-rich protein 2B	SPR2B_MOUSE	5	0.29
P00493	Hypoxanthine-guanine phosphoribosyltransferase	HPRT_MOUSE	13	0.29
P46638	Ras-related protein Rab-11B	RB11B_MOUSE	16	0.29
Q07076	Annexin A7	ANXA7_MOUSE	23	0.29
Q61879	Myosin-10	MYH10_MOUSE	125	0.29
Q8K353	Cysteine-rich and transmembrane domain-containing protein 1	CYTM1_MOUSE	2	0.29
Q8VDW0	ATP-dependent RNA helicase DDX39A	DX39A_MOUSE	26	0.29
Q9CYH2	Redox-regulatory protein FAM213A	F213A_MOUSE	14	0.29

Accession Number	Protein Name (Wt ALI Day 14 mMECs)	Gene name	Peptide count	emPAI
Q9D103	Interferon-induced transmembrane protein 1	IFM1_MOUSE	2	0.29
Q9R112	Sulfide:quinone oxidoreductase, mitochondrial	SQRD_MOUSE	32	0.29
O54782	Epididymis-specific alpha-mannosidase	MA2B2_MOUSE	44	0.28

Table S6 Proteins detected by MS analysis of *Bpifa1*$^{-/-}$ ALI Day mMEC washes

Accession Number	Protein Name (*Bpifa1*$^{-/-}$ ALI Day 14 mMECs)	Gene name	Peptide count	emPAI
P08071	Lactotransferrin	TRFL_MOUSE	47	247.93
Q921I1	Serotransferrin	TRFE_MOUSE	40	13.69
O09049	Regenerating islet-derived protein 3-gamma	REG3G_MOUSE	8	8.04
O09131	Glutathione S-transferase omega-1	GSTO1_MOUSE	17	6.64
P11672	Neutrophil gelatinase-associated lipocalin	NGAL_MOUSE	9	5.66
P60710	Actin, cytoplasmic 1	ACTB_MOUSE	23	5.11
Q61147	Ceruloplasmin	CERU_MOUSE	55	4.58
P08074	Carbonyl reductase [NADPH] 2	CBR2_MOUSE	16	4.36
Q06890	Clusterin	CLUS_MOUSE	22	3.32
P10649	Glutathione S-transferase Mu 1	GSTM1_MOUSE	18	3.22
P50446	Keratin, type II cytoskeletal 6A	K2C6A_MOUSE	35	2.43
Q8BND5	Sulfhydryl oxidase 1	QSOX1_MOUSE	43	2.42
P10107	Annexin A1	ANXA1_MOUSE	24	2.39
O35639	Annexin A3	ANXA3_MOUSE	24	2.36
P11679	Keratin, type II cytoskeletal 8	K2C8_MOUSE	33	2.22
P07356	Annexin A2	ANXA2_MOUSE	23	2.12
Q922U2	Keratin, type II cytoskeletal 5	K2C5_MOUSE	34	2.11
Q9DCV7	Keratin, type II cytoskeletal 7	K2C7_MOUSE	35	2.1
Q9Z331	Keratin, type II cytoskeletal 6B	K2C6B_MOUSE	36	2.03
Q61414	Keratin, type I cytoskeletal 15	K1C15_MOUSE	32	2
P10605	Cathepsin B	CATB_MOUSE	15	1.94
P19001	Keratin, type I cytoskeletal 19	K1C19_MOUSE	35	1.92
P26040	Ezrin	EZRI_MOUSE	39	1.76
P62962	Profilin-1	PROF1_MOUSE	9	1.74
Q61398	Procollagen C-endopeptidase enhancer 1	PCOC1_MOUSE	23	1.73
P24472	Glutathione S-transferase A4	GSTA4_MOUSE	12	1.66
Q61646	Haptoglobin	HPT_MOUSE	20	1.63
Q61362	Chitinase-3-like protein 1	CH3L1_MOUSE	22	1.55
Q07797	Galectin-3-binding protein	LG3BP_MOUSE	26	1.41
O08709	Peroxiredoxin-6	PRDX6_MOUSE	15	1.4
P08249	Malate dehydrogenase, mitochondrial	MDHM_MOUSE	24	1.4
P01027	Complement C3	CO3_MOUSE	111	1.32
P35700	Peroxiredoxin-1	PRDX1_MOUSE	14	1.3
P50404	Pulmonary surfactant-associated protein D	SFTPD_MOUSE	23	1.3
P05213	Tubulin alpha-1B chain	TBA1B_MOUSE	22	1.26
P17182	Alpha-enolase	ENOA_MOUSE	28	1.23
P50543	Protein S100-A11	S10AB_MOUSE	5	1.22
Q61781	Keratin, type I cytoskeletal 14	K1C14_MOUSE	35	1.18
P08228	Superoxide dismutase [Cu-Zn]	SODC_MOUSE	11	1.14
P47739	Aldehyde dehydrogenase, dimeric NADP-preferring	AL3A1_MOUSE	25	1.12
Q9CQV3	Serpin B11	SPB11_MOUSE	24	1.07

Accession Number	Protein Name (*Bpifa1*$^{-/-}$ ALI Day 14 mMECs)	Gene name	Peptide count	emPAI
Q9QWL7	Keratin, type I cytoskeletal 17	K1C17_MOUSE	33	1.06
P28654	Decorin	PGS2_MOUSE	23	1.04
P10126	Elongation factor 1-alpha 1	EF1A1_MOUSE	23	1
Q8BGZ7	Keratin, type II cytoskeletal 75	K2C75_MOUSE	36	1
P56480	ATP synthase subunit beta, mitochondrial	ATPB_MOUSE	30	0.98
P30412	Peptidyl-prolyl cis-trans isomerase C	PPIC_MOUSE	11	0.97
P05784	Keratin, type I cytoskeletal 18	K1C18_MOUSE	32	0.95
P06797	Cathepsin L1	CATL1_MOUSE	12	0.94
P08730	Keratin, type I cytoskeletal 13	K1C13_MOUSE	31	0.94
P19157	Glutathione S-transferase P 1	GSTP1_MOUSE	10	0.93
Q61176	Arginase-1	ARGI1_MOUSE	18	0.88
P07744	Keratin, type II cytoskeletal 4	K2C4_MOUSE	31	0.86
Q8VCT4	Carboxylesterase 1D	CES1D_MOUSE	27	0.86
P47738	Aldehyde dehydrogenase, mitochondrial	ALDH2_MOUSE	26	0.85
P40142	Transketolase	TKT_MOUSE	34	0.84
P57780	Alpha-actinin-4	ACTN4_MOUSE	61	0.84
Q8VED5	Keratin, type II cytoskeletal 79	K2C79_MOUSE	32	0.84
P52480	Pyruvate kinase PKM	KPYM_MOUSE	36	0.83
Q8BFZ3	Beta-actin-like protein 2	ACTBL_MOUSE	24	0.82
Q6IFX2	Keratin, type I cytoskeletal 42	K1C42_MOUSE	33	0.77
P63101	14-3-3 protein zeta/delta	1433Z_MOUSE	19	0.75
Q62266	Cornifin-A	SPR1A_MOUSE	13	0.74
Q61468	Mesothelin	MSLN_MOUSE	29	0.73
O88844	Isocitrate dehydrogenase [NADP] cytoplasmic	IDHC_MOUSE	30	0.72
Q00493	Carboxypeptidase E	CBPE_MOUSE	28	0.71
Q03265	ATP synthase subunit alpha, mitochondrial	ATPA_MOUSE	36	0.71
P47791	Glutathione reductase, mitochondrial	GSHR_MOUSE	25	0.7
P08207	Protein S100-A10	S10AA_MOUSE	5	0.69
P24369	Peptidyl-prolyl cis-trans isomerase B	PPIB_MOUSE	15	0.69
P17742	Peptidyl-prolyl cis-trans isomerase A	PPIA_MOUSE	14	0.67
P33267	Cytochrome P450 2F2	CP2F2_MOUSE	29	0.67
Q93092	Transaldolase	TALDO_MOUSE	23	0.66
Q61508	Extracellular matrix protein 1	ECM1_MOUSE	37	0.64
P17563	Selenium-binding protein 1	SBP1_MOUSE	31	0.62
Q9DCD0	6-phosphogluconate dehydrogenase, decarboxylating	6PGD_MOUSE	29	0.61
P26043	Radixin	RADI_MOUSE	39	0.6
P05202	Aspartate aminotransferase, mitochondrial	AATM_MOUSE	29	0.59
Q3UV17	Keratin, type II cytoskeletal 2 oral	K22O_MOUSE	39	0.58
Q9WUU7	Cathepsin Z	CATZ_MOUSE	14	0.58
P16110	Galectin-3	LEG3_MOUSE	10	0.57
Q3TTY5	Keratin, type II cytoskeletal 2 epidermal	K22E_MOUSE	43	0.57
O88593	Peptidoglycan recognition protein 1	PGRP1_MOUSE	10	0.56

Accession Number	Protein Name (*Bpifa1*$^{-/-}$ ALI Day 14 mMECs)	Gene name	Peptide count	emPAI
P16858	Glyceraldehyde-3-phosphate dehydrogenase	G3P_MOUSE	21	0.55
P06151	L-lactate dehydrogenase A chain OS	LDHA_MOUSE	23	0.54
P14152	Malate dehydrogenase, cytoplasmic	MDHC_MOUSE	21	0.54
Q9Z2K1	Keratin, type I cytoskeletal 16	K1C16_MOUSE	35	0.54
Q61171	Peroxiredoxin-2	PRDX2_MOUSE	10	0.53
P05064	Fructose-bisphosphate aldolase A	ALDOA_MOUSE	23	0.49
P54116	Erythrocyte band 7 integral membrane protein	STOM_MOUSE	17	0.49
P27773	Protein disulfide-isomerase A3	PDIA3_MOUSE	35	0.48
Q8BPB5	EGF-containing fibulin-like extracellular matrix protein 1	FBLN3_MOUSE	27	0.48
P11499	Heat shock protein HSP 90-beta	HS90B_MOUSE	40	0.47
P23492	Purine nucleoside phosphorylase	PNPH_MOUSE	19	0.47
Q8VDD5	Myosin-9	MYH9_MOUSE	127	0.47
Q9Z0K8	Pantetheinase	VNN1_MOUSE	23	0.47
Q6NXH9	Keratin, type II cytoskeletal 73	K2C73_MOUSE	37	0.46
Q7TPR4	Alpha-actinin-1	ACTN1_MOUSE	60	0.45
Q9ER10	Brain-specific serine protease 4	BSSP4_MOUSE	15	0.45
P11276	Fibronectin	FINC_MOUSE	108	0.44
P15626	Glutathione S-transferase Mu 2	GSTM2_MOUSE	18	0.44
Q6IFZ6	Keratin, type II cytoskeletal 1b	K2C1B_MOUSE	39	0.44
Q61805	Lipopolysaccharide-binding protein	LBP_MOUSE	19	0.43
P08113	Endoplasmin	ENPL_MOUSE	47	0.41
Q9JII6	Alcohol dehydrogenase [NADP(+)]	AK1A1_MOUSE	23	0.41
P04104	Keratin, type II cytoskeletal 1	K2C1_MOUSE	35	0.4
P18760	Cofilin-1	COF1_MOUSE	12	0.39
Q571E4	N-acetylgalactosamine-6-sulfatase	GALNS_MOUSE	25	0.39
P10810	Monocyte differentiation antigen CD14	CD14_MOUSE	16	0.38
Q01853	Transitional endoplasmic reticulum ATPase	TERA_MOUSE	45	0.38
Q9DAU7	WAP four-disulfide core domain protein 2	WFDC2_MOUSE	6	0.38
Q9QYB1	Chloride intracellular channel protein 4	CLIC4_MOUSE	17	0.38
Q61581	Insulin-like growth factor-binding protein 7	IBP7_MOUSE	18	0.37
P06745	Glucose-6-phosphate isomerase	G6PI_MOUSE	32	0.36
P58252	Elongation factor 2	EF2_MOUSE	52	0.35
Q9R0P3	S-formylglutathione hydrolase	ESTD_MOUSE	16	0.35
P09803	Cadherin-1	CADH1_MOUSE	33	0.34
P17751	Triosephosphate isomerase	TPIS_MOUSE	18	0.34
Q60930	Voltage-dependent anion-selective channel protein 2	VDAC2_MOUSE	16	0.34
P35980	60S ribosomal protein L18	RL18_MOUSE	9	0.33
Q9WV54	Acid ceramidase	ASAH1_MOUSE	21	0.33
P09103	Protein disulfide-isomerase	PDIA1_MOUSE	39	0.32
P0CG49	Polyubiquitin-B	UBB_MOUSE	28	0.32

Accession Number	Protein Name (*Bpifa1*$^{-/-}$ ALI Day 14 mMECs)	Gene name	Peptide count	emPAI
P18242	Cathepsin D	CATD_MOUSE	20	0.32
P05201	Aspartate aminotransferase, cytoplasmic	AATC_MOUSE	27	0.31
P61027	Ras-related protein Rab-10	RAB10_MOUSE	17	0.31
O70570	Polymeric immunoglobulin receptor	PIGR_MOUSE	38	0.3
P14211	Calreticulin	CALR_MOUSE	27	0.3
P23780	Beta-galactosidase	BGAL_MOUSE	28	0.3
P97449	Aminopeptidase N	AMPN_MOUSE	51	0.3
Q9DB20	ATP synthase subunit O, mitochondrial	ATPO_MOUSE	14	0.3
P47963	60S ribosomal protein L13	RL13_MOUSE	14	0.29
P21956	Lactadherin	MFGM_MOUSE	23	0.28
P25785	Metalloproteinase inhibitor 2	TIMP2_MOUSE	14	0.28
P61979	Heterogeneous nuclear ribonucleoprotein K	HNRPK_MOUSE	27	0.28
Q60692	Proteasome subunit beta type-6	PSB6_MOUSE	11	0.28
Q61503	5~-nucleotidase	5NTD_MOUSE	32	0.28
Q9CZU6	Citrate synthase, mitochondrial	CISY_MOUSE	21	0.28
P35441	Thrombospondin-1	TSP1_MOUSE	70	0.27
Q8BHL4	Retinoic acid-induced protein 3	RAI3_MOUSE	13	0.26
Q9Z1Q5	Chloride intracellular channel protein 1	CLIC1_MOUSE	17	0.26
P02535	Keratin, type I cytoskeletal 10	K1C10_MOUSE	28	0.25
P20029	78 kDa glucose-regulated protein	GRP78_MOUSE	39	0.25
Q6IME9	Keratin, type II cytoskeletal 72	K2C72_MOUSE	34	0.25
P62259	14-3-3 protein epsilon	1433E_MOUSE	18	0.24
O88968	Transcobalamin-2	TCO2_MOUSE	23	0.22
P11214	Tissue-type plasminogen activator	TPA_MOUSE	31	0.22
Q8K354	Carbonyl reductase [NADPH] 3	CBR3_MOUSE	20	0.22
P48962	ADP/ATP translocase 1	ADT1_MOUSE	22	0.21
Q61598	Rab GDP dissociation inhibitor beta	GDIB_MOUSE	28	0.21
Q9D312	Keratin, type I cytoskeletal 20	K1C20_MOUSE	32	0.21
Q9R118	Serine protease HTRA1	HTRA1_MOUSE	21	0.2
P24549	Retinal dehydrogenase 1	AL1A1_MOUSE	23	0.19
P38647	Stress-70 protein, mitochondrial	GRP75_MOUSE	43	0.19
P48036	Annexin A5	ANXA5_MOUSE	25	0.19
P97494	Glutamate--cysteine ligase catalytic subunit	GSH1_MOUSE	34	0.19
Q9JJ00	Phospholipid scramblase 1	PLS1_MOUSE	13	0.19
P09405	Nucleolin	NUCL_MOUSE	48	0.18
P37040	NADPH--cytochrome P450 reductase	NCPR_MOUSE	35	0.18
Q61990	Poly(rC)-binding protein 2	PCBP2_MOUSE	18	0.18
Q8VDN2	Sodium/potassium-transporting ATPase subunit alpha-1	AT1A1_MOUSE	53	0.18
Q9WU78	Programmed cell death 6-interacting protein	PDC6I_MOUSE	52	0.18
P29268	Connective tissue growth factor	CTGF_MOUSE	24	0.17
Q8BG05	Heterogeneous nuclear ribonucleoprotein	ROA3_MOUSE	20	0.17

Accession Number	Protein Name (*Bpifa1*$^{-/-}$ ALI Day 14 mMECs)	Gene name	Peptide count	emPAI
	A3			
Q8VEM8	Phosphate carrier protein, mitochondrial	MPCP_MOUSE	21	0.17
Q99K85	Phosphoserine aminotransferase	SERC_MOUSE	27	0.17
P06801	NADP-dependent malic enzyme	MAOX_MOUSE	32	0.16
Q60854	Serpin B6	SPB6_MOUSE	23	0.16
Q9WV32	Actin-related protein 2/3 complex subunit 1B	ARC1B_MOUSE	19	0.16
O88342	WD repeat-containing protein 1	WDR1_MOUSE	37	0.15
P07724	Serum albumin	ALBU_MOUSE	42	0.15
P09411	Phosphoglycerate kinase 1	PGK1_MOUSE	29	0.15
O35737	Heterogeneous nuclear ribonucleoprotein H	HNRH1_MOUSE	25	0.14
O54990	Prominin-1	PROM1_MOUSE	41	0.14
P29758	Ornithine aminotransferase, mitochondrial	OAT_MOUSE	23	0.14
Q8R2Y2	Cell surface glycoprotein MUC18	MUC18_MOUSE	34	0.14
P21981	Protein-glutamine gamma-glutamyltransferase 2	TGM2_MOUSE	36	0.13
P46664	Adenylosuccinate synthetase isozyme 2	PURA2_MOUSE	27	0.13
Q91VI7	Ribonuclease inhibitor	RINI_MOUSE	27	0.13
Q9D379	Epoxide hydrolase 1	HYEP_MOUSE	29	0.13
O09159	Lysosomal alpha-mannosidase	MA2B1_MOUSE	47	0.12
O54782	Epididymis-specific alpha-mannosidase	MA2B2_MOUSE	44	0.12
P13597	Intercellular adhesion molecule 1	ICAM1_MOUSE	26	0.11
P23953	Carboxylesterase 1C	EST1C_MOUSE	25	0.11
P42932	T-complex protein 1 subunit theta	TCPQ_MOUSE	39	0.11
P63038	60 kDa heat shock protein, mitochondrial	CH60_MOUSE	36	0.11
Q68FD5	Clathrin heavy chain 1	CLH1_MOUSE	95	0.11
P17879	Heat shock 70 kDa protein 1B	HS71B_MOUSE	37	0.1
Q01279	Epidermal growth factor receptor	EGFR_MOUSE	66	0.1
Q61490	CD166 antigen	CD166_MOUSE	29	0.1
Q61656	Probable ATP-dependent RNA helicase DDX5	DDX5_MOUSE	35	0.1
Q69ZN7	Myoferlin	MYOF_MOUSE	131	0.1
Q8K2I4	Beta-mannosidase	MANBA_MOUSE	49	0.1
Q8R081	Heterogeneous nuclear ribonucleoprotein L	HNRPL_MOUSE	24	0.1
Q9DC53	Copine-8	CPNE8_MOUSE	33	0.1
P12265	Beta-glucuronidase	BGLR_MOUSE	33	0.09
Q8BHN3	Neutral alpha-glucosidase AB	GANAB_MOUSE	51	0.09
Q8JZM8	Mucin-4	MUC4_MOUSE	115	0.09
Q61851	Fibroblast growth factor receptor 3	FGFR3_MOUSE	35	0.08
Q8VEK3	Heterogeneous nuclear ribonucleoprotein U	HNRPU_MOUSE	43	0.08
Q99K30	Epidermal growth factor receptor kinase substrate 8-like protein 2	ES8L2_MOUSE	40	0.08
P17710	Hexokinase-1	HXK1_MOUSE	57	0.06

Accession Number	Protein Name (*Bpifa1*$^{-/-}$ ALI Day 14 mMECs)	Gene name	Peptide count	emPAI
P97467	Peptidyl-glycine alpha-amidating monooxygenase	AMD_MOUSE	51	0.06
P10493	Nidogen-1	NID1_MOUSE	46	0.05
Q80X90	Filamin-B	FLNB_MOUSE	146	0.05
Q8BTM8	Filamin-A	FLNA_MOUSE	143	0.05
Q9JKF1	Ras GTPase-activating-like protein IQGAP1	IQGA1_MOUSE	93	0.03
Q05793	Basement membrane-specific heparan sulfate proteoglycan core protein	PGBM_MOUSE	151	0.02